

Recent advances in novel therapeutic molecules and targets for inflammatory diseases

Edited by

Shuai Wang, Shaogui Wang and Xiaojuan Chao

Published in

Frontiers in Pharmacology



FRONTIERS EBOOK COPYRIGHT STATEMENT

The copyright in the text of individual articles in this ebook is the property of their respective authors or their respective institutions or funders. The copyright in graphics and images within each article may be subject to copyright of other parties. In both cases this is subject to a license granted to Frontiers.

The compilation of articles constituting this ebook is the property of Frontiers.

Each article within this ebook, and the ebook itself, are published under the most recent version of the Creative Commons CC-BY licence. The version current at the date of publication of this ebook is CC-BY 4.0. If the CC-BY licence is updated, the licence granted by Frontiers is automatically updated to the new version.

When exercising any right under the CC-BY licence, Frontiers must be attributed as the original publisher of the article or ebook, as applicable.

Authors have the responsibility of ensuring that any graphics or other materials which are the property of others may be included in the CC-BY licence, but this should be checked before relying on the CC-BY licence to reproduce those materials. Any copyright notices relating to those materials must be complied with.

Copyright and source acknowledgement notices may not be removed and must be displayed in any copy, derivative work or partial copy which includes the elements in question.

All copyright, and all rights therein, are protected by national and international copyright laws. The above represents a summary only. For further information please read Frontiers' Conditions for Website Use and Copyright Statement, and the applicable CC-BY licence.

ISSN 1664-8714
ISBN 978-2-83251-338-5
DOI 10.3389/978-2-83251-338-5

About Frontiers

Frontiers is more than just an open access publisher of scholarly articles: it is a pioneering approach to the world of academia, radically improving the way scholarly research is managed. The grand vision of Frontiers is a world where all people have an equal opportunity to seek, share and generate knowledge. Frontiers provides immediate and permanent online open access to all its publications, but this alone is not enough to realize our grand goals.

Frontiers journal series

The Frontiers journal series is a multi-tier and interdisciplinary set of open-access, online journals, promising a paradigm shift from the current review, selection and dissemination processes in academic publishing. All Frontiers journals are driven by researchers for researchers; therefore, they constitute a service to the scholarly community. At the same time, the *Frontiers journal series* operates on a revolutionary invention, the tiered publishing system, initially addressing specific communities of scholars, and gradually climbing up to broader public understanding, thus serving the interests of the lay society, too.

Dedication to quality

Each Frontiers article is a landmark of the highest quality, thanks to genuinely collaborative interactions between authors and review editors, who include some of the world's best academicians. Research must be certified by peers before entering a stream of knowledge that may eventually reach the public - and shape society; therefore, Frontiers only applies the most rigorous and unbiased reviews. Frontiers revolutionizes research publishing by freely delivering the most outstanding research, evaluated with no bias from both the academic and social point of view. By applying the most advanced information technologies, Frontiers is catapulting scholarly publishing into a new generation.

What are Frontiers Research Topics?

Frontiers Research Topics are very popular trademarks of the *Frontiers journals series*: they are collections of at least ten articles, all centered on a particular subject. With their unique mix of varied contributions from Original Research to Review Articles, Frontiers Research Topics unify the most influential researchers, the latest key findings and historical advances in a hot research area.

Find out more on how to host your own Frontiers Research Topic or contribute to one as an author by contacting the Frontiers editorial office: frontiersin.org/about/contact

Recent advances in novel therapeutic molecules and targets for inflammatory diseases

Topic editors

Shuai Wang — Guangzhou University of Chinese Medicine, China

Shaogui Wang — Guangzhou University of Chinese Medicine, China

Xiaojuan Chao — The First Affiliated Hospital of Sun Yat-sen University, China

Citation

Wang, S., Wang, S., Chao, X., eds. (2023). *Recent advances in novel therapeutic molecules and targets for inflammatory diseases*. Lausanne: Frontiers Media SA. doi: 10.3389/978-2-83251-338-5

Table of contents

- 05 **Editorial: Recent advances in novel therapeutic molecules and targets for inflammatory diseases**
Feng Li, Shaogui Wang, Xiaojuan Chao and Shuai Wang
- 08 **Design, synthesis and biological evaluation of novel O-substituted tryptanthrin oxime derivatives as c-Jun N-terminal kinase inhibitors**
Igor A. Schepetkin, Anastasia R. Kovrizhina, Ksenia S. Stankevich, Andrei I. Khlebnikov, Liliya N. Kirpotina, Mark T. Quinn and Matthew J. Cook
- 22 **Identification of lncRNA DLEU2 as a potential diagnostic biomarker and anti-inflammatory target for ulcerative colitis**
Qiuling Lin, Dingguo Zhang, Jian Zhang, Weixiang Luo, Zhenglei Xu, Jun Yao and Lisheng Wang
- 30 **Ginsenoside Rc, as an FXR activator, alleviates acetaminophen-induced hepatotoxicity via relieving inflammation and oxidative stress**
Yadi Zhong, Yingjian Chen, Zhisen Pan, Kaijia Tang, Guangcheng Zhong, Jingyi Guo, Tianqi Cui, Tianyao Li, Siwei Duan, Xiaoying Yang, Yong Gao, Qi Wang and Dong Zhang
- 47 **Bufadienolides originated from toad source and their anti-inflammatory activity**
Denglang Zou, Qiqi Wang, Tao Chen, Duocheng Sang, Tingqin Yang, Yuhan Wang, Mengze Gao, Fangfang He, Yulin Li, Liangliang He and Duojie Longzhu
- 64 **Inflammatory signaling on cytochrome P450-mediated drug metabolism in hepatocytes**
Xiaokang Wang, Jiaoyu Rao, Zhiyi Tan, Tianrong Xun, Jingqian Zhao and Xixiao Yang
- 79 **Inhibition of colon cancer K-Ras^{G13D} mutation reduces cancer cell proliferation but promotes stemness and inflammation via RAS/ERK pathway**
Yan Qi, Hong Zou, XiaoHui Zhao, Joanna Kapeleris, Michael Monteiro, Feng Li, Zhi Ping Xu, Yizhen Deng, Yanheng Wu, Ying Tang and Wenyi Gu
- 95 **Ginsenoside Rc attenuates DSS-induced ulcerative colitis, intestinal inflammatory, and barrier function by activating the farnesoid X receptor**
Kaijia Tang, Danli Kong, Yuan Peng, Jingyi Guo, Yadi Zhong, Haibing Yu, Zhenhua Mai, Yanling Chen, Yingjian Chen, Tianqi Cui, Siwei Duan, Tianyao Li, Naihua Liu, Dong Zhang, Yuanlin Ding and Jiawen Huang

- 109 **Monocyte to high-density lipoprotein and apolipoprotein A1 ratios are associated with bone homeostasis imbalance caused by chronic inflammation in postmenopausal women with type 2 diabetes mellitus**
Rong Huang, Yang Chen, Mei Tu and Wei Wang
- 118 **Mouse promyelocytic leukemia zinc finger protein (PLZF) regulates hepatic lipid and glucose homeostasis dependent on SIRT1**
Huiling Hu, Nannan Sun, Haiyan Du, Yuqing He, Kunyi Pan, Xiuli Liu, Xiaoxia Lu, Jie Wei, Mianmian Liao and Chaohui Duan



OPEN ACCESS

EDITED AND REVIEWED BY
Dieter Steinhilber,
Goethe University Frankfurt, Germany

*CORRESPONDENCE

Feng Li,
✉ li_fengfeng@163.com
Shaogui Wang,
✉ wangshaogui@gzucm.edu.cn
Xiaojuan Chao,
✉ chxj2018@163.com
Shuai Wang,
✉ wangs91@163.com

SPECIALTY SECTION

This article was submitted to
Inflammation Pharmacology,
a section of the journal
Frontiers in Pharmacology

RECEIVED 12 December 2022
ACCEPTED 19 December 2022
PUBLISHED 04 January 2023

CITATION

Li F, Wang S, Chao X and Wang S (2023),
Editorial: Recent advances in novel
therapeutic molecules and targets for
inflammatory diseases.
Front. Pharmacol. 13:1121821.
doi: 10.3389/fphar.2022.1121821

COPYRIGHT

© 2023 Li, Wang, Chao and Wang. This is
an open-access article distributed under
the terms of the [Creative Commons
Attribution License \(CC BY\)](#). The use,
distribution or reproduction in other
forums is permitted, provided the original
author(s) and the copyright owner(s) are
credited and that the original publication in
this journal is cited, in accordance with
accepted academic practice. No use,
distribution or reproduction is permitted
which does not comply with these terms.

Editorial: Recent advances in novel therapeutic molecules and targets for inflammatory diseases

Feng Li^{1*}, Shaogui Wang^{2*}, Xiaojuan Chao^{3*} and Shuai Wang^{4*}

¹Infectious Diseases Institute, Guangzhou Eighth People's Hospital, Guangzhou Medical University, Guangzhou, China, ²Guangdong Provincial Key Laboratory of Translational Cancer Research of Chinese Medicines, Joint International Research Laboratory of Translational Cancer Research of Chinese Medicines, International Institute for Translational Chinese Medicine, School of Pharmaceutical Sciences, Guangzhou University of Chinese Medicine, Guangzhou, China, ³Institute of Precision Medicine, The First Affiliated Hospital, Sun Yat-sen University, Guangzhou, China, ⁴Institute of Molecular Rhythm and Metabolism, School of Pharmaceutical Sciences, Guangzhou University of Chinese Medicine, Guangzhou, China

KEYWORDS

inflammatory diseases, biomarkers, targets, inflammation, compounds

Editorial on the Research Topic

[Recent advances in novel therapeutic molecules and targets for inflammatory diseases](#)

Inflammatory diseases are composed of numerous disorders and conditions that are characterized by inflammation, such as inflammatory bowel disease, hepatitis, and rheumatoid arthritis (Okim et al., 2012). In pathological conditions with inflammatory diseases, the immune system mistakenly attacks healthy cells or tissues, resulting in chronic pain, redness, swelling, stiffness, and damage to the body (Marchetti et al., 2005). Inflammatory diseases have been linked to several potential causes, including diet, stress, and sleep disorders. Anti-inflammatory drugs help to prevent or minimize disease progression. However, common medications used are frequently accompanied by serious adverse effects. There is an urgent need to develop new therapies for inflammatory diseases and elucidate the critical genes and inner mechanism.

Diagnostic biomarkers are useful in the therapeutics of diseases at multiple aspects along the patient's diagnostic and treatment course. There are various inflammatory biomarkers including cytokines/chemokines, acute phase proteins, immune-related effectors, reactive oxygen and nitrogen species, prostaglandins and cyclooxygenase-related factors, transcription factors, and growth factors (Brenner et al., 2014). Lin et al. demonstrated that lncRNA DLEU2 in the intestinal mucosa was dysregulated upon gut inflammation and could act as a diagnostic biomarker for ulcerative colitis (Lin et al.). They identified DLEU2 as an anti-inflammatory lncRNA which inhibits gut inflammation by negatively regulating the NF- κ B signaling pathway (Lin et al.). Huang et al. reported that MHR (monocyte to high-density lipoprotein ratio) and MAR (monocyte to apolipoprotein A1 ratio) were ideal pro-inflammatory markers to reflect bone homeostasis imbalance caused by chronic inflammation in the bone microenvironment of postmenopausal women with type 2 diabetes mellitus (Huang et al.). These researchers expanded the Research Topic of biomarkers to inflammatory diseases.

Finding the right therapeutic targets is the most important approach in anti-inflammatory drug discovery. Many targets are responsible for the anti-inflammatory actions, such as inhibition of cytokine signaling, decreasing leucocyte activation, chemotaxis, and recruitment. Researchers have characterized several targets in this Research Topic. K-Ras is a well-studied oncogene. Qi et al. reported that inhibition of K-Ras^{G13D} mutation promoted cancer stemness and inflammation via RAS/ERK pathway (Qi et al.). This finding may be important for understanding the effects of K-Ras^{G13D} mutation on promoting cancer stemness and inflammation when employing targeted therapies to K-Ras^{G13D}.

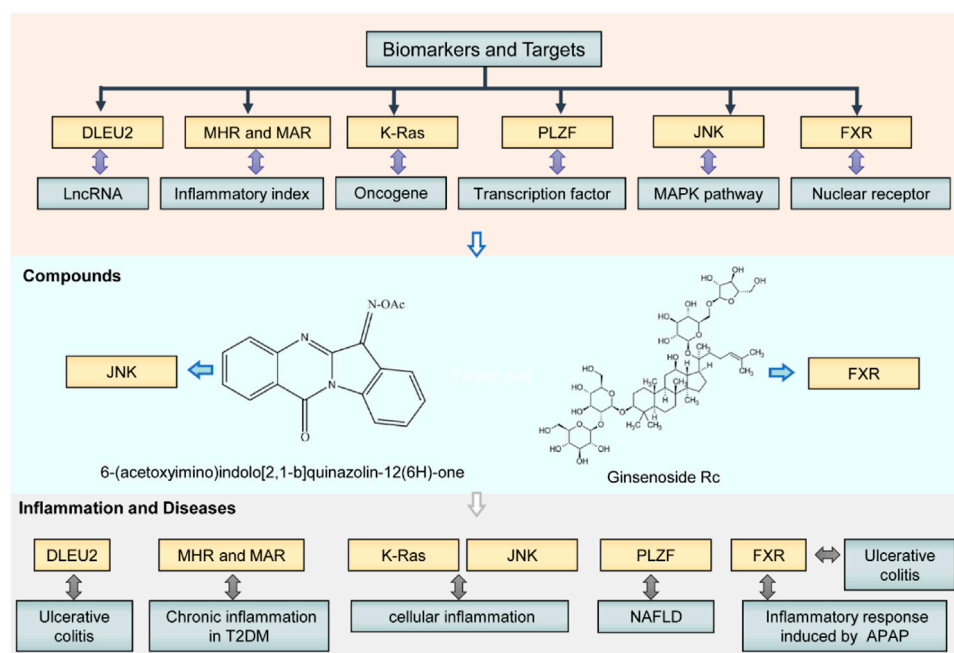


FIGURE 1

Biomarkers, targets, and compounds for the management of inflammatory diseases in this Research Topic. These biomarkers and targets consist of lncRNA, oncogene, key protein of signaling pathways, and transcriptional factor (e.g., nuclear receptor). Therapeutic agents include natural (e.g., Ginsenoside Rc) and synthetic compounds (e.g., O-substituted tryptanthrin oxime derivatives). NAFLD, non-alcoholic fatty liver disease; T2DM, type 2 diabetes mellitus; APAP, acetaminophen.

mutations in clinical practice. Promyelocytic leukemia zinc finger protein (PLZF) is a transcription factor that acts in regulating a variety of biological processes, such as spermatogenesis, stem cell maintenance, immune regulation, and invariant natural killer T cell (iNKT) development. Hu et al. demonstrated that PLZF, upregulated in mice with non-alcoholic fatty liver disease, was an essential regulator of hepatic lipid and glucose metabolism (Hu et al.). PLZF activates SREBP-1c gene transcription by binding directly to the promoter, inducing repressor-to-activator conversion.

Target-based small molecule drug discovery is an important research direction for inflammatory diseases. Schepetkin et al. designed, synthesized, and evaluated several novel analogs of O-substituted tryptanthrin oxime derivatives as c-Jun N-terminal kinase (JNK) inhibitors. Some of these compounds had a high affinity for JNK1-3 and potently inhibited LPS-induced nuclear NF- κ B/AP-1 activation and IL-6 production in human monocytic cells (Schepetkin et al.). Ginsenoside Rc (Rc) is a major component of Panax ginseng. Tang et al. reported that Rc potentially ameliorated inflammatory response and barrier function to protect the gut from DSS-induced colitis (Tang et al.). Zhong et al. showed that Rc alleviated acetaminophen-induced hepatotoxicity by relieving inflammation and oxidative stress (Zhong et al.). Both studies indicated that Rc could be a ligand of FXR by binding with the protein domain. Thus, signaling inhibitors and ligands of nuclear receptors may represent novel anti-inflammatory therapies for the inhibition of multiple cytokines and inflammatory signaling pathways.

Overall, we identified a series of attractive diagnostic biomarkers, therapeutic targets, and compounds for the intervention of inflammatory diseases (Figure 1). These biomarkers and targets consist of lncRNA, oncogene, protein of signaling pathways, and

transcriptional factor (e.g., nuclear receptor). Therapeutic agents include natural (e.g., Ginsenoside Rc) and synthetic compounds (e.g., O-substituted tryptanthrin oxime derivatives) (Figure 1). The researchers also delineated intricate gene-chemical relationships and molecular mechanisms in inflammatory disease development. All these findings may yield novel anti-inflammatory lead structures with proven efficacy and pharmacokinetics *in vivo* to manage inflammatory diseases in the future. Further studies would identify the patients who would benefit from a particular anti-inflammatory drug action, making treatment for disease state more personalized and effective.

Author contributions

FL drafted the manuscript; SGW, XC and SW reviewed and edited the manuscript.

Funding

This work was supported by the National Natural Science Foundation of China (No. 82104238 to FL, 82000612 to SGW).

Conflict of interest

The authors declare that the research was conducted in the absence of any commercial or financial relationships that could be construed as a potential conflict of interest.

Publisher's note

All claims expressed in this article are solely those of the authors and do not necessarily represent those of their affiliated

organizations, or those of the publisher, the editors and the reviewers. Any product that may be evaluated in this article, or claim that may be made by its manufacturer, is not guaranteed or endorsed by the publisher.

References

Brenner, D. R., Scherer, D., Muir, K., Schildkraut, J., Boffetta, P., Spitz, M. R., et al. (2014). A review of the application of inflammatory biomarkers in epidemiologic cancer research. *Cancer Epidemiol. Biomarkers Prev.* 23 (9), 1729–1751. doi:10.1158/1055-9965.EPI-14-0064

Marchetti, B., and Abbracchio, M. P. (2005). To be or not to be (inflamed)--is that the question in anti-inflammatory drug therapy of neurodegenerative disorders? *Trends Pharmacol. Sci.* 26 (10), 517–525. doi:10.1016/j.tips.2005.08.007

Okin, D., and Medzhitov, R. (2012). Evolution of inflammatory diseases. *Curr. Biol.* 22 (17), R733–R740. doi:10.1016/j.cub.2012.07.029



OPEN ACCESS

EDITED BY

Shuai Wang,
Guangzhou University of Chinese
Medicine, China

REVIEWED BY

Xiang Luo,
Guangzhou University of Chinese
Medicine, China
Subhendu Ghosh,
University of Delhi, India

*CORRESPONDENCE

Mark T. Quinn,
mquinn@montana.edu
Matthew J. Cook,
matthew.cook6@montana.edu

SPECIALTY SECTION

This article was submitted to
Inflammation Pharmacology,
a section of the journal
Frontiers in Pharmacology

RECEIVED 31 May 2022

ACCEPTED 22 August 2022

PUBLISHED 12 September 2022

CITATION

Schepetkin IA, Kovrizhina AR,
Stankevich KS, Khlebnikov AI,
Kirpotina LN, Quinn MT and Cook MJ
(2022), Design, synthesis and biological
evaluation of novel O-substituted
tryptanthrin oxime derivatives as c-Jun
N-terminal kinase inhibitors.
Front. Pharmacol. 13:958687.
doi: 10.3389/fphar.2022.958687

COPYRIGHT

© 2022 Schepetkin, Kovrizhina,
Stankevich, Khlebnikov, Kirpotina,
Quinn and Cook. This is an open-access
article distributed under the terms of the
[Creative Commons Attribution License](#)
(CC BY). The use, distribution or
reproduction in other forums is
permitted, provided the original
author(s) and the copyright owner(s) are
credited and that the original
publication in this journal is cited, in
accordance with accepted academic
practice. No use, distribution or
reproduction is permitted which does
not comply with these terms.

Design, synthesis and biological evaluation of novel O-substituted tryptanthrin oxime derivatives as c-Jun N-terminal kinase inhibitors

Igor A. Schepetkin¹, Anastasia R. Kovrizhina²,
Ksenia S. Stankevich³, Andrei I. Khlebnikov², Liliya N. Kirpotina¹,
Mark T. Quinn^{1*} and Matthew J. Cook^{3*}

¹Department of Microbiology and Cell Biology, Montana State University, Bozeman, MT, United States,
²Kizhner Research Center, Tomsk Polytechnic University, Tomsk, Russia, ³Department of Chemistry
and Biochemistry, Montana State University, Bozeman, MT, United States

The c-Jun N-terminal kinase (JNK) family includes three proteins (JNK1-3) that regulate many physiological processes, including inflammatory responses, morphogenesis, cell proliferation, differentiation, survival, and cell death. Therefore, JNK represents an attractive target for therapeutic intervention. Herein, a panel of novel tryptanthrin oxime analogs were synthesized and evaluated for JNK1-3 binding (K_d) and inhibition of cellular inflammatory responses (IC_{50}). Several compounds exhibited submicromolar JNK binding affinity, with the most potent inhibitor being 6-(acetoxymino)indolo[2,1-*b*]quinazolin-12(6*H*)-one (**1j**), which demonstrated high JNK1-3 binding affinity (K_d = 340, 490, and 180 nM for JNK1, JNK2, and JNK3, respectively) and inhibited lipopolysaccharide (LPS)-induced nuclear factor- κ B/activating protein 1 (NF- κ B/AP-1) transcription activity in THP-1Blue cells and interleukin-6 (IL-6) production in MonoMac-6 monocytic cells (IC_{50} = 0.8 and 1.7 μ M, respectively). Compound **1j** also inhibited LPS-induced production of several other proinflammatory cytokines, including IL-1 α , IL-1 β , granulocyte-macrophage colony-stimulating factor (GM-CSF), monocyte chemoattractant protein-1 (MCP-1), and tumor necrosis factor (TNF) in MonoMac-6 cells. Likewise, **1j** inhibited LPS-induced c-Jun phosphorylation in MonoMac-6 cells, directly confirming JNK inhibition. Molecular modeling suggested modes of binding interaction of selected compounds in the JNK3 catalytic site that were in agreement with the experimental JNK3 binding data. Our results demonstrate the potential for developing anti-inflammatory drugs based on these nitrogen-containing heterocyclic systems.

KEYWORDS

anti-inflammatory, 11H-indeno[1,2-*b*]quinoxalin-11-one, interleukin-6, c-Jun N-terminal kinase, nuclear factor- κ B, oxime, tryptanthrin

1 Introduction

c-Jun N-terminal kinases (JNKs) are members of the mitogen-activated protein kinase (MAPK) family and mediate eukaryotic cell responses to abiotic and biotic stress (Kyriakis et al., 1994). The JNK pathway is a highly complex cassette within the MAPK signaling network (Johnson and Lapadat, 2002). JNK activation can be induced by other MAPKs, as well as G protein-coupled receptors (GPCRs), which feed information into the JNK signaling pathway. Moreover, it has been demonstrated that JNKs can undergo significant autophosphorylation (Vogel et al., 2009; Wang et al., 2020). Despite the name, activated JNKs can phosphorylate an number of proteins in addition to *c-Jun*, with close to 100 protein substrates known to date (Hammouda et al., 2020). Specific JNK3 substrates have also been identified, including voltage-dependent anion channel (VDAC) (Gupta and Ghosh, 2015; Gupta, 2017; Gupta and Ghosh, 2017). Nevertheless, *c-Jun* is a major substrate for JNKs, and its phosphorylation is closely tied to activator protein 1 (AP-1) activation.

The human genome contains three closely related genes (JNK1, JNK2, and JNK3), with each gene encoding multiple isoforms (Ha et al., 2019). JNK1 and JNK2 are expressed in a wide variety of tissues throughout the body, whereas JNK3 is mainly expressed in neurons and to a lesser extent in the heart and testes (Bode and Dong, 2007). Although the structure and sequences of all JNKs are similar, containing well conserved features observed in other MAPKs, JNK1 and JNK3 closely resemble each other, with JNK2 containing sequence differences in the kinase domain (Gupta et al., 1996). Despite the multifaceted role of JNKs in cell signaling, JNK has still been viewed as a promising target for several disease areas (Lai et al., 2020; Yung and Giacca, 2020; Abdelrahman et al., 2021). Our interest comes from its role in mediating inflammatory and immunological responses (Lai et al., 2020; Chen et al., 2021). Indeed, JNK inhibition has been demonstrated to downregulate the production of several proinflammatory transcription factors and cytokines (Kaminska et al., 2009; Lai et al., 2020). Due to the physiological isoform distribution within the body, therapeutic selectivity between the JNK isoforms could have major therapeutic benefits. JNK1/2 are attractive targets for treating

chronic inflammatory diseases, such as rheumatoid arthritis, whereas JNK3 could be a promising target for treating neuroinflammation (Mehan et al., 2011; Kersting et al., 2013; Cubero et al., 2015).

Due to the potential clinical significance of the JNKs, many groups have sought to develop inhibitors for these targets (Gehringer et al., 2015; Cho and Hah, 2021). The first potent inhibitor reported was SP600125 (Figure 1), which exhibited pan-JNK activity but also inhibited numerous other MAPKs (Bennett et al., 2001). We examined other heterocyclic structures and found that derivatives of indeno[1,2-*b*]quinoxalinone oxime (IQ-1) were both potent and selective (Figure 1) (Schepetkin et al., 2012; Schepetkin et al., 2019). Indeed, these IQ-1 derivatives were equipotent with SP600125 and had much higher selectivity profiles, with significant binding only seen at CK1 δ and JNK1-3 when tested against a panel of kinases (Schepetkin et al., 2012; Schepetkin et al., 2019). Additionally, these compounds were shown to downregulate proinflammatory responses in human monocytic cell lines and in animal models (Schepetkin et al., 2012; Schepetkin et al., 2015; Schepetkin et al., 2019; Kirpotina et al., 2020; Seledtsov et al., 2020). More recently, we discovered that other planar heterocyclic core structures could provide similar and complementary activity, with oxime derivatives of the natural product tryptanthrin (TRYP-Ox) proving especially effective (Schepetkin et al., 2019; Kirpotina et al., 2020). Herein, we report our investigation of the effect that chemical modification of the oxime group has on the biological activity of the TRYP-Ox scaffold. The premise of this study was to determine the role of the oxime functionality in enzymatic binding, cellular mediation of inflammatory responses, and phosphorylation of *c-Jun*.

2 Results and discussion

2.1 Chemistry

Our previous studies on indenoquinoxaline and tryptanthrin structures demonstrated that the oxime was crucial for JNK inhibition (Schepetkin et al., 2012; Schepetkin et al., 2019). We therefore examined the effect that substitution of the oxime OH

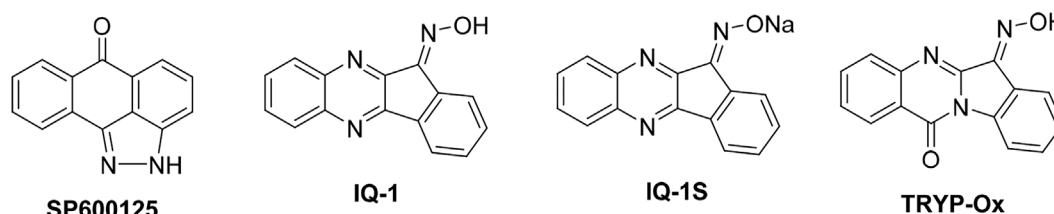
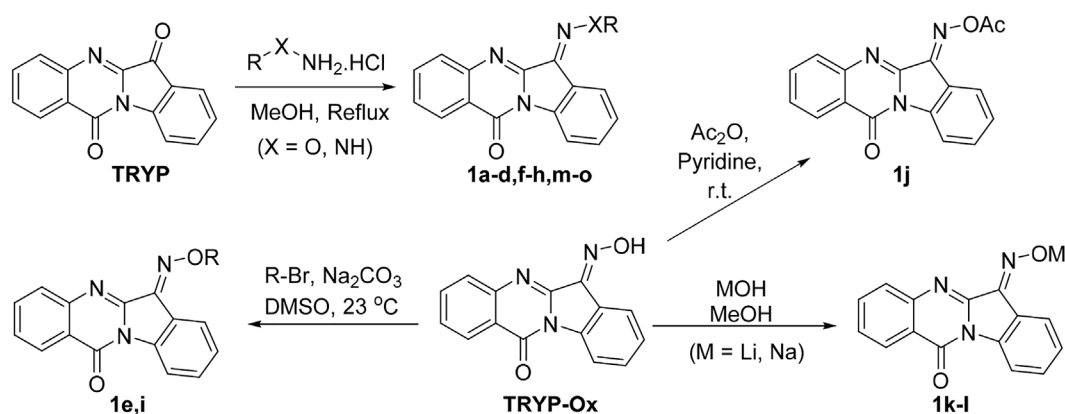


FIGURE 1
Chemical structures of several JNK inhibitors.



SCHEME 1
Synthetic routes to tryptanthrin derivatives.

had on JNK inhibitory activity. To accomplish this, we synthesized a range of tryptanthrin derivatives where the oxime group was replaced (**1a-o**). The synthesis of these compounds was achieved from tryptanthrin (TRYP) or the previously reported TRYP-Ox (Scheme 1). Substituted oximes and hydrazones were synthesized through direct condensation of the corresponding hydroxylamine ether, hydrazine, or semicarbazide with TRYP. Alternatively, TRYP-Ox could undergo base-mediated alkylation or acylation to provide the O-alkyl and O-acyl derivatives. Lithium and sodium salts were obtained through treatment with LiOH and NaOH, respectively. All compounds were obtained as mixtures of *E/Z* isomers; however, the interconversion of (*E/Z*) oximes and oxime ethers in solution is well established (Diethelm-Varela et al., 2021).

2.2 Evaluation of compound biological activity

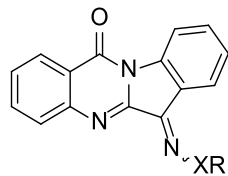
Prior to evaluation in both enzymatic and cellular assays, we measured the cytotoxicity of compounds **1a-o** in human monocytic THP-1Blue and MonoMac-6 cells following a 24 h incubation. All compounds reported in this study had no effect on cell viability at concentrations up to 50 μ M (data not shown), which is similar to the lack of toxicity observed for the parent compounds (Schepetkin et al., 2019; Kirpotina et al., 2020). The compounds were evaluated for their ability to bind to JNK1-3 and compared with previously reported TRYP-Ox, a JNK inhibitor (Schepetkin et al., 2019). We used the KINOMEScan ATP site-dependent binding assay, which reflects biologically relevant behavior of the kinases (Fabian et al., 2005; Karaman et al., 2008). The JNK pathway can be activated through Toll-like receptor 4 (TLR4), leading to the activation of transcription

factors NF- κ B and AP-1 [reviewed in (Aggarwal, 2000; Guha and Mackman, 2001; Takeuchi and Akira, 2001)]. Thus, to assess the anti-inflammatory activity of test derivatives, compounds **1a-o** were also evaluated for their ability to inhibit lipopolysaccharide (LPS)-induced NF- κ B/AP-1 reporter activity and IL-6 production in THP-1Blue and MonoMac-6 cells, respectively (Schepetkin et al., 2012).

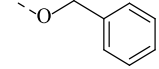
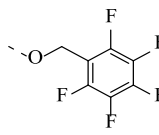
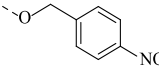
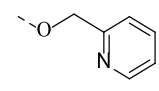
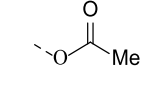
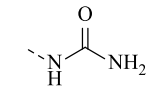
In particular, O-alkyl substituted oximes had little to no JNK binding affinity and did not inhibit cellular anti-inflammatory responses. O-Acyl groups, however, provided very similar JNK binding affinities to the parent oxime, with increased cellular anti-inflammatory activity. This suggested that the ester C-O bond was cleaved in both assays with substitution increasing cellular uptake. The aim of this study was to investigate the effect oxime group modification of the tryptanthrin oxime scaffold had on both JNK binding and cellular activity. Importantly, these results will help determine whether the two structures share a common binding epitope and what, if any, key differences in structure-activity relationship (SAR) exist between the two series.

Our baseline for biological activity was the unsubstituted oxime (TRYP-Ox), which exhibited pan-JNK binding with JNK-1/3 selectivity over JNK-2. Additionally, TRYP-Ox inhibited cytokine production in LPS-stimulated THP-1Blue and MonoMac-6 cells with IC_{50} values of 3.8 and 3.2 μ M, respectively (Schepetkin et al., 2019). Upon O-alkylation, the biological profile of these molecules changed, with increased JNK-3 selectivity, albeit with decreased binding affinity. Simple alkyl groups (**1a-d**) gave moderate JNK-3 selectivity with 2-4-fold higher binding over JNK-1 and 4-6-fold over JNK-2 (Table 1). Additionally, these compounds were poorly active (or inactive) in the cellular assay, suggesting poor cellular uptake and/or microsomal instability within the cells. This selectivity trend is even more pronounced in methylene nitrile ether **1e**, which

TABLE 1 Binding affinity (K_d) of compounds 1a-o and their inhibitory effect on LPS-induced NF- κ B/AP-1 transcriptional activity in THP-1Blue cells and IL-6 production in MonoMac-6 cells.



TRYP-Ox, 1a-1p

Compd.	XR	Binding affinity			THP-1Blue NF- κ B/AP-1	MonoMac-6 IL-6 production
		JNK1	JNK2	JNK3		
	K_d (μ M)			IC_{50} (μ M)		
TRYP-Ox ^a	-OH	0.15 \pm 0.081 ^a	1.0 \pm 0.14 ^a	0.275 \pm 0.21 ^a	3.8 \pm 1.1 ^a	3.2 \pm 1.2 ^a
1a	-OCH ₃	3.1 \pm 0.8	5.6 \pm 0.4	1.4 \pm 0.2	20.8 \pm 5.3	23.5 \pm 1.8
1b	-OC ₂ H ₅	3.2 \pm 1.2	5.4 \pm 0.6	1.2 \pm 0.4	N.A.	N.A.
1c	-OCH ₂ CH=CH ₂	3.6 \pm 0.7	4.1 \pm 0.1	0.85 \pm 0.01	18.9 \pm 1.8	N.A.
1d	-OC(CH ₃) ₃	9.3 \pm 0.5	12.0 \pm 1.4	2.3 \pm 0.3	N.A.	N.A.
1e	OCH ₂ CN	19.5 \pm 3.5	17.5 \pm 2.1	1.5 \pm 0.6	N.A.	N.A.
1f		n.d.	n.d.	N.B.	N.A.	N.A.
1g		n.d.	n.d.	N.B.	N.A.	N.A.
1h		Poor solubility ^b			N.A.	N.A.
1i		4.0 \pm 0.9	3.9 \pm 0.4	1.5 \pm 0.1	N.A.	N.A.
1j		0.34 \pm 0.04	0.49 \pm 0.01	0.18 \pm 0.04	0.8 \pm 0.2	1.7 \pm 0.1
1k	-OLi	0.47 \pm 0.03	0.62 \pm 0.035	0.17 \pm 0.03	0.9 \pm 0.1	1.1 \pm 0.2
1l	-ONa	0.44 \pm 0.07	0.58 \pm 0.014	0.22 \pm 0.04	0.9 \pm 0.2	1.8 \pm 0.2
1m	-NH ₂	Poor solubility ^b			N.A.	N.A.
1n	-NHPh	Poor solubility ^b			N.A.	N.A.
1o		0.47 \pm 0.03	0.62 \pm 0.035	0.17 \pm 0.03	3.3 \pm 0.1	6.6 \pm 1.2

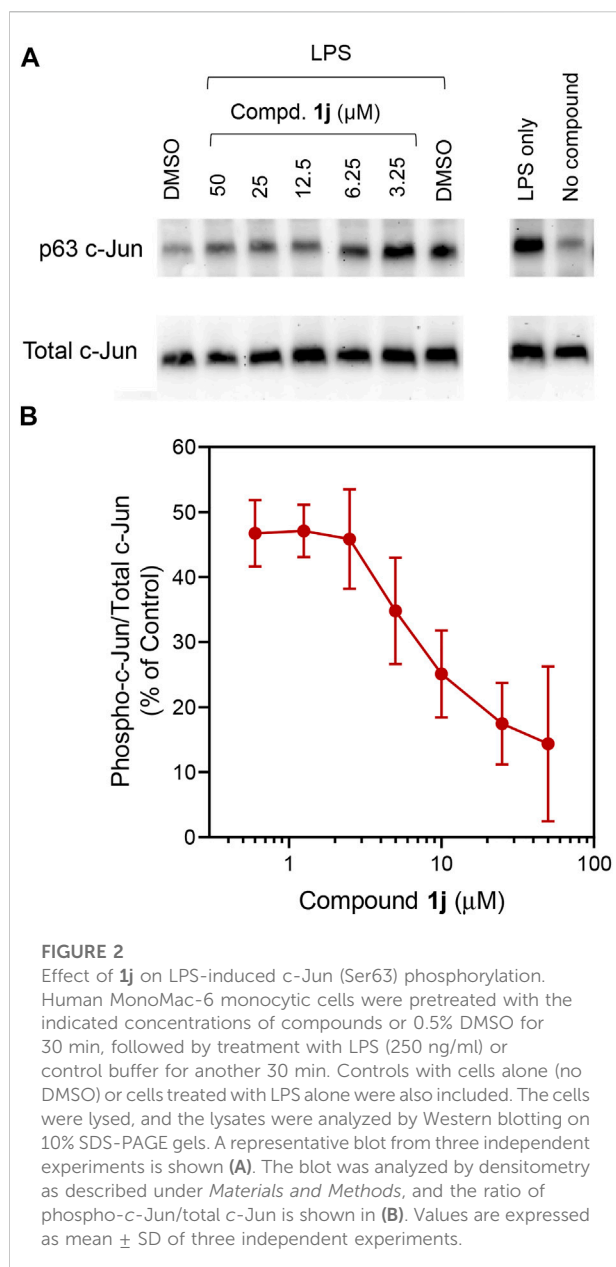
^aData for from (Schepetkin et al., 2019).

^bCompound was insufficiently soluble in dimethyl sulfoxide (DMSO) for the binding affinity assay.

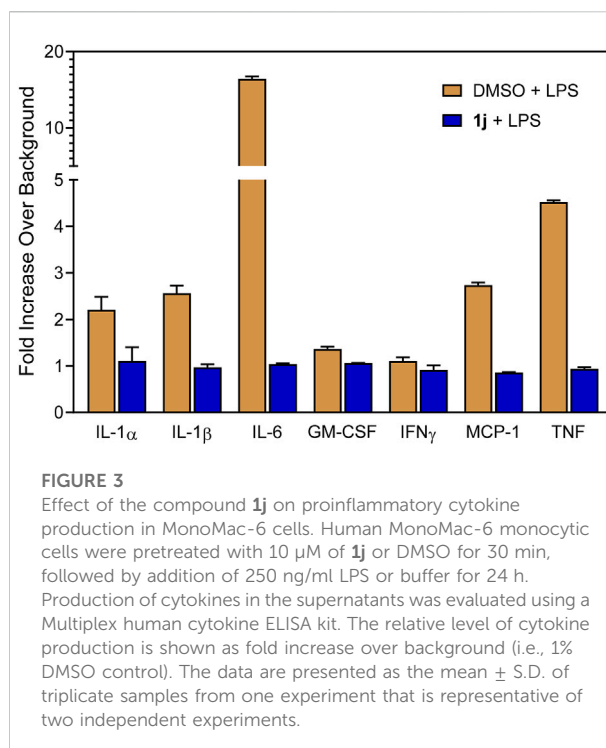
N.A., no inhibition at concentrations \leq 50 μ M; n.d., not determined; N.B., no JNK binding at concentrations \leq 30 μ M.

showed >10-fold discrimination for JNK-3 over JNK-1/2, again with no cellular activity. *O*-Benzyl oxime ethers (**1f-h**) were inactive, whereas 2-pyridyl ether (**1i**) exhibited moderate JNK activity and selectivity, demonstrating the tolerance of aromatic

groups when a basic group was present. Similarly to the **IQ-1** series (Schepetkin et al., 2012), acylated oxime (**1j**) provided comparable enzymatic activity to **TRYP-Ox** but with enhanced anti-inflammatory activity. Likewise, lithium and sodium oxime



salts (**1k,l**) gave similar profiles to **TRYP-Ox** but with more potent cellular function. The dichotomy between the enzymatic and cellular data for these three compounds (**2j-l**) compared to **TRYP-Ox** suggested that their increased solubility led to increased cellular uptake; however, the active ligand was still **TRYP-Ox**. Indeed, the measured pK_a range of diaryl oximes is 8–11, leading to rapid protonation in pH 7.4 buffer solution (Mangold et al., 1989). Hydrazone derivatives (**1m-n**) were poorly soluble and inactive in cellular assays. Semicarbazone variant (**1o**) had a much better solubility profile, exhibiting sub-micromolar binding affinities with all JNK isoforms tested and moderate inhibition of anti-inflammatory activity.



When comparing the enzymatic and cellular data from the **TRYP-Ox** series to the **IQ-1** series (Schepetkin et al., 2012), there was a clear difference. Specifically, O-substitution was much better tolerated in the tryptanthrin analogs, with alkyl groups still providing moderate JNK-binding and selectivity, although aromatic substituted alkyl groups were inactive in the absence of a basic group. The effect of acetyl substitution (**1j**) and deprotonation (**1k,j**) mirrored that of **IQ-1** and **IQ-1S**, with similar levels of binding affinity and higher efficacy in the cellular assays (Mangold et al., 1989; Schepetkin et al., 2012). This similar trend further supports the hypothesis that the increased cellular activity is due to higher solubility and/or cellular permeability.

In order to probe whether the increased anti-inflammatory activity observed for **1j** was a result of JNK inhibition, we evaluated its effect on c-Jun phosphorylation in MonoMac-6 monocytic cells. These cells were pretreated with the compounds, stimulated with LPS (250 ng/ml), and the level of phospho-c-Jun (S63) was determined (Figure 2A). Although phosphorylation can occur at S63/73 and T91/93 (Morton et al., 2003; Vinciguerra et al., 2008; Madeo et al., 2010), S63 activation occurs in all cases. Therefore, anti-phosphoS63 antibody was selected and benchmarked against total c-Jun. Indeed, we saw a dose-dependent inhibition of phosphorylation (Figure 2B) similar to our previous studies with **TRYP-Ox** (Schepetkin et al., 2019), providing further evidence for the increased cell permeability and conversion to **TRYP-Ox**. The effect that compound **1j** had on production of proinflammatory cytokines was investigated using a Multiplex human cytokine

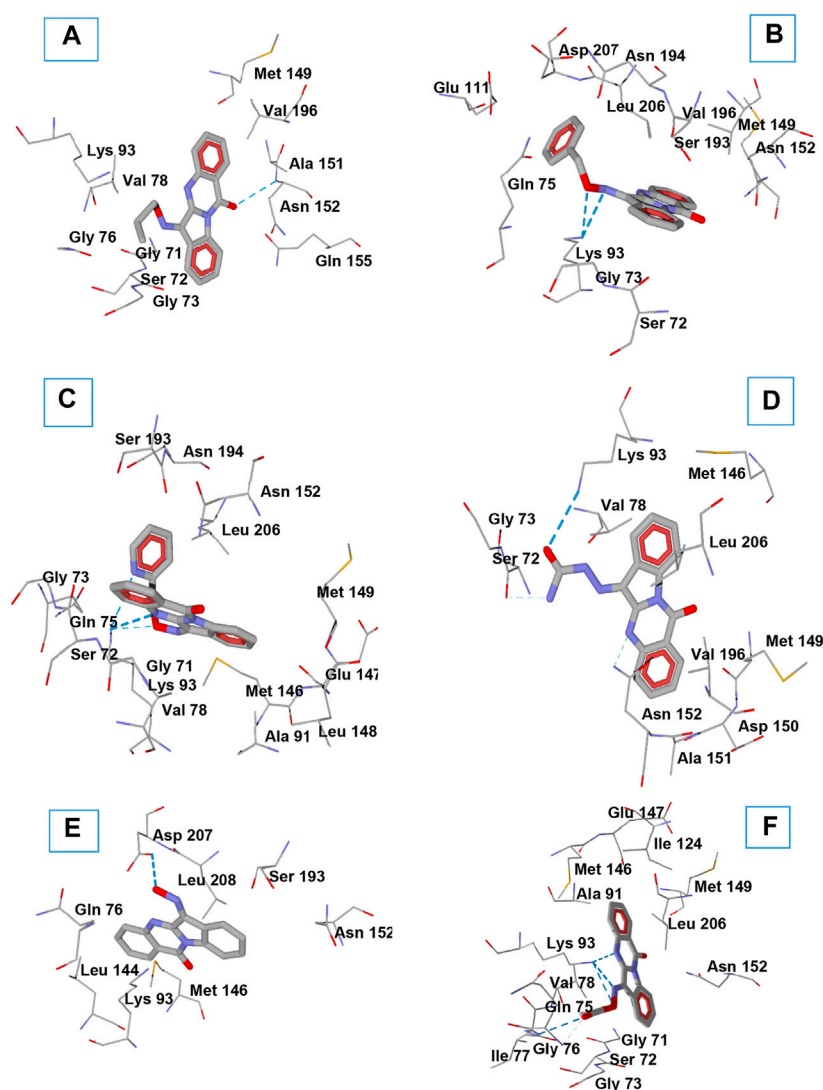


FIGURE 4

Docking poses of compounds **1c** (A), **1f** (B), **1i** (C), **1o** (D), **TRYP-Ox** (E), and **1j** (F) in JNK3 (PDB code 1PMV). H-bonds are shown in blue dashed lines. Residues within 3 Å of each pose are visible.

ELISA kit against seven different cytokines and chemokines. Compound **1j**, at a concentration of 10 μ M, completely inhibited the secretion of IL-1 α , IL-1 β , IL-6, tumor necrosis factor (TNF), monocyte chemoattractant protein-1 (MCP-1), and granulocyte-macrophage colony-stimulating factor (GM-CSF) in LPS-stimulated MonoMac-6 cells compared with dimethyl sulfoxide (DMSO)-treated control cells. The effect on interferon- γ (IFN- γ) production was inconclusive because of low production of this cytokine after LPS treatment of MonoMac-6 cells (Figure 3). These data further demonstrate the anti-inflammatory activity of **1j**.

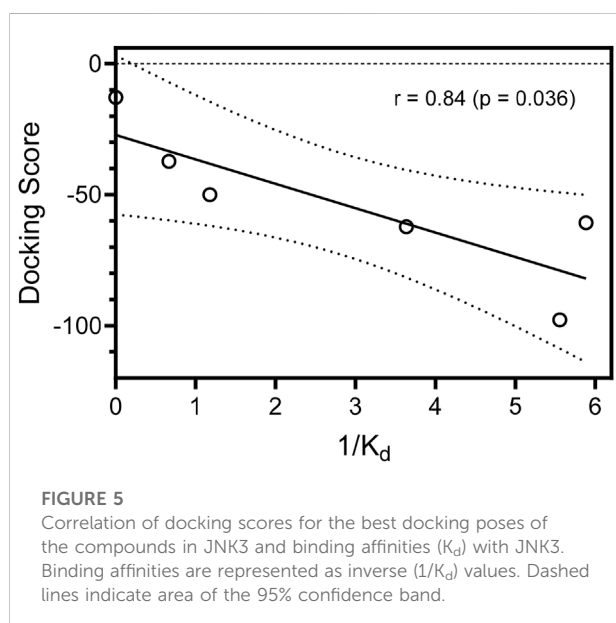
2.3 Molecular modeling

In order to gain insight into interactions of the investigated compounds and explain some observations made in structure-activity relationship analysis, we performed molecular docking of **TRYP-Ox** (Schepetkin et al., 2019), **1c**, **1f**, **1i**, **1j**, and **1o** into the JNK3 binding site (PDB: 1PMV) using Molegro Virtual Docker (MVD) software. Note that these compounds exist as mixtures of *Z* and *E* isomers with respect to the exocyclic C=N bond. These geometric isomers are prone to interconversion (Dugave and Demange, 2003; Blanco et al., 2009). Therefore, we obtained

TABLE 2 MVD docking scores (DS) for the best docking poses, absolute differences Δ DS between *Z* and *E* isomers, and key interactions with the binding site of JNK3 (PDB: 1PMV) for compounds 1c, 1f, 1i, 1o, 1j, and TRYP-Ox.

Compd.	JNK3 K_d (μ M) ^a	DS (units)	Δ DS (units)	Characteristics of binding to JNK3
<i>Z</i> 1c	0.85 \pm 0.01	−50.03	4.39	HB: Asn152 (amide oxygen) VdW: Ile70 (pDS = −14.56)
<i>E</i> 1f	N.B.	−12.85	44.99	HB: Lys93 (oxime oxygen and nitrogen atoms) VdW: Leu206 (pDS = −13.66)
<i>Z</i> 1i	1.5 \pm 0.1	−37.26	31.63	HB: Lys93 (oxime oxygen, weak; nitrogen atoms in pyridine and tryptanthrin moieties) VdW: Val78 (pDS = −14.54)
<i>E</i> 1j	0.18 \pm 0.04	−97.78	24.33	HB: Lys93 (heterocycle nitrogen, oxime nitrogen and oxygen); Gly76 (acetyl oxygen); Gln75 (acetyl oxygen, weak) VdW: Val78 (pDS = −17.36)
<i>E</i> -1o	0.17 \pm 0.03	−60.71	9.01	HB: Lys93 (semicarbazone oxygen); Ser72 (semicarbazone NH ₂ , weak); Asn152 (heterocycle nitrogen, weak) VdW: Val78 (pDS = −12.46)
<i>Z</i> TRYP-Ox	0.275 \pm 0.21	−62.22	27.90	HB: Asp207 (OH group) VdW: Leu206 (pDS = −15.51)

^aBinding affinity measured on a mixture of isomers. N.B., no JNK binding at concentrations \leq 30 μ M. HB, hydrogen bond; VdW, strong van der Waals interaction; pDS, partial docking score for van der Waals interaction.



docking poses for both *Z* and *E* isomers. The best docking poses are shown in Figure 4, and key interactions of the compounds with the kinase residues are presented in Table 2.

The MolDock docking scores (DS) differ by 4.4–45 units between the isomeric oxime structures. For compounds 1f, 1j, and 1o bound to JNK3, the lower (more negative) DS corresponds to the *E* isomer, while in the other cases, compounds bound to the kinase binding site preferably in the *Z* isomer form. We benchmarked our docking scores against measured binding affinities with JNK3 and found a significant

correlation ($r = 0.84$; $p = 0.036$) between experimentally and computationally derived data (Figure 5).

O-Substitution of TRYP-Ox with an allyl group (1c) led to a docking pose with a H-bonding interaction of the ligand with JNK3 via the amide carbonyl group of the tryptanthrin fragment with the allyl moiety located in a hydrophobic region (Figure 4A). This hydrophobic pocket can accommodate small linear alkyl groups (1a–c) with similar efficiency; however, benzyl groups (1f) were too large, leading to a change in binding pose and loss of binding affinity. Interestingly, the isosteric (2-pyridyl)methyl group (1i) exhibited modest binding to JNK3, and the docking results indicated H-bonding between Lys93 and the pyridyl nitrogen (Figure 4C). Introducing a semicarbazone fragment to the oxime group of TRYP-Ox brings additional H-bond donors and acceptors into molecule 1o. On the interaction with JNK3, this fragment was H-bonded to Lys93 via the semicarbazone oxygen atom. Additionally, weak H-bonds to Ser72 and Asn152 were formed, with participation of the NH₂ group and heterocyclic nitrogen atom (Figure 4D). These interactions, along with a noticeable van der Waals attraction between the ligand and Val78 (Table 2), led to an increased affinity with JNK3 (Table 1). Of note, these additional polar interactions, which led to the increased binding of compound 1o, resulted in a different pose to that of the unsubstituted oxime TRYP-Ox (Figure 4E). The most negative DS value corresponded to compound 1j, which is anchored within the binding site by several H-bonds (Figure 4F).

JNKs are directly involved in controlling regulation of NF- κ B/AP-1 transcriptional activity; therefore, drug discovery efforts have focused on the development of JNK inhibitors for treatment of inflammatory diseases (Bennett et al., 2003; Wagner and

Laufer, 2006; Jung et al., 2010). One of the targets of activated JNKs is c-Jun, which is specifically phosphorylated on Ser63 and/or Ser73, making this protein capable of binding AP-1 sites in the nucleus (Hibi et al., 1993). Although AP-1 and NF- κ B are regulated by different signaling pathways, cross-talk between these pathways occurs, mediated in part by the ability of certain Jun and Fos family proteins to interact with the p65 subunit of NF- κ B (Fujioka et al., 2004). Here, we report novel and potent JNK inhibitors with a tryptanthrin scaffold that had high JNK1-3 binding affinity and inhibited LPS-induced NF- κ B/AP-1 transcription activity in THP-1Blue cells and IL-6 production in MonoMac-6 cells. The present work supports our previous studies suggesting that tryptanthrin is a good scaffold for the development JNK inhibitors (Schepetkin et al., 2012; Schepetkin et al., 2015). The tryptanthrin molecule has a rigid flat aromatic ring structure. Other tri- and tetracyclic planar fragments have also been reported as kinase inhibitor scaffolds for Aurora A kinase (Warner et al., 2006) and JNK (Bennett et al., 2001). In general, flat ring structures have been identified as kinase-specific privileged structures; i.e., compounds containing these fragments are enriched for kinase targets, compared with other target classes (Posy et al., 2011). Thus, although oxime side groups may contribute important interactions in the JNK binding site (Schepetkin et al., 2012; Schepetkin et al., 2015; Schepetkin et al., 2019; Liakhov et al., 2021; Schepetkin et al., 2021), the tetracyclic nucleus seems to be responsible for proper ligand positioning. Docking experiments performed in the present study and in our previous work (Schepetkin et al., 2019) show that the tryptanthrin nucleus stipulates good complementarity of the ligands to the JNK1-3 binding sites with similar orientations of the tetracyclic moiety. Comparison of docking poses of the most potent JNK inhibitors (**TRYP-Ox**, **1j**, **1o**) with the published coordinates of ATP (Xie et al., 1998) showed that the oxime moiety of the compounds is positioned in an orientation similar to that of the ATP purine base, which is anchored deep in the ATP-binding site among Gly71, Ser72, Gly73, Gln75, Val78, Lys93, Leu148, Met149, Asp150, Ala151, Asn152, Ser193, Asn194, Ile195, Val196, Leu206, and Asp207.

3 Conclusion

In summary, fifteen novel analogs of **TRYP-Ox** were synthesized and characterized. The reactions of ketone oximation and oxime alkylation were investigated based on this heterocyclic system. Compounds **1j**, **k**, **l** had high affinity for JNK1-3 ($K_d < 1 \mu\text{M}$) and also potently inhibited LPS-induced nuclear NF- κ B/AP-1 activation and IL-6 production in human monocytic cells. Our molecular modeling showed that compounds **1c**, **1i**, and **TRYP-Ox** bound to JNK3, preferably as *Z* isomers, while for **1f**, **1j**, and **1o**, the docking poses of *E* isomers were characterized by more negative docking scores. Differences

in the JNK3 binding affinities of **TRYP-Ox** and its derivatives can be well explained by H-bonding patterns of the ligands and magnitudes of their docking scores.

4 Experimental section

4.1 Chemistry

Tryptanthrin was purchased from Combi-Blocks (San Diego, CA, United States). All the other starting reagents were purchased from Sigma-Aldrich. The chemicals were of analytical grade and used without further purification. Reaction progress was monitored by thin-layer chromatography (TLC) with UV detection using pre-coated silica gel F254 (Merck). Melting points (m.p.) were determined using an electrothermal Mel-Temp capillary melting point apparatus. HPLC-MS analysis was performed on a Zorbax Eclipse Plus C18 2.1 mm \times 50 mm 1.8 micron. Elemental analysis was performed with a Carlo Erba instrument. IR spectra were recorded on a FT-IR spectrometer Nicolet 5700 with KBr pellets. NMR spectra were recorded on a Bruker Avance III HD instrument (operating frequency ^1H -400 MHz; ^{13}C -100 MHz). Purity of the compounds, according to the NMR data, were at least 98%.

4.1.1 General procedure of the tryptanthrin oximation by O-alkyl-hydroxylamine hydrochlorides and hydrazines

A mixture of tryptanthrin (**TRYP**) (0.5 mmol) and substituted hydroxylamine or hydrazine (0.7 mmol) in MeOH (10 ml) were refluxed for 3–8 h and monitored by TLC. The mixture was then cooled and poured into water (100 ml). The resulting precipitate was filtered, washed with water, and recrystallized from EtOH to give **1a-d**, **f-h**, **m-o** as colorless or flaxen solids.

4.1.2 General procedure of alkylation of tryptanthrin oximes

Compounds **1e** and **1i** were synthesized as described previously (Schepetkin et al., 2019). To a suspension of **TRYP-Ox** (1.0 mmol) and Na_2CO_3 (0.127 g, 1.2 mmol) in DMSO (5 ml), was added dropwise a solution of alkyl bromide (1.5 mmol) in DMSO (5 ml). The mixture was stirred overnight at room temperature and poured into 200 ml of water. The resulting precipitate was filtered and recrystallized from EtOH.

4.1.3 General procedure for the synthesis of TRYP-Ox salts (**1k** and **1l**)

Compounds **1k** and **1l** were prepared from **TRYP-Ox** (0.263 g, 1.0 mmol) by treatment with an excess of corresponding LiOH (36 mg, 1.5 mmol) or NaOH (60 mg,

1.5 mmol) in refluxing MeOH (10 ml) for 3 h (TLC monitoring). After cooling the precipitate was filtered and recrystallized from EtOH.

4.1.3.1 6-(methoxyimino)indolo[2,1-b]quinazolin-12(6H)-one (1a)

Yield 73%, a flaxen solid. M.p. 218°C. ¹H NMR (CDCl₃), δ, ppm: 8.64 (1H, d, *J* = 8.1 Hz), 8.41 (1H, dd, *J* = 8.0, 1.6 Hz), 8.28 (1H, d, *J* = 7.6 Hz), 7.96 (1H, dd, *J* = 8.1, 1.2 Hz), 7.79 (1H, ddd, *J* = 8.3, 7.2, 1.6 Hz), 7.59 (1H, td, *J* = 8.0, 1.2 Hz), 7.55 (1H, ddd, *J* = 8.0, 7.5, 1.1 Hz), 7.37 (1H, td, *J* = 7.7, 1.1 Hz), 4.41 (3H, s). ¹³C NMR (CDCl₃), δ, ppm: 159.2, 148.1, 147.2, 144.7, 140.2, 134.8, 133.1, 129.0, 128.3, 128.1, 127.2, 126.9, 122.2, 119.0, 117.3, 65.2. Found, %: C 69.60, H 3.97, N 15.30. C₁₆H₁₁N₃O₂. Calculated, %: C 69.31, H 4.00, N 15.15. HRMS (ESI-TOF) *m/z*: [M + H]⁺ Calcd. for C₁₆H₁₂N₃O₂ 278.0930, found 278.0919.

4.1.3.2 6-(ethoxyimino)indolo[2,1-b]quinazolin-12(6H)-one (1b)

Yield 89%, a flaxen solid. M.p. 117°C. ¹H NMR (CDCl₃), δ, ppm: 8.65 (1H, d, *J* = 8.1 Hz), 8.41 (1H, dd, *J* = 8.0, 1.6 Hz), 8.30 (1H, d, *J* = 7.7 Hz), 7.96 (1H, dd, *J* = 8.2, 1.2 Hz), 7.79 (1H, ddd, *J* = 8.3, 7.1, 1.6 Hz), 7.58 (1H, td, *J* = 8.0, 1.2 Hz), 7.55 (1H, ddd, *J* = 8.1, 7.0, 1.3 Hz), 7.37 (1H, td, *J* = 7.7, 1.0 Hz), 4.68 (2H, q, *J* = 7.1 Hz), 1.52 (3H, t, *J* = 7.1 Hz). ¹³C NMR (CDCl₃), δ, ppm: 159.3, 148.2, 147.3, 144.5, 140.1, 134.7, 132.9, 129.0, 128.2, 128.0, 127.2, 126.9, 122.1, 119.1, 117.2, 73.5, 14.9. Found, %: C 70.33, H 4.31, N 14.62. C₁₇H₁₃N₃O₂. Calculated, %: C 70.09, H 4.50, N 14.42. HRMS (ESI-TOF) *m/z*: [M + H]⁺ Calcd. for C₁₇H₁₄N₃O₂ 292.1086, found 292.1079.

4.1.3.3 6-((allyloxy)imino)indolo[2,1-b]quinazolin-12(6H)-one (1c)

Yield 86%, a flaxen solid. M.p. 163°C. ¹H NMR (CDCl₃), δ, ppm: 8.65 (1H, d, *J* = 8.1 Hz), 8.42 (1H, dd, *J* = 7.9, 1.6 Hz), 8.31 (1H, d, *J* = 7.7 Hz), 7.96 (1H, d, *J* = 7.8 Hz), 7.80 (1H, ddd, *J* = 8.4, 7.2, 1.6 Hz), 7.60 (1H, td, *J* = 7.9, 1.3 Hz), 7.56 (1H, ddd, *J* = 8.1, 7.0, 1.0 Hz), 7.38 (1H, td, *J* = 7.7, 1.1 Hz), 6.18 (1H, ddt, *J* = 17.2, 10.4, 5.9 Hz), 5.48 (1H, dd, *J* = 17.2, 1.5 Hz), 5.38 (1H, dd, *J* = 10.5, 1.3 Hz), 5.12 (2H, d, *J* = 5.9 Hz). ¹³C NMR (CDCl₃), δ, ppm: 159.2, 148.1, 147.3, 145.0, 140.2, 134.8, 133.1, 132.8, 129.0, 128.4, 128.1, 127.2, 127.0, 122.2, 119.5, 119.1, 117.3, 76.8. Found, %: C 71.56, H 4.19, N 14.02. C₁₈H₁₃N₃O₂. Calculated, %: C 71.28, H 4.32, N 13.85. HRMS (ESI-TOF) *m/z*: [M + H]⁺ Calcd. for C₁₈H₁₄N₃O₂ 304.1086, found 304.1086.

4.1.3.4 6-(tert-butoxyimino)indolo[2,1-b]quinazolin-12(6H)-one (1d)

Yield 50%, a flaxen solid. M.p. 229°C. *E*-isomer: ¹H NMR (CDCl₃), δ, ppm: 8.67 (1H, d, *J* = 8.1 Hz), 8.42 (1H, dd, *J* = 8.0, 1.6 Hz), 8.33 (1H, d, *J* = 7.6 Hz), 7.95 (1H, d, *J* = 8.1 Hz), 7.79 (1H, ddd, *J* = 8.3, 7.2, 1.6 Hz), 7.58 (1H, td, *J* = 8.0, 1.1 Hz), 7.57–7.52 (1H, m), 7.38 (1H, t, *J* = 7.9 Hz), 1.59 (s, 9H). ¹³C NMR (CDCl₃),

δ, ppm: 159.4, 148.4, 147.5, 144.0, 139.9, 134.6, 132.5, 128.9, 128.1, 127.8, 127.2, 126.8, 122.0, 119.5, 117.2, 83.8, 27.9. *Z*-isomer: ¹H NMR (CDCl₃), δ, ppm: 8.67 (1H, d, *J* = 8.1 Hz), 8.42 (1H, dd, *J* = 8.0, 1.6 Hz), 8.33 (1H, d, *J* = 7.6 Hz), 7.95 (1H, d, *J* = 8.1 Hz), 7.79 (1H, ddd, *J* = 8.3, 7.2, 1.6 Hz), 7.58 (1H, td, *J* = 8.0, 1.1 Hz), 7.57–7.52 (1H, m), 7.38 (1H, t, *J* = 7.9 Hz), 1.70 (s, 9H). ¹³C NMR (CDCl₃), δ, ppm: 159.4, 148.4, 147.5, 144.0, 139.9, 134.4, 131.1, 128.5, 128.1, 127.7, 127.0, 126.8, 122.0, 119.5, 117.3, 83.8, 27.64. Found, %: C 71.68, H 5.26, N 13.28. C₁₉H₁₇N₃O₂. Calculated, %: C 71.46, H 5.37, N 13.16. HRMS (ESI-TOF) *m/z*: [M + H]⁺ Calcd. for C₁₉H₁₈N₃O₂ 320.1399, found 320.1404.

4.1.3.5 2-(((12-oxoindolo[2,1-b]quinazolin-6(12H)-ylidene)amino)oxy)acetonitrile (1e)

Compound **2e** was synthesized according to the general procedure of alkylation from **TRYP-Ox** (0.263 g, 1.0 mmol) and 2-bromoacetonitrile (0.104 ml, 1.5 mmol). Yield 3% (10 mg), dark brown crystals. M.p. 224°C. ¹H NMR (CDCl₃), δ, ppm: 8.67 (1H, d, *J* = 8.1 Hz), 8.44 (1H, dd, *J* = 7.9, 1.5 Hz), 8.26 (1H, d, *J* = 7.7 Hz), 7.97 (1H, d, *J* = 7.8 Hz), 7.83 (1H, ddd, *J* = 8.3, 7.2, 1.5 Hz), 7.67 (1H, td, *J* = 7.8, 1.3 Hz), 7.61 (1H, ddd, *J* = 8.2, 7.2, 1.2 Hz), 7.41 (1H, ddd, *J* = 7.7, 7.7, 1.0 Hz), 5.24 (2H, s). ¹³C NMR (CDCl₃), δ, ppm: 158.9, 147.6, 146.8, 145.7, 140.9, 135.1, 134.4, 133.1, 129.7, 129.2, 128.8, 127.3, 127.1, 122.4, 118.3, 117.5, 61.4. HRMS (ESI-TOF) *m/z*: [M + H]⁺ Calcd. for C₁₇H₁₁N₄O₂ 303.0882, found 303.0885.

4.1.3.6 6-((benzyloxy)imino)indolo[2,1-b]quinazolin-12(6H)-one (1f)

Yield 96%, a flaxen solid. M.p. 206°C. *E*-isomer: ¹H NMR (CDCl₃), δ, ppm: 8.65 (1H, d, *J* = 8.1 Hz), 8.43 (1H, dd, *J* = 8.0, 1.6 Hz), 8.25 (1H, d, *J* = 8.1 Hz), 7.97 (1H, d, *J* = 7.8 Hz), 7.81 (1H, ddd, *J* = 8.5, 7.2, 1.5 Hz), 7.62–7.54 (2H, m), 7.51 (2H, d, *J* = 6.6 Hz), 7.46–7.38 (3H, m), 7.33 (1H, t, *J* = 7.7 Hz), 5.66 (2H, s). ¹³C NMR (CDCl₃), δ, ppm: 159.3, 148.2, 147.3, 145.1, 140.2, 136.1, 134.8, 133.2, 129.0, 128.9, 128.8, 128.7, 128.5, 128.1, 127.3, 127.0, 122.2, 119.1, 117.2, 76.8. *Z*-isomer: ¹H NMR (CDCl₃), δ, ppm: 8.58 (1H, d, *J* = 8.1 Hz), 8.43 (1H, dd, *J* = 8.0, 1.6 Hz), 8.25 (1H, d, *J* = 8.1 Hz), 7.94 (1H, d, *J* = 7.8 Hz), 7.81 (1H, ddd, *J* = 8.5, 7.2, 1.5 Hz), 7.62–7.54 (2H, m), 7.51 (2H, d, *J* = 6.6 Hz), 7.46–7.38 (3H, m), 7.33 (1H, t, *J* = 7.7 Hz), 5.62 (2H, s). Found, %: C 75.02, H 4.02, N 12.01. C₂₂H₁₅N₃O₂. Calculated, %: C 74.78, H 4.28, N 11.89. HRMS (ESI-TOF) *m/z*: [M + H]⁺ Calcd. for C₂₂H₁₆N₃O₂ 354.123, found 354.1257.

4.1.3.7 6-(((pentafluorophenyl)methoxy)imino)indolo[2,1-b]quinazolin-12(6H)-one (1g)

Yield 90%, a flaxen solid. M.p. 183°C. *E*-isomer: ¹H NMR (CDCl₃), δ, ppm: 8.63 (1H, d, *J* = 8.1 Hz), 8.41 (1H, dd, *J* = 8.0, 1.6 Hz), 8.14 (1H, d, *J* = 7.3 Hz), 7.96 (1H, d, *J* = 7.9 Hz), 7.81 (1H, t, *J* = 7.7 Hz), 7.59 (2H, t, *J* = 8.0 Hz), 7.35 (1H, t, *J* = 7.7 Hz), 5.73 (s, 2H). ¹³C NMR (CDCl₃), δ, ppm: 159.1, 147.7, 147.5 – 147.1 and 143.7–143.3 (2 × m), 147.1,

146.3–145.9 and 143.7–143.2 (2 × m), 146.0, 140.5, 134.9, 139.2–138.8 and 136.7–136.3 (2 × m), 133.7, 129.1, 128.6, 128.4, 127.3, 127.0, 122.3, 118.8, 117.3, 66.1. *Z*-isomer: ¹H NMR (CDCl₃), δ, ppm: 8.55 (1H, d, *J* = 8.1 Hz), 8.41 (1H, dd, *J* = 8.0, 1.6 Hz), 8.14 (1H, d, *J* = 7.3 Hz), 7.92 (1H, d, *J* = 7.9 Hz), 7.77 (1H, d, *J* = 7.7 Hz), 7.55 (2H, t, *J* = 8.0 Hz), 7.35 (1H, t, *J* = 7.7 Hz), 5.64 (s, 2H). ¹³C NMR (CDCl₃), δ, ppm: 159.0, 147.4, 147.5–147.1 and 143.7–143.3 (2 × m), 146.3–145.9 and 143.7–143.2 (2 × m), 144.0, 142.7, 139.8, 134.6, 139.2–138.8 and 136.7–136.3 (2 × m), 132.2, 128.1, 128.6, 128.4, 127.1, 126.7, 121.4, 118.8, 117.4, 65.7. HRMS (ESI-TOF) *m/z*: [M + H]⁺ Calcd. for C₂₂H₁₁F₅N₃O₂ 444.0771, found 444.0766.

4.1.3.8 6-(((4-nitrobenzyl)oxy)imino)indolo[2,1-b]quinazolin-12(6H)-one (1h)

Yield 95%, a flaxen solid. M.p. 219°C. *E*-isomer: ¹H NMR (CDCl₃), δ, ppm: 8.68 (1H, d, *J* = 8.1 Hz), 8.43 (1H, dd, *J* = 7.9, 1.6 Hz), 8.31–8.25 (3H, m), 7.95 (1H, d, *J* = 7.9 Hz), 7.81 (1H, ddd, *J* = 8.3, 7.2, 1.6 Hz), 7.68–7.56 (4H, m), 7.38 (1H, t, *J* = 7.6 Hz), 5.75 (2H, s). ¹³C NMR (CDCl₃), δ, ppm: 159.1, 148.1, 147.8, 147.1, 146.0, 143.7, 140.5, 134.9, 133.7, 129.1, 128.7, 128.5, 128.4, 127.3, 127.1, 124.1, 122.3, 118.9, 117.5, 78.0. *Z*-isomer: ¹H NMR (CDCl₃), δ, ppm: 8.59 (1H, d, *J* = 8.1 Hz), 8.45 (1H, dd, *J* = 7.9, 1.6 Hz), 8.31–8.25 (3H, m), 7.95 (1H, d, *J* = 7.9 Hz), 7.81 (1H, ddd, *J* = 8.3, 7.2, 1.6 Hz), 7.68–7.56 (4H, m), 7.34 (1H, t, *J* = 7.6 Hz), 5.75 (2H, s). ¹³C NMR (CDCl₃), δ, ppm: 159.0, 148.1, 147.8, 147.4, 147.0, 144.6, 139.8, 134.7, 132.3, 129.7, 129.2, 128.7, 128.3, 127.2, 126.7, 123.9, 121.4, 119.1, 117.5, 77.6. Found, %: C 66.59, H 3.42, N 14.24. C₂₂H₁₄N₄O₄. Calculated, %: C 66.33, H 3.54, N 14.06. HRMS (ESI-TOF) *m/z*: [M + H]⁺ Calcd. for C₂₂H₁₅N₄O₄ 399.1093, found 399.1116.

4.1.3.9 6-((pyridin-2-ylmethoxy)imino)indolo[2,1-b]quinazolin-12(6H)-one (1i)

Compound **2i** was synthesized according to the general procedure of alkylation from **TRYP-Ox** (0.263 g, 1.0 mmol), 2-(bromomethyl)pyridine hydrobromide (0.3794 g, 1.5 mmol) and Na₂CO₃ (0.2861 g, 2.7 mmol). Yield 18% (64 mg), light green crystals. M.p. 199–200°C. ¹H NMR (CDCl₃), δ, ppm: 8.72–8.62 (2H, m), 8.42 (1H, d, *J* = 7.9 Hz), 8.36 (1H, d, *J* = 7.7 Hz), 7.95 (1H, d, *J* = 8.2 Hz), 7.85–7.74 (2H, m), 7.67–7.51 (3H, m), 7.37 (1H, dd, *J* = 7.7, 7.7 Hz), 7.32 (1H, dd, *J* = 7.6, 5.0 Hz), 5.82 (2H, s). ¹³C NMR (CDCl₃), δ, ppm: 159.2, 156.2, 148.8, 148.0, 147.2, 145.9, 140.4, 138.0, 134.9, 133.5, 129.0, 128.7, 128.3, 127.3, 127.1, 123.5, 122.6, 122.3, 119.0, 117.3, 79.4. HRMS (ESI-TOF) *m/z*: [M + H]⁺ Calcd. for C₂₁H₁₅N₄O₂ 355.1195, found 355.1215.

4.1.3.10 The synthesis of 6-(acetoxymino)indolo[2,1-b]quinazolin-12(6H)-one (1j)

Prepared from **TRYP-Ox** (80.0 mg, 0.3 mmol) and acetic anhydride (0.468 ml, 4.5 mmol) in pyridine (5 ml) at 0°C. Then

the mixture was poured into the water (150 ml), filtered and recrystallized from EtOH. Yield 78%, a colorless solid. M.p. 262°C. *E*-isomer: ¹H NMR (CDCl₃), δ, ppm: 8.67 (1H, d, *J* = 8.1 Hz), 8.42 (1H, dd, *J* = 7.8, 1.5 Hz), 8.34 (1H, d, *J* = 7.4 Hz), 7.97 (1H, dd, *J* = 8.2, 1.2 Hz), 7.83 (1H, ddd, *J* = 8.2, 7.2, 1.6 Hz), 7.69 (1H, ddd, *J* = 7.9, 7.9, 1.3 Hz), 7.61 (1H, ddd, *J* = 8.1, 7.2, 1.2 Hz), 7.43 (1H, ddd, *J* = 7.7, 7.7, 1.0 Hz), 2.50 (3H, s). ¹³C NMR (CDCl₃), δ, ppm: 167.7, 158.9, 149.9, 147.2, 146.9, 141.6, 135.1, 135.1, 129.6, 129.5, 129.0, 127.4, 127.2, 122.6, 118.2, 117.7, 19.6. *Z*-isomer: ¹H NMR (CDCl₃), δ, ppm: 8.58 (1H, d, *J* = 8.1 Hz), 8.42 (1H, dd, *J* = 7.8, 1.5 Hz), 8.34 (1H, d, *J* = 7.4 Hz), 8.04 (1H, d, *J* = 8.2 Hz), 7.83 (1H, ddd, *J* = 8.2, 7.2, 1.6 Hz), 7.69 (1H, ddd, *J* = 7.9, 7.9, 1.3 Hz), 7.61 (1H, ddd, *J* = 8.1, 7.2, 1.2 Hz), 7.39 (1H, dd, *J* = 7.7, 7.7 Hz), 2.47 (3H, s). ¹³C NMR (CDCl₃), δ, ppm: 168.2, 158.7, 149.9, 147.2, 146.9, 141.9, 134.9, 134.1, 130.0, 129.8, 129.0, 127.4, 127.0, 123.2, 118.2, 117.5, 19.6. Found, %: C 69.62, H 3.77, N 14.83. C₁₇H₁₁N₃O₃. Calculated, %: C 69.31, H 4.00, N 15.15. HRMS (ESI-TOF) *m/z*: [M + H]⁺ Calcd. for C₁₇H₁₂N₃O₃ 306.0879, found 306.0898.

4.1.3.11 6-(hydroximino)indolo[2,1-b]quinazolin-12(6H)-one lithium salt (1k)

Yield 34%, colorless crystals. M.p. 399°C. ¹H NMR (DMSO-*d*₆), δ, ppm: 8.64–8.58 (2H, m), 8.25 (1H, dd, *J* = 7.9, 1.6 Hz), 7.74 (1H, ddd, *J* = 8.4, 6.9, 1.6 Hz), 7.67 (1H, dd, *J* = 8.3, 1.2 Hz), 7.35 (1H, ddd, *J* = 8.0, 6.8, 1.3 Hz), 7.31–7.24 (2H, m). ¹³C NMR (DMSO-*d*₆), δ, ppm: 159.7, 152.3, 149.5, 145.6, 133.7, 132.3, 126.5, 126.3, 126.2, 124.5, 122.9, 119.5, 119.5, 118.5, 115.4. Found, %: C 66.67, H 2.98, N 15.28. C₁₅H₈LiN₃O₂. Calculated, %: C 66.93, H 3.00, N 15.61.

4.1.3.12 6-(hydroximino)indolo[2,1-b]quinazolin-12(6H)-one sodium salt (1l)

Yield 88%, colorless crystals. M.p. >400°C, decomp. ¹H NMR (DMSO-*d*₆), δ, ppm: 8.59 (1H, d, *J* = 8 Hz), 8.57 (1H, dd, *J* = 7.9, 1.4 Hz), 8.26 (1H, dd, *J* = 8.0, 1.5 Hz), 7.79 (1H, ddd, *J* = 8.3, 6.8, 1.6 Hz), 7.74 (1H, d, *J* = 7.4 Hz), 7.45–7.35 (2H, m), 7.32 (1H, ddd, *J* = 7.5, 7.5, 1.3 Hz). ¹³C NMR (DMSO-*d*₆), δ, ppm: 159.4, 151.3, 148.8, 145.0, 134.1, 134.0, 126.9, 126.4, 126.4, 124.1, 121.6, 121.6, 119.5, 119.5, 115.6. Found, %: C 63.42, H 2.68, N 14.70. C₁₅H₈NaN₃O₂. Calculated, %: C 63.16, H 2.83, N 14.73. HRMS (ESI-TOF) *m/z*: [M + H]⁺ Calcd. for C₁₅H₉N₃NaO₂ 286.05925, found 286.0592.

4.1.3.13 6-hydrazonoindolo[2,1-b]quinazolin-12(6H)-one (1m)

Yield 93%, an orange solid. M.p. >400°C with decomposition. ¹H NMR (CDCl₃), δ, ppm: 11.21 (2H, s), 8.63 (1H, d, *J* = 8.1 Hz), 8.46 (1H, d, *J* = 7.9 Hz), 8.04 (1H, d, *J* = 8.0 Hz), 7.92 (1H, d, *J* = 7.7 Hz), 7.85 (1H, t, *J* = 7.0 Hz), 7.68 (1H, t, *J* = 8.1 Hz), 7.44 (1H, t, *J* = 7.5 Hz), 7.37 (1H, td, *J* = 7.9, 0.9 Hz). ¹³C NMR (CDCl₃), δ, ppm: 159.1, 147.3, 146.1, 138.5, 135.3, 134.5, 130.9, 128.5, 127.7, 127.5, 126.5, 125.6, 119.0, 118.1, 117.1. Found, %: C 68.83, H 3.66,

N 21.62. $C_{15}H_{10}N_4O$. Calculated, %: C 68.69, H 3.84, N 21.36. HRMS (ESI-TOF) m/z : $[M + H]^+$ Calcd. for $C_{15}H_{11}N_4O$ 263.0933, found 263.0934.

4.1.3.14 6-(2-phenylhydrazono)indolo[2,1-b]quinazolin-12(6H)-one (1n)

Yield 90%, an orange solid. M.p. 223°C. 1H NMR ($CDCl_3$), δ , ppm: 13.48 (1H, s), 8.58 (1H, d, $J = 7.7$ Hz), 8.46 (1H, d, $J = 7.9$ Hz), 7.89 (1H, d, $J = 7.5$ Hz), 7.83–7.80 (2H, m), 7.55 (1H, dt, $J = 8.2, 4.2$ Hz), 7.50–7.36 (6H, m), 7.11 (1H, t, $J = 7.2$ Hz). ^{13}C NMR ($CDCl_3$), δ , ppm: 159.0, 147.0, 146.2, 142.8, 138.4, 137.2, 135.3, 134.5, 129.7, 128.5, 127.5, 127.5, 126.5, 123.7, 121.5, 119.2, 117.1, 114.7. Found, %: C 74.79, H 3.98, N 16.42. $C_{21}H_{14}N_4O$. Calculated, %: C 74.54, H 4.17, N 16.56. HRMS (ESI-TOF) m/z : $[M + H]^+$ Calcd. for $C_{21}H_{15}N_4O$ 339.1246, found 339.1263.

4.1.3.15 2-(12-oxoindolo[2,1-b]quinazolin-6(12H)-ylidene)hydrazinecarboxamide (1o)

Yield 91%, a yellow solid. M.p. 266°C. 1H NMR ($CDCl_3$), δ , ppm: 12.62 (1H, s), 8.68 (1H, d, $J = 8.1$ Hz), 8.49 (1H, dd, $J = 8.1, 1.5$ Hz), 8.10 (1H, d, $J = 8.0$ Hz), 7.90–7.83 (2H, m), 7.71–7.68 (1H, m), 7.55 (1H, td, $J = 7.9, 1.3$ Hz), 7.43 (1H, td, $J = 7.5, 0.7$ Hz). ^{13}C NMR ($CDCl_3$), δ , ppm: 159.0, 155.8, 147.4, 146.4, 141.9, 138.5, 135.1, 134.6, 131.3, 130.0, 128.5, 127.7, 126.8, 125.6, 120.5, 117.5. Found, %: C 63.22, H 3.51, N 22.62. $C_{16}H_{11}N_5O_2$. Calculated, %: C 62.95, H 3.63, N 22.94. HRMS (ESI-TOF) m/z : $[M + H]^+$ Calcd. for $C_{16}H_{12}N_5O_2$ 306.0991, found 306.1006.

4.2 Methods for biological analysis

4.2.1 Kinase K_d determination

Selected compounds were submitted for dissociation constant (K_d) determination using the KINOMEScan platform (Eurofins Pharma Discovery, San Diego, CA, United States), as described previously (Karaman et al., 2008). In brief, kinases were produced and displayed on T7 phage or expressed in HEK-293 cells. Binding reactions were performed at room temperature for 1 h, and the fraction of kinase not bound to test compound was determined by capture with an immobilized affinity ligand and quantified by quantitative polymerase chain reaction. Primary screening at fixed concentrations of compounds was performed in duplicate. For dissociation constant K_d determination, a 12-point half-log dilution series (a maximum concentration of 33 μM) was used. Assays were performed in duplicate, and their average mean value is displayed.

4.2.2 Cell culture

All cells were cultured at 37°C in a humidified atmosphere containing 5% CO_2 . THP-1Blue cells obtained from InvivoGen (San Diego, CA, United States) were cultured in RPMI 1640 medium (Mediatech Inc., Herndon, VA, United States)

supplemented with 10% (v/v) fetal bovine serum (FBS), 4.5 g/L glucose, 100 $\mu g/ml$ streptomycin, 100 U/mL penicillin, 100 $\mu g/ml$ phleomycin (Zeocin), and 10 $\mu g/ml$ blasticidin S. Human monocyte-macrophage MonoMac-6 cells (Deutsche Sammlung von Mikroorganismen und Zellkulturen GmbH, Braunschweig, Germany) were grown in RPMI 1640 medium supplemented with 10% (v/v) FBS, 10 $\mu g/ml$ bovine insulin, 100 $\mu g/ml$ streptomycin, and 100 U/mL penicillin.

4.2.3 Analysis of AP-1/NF- κB activation

Activation of AP-1/NF- κB was measured using an alkaline phosphatase reporter gene assay in THP1-Blue cells. Human monocytic THP-1Blue cells are stably transfected with a secreted embryonic alkaline phosphatase gene that is under the control of a promoter inducible by AP-1/NF- κB . THP-1Blue cells (2×10^5 cells/well) were pretreated with test compound or DMSO (1% final concentration) for 30 min, followed by addition of 250 ng/ml LPS (from *Escherichia coli* K-235; Sigma Chemical Co., St. Louis, MO, United States) for 24 h, and alkaline phosphatase activity was measured in cell supernatants using QUANTI-Blue mix (InvivoGen) with absorbance at 655 nm and compared with positive control samples (LPS). The concentrations of compound that caused 50% inhibition of the AP-1/NF- κB reporter activity (IC_{50}) were calculated.

4.2.4 Cytokine analysis

Human IL-6 ELISA kit (BD Biosciences, San Jose, CA, United States) was used to confirm the inhibitory effect of selected compounds on IL-6 production. MonoMac-6 cells were plated in 96-well plates at a density of 2×10^5 cells/well in culture medium supplemented with 3% (v/v) endotoxin-free FBS. Cells were pretreated with test compound or DMSO (1% final concentration) for 30 min, followed by addition of 250 ng/ml LPS for 24 h. IC_{50} values for IL-6 production were calculated by plotting the percentage inhibition against the logarithm of inhibitor concentration (at least five points). Multiplex human cytokine ELISA kit from Anogen (Mississauga, ON, Canada) was used to evaluate various cytokines (IL-1 α , IL-1 β , IL-6, GM-CSF, MCP-1, IFN γ , and TNF) in the supernatants of MonoMac-6 cells.

4.2.5 Cytotoxicity assay

Cytotoxicity was analyzed with a CellTiter-Glo Luminescent Cell Viability Assay Kit from Promega (Madison, WI, United States), according to the manufacturer's protocol. Cells were treated with the compound under investigation and cultivated for 24 h. After treatment, the cells were allowed to equilibrate to room temperature for 30 min, substrate was added, and the luminescence measured using a Fluoroscan Ascent FL (Thermo Fisher Scientific, Waltham, MA, United States). The cell IC_{50} values were calculated by plotting the percentage inhibition against the logarithm of inhibitor concentration (at least five points).

4.2.6 Western blotting

MonoMac-6 monocytic cells (10^7 cells) were incubated with different concentrations of compound **1j** (final DMSO concentration of 0.5%) for 30 min at 37°C and then treated with LPS (250 ng/ml) or buffer for another 30 min at 37°C. Cells were washed twice with ice-cold phosphate buffer solution (pH 7.4), and cell lysates were prepared using lysis buffer (Cell Signaling Technology, Danvers, MA, United States). Cell lysates were separated on ExpressPlus 10% PAGE Gels (GenScript, Piscataway, NJ, United States) using TRIS-MOPS running buffer and transferred to nitrocellulose membranes. The blots were blocked overnight at 4°C in TRIS buffer (pH 7.4) + 0.1% Tween-20 (TBST) + 2.5% bovine serum albumin and probed with antibodies against phospho-c-Jun (Ser63) (Cell Signaling Technology), followed by horseradish peroxidase-conjugated secondary antibody (Cell Signaling Technology), and the blots were developed using Super-Signal West Femto chemiluminescent substrate (Thermo Fisher Scientific) and visualized with a FluorChem FC2 imaging system (Alpha Innotech Corporation, San Leandro, CA, United States). For measurement of total c-Jun signal, we stripped and reprobed the same Western blots that were used for phospho-c-Jun blots. Briefly, the membranes were washed 4 times for 5 min with TBST, incubated for 30 min at 50°C in TRIS buffer (pH 6.3) + 2% sodium dodecyl sulfate + 0.63% β -mercaptoethanol and then washed 6 times for 5 min each wash in TBST. The membranes were blocked again and probed for total c-Jun, followed by horseradish peroxidase-conjugated secondary antibody (both reagents from Cell Signaling Technology), developed, and visualized as described above. Quantitation of the luminescent signals were performed using AlphaView software.

4.3 Molecular docking

Geometries of JNK3 protein was obtained by downloading crystal structures from the Protein Data Bank (PDB entry code 1PMV) into Molegro software (Molegro ApS, Aarhus, Denmark). All solvent molecules were removed. A search space was chosen for each of the receptors as a sphere centered on co-crystallized ligand present in the corresponding PDB structure. Radius of the sphere was equal to 10 Å. The sphere completely encompassed the co-crystallized ligand and the binding site. Side chains of all amino acid residues of a receptor within the corresponding sphere were regarded as flexible during docking. The number of such residues was equal to 39. The flexible residues were treated with default settings of “Setup Sidechain Flexibility” tool in Molegro, and a softening parameter of 0.7 was applied during flexible docking, according to the standard protocol using the Molegro Virtual Docker 6.0 (MVD) program. Before docking, structures of compounds were pre-optimized using HyperChem software (HyperCube, Gainesville, FL, United States) with the MM+

force field and saved in Tripos MOL2 format (Tripos, St. Louis, MO, United States). The ligand structures were imported into MVD. The options “Create explicit hydrogens,” “Assign charges (calculated by MVD),” and “Detect flexible torsions in ligands” were enabled during importing. Appropriate protonation states of the ligands were also automatically generated at this step. Each ligand was subjected to 30 docking runs with respect to a given receptor structure using MVD software. The docking pose with the lowest MolDock docking score (Thomsen et al., 2006) was selected for each ligand and analyzed using the built-in tools of MVD.

Data availability statement

The raw data supporting the conclusion of this article will be made available by the authors, without undue reservation.

Author contributions

Conceptualization, IS, AKh, MQ, and MC; methodology, IS, AKh, KS, and MC; formal analysis, IS, AKo, KS, LK, and AKh; investigation, IS, AKo, KS, LK, and AKh; resources, AKh, MQ, and MC; writing—original draft preparation, IS and AKo; writing—review and editing, IS, AKo, KS, AKh, MQ, and MC; supervision, AKh, MQ, and MC; funding acquisition, AKh, MQ, and MC. All authors have read and agreed to the published version of the manuscript.

Funding

This research was supported in part by National Institutes of Health IDeA Program Grants GM115371 and GM103474; USDA National Institute of Food and Agriculture Hatch project 1009546; the Montana State University Agricultural Experiment Station; and Tomsk Polytechnic University development program Priority 2030 (project Priority-2030-NIP/IZ-009-0000-2022).

Acknowledgments

KS gratefully acknowledges the Fulbright Commission for a Scholarship.

Conflict of interest

The authors declare that the research was conducted in the absence of any commercial or financial relationships that could be construed as a potential conflict of interest.

Publisher's note

All claims expressed in this article are solely those of the authors and do not necessarily represent those of their affiliated

References

- Abdelrahman, K. S., Hassan, H. A., Abdel-Aziz, S. A., Marzouk, A. A., Narumi, A., Konno, H., et al. (2021). JNK signaling as a target for anticancer therapy. *Pharmacol. Rep.* 73 (2), 405–434. doi:10.1007/s43440-021-00238-y
- Aggarwal, B. B. (2000). Tumour necrosis factors receptor associated signalling molecules and their role in activation of apoptosis, JNK and NF-kappaB. *Ann. Rheum. Dis.* 59, i6–16. doi:10.1136/ard.59.suppl_1.i6
- Bennett, B. L., Sasaki, D. T., Murray, B. W., O'Leary, E. C., Sakata, S. T., Xu, W., et al. (2001). SP600125, an anthrapyrazolone inhibitor of Jun N-terminal kinase. *Proc. Natl. Acad. Sci. U. S. A.* 98 (24), 13681–13686. doi:10.1073/pnas.251194298
- Bennett, B. L., Satoh, Y., and Lewis, A. J. (2003). Jnk: A new therapeutic target for diabetes. *Curr. Opin. Pharmacol.* 3 (4), 420–425. doi:10.1016/s1471-4892(03)00068-7
- Blanco, F., Alkorta, I., and Elguero, J. (2009). Barriers about double carbon-nitrogen bond in imine derivatives (aldimines, oximes, hydrazones, azines). *Croat. Chem. Acta* 82 (1), 173.
- Bode, A. M., and Dong, Z. (2007). The functional contrariety of JNK. *Mol. Carcinog.* 46 (8), 591–598. doi:10.1002/mc.20348
- Chen, J., Ye, C., Wan, C., Li, G., Peng, L., Peng, Y., et al. (2021). The roles of c-jun N-terminal kinase (JNK) in infectious diseases. *Int. J. Mol. Sci.* 22 (17), 9640. doi:10.3390/ijms22179640
- Cho, H., and Hah, J. M. (2021). A perspective on the development of c-jun N-terminal kinase inhibitors as therapeutics for alzheimer's disease: Investigating structure through docking studies. *Biomedicines* 9 (10), 1431. doi:10.3390/biomedicines9101431
- Cubero, F. J., Zhao, G., Nevzorova, Y. A., Hatting, M., Al Masaoudi, M., Verdier, J., et al. (2015). Haematopoietic cell-derived Jnk1 is crucial for chronic inflammation and carcinogenesis in an experimental model of liver injury. *J. Hepatol.* 62 (1), 140–149. doi:10.1016/j.jhep.2014.08.029
- Diethelm-Varela, B., Kumar, A., Lynch, C., Immler, G. H., Deschamps, J. R., Li, Y., et al. (2021). Stereoisomerization of human constitutive androstane receptor agonist CITCO. *Tetrahedron* 79, 131886. doi:10.1016/j.tet.2020.131886
- Dugave, C., and Demange, L. (2003). Cis-trans isomerization of organic molecules and biomolecules: Implications and applications. *Chem. Rev.* 103 (7), 2475–2532. doi:10.1021/cr0104375
- Fabian, M. A., Biggs, W. H., Treiber, D. K., Atteridge, C. E., Azimioara, M. D., Benedetti, M. G., et al. (2005). A small molecule-kinase interaction map for clinical kinase inhibitors. *Nat. Biotechnol.* 23 (3), 329–336. doi:10.1038/nbt1068
- Fujioka, S., Niu, J., Schmidt, C., Sclabas, G. M., Peng, B., Uwagawa, T., et al. (2004). NF-kappaB and AP-1 connection: Mechanism of NF-kappaB-dependent regulation of AP-1 activity. *Mol. Cell. Biol.* 24 (17), 7806–7819. doi:10.1128/MCB.24.17.7806-7819.2004
- Gehring, M., Muth, F., Koch, P., and Laufer, S. A. (2015). c-Jun N-terminal kinase inhibitors: a patent review (2010–2014). *Expert Opin. Ther. Pat.* 25 (8), 849–872. doi:10.1517/13543776.2015.1039984
- Guha, M., and Mackman, N. (2001). LPS induction of gene expression in human monocytes. *Cell. Signal.* 13 (2), 85–94. doi:10.1016/s0898-6568(00)00149-2
- Gupta, R., and Ghosh, S. (2017). Phosphorylation of purified mitochondrial Voltage-Dependent Anion Channel by c-Jun N-terminal Kinase-3 modifies channel voltage-dependence. *Biochim. Open* 4, 78–87. doi:10.1016/j.biopen.2017.03.002
- Gupta, R., and Ghosh, S. (2015). Phosphorylation of voltage-dependent anion channel by c-Jun N-terminal Kinase-3 leads to closure of the channel. *Biochem. Biophys. Res. Commun.* 459 (1), 100–106. doi:10.1016/j.bbrc.2015.02.077
- Gupta, R. (2017). Phosphorylation of rat brain purified mitochondrial Voltage-Dependent Anion Channel by c-Jun N-terminal kinase-3 modifies open-channel noise. *Biochem. Biophys. Res. Commun.* 490 (4), 1221–1225. doi:10.1016/j.bbrc.2017.06.194
- Gupta, S., BarreTT, T., Whitmarsh, A. J., Cavanagh, J., Sluss, H. K., Derijard, B., et al. (1996). Selective interaction of JNK protein kinase isoforms with transcription factors. *EMBO J.* 15 (11), 2760–2770. doi:10.1002/j.1460-2075.1996.tb00636.x
- Ha, J., Kang, E., Seo, J., and Cho, S. (2019). Phosphorylation dynamics of JNK signaling: Effects of dual-specificity phosphatases (DUSPs) on the JNK pathway. *Int. J. Mol. Sci.* 20 (24), E6157. doi:10.3390/ijms20246157
- Hammouda, M. B., Ford, A. E., Liu, Y., and Zhang, J. Y. (2020). The JNK signaling pathway in inflammatory skin disorders and cancer. *Cells* 9 (4), E857. doi:10.3390/cells9040857
- Hibi, M., Lin, A., Smeal, T., Minden, A., and Karin, M. (1993). Identification of an oncoprotein- and UV-responsive protein kinase that binds and potentiates the c-Jun activation domain. *Genes Dev.* 7 (11), 2135–2148. doi:10.1101/gad.7.11.2135
- Johnson, G. L., and Lapadat, R. (2002). Mitogen-activated protein kinase pathways mediated by ERK, JNK, and p38 protein kinases. *Science* 298 (5600), 1911–1912. doi:10.1126/science.1072682
- Jung, D. H., Park, H. J., Byun, H. E., Park, Y. M., Kim, T. W., Kim, B. O., et al. (2010). Diosgenin inhibits macrophage-derived inflammatory mediators through downregulation of CK2, JNK, NF-kappaB and AP-1 activation. *Int. Immunopharmacol.* 10 (9), 1047–1054. doi:10.1016/j.intimp.2010.06.004
- Kaminska, B., Gozdz, A., Zawadzka, M., Ellert-Miklaszewska, A., and Lipko, M. (2009). MAPK signal transduction underlying brain inflammation and gliosis as therapeutic target. *Anat. Rec.* 292 (12), 1902–1913. doi:10.1002/ar.21047
- Karaman, M. W., Herrgard, S., Treiber, D. K., Gallant, P., Atteridge, C. E., Campbell, B. T., et al. (2008). A quantitative analysis of kinase inhibitor selectivity. *Nat. Biotechnol.* 26 (1), 127–132. doi:10.1038/nbt1358
- Kersting, S., Reinecke, K., Hilgert, C., Janot, M. S., Haarmann, E., Albrecht, M., et al. (2013). Knockout of the c-Jun N-terminal Kinase 2 aggravates the development of mild chronic dextran sulfate sodium colitis independently of expression of intestinal cytokines TNF alpha, TGFbeta1, and IL-6. *J. Inflamm. Res.* 6, 13–23. doi:10.2147/JIR.S36415
- Kirpotina, L. N., Schepetkin, I. A., Hammaker, D., Kuhs, A., Khlebnikov, A. I., and Quinn, M. T. (2020). Therapeutic effects of tryptanthrin and tryptanthrin-6-oxime in models of rheumatoid arthritis. *Front. Pharmacol.* 11, 1145. doi:10.3389/fphar.2020.01145
- Kyriakis, J. M., Banerjee, P., Nikolakaki, E., Dai, T., Rubie, E. A., Ahmad, M. F., et al. (1994). The stress-activated protein kinase subfamily of c-Jun kinases. *Nature* 369 (6476), 156–160. doi:10.1038/369156a0
- Lai, B. N., Wu, C. H., and Lai, J. H. (2020). Activation of c-jun N-terminal kinase, a potential therapeutic target in autoimmune arthritis. *Cells* 9 (11), E2466. doi:10.3390/cells9112466
- Liakhov, S. A., Schepetkin, I. A., Karpenko, O. S., Duma, H. I., Haidarzhly, N. M., Kirpotina, L. N., et al. (2021). Novel c-jun N-terminal kinase (JNK) inhibitors with an 11H-Indeno[1, 2-b]quinoxalin-11-one scaffold. *Molecules* 26 (18), 5688. doi:10.3390/molecules26185688
- Madeo, A., Lappano, R., Galgani, M. G., Asperi-Camp, Ani, A., Maggiolini, M., et al. (2010). c-Jun activation is required for 4-hydroxytamoxifen-induced cell death in breast cancer cells. *Oncogene* 29 (7), 978–991. doi:10.1038/onc.2009.400
- Mangold, J. B., Spina, A., and McCann, D. J. (1989). Sulfation of mono- and diaryl oximes by aryl sulfotransferase isozymes. *Biochim. Biophys. Acta* 991 (3), 453–458. doi:10.1016/0304-4165(89)90072-x
- Mehan, S., Meena, H., Sharma, D., and Sankhla, R. (2011). Jnk: A stress-activated protein kinase therapeutic strategies and involvement in alzheimer's and various neurodegenerative abnormalities. *J. Mol. Neurosci.* 43 (3), 376–390. doi:10.1007/s12031-010-9454-6
- Morton, S., Davis, R. J., McLaren, A., and Cohen, P. (2003). A reinvestigation of the multisite phosphorylation of the transcription factor c-Jun. *EMBO J.* 22 (15), 3876–3886. doi:10.1093/emboj/cdg388
- Posy, S. L., Hermsmeier, M. A., Vaccaro, W., Ott, K. H., Todderud, G., Lippy, J. S., et al. (2011). Trends in kinase selectivity: Insights for target class-focused library screening. *J. Med. Chem.* 54 (1), 54–66. doi:10.1021/jm101195a
- Schepetkin, I. A., Khlebnikov, A. I., Potapov, A. S., Kovrizhina, A. R., Matveevskaya, V. V., Belyanin, M. L., et al. (2019). Synthesis, biological evaluation, and molecular modeling of 11H-indeno[1, 2-b]quinoxalin-11-one

derivatives and tryptanthrin-6-oxime as c-Jun N-terminal kinase inhibitors. *Eur. J. Med. Chem.* 161, 179–191. doi:10.1016/j.ejmech.2018.10.023

Schepetkin, I. A., Kirpotina, L. N., Hammaker, D., Kochetkova, I., Khlebnikov, A. I., Lyakhov, S. A., et al. (2015). Anti-inflammatory effects and joint protection in collagen-induced arthritis after treatment with IQ-1S, a selective c-jun N-terminal kinase inhibitor. *J. Pharmacol. Exp. Ther.* 353 (3), 505–516. doi:10.1124/jpet.114.220251

Schepetkin, I. A., Kirpotina, L. N., Khlebnikov, A. I., Hanks, T. S., Kochetkova, I., Pascual, D. W., et al. (2012). Identification and characterization of a novel class of c-Jun N-terminal kinase inhibitors. *Mol. Pharmacol.* 81 (6), 832–845. doi:10.1124/mol.111.077446

Schepetkin, I. A., Plotnikov, M. B., Khlebnikov, A. I., Plotnikova, T. M., and Quinn, M. T. (2021). Oximes: Novel therapeutics with anticancer and anti-inflammatory potential. *Biomolecules* 11 (6), 777. doi:10.3390/biom11060777

Seledtsov, V. I., Malashchenko, V. V., Meniailo, M. E., Atochin, D. N., Seledtsova, G. V., and Schepetkin, I. A. (2020). Inhibitory effect of IQ-1S, a selective c-Jun N-terminal kinase (JNK) inhibitor, on phenotypical and cytokine-producing characteristics in human macrophages and T-cells. *Eur. J. Pharmacol.*, 173116. doi:10.1016/j.ejphar.2020.173116

Takeuchi, O., and Akira, S. (2001). Toll-like receptors; their physiological role and signal transduction system. *Int. Immunopharmacol.* 1 (4), 625–635. doi:10.1016/s1567-5769(01)00010-8

Thomsen, R., Christensen, M. H., and MolDock (2006). MolDock: A new technique for high-accuracy molecular docking. *J. Med. Chem.* 49 (11), 3315–3321. doi:10.1021/jm051197e

Vinciguerr, M., Esposito, I., Salzano, S., Madeo, A., Nagel, G., Maggiolini, M., et al. (2008). Negative charged threonine 95 of c-Jun is essential for c-Jun N-terminal kinase-dependent phosphorylation of threonine 91/93 and stress-induced c-Jun biological activity. *Int. J. Biochem. Cell Biol.* 40 (2), 307–316. doi:10.1016/j.biocel.2007.08.001

Vogel, J., Anand, V. S., Ludwig, B., NawoSchik, S., Dunlop, J., and Braithwaite, S. P. (2009). The JNK pathway amplifies and drives subcellular changes in tau phosphorylation. *Neuropharmacology* 57 (5–6), 539–550. doi:10.1016/j.neuropharm.2009.07.021

Wagner, G., and Laufer, S. (2006). Small molecular anti-cytokine agents. *Med. Res. Rev.* 26 (1), 1–62. doi:10.1002/med.20042

Wang, S., Li, H., Weng, S., Li, C., and He, J. (2020). White spot syndrome virus establishes a novel IE1/JNK/c-Jun positive feedback loop to drive replication. *Iscience* 23 (1), 100752. doi:10.1016/j.isci.2019.100752

Warner, S. L., Bashyam, S., Vankayalapati, H., Bearss, D. J., Han, H., Mahadevan, D., et al. (2006). Identification of a lead small-molecule inhibitor of the Aurora kinases using a structure-assisted, fragment-based approach. *Mol. Cancer Ther.* 5 (7), 1764–1773. doi:10.1158/1535-7163.MCT-05-0524

Xie, X. L., Gu, Y., Fox, T., Coll, J. T., Fleming, M. A., Markland, W., et al. (1998). Crystal structure of JNK3: A kinase implicated in neuronal apoptosis. *Structure* 6 (8), 983–991. doi:10.1016/s0969-2126(98)00100-2

Yung, J. H. M., and Giacca, A. (2020). Role of c-jun N-terminal kinase (JNK) in obesity and type 2 diabetes. *Cells* 9 (3), E706. doi:10.3390/cells9030706



OPEN ACCESS

EDITED BY

Shaogui Wang,
Guangzhou University of Chinese
Medicine, China

REVIEWED BY

Liubing Hu,
Jinan University, China
Hua Sun,
Henan University, China

*CORRESPONDENCE

Jun Yao,
yj_1108@126.com
Lisheng Wang,
wangls168@163.com

[†]These authors have contributed equally
to this work

SPECIALTY SECTION

This article was submitted to
Inflammation Pharmacology,
a section of the journal
Frontiers in Pharmacology

RECEIVED 11 July 2022

ACCEPTED 19 August 2022

PUBLISHED 14 September 2022

CITATION

Lin Q, Zhang D, Zhang J, Luo W, Xu Z,
Yao J and Wang L (2022), Identification
of lncRNA DLEU2 as a potential
diagnostic biomarker and anti-
inflammatory target for
ulcerative colitis.
Front. Pharmacol. 13:991448.
doi: 10.3389/fphar.2022.991448

COPYRIGHT

© 2022 Lin, Zhang, Zhang, Luo, Xu, Yao
and Wang. This is an open-access article
distributed under the terms of the
[Creative Commons Attribution License](#)
(CC BY). The use, distribution or
reproduction in other forums is
permitted, provided the original
author(s) and the copyright owner(s) are
credited and that the original
publication in this journal is cited, in
accordance with accepted academic
practice. No use, distribution or
reproduction is permitted which does
not comply with these terms.

Identification of lncRNA DLEU2 as a potential diagnostic biomarker and anti-inflammatory target for ulcerative colitis

Qiuling Lin^{1†}, Dingguo Zhang^{2†}, Jian Zhang^{3†}, Weixiang Luo⁴,
Zhenglei Xu², Jun Yao^{2*} and Lisheng Wang^{2*}

¹Department of General Practice, Shenzhen People's Hospital (The Second Clinical Medical College, Jinan University; The First Affiliated Hospital, Southern University of Science and Technology), Shenzhen, Guangdong, China, ²Department of Gastroenterology, Shenzhen People's Hospital (The Second Clinical Medical College, Jinan University; The First Affiliated Hospital, Southern University of Science and Technology), Shenzhen, Guangdong, China, ³Department of Plastic Surgery, Sun Yat-Sen Memorial Hospital, Sun Yat-Sen University, Guangzhou, Guangdong, China, ⁴Department of Nursing, Shenzhen People's Hospital (The Second Clinical Medical College, Jinan University; The First Affiliated Hospital, Southern University of Science and Technology), Shenzhen, Guangdong, China

The incidence of ulcerative colitis (UC) in China has significantly increased over the past 10 years. Here we aim to explore potential diagnostic biomarkers and anti-inflammatory targets associated with UC. Patients with UC were enrolled in this study. The expression of lncRNAs and mRNAs in the nidus of the gut mucosa and adjacent normal mucosa samples was evaluated by RNA sequencing. The role of DLEU2 in inflammation and NF- κ B signaling pathway was examined by RT-qPCR, Western blotting, and ELISA with human macrophage-like cells derived from THP-1. 564 lncRNAs and 859 mRNAs are significantly altered in the nidus of the gut mucosa of UC patients. Among the differentially expressed lncRNAs, DLEU2 changes the most. The expression of DLEU2 is negatively associated with inflammatory factors such as *TNF- α* , *IL-1 α* , *IL-1 β* , *IL-6*, and *NLRP3*. Mechanistically, DLEU2 exerts anti-inflammatory activity by inhibiting the NF- κ B signaling pathway. In conclusion, the lncRNA DLEU2 in the intestinal mucosa is dysregulated upon gut inflammation and may act as a diagnostic biomarker and a therapeutic target for UC.

KEYWORDS

ulcerative colitis, DLEU2, inflammatory factors, NF- κ B, lncRNA

Introduction

Ulcerative colitis (UC) is an immune-mediated chronic nonspecific inflammatory disease of the colon and rectum, belonging to inflammatory bowel disease (IBD). The etiology and pathogenesis of UC are not fully understood (Russell and Satsangi, 2004; Irving and Gibson, 2008; Tozlu et al., 2021). The incidence of UC in Asia is much lower than that in Europe, but it has increased significantly in China in recent years

(Kaplan, 2015; Gearry, 2016; Yang, 2016). Thus, a deeper understanding of its pathogenesis, diagnosis, and treatment is urgently required.

The pathogenesis of UC is affected by many factors, including genetic susceptibility, epithelial barrier defects, immune response disorders, and environmental factors. UC classification is critical for the clinical management of patients due to the heterogeneous and varying disease courses. Several specific genes have been identified as biomarkers which closely related to UC pathogenesis (Lee et al., 2018). Wang et al. found that Aquaporin (AQP) four deficiency alleviates experimental colitis in mice (Wang G. et al., 2019). Su et al. found that AA genotype of HSP70-2 polymorphisms was associated with severe UC, and HSP70-2 polymorphism may be used to predict UC phenotypes (Nam et al., 2007). TNF- α is the major pro-inflammatory factor of intestinal epithelial cell proliferation and apoptosis, and the expression of TNF- α in intestinal mucosa increased in DSS-induced UC mice, suggesting that TNF- α is involved in colonic inflammation (Watson and Hughes, 2012; Billmeier et al., 2016; Abraham et al., 2017; Schreurs et al., 2019; Hu et al., 2020).

Long non-coding RNAs (lncRNAs) are a class of non-coding RNAs (ncRNAs) defined by a transcript length of >200 nucleotides (Ma et al., 2013). LncRNAs have been implicated as potential therapeutic targets in various diseases such as cancers, metabolic diseases, and inflammatory diseases (Winkle et al., 2021). We found that a lncRNA named Deleted in Lymphocytic Leukemia 2 (DLEU2) was up-regulated in the nidus of the intestinal mucosa of UC patients. DLEU2 is located on chromosome 13q14 and was originally identified as a potential tumor regulator gene (Garding et al., 2013). However, the role of lncRNA DLEU2 in UC remains unknown.

In this study, we compared lncRNA levels between the nidus of the intestinal mucosa and adjacent normal mucosa in UC patients by RNA sequencing. And the role of DLEU2 in inflammation was investigated *in vitro*. DLEU2 is identified to be a potential anti-inflammatory lncRNA and inhibits gut inflammation by negatively regulating the NF- κ B signaling pathway. The lncRNA DLEU2 is suggested to be a diagnostic biomarker and anti-inflammation target for UC.

Materials and methods

Materials

Anti-IL-1 β antibody (AF-401) was purchased from R&D systems (Minneapolis, MN). anti-p-p65 antibody (3031), anti- β -actin antibody (4970S), and HRP-conjugated goat-anti-rabbit IgG (7074S) were obtained from Cell Signaling

Technology (Beverly, MA). HRP-conjugated donkey-anti-goat IgG antibody (A0181) was purchased from Beyotime (Shanghai, China). 96T Human TNF- α ELISA kit (CHE0019-096) and 96T Human IL-6 ELISA kit (CHE0009-096) were obtained from 4A Biotech Co., Ltd. (Beijing, China). PrimeScript RT Master Mix reagent kit (R122) and SYBR Green Master Mix (Q141) were purchased from Vazyme (Nanjing, China). Phorbol myristic acetate (PMA, P8139) was purchased from Sigma (St. Louis, MO).

Subjects and samples collection

A total of four UC patients were included in the study who presented typical UC symptoms. The nidus of the intestinal mucosa and adjacent normal mucosa were taken from subjects during colonoscopy, respectively (>100 ng).

RNA sequencing and data analysis

Total RNA of the mucosa samples was isolated by Trizol reagent (Invitrogen, Carlsbad, CA, United States), and its quantity and purity were analyzed by Bioanalyzer 2100 and RNA 1000 Nano LabChip Kit (Agilent, CA, United States) with a standard of RIN number >7.0, respectively. After the quality check, ribosomal RNA was removed from 5 μ g of total RNA by using Ribo-ZeroTM rRNA Removal Kit (Illumina, San Diego, United States). The paired-end sequencing was performed on Illumina NovaseqTM 6000 platform. Reads were mapped into the genome of *Homo sapiens* by hisat2 Ver 2.0.4 (Kim et al., 2019), and assembled by stringtie Ver 1.3.4 (Pertea et al., 2016) with default parameters. StringTie was used to perform expression levels for mRNAs and lncRNAs by calculating FPKM (Pertea et al., 2016). The differentially expressed mRNAs and lncRNAs were selected with log₂ (fold change) ≥ 1 or log₂ (fold change) ≤ -1 and with statistical significance *p* value < 0.05 by R package edgeR or DESeq2 (Love et al., 2014). KEGG enrichment analyses were used to screen the signaling pathways involved.

Cell culture

The THP-1 human monocytic leukemia cell line was purchased from the American Type Culture Collection. The cells were cultured in RPMI-1640 medium (HyClone; Cytiva) containing 10% fetal bovine serum (FBS; HyClone; Cytiva) and 1% penicillin/streptomycin (Invitrogen; Thermo Fisher Scientific, Inc.) in a humidified atmosphere of 5% CO₂ at 37°C. The cells were stimulated with 100 nM PMA in RPMI 1640 medium for 72 h.

TABLE 1 Primers used in RT-qPCR.

	Forward (5'–3' sequence)	Reverse (5'–3' sequence)
<i>GAPDH</i>	GGTCGGAGTCAACGGATTGG	CCATGGGTGGAATCATATTGGAAC
<i>DLEU2</i>	CGGGGTGGCTCTAACGAAT	GTGGCGCTATACTCTCGGAC
<i>TNF-α</i>	CCTCTCTCTAATCAGCCCTCTG	GAGGACCTGGGAGTAGATGAG
<i>IL-1α</i>	TGGTAGTAGCAACCAACGGGA	ACTTTGATTGAGGGCGTCATTG
<i>IL-1β</i>	ATGATGGCTTATTACAGTGGCAA	GTCGGAGATTCGTAGCTGGA
<i>IL-6</i>	ACTCACCTCTTCAGAACGAATTG	CCATCTTTGGAAGGTTTCAGGTTG
<i>NLRP3</i>	GATCTTCGCTGCGATCAACAG	CGTGCATTATCTGAACCCAC

Transient transfection and quantification

A DLEU2 expression vector was constructed by IGEbio (Guangzhou, China) using the pcDNA3.1(+) vector. DLEU2 siRNA and negative control siRNA were designed and synthesized by IGEbio (Guangzhou, China). siRNA for DLEU2 was as follows: 5'-AGUCUACGUUGGAGGUAA A-3'. Transient transfection was performed using Lipofectamine 2000 Reagent (Sigma-Aldrich, United States). The PMA-differentiated THP-1 cells were transfected with siDLEU2, pcDNA-DLEU2, or controls for 8 h, and further incubated for 24 h with LPS (1 µg/ml) stimulation. Total RNA was isolated and purified using Trizol reagent (Invitrogen, Carlsbad, CA, United States) following the manufacturer's procedure. Using GAPDH as an internal reference, the relative expression levels of TNF-α, IL-1α, IL-1β, IL-6, NLRP3, and DLEU2 were measured by qPCR with $2^{-\Delta\Delta C_t}$ method. Amplification reactions consisted of an initial denaturation at 95°C for 3 min, 40 cycles of denaturation at 95°C for 15 s, annealing at 60°C for 30 s, and extension at 72°C for 30 s. GAPDH was used as an internal control. Primer sequences are shown in Table 1.

Western blotting

Total proteins were harvested from human macrophage-like cells derived from THP-1. After transfection, cells in each group were washed by pre-cooling PBS, 100 µl cell lysate was added, lysed at 4°C for 30 min, and centrifuged at 12,000 r/min for 10 min at 4°C to extract proteins. Protein concentration was detected by BCA protein concentration assay kit (Invitrogen, United States). The protein gels were transferred to polyvinylidene fluoride (PVDF) membrane by SDS-PAGE reaction of 30 µg total protein per swimming lane. 5% defatted milk powder was sealed for 1 h, and protein primary antibody (1:1000) was added, respectively, and incubated in a shaker for 24 h (4°C). After washing the film with TBST, the film was incubated with a secondary antibody (1:2000) at room temperature for 1 h. TBST was washed and

ECL developed. The gray values of the strips were detected by Gel imaging system and Quantity one software.

Statistical analysis

Data were analyzed using SPSS version 17.0 statistical software (SPSS, Inc.). Measurement data are expressed as the mean ± standard deviation. An unpaired Student's t-test was employed to examine the difference between the two groups. $p < 0.05$ was considered to indicate a statistically significant difference.

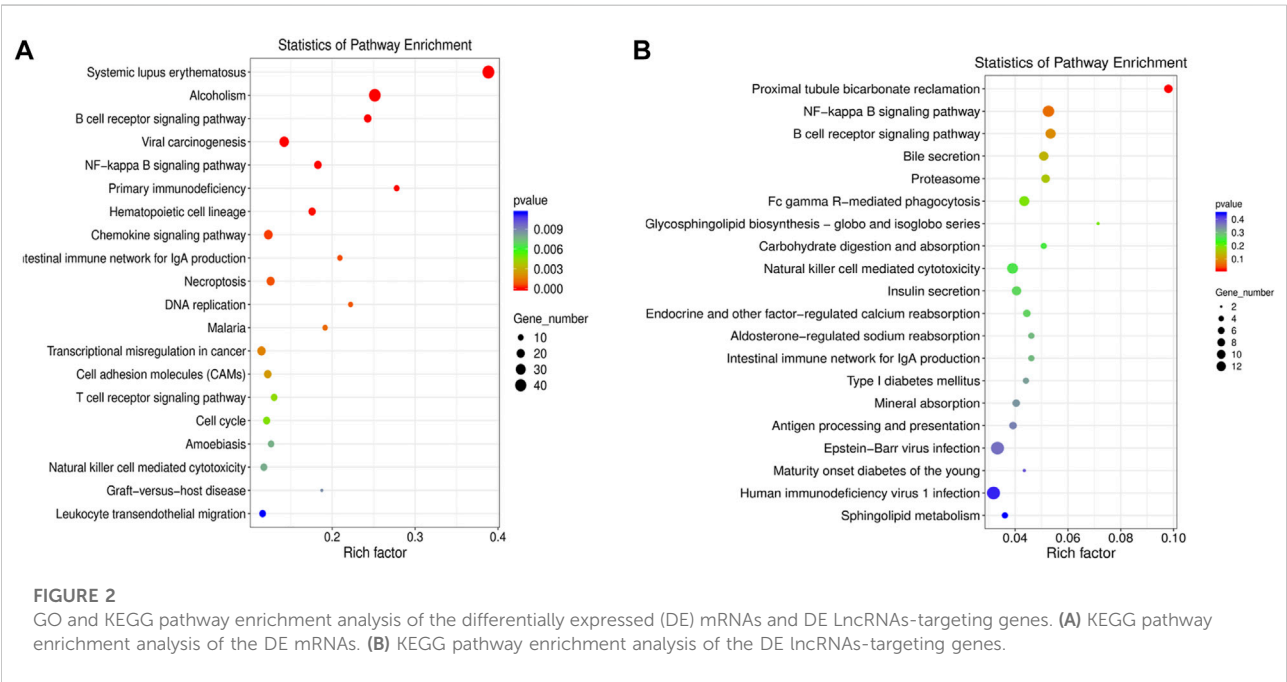
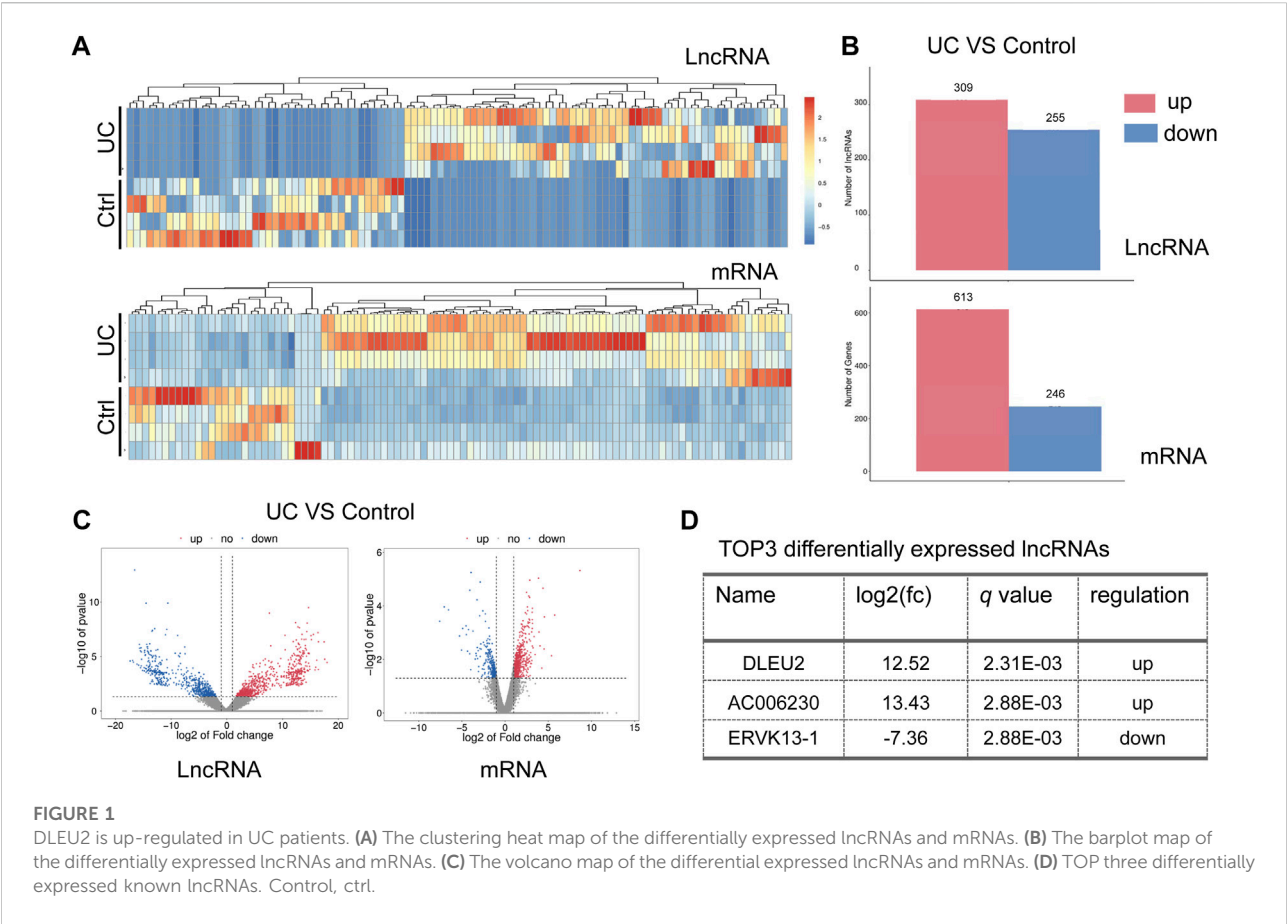
Results

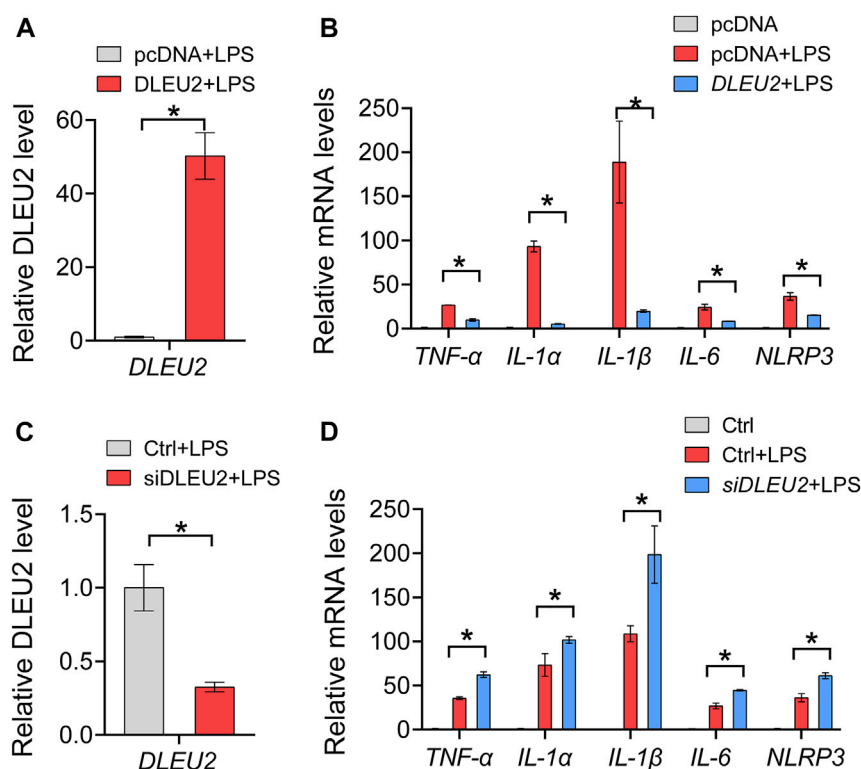
DLEU2 is up-regulated in UC

A comparison of RNA expression was made between samples of the nidus of the intestinal mucosa (colitis) and adjacent normal mucosa (control). An overall change of lncRNAs and mRNAs in the intestinal mucosa of UC was observed (Figure 1A). A total of 564 lncRNAs (309 up-regulated and 255 down-regulated) were significantly altered compared to control (Figures 1B,C). And a total of 859 mRNAs (613 up-regulated and 246 down-regulated) were significantly changed ($p < 0.05$) (Figures 1B,C). Of note, the up-regulated DLEU2 changes the most in the differentially expressed (DE) lncRNAs (Figure 1D).

NF-κB signaling pathway is associated with UC

The DE mRNAs and lncRNAs were analyzed by KEGG pathway enrichment analyses. The DE mRNAs were mainly enriched in inflammation-related pathways including systemic lupus erythematosus, alcoholism, B cell receptor signaling pathway, viral carcinogenesis, and NF-κB signaling pathway (Figure 2A). We further performed functional enrichment



**FIGURE 3**

DLEU2 inhibits NF-κB-related inflammation cytokines. (A) The expression level of DLEU2 in DLEU2 and pcDNA (control) treated THP-1 cells. (B) Effects of DLEU2 overexpression on level of inflammation cytokines in THP-1 cells. (C) The expression level of DLEU2 in siDLEU2 and negative control transfected THP-1 cells. (D) Effects of DLEU2 knockdown on level of inflammation cytokines in THP-1 cells. $n = 5$ per group. $p < 0.05$ (t -test).

analysis of DE lncRNAs-targeting genes. The DE lncRNA-targeting genes were mainly enriched in proximal tubule bicarbonate reclamation, NF-κB signaling pathway, B cell receptor signaling pathway, bile secretion, and proteasome (Figure 2B). Taking together, the results of enrichment analyses suggested several inflammation-related pathways related to UC. Among them, the signaling pathway NF-κB is closely associated with gut inflammation.

DLEU2 down-regulated expression of inflammatory genes

We further tested the effects of the DLEU2 on inflammation with macrophage-like cells derived from THP-1. The overexpression and knockdown efficiency of DLEU2 was verified by the RT-qPCR (Figures 3A,C). The expression levels of *TNF-α*, *IL-1α*, *IL-1β*, *IL-6*, and *NLRP3* in THP-1 cells were significantly decreased upon DLEU2 overexpression (Figure 3B). Consistently, these inflammatory factors were significantly increased in the siDLEU2 group compared with the control group (Figure 3D). Overall, DLEU2 inhibits inflammation *in vitro*.

DLEU2 inhibits NF-κB signaling pathway

Of note, the abovementioned inflammatory genes (i.e., *TNF-α*, *IL-1α*, *IL-1β*, *IL-6*, and *NLRP3*) are direct targets of NF-κB. We further investigated the effect of DLEU2 on protein levels of NF-κB-regulated inflammatory factors. DLEU2 significantly decreased levels of TNF-α and IL-6 in LPS-treated THP-1 cells (Figure 4A). In addition, Western blotting assay revealed that the expression levels of IL-1β and phosphorylated NF-κB p65 (p-p65) were also significantly decreased by DLEU2 (Figures 4B,C). Taken together, these results indicate that DLEU2 inactivates the NF-κB signaling pathway to exert anti-inflammatory effects.

Discussion

In this study, the expression of lncRNAs and mRNAs between the nidus of the intestinal mucosa and adjacent normal mucosa in UC patients were measured and compared. DLEU2 is the most significant DE lncRNA in the intestinal mucosa. DLEU2 was identified as an anti-inflammatory lncRNA. The anti-inflammatory effect of DLEU2 was validated *in vitro*.

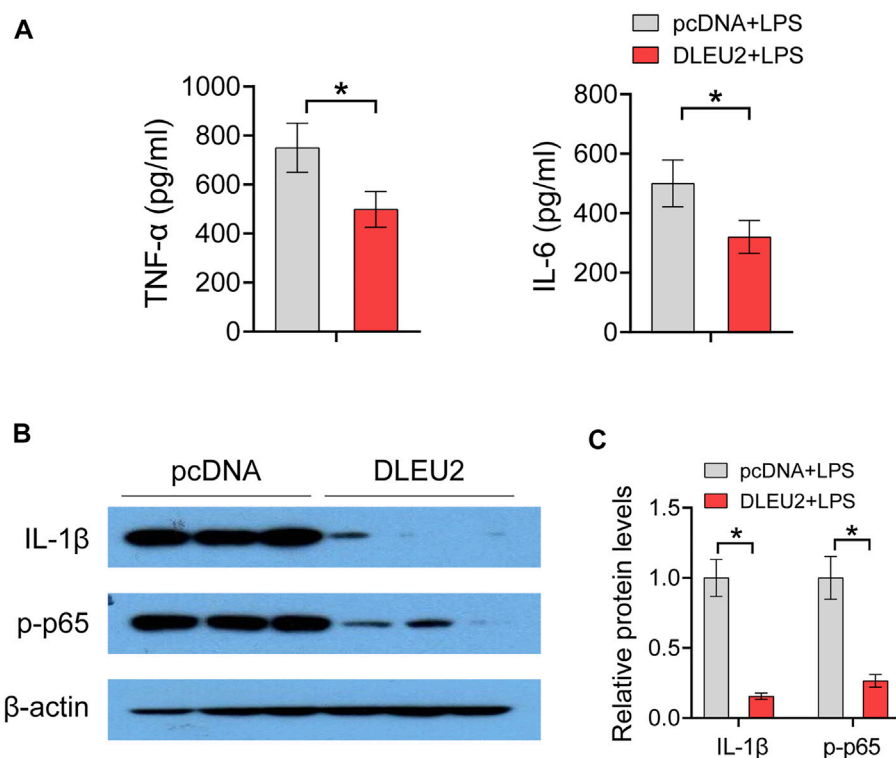


FIGURE 4

DLEU2 inhibits NF-κB signaling pathway. (A) The level of IL-6 and TNF-α protein in THP-1 cells transfected with DLEU2 or pcDNA. (B) The protein expression level of IL-1β and p-p65 in THP-1 cells transfected with DLEU2 or pcDNA. (C) Quantification data of (B). $n = 3$ per group. $p < 0.05$ (t -test).

Mechanistically, DLEU2 inhibits inflammation by negatively regulating the NF-κB signaling pathway, suggesting DLEU2 may serve as a novel biomarker and therapeutic target for UC.

The DE mRNAs and lncRNAs were mainly enriched in NF-κB signaling pathway in UC patients, which indicates the pathological process and inflammatory response of UC are closely associated with NF-κB pathway (Bing et al., 2017; Shen et al., 2019; Tian et al., 2019; Wang L. et al., 2019; Qiu et al., 2020). The interactions of DLEU2 and NF-κB may also be implicated in other physiology and diseases. In previous studies, DLEU2 was often related to cell proliferation and tumor progression. Mikael et al. found that the inactivation of DLEU2 promotes cell proliferation and tumor progression (Lerner et al., 2009). Angela et al. found that DLEU1 and DLEU2 mapped to a critical region at chromosomal band 13q14.3 that is recurrently deleted in solid tumors and hematopoietic malignancies like chronic lymphocytic leukemia. The tumor suppressor mechanism at 13q14.3 is a cluster of genes controlled by two lncRNA genes that are regulated by DNA-methylation and histone modifications and whose members all regulate NF-κB (Garding et al., 2013). Our study reveals that DLEU2 inhibits NF-κB signaling pathway in

THP-1 cells. DLEU2 maps at chromosome 13q14.3. The 13q14.3 locus contains C13ORF1, KPNA3, miR-15a/16-1, and RFP2 (Garding et al., 2013). These factors were found to positively regulate NF-κB activity (Garding et al., 2013). These results suggest that DLEU2 may regulate NF-κB through C13ORF1, KPNA3, miR-15a/16-1, and RFP2.

Besides DLEU2, other DE mRNAs and lncRNAs may also play roles in UC. SLC51A gene is involved in bile secretion. Nazzareno et al. found that SLC51, one of the newest members of the solute carrier family, played a critical role in the transport of bile acids, conjugated steroids, and structurally-related molecules across the basolateral membrane of many epithelial cells. In particular, SLC51A appears to be essential for intestinal bile acid absorption, and thus for dietary lipid absorption (Ballatori et al., 2013). Protooncogene TCL1b functions as an Akt kinase co-activator that exhibits oncogenic potency *in vivo* (Hashimoto et al., 2013). We found that TCL1b was highly expressed in the lesion location of the intestinal mucosa, which indicates TCL1b may also relate to the pathological changes in UC.

In conclusion, DLEU2 is identified to be an anti-inflammatory factor and inhibits inflammation by negatively regulating the NF-κB signaling pathway. The lncRNA DLEU2 in the intestinal mucosa is dysregulated upon gut

inflammation and may act as a diagnostic biomarker and a therapeutic target for UC.

Data availability statement

RNA-seq data have been deposited into the NCBI SRA database (PRJNA866700). The analyzed data sets generated during the study are available from the corresponding author on reasonable request.

Ethics statement

The studies involving human participants were reviewed and approved by The study was approved by the Shenzhen People's Hospital with the authorization number LL-KY-2021690. The patients/participants provided their written informed consent to participate in this study.

Author contributions

QL and LW designed the study; QL, DZ, WL, ZX, and WL performed experiments; QL, DZ, JZ, and JY collected and analyzed data; QL, DZ, and WL wrote the manuscript.

References

- Abraham, B. P., Ahmed, T., and Ali, T. (2017). Inflammatory bowel disease: Pathophysiology and current therapeutic approaches. *Handb. Exp. Pharmacol.* 239, 115–146. doi:10.1007/164_2016_122
- Ballatori, N., Christian, W. V., Wheeler, S. G., and Hammond, C. L. (2013). The heteromeric organic solute transporter, OST α -OST β /SLC51: A transporter for steroid-derived molecules. *Mol. Asp. Med.* 34 (2–3), 683–692. doi:10.1016/j.mam.2012.11.005
- Billmeier, U., Dieterich, W., Neurath, M. F., and Atreya, R. (2016). Molecular mechanism of action of anti-tumor necrosis factor antibodies in inflammatory bowel diseases. *World J. Gastroenterol.* 22 (42), 9300–9313. doi:10.3748/wjg.v22.i42.9300
- Bing, X., Xuelei, L., Wanwei, D., Linlang, L., and Keyan, C. (2017). EGCG maintains Th1/Th2 balance and mitigates ulcerative colitis induced by dextran sulfate sodium through TLR4/MyD88/NF- κ B signaling pathway in rats. *Can. J. Gastroenterol. Hepatol.* 2017, 3057268. doi:10.1155/2017/3057268
- Garding, A., Bhattacharya, N., Claus, R., Ruppel, M., Tschuch, C., Filarsky, K., et al. (2013). Epigenetic upregulation of lncRNAs at 13q14.3 in leukemia is linked to the in Cis downregulation of a gene cluster that targets NF- κ B. *PLoS Genet.* 9 (4), e1003373. doi:10.1371/journal.pgen.1003373
- Geary, R. B. (2016). IBD and environment: Are there differences between east and west. *Dig. Dis.* 34 (1–2), 84–89. doi:10.1159/000442933
- Hashimoto, M., Suizu, F., Tokuyama, W., Noguchi, H., Hirata, N., Matsuda-Lennikov, M., et al. (2013). Protooncogene TCL1b functions as an Akt kinase co-activator that exhibits oncogenic potency in vivo. *Oncogenesis* 2 (9), e70. doi:10.1038/oncsis.2013.30
- Hu, L., Chen, H., Zhang, X., Feng, Z., Zhang, H., and Meng, Q. (2020). Rosiglitazone ameliorates radiation-induced intestinal inflammation in rats by inhibiting NLRP3 inflammasome and TNF- α production. *J. Radiat. Res.* 61 (6), 842–850. doi:10.1093/jrr/rtaa062
- Irving, P. M., and Gibson, P. R. (2008). Infections and IBD. *Nat. Clin. Pract. Gastroenterol. Hepatol.* 5 (1), 18–27. doi:10.1038/ncpgasthep1004
- Kaplan, G. G. (2015). The global burden of IBD: From 2015 to 2025. *Nat. Rev. Gastroenterol. Hepatol.* 12 (12), 720–727. doi:10.1038/nrgastro.2015.150
- Kim, D., Paggi, J. M., Park, C., Bennett, C., and Salzberg, S. L. (2019). Graph-based genome alignment and genotyping with HISAT2 and HISAT-genotype. *Nat. Biotechnol.* 37 (8), 907–915. doi:10.1038/s41587-019-0201-4
- Lee, S. H., Kwon, J. E., and Cho, M. L. (2018). Immunological pathogenesis of inflammatory bowel disease. *Intest. Res.* 16 (1), 26–42. doi:10.5217/ir.2018.16.1.26
- Lerner, M., Harada, M., Lovén, J., Castro, J., Davis, Z., Oscier, D., et al. (2009). DLEU2, frequently deleted in malignancy, functions as a critical host gene of the cell cycle inhibitory microRNAs miR-15a and miR-16-1. *Exp. Cell Res.* 315 (17), 2941–2952. doi:10.1016/j.yexcr.2009.07.001
- Love, M. I., Huber, W., and Anders, S. (2014). Moderated estimation of fold change and dispersion for RNA-seq data with DESeq2. *Genome Biol.* 15 (12), 550. doi:10.1186/s13059-014-0550-8
- Ma, L., Bajic, V. B., and Zhang, Z. (2013). On the classification of long non-coding RNAs. *RNA Biol.* 10 (6), 925–933. doi:10.4161/rna.24604
- Nam, S. Y., Kim, N., Kim, J. S., Lim, S. H., Jung, H. C., and Song, I. S. (2007). Heat shock protein gene 70-2 polymorphism is differentially associated with the clinical phenotypes of ulcerative colitis and Crohn's disease. *J. Gastroenterol. Hepatol.* 22 (7), 1032–1038. doi:10.1111/j.1440-1746.2007.04927.x
- Perlea, M., Kim, D., Perlea, G. M., Leek, J. T., and Salzberg, S. L. (2016). Transcript-level expression analysis of RNA-seq experiments with HISAT, StringTie and Ballgown. *Nat. Protoc.* 11 (9), 1650–1667. doi:10.1038/nprot.2016.095
- Qiu, S., Li, P., Zhao, H., and Li, X. (2020). Maresin 1 alleviates dextran sulfate sodium-induced ulcerative colitis by regulating NRF2 and TLR4/NF- κ B signaling pathway. *Int. Immunopharmacol.* 78, 106018. doi:10.1016/j.intimp.2019.106018
- Russell, R. K., and Satsangi, J. (2004). Ibd: A family affair. *Best. Pract. Res. Clin. Gastroenterol.* 18 (3), 525–539. doi:10.1016/j.bpg.2003.12.006
- Schreurs, R. R. C. E., Baumdick, M. E., Sagebiel, A. F., Kaufmann, M., Mokry, M., Klarenbeek, P. L., et al. (2019). Human fetal TNF- α -cytokine-producing CD4+

Funding

This work was supported by Shenzhen Technical Research and Development Project (JCYJ20210324113803011) and Natural Science Foundation of Guangdong Province (2018A030313900).

Conflict of interest

The authors declare that the research was conducted in the absence of any commercial or financial relationships that could be construed as a potential conflict of interest.

The reviewer LH declared a shared affiliation with all the author(s) at the time of review.

Publisher's note

All claims expressed in this article are solely those of the authors and do not necessarily represent those of their affiliated organizations, or those of the publisher, the editors and the reviewers. Any product that may be evaluated in this article, or claim that may be made by its manufacturer, is not guaranteed or endorsed by the publisher.

effector memory T cells promote intestinal development and mediate inflammation early in life. *Immunity* 50 (2), 462–476. doi:10.1016/j.immuni.2018.12.010

Shen, J., Cheng, J., Zhu, S., Zhao, J., Ye, Q., Xu, Y., et al. (2019). Regulating effect of baicalin on IKK/I κ B/NF- κ B signaling pathway and apoptosis-related proteins in rats with ulcerative colitis. *Int. Immunopharmacol.* 73, 193–200. doi:10.1016/j.intimp.2019.04.052

Tian, X., Peng, Z., Luo, S., Zhang, S., Li, B., Zhou, C., et al. (2019). Aesculin protects against DSS-Induced colitis through activating PPAR γ and inhibiting NF- κ B pathway. *Eur. J. Pharmacol.* 857, 172453. doi:10.1016/j.ejphar.2019.172453

Tozlu, M., Cash, B., Younes, M., and Ertan, A. (2021). Dilemma in post-IBD patients with IBS-D symptoms: A 2020 overview. *Expert Rev. Gastroenterol. Hepatol.* 15 (1), 5–8. doi:10.1080/17474124.2021.1829469

Wang, G., Xu, B., Shi, F., Du, M., Li, Y., Yu, T., et al. (2019). Protective effect of methane-rich saline on acetic acid-induced ulcerative colitis via blocking the TLR4/

NF- κ B/MAPK pathway and promoting IL-10/JAK1/STAT3-mediated anti-inflammatory response. *Oxid. Med. Cell. Longev.* 2019, 7850324. doi:10.1155/2019/7850324

Wang, L., Tang, H., Wang, C., Hu, Y., Wang, S., and Shen, L. (2019). Aquaporin 4 deficiency alleviates experimental colitis in mice. *FASEB J.* 33 (8), 8935–8944. doi:10.1096/fj.201802769RR

Watson, A. J., and Hughes, K. R. (2012). TNF- α -induced intestinal epithelial cell shedding: Implications for intestinal barrier function. *Ann. N. Y. Acad. Sci.* 1258, 1–8. doi:10.1111/j.1749-6632.2012.06523.x

Winkle, M., El-Daly, S. M., Fabbri, M., and Calin, G. A. (2021). Noncoding RNA therapeutics-challenges and potential solutions. *Nat. Rev. Drug Discov.* 20, 629–651. doi:10.1038/s41573-021-00219-z

Yang, S. K. (2016). Personalizing IBD therapy: The asian perspective. *Dig. Dis.* 34 (1–2), 165–174. doi:10.1159/000443134



OPEN ACCESS

EDITED BY

Xiaojuan Chao,
University of Kansas Medical Center,
United States

REVIEWED BY

Yinliang Zhang,
Tianjin Medical University, China
Denglang Zou,
Qinghai Normal University, China

*CORRESPONDENCE

Xiaoying Yang,
yxyxiaoliqq@163.com
Yong Gao,
gaoyong@gzucm.edu.cn
Qi Wang,
wangqi@gzucm.edu.cn
Dong Zhang,
zhangdongvonhbxg@163.com

[†]These authors have contributed equally to this work and share first authorship

SPECIALTY SECTION

This article was submitted to
Inflammation Pharmacology,
a section of the journal
Frontiers in Pharmacology

RECEIVED 25 August 2022

ACCEPTED 21 September 2022

PUBLISHED 07 October 2022

CITATION

Zhong Y, Chen Y, Pan Z, Tang K,
Zhong G, Guo J, Cui T, Li T, Duan S,
Yang X, Gao Y, Wang Q and Zhang D
(2022), Ginsenoside Rc, as an FXR
activator, alleviates acetaminophen-
induced hepatotoxicity via relieving
inflammation and oxidative stress.
Front. Pharmacol. 13:1027731.
doi: 10.3389/fphar.2022.1027731

COPYRIGHT

© 2022 Zhong, Chen, Pan, Tang, Zhong,
Guo, Cui, Li, Duan, Yang, Gao, Wang and
Zhang. This is an open-access article
distributed under the terms of the
[Creative Commons Attribution License](#)
(CC BY). The use, distribution or
reproduction in other forums is
permitted, provided the original
author(s) and the copyright owner(s) are
credited and that the original
publication in this journal is cited, in
accordance with accepted academic
practice. No use, distribution or
reproduction is permitted which does
not comply with these terms.

Ginsenoside Rc, as an FXR activator, alleviates acetaminophen-induced hepatotoxicity *via* relieving inflammation and oxidative stress

Yadi Zhong^{1,2†}, Yingjian Chen^{2†}, Zhisen Pan^{3†}, Kaijia Tang^{2†},
Guangcheng Zhong², Jingyi Guo², Tianqi Cui², Tianyao Li²,
Siwei Duan², Xiaoying Yang^{4*}, Yong Gao^{2*}, Qi Wang^{2*} and
Dong Zhang^{1*}

¹The Fourth Clinical Medical College of Guangzhou University of Chinese Medicine, Shenzhen, China,

²Science and Technology Innovation Center, Guangzhou University of Chinese Medicine, Guangzhou, China, ³The First Clinical Medical College of Guangzhou University of Chinese Medicine, Guangzhou, China, ⁴Jiangsu Key Laboratory of Immunity and Metabolism, Department of Pathogen Biology and Immunology, Xuzhou Medical University, Xuzhou, China

Acetaminophen (APAP) intake leads to excessive NAPQI deposition, stimulating inflammatory and oxidative stress and causing fatal liver injury. However, the detailed molecular mechanism involved is unknown, and effective therapeutic approaches remain insufficient. In this study, we discovered that treatment with ginsenoside Rc can prevent the inflammatory response caused by APAP and oxidative stress in mouse primary hepatocytes (MPHs), along with the corresponding changes in related genes. Additionally, Ginsenoside Rc effectively alleviates APAP-induced cellular apoptosis and NAPQI accumulation in MPHs. *In vivo*, Ginsenoside Rc administration remarkably attenuates APAP-induced hepatotoxicity, repairing liver damage and improving survival. Moreover, Ginsenoside Rc treatment modulates genes involved in APAP metabolism, leading to a decrease in NAPQI and resulting in the alleviation of fatal oxidative stress and inflammatory response after APAP exposure, along with the expression of their related indicators. Furthermore, our RNA-seq and molecular docking analysis implies that FXR expression and FXR transcriptional activity are stimulated by Ginsenoside Rc treatment. Notably, due to the lack of FXR in mice and MPHs, ginsenoside Rc can no longer play its original protective role against hepatotoxicity and cell damage caused by APAP, and it is difficult to improve the corresponding survival rate and prevent hepatic apoptosis, NAPQI generation, fatal oxidative stress, and the inflammatory response induced by APAP and the expression of related genes. In summary, our results indicate that Ginsenoside Rc could act as an effective FXR activator and effectively regulate FXR-induced antioxidant stress and eliminate inflammation while also having an anti-apoptotic function.

KEYWORDS

ginsenoside Rc, FXR, acetaminophen, acute liver failure, inflammation, oxidative stress

Introduction

Acetaminophen (APAP) is an antipyretic analgesic that is widely used in clinical practice. It can have a safe therapeutic effect when taken at a reasonable dose (1–4 g/d). However, if the dosage of APAP is too high, it can easily cause acute liver injury (Tsai et al., 2015) or even an emergency outbreak of FLF (Fatty Liver Foundation) liver failure (Soeda et al., 2014). In China, APAP is one of the three main causes of acute liver failure (Gao et al., 2020b). APAP is metabolized by hepatocyte cytochrome P450 (CYP450), and converted to the active intermediate N-acetyl-p-benzoquinimide (NAPQI). Too much APAP causes NAPQI to consume all of the glutathione (GSH). It combines to form APAP adducts, causing mitochondria to lose their normal functions, produce reactive oxygen species (ROS) and release mitochondrial cell death factors, leading to liver necrosis (Chen D. et al., 2019; Chen et al., 2020). As the only approved antidote for ALILI (Acetaminophen-induced liver injury), N-acetyl-cysteine (NAC) can cause nausea and other adverse reactions, and its utility is limited to the early days of treatment. Later treatment with NAC may even damage liver regeneration (Yin et al., 2010; Gao et al., 2020a). Therefore, it is necessary to find a new and effective treatment method for acute liver injury caused by APAP. Reducing APAP-induced oxidative stress and inflammation may be an effective strategy.

The nuclear receptor farnesoid X receptor (FXR; NR1H4) potently regulates lipid, bile acid (BA), and glucose metabolism. Bile acids regulate the bile acid balance, inflammation, and lipid and glucose metabolism by activating the nuclear receptor FXR and membrane G protein-coupled receptor TGR5. Cholestasis can lead to the accumulation of BAs in the liver. FXR is not only expressed in the liver, but also exists in the intestine to control the reabsorption of bile acids, acting as a key regulator of bile acid enterohepatic circulation (Anakk et al., 2011; Baghdasaryan et al., 2011). It also plays an essential role in the metabolism of xenobiotics (Fiorucci et al., 2012). FXR induces transcriptional repression with small heterodimer partners (SHP), thereby inhibiting the transactivation of human NTCP and CYP7A1 genes. This mechanism can prevent bile acid overload and liver cell damage during cholestasis (Bechmann et al., 2013). In addition, FXR combines with bound bile acids to induce fibroblast growth factor (FGF)-15 to reduce the transcription of cytochrome P450 enzyme (Cyp7a1) in hepatocytes, further inhibiting the *de novo* synthesis of bile acids (Hartmann et al., 2018). Previous studies have shown that FXR and SHP strictly regulate the physiological concentration and homeostasis of bile acids through a multistep feedback loop, and ultimately inhibit cytochrome P450 (CYP7A1) (Anakk et al., 2011). Therefore, FXR may be a target protein mediating drug-induced liver injury and play an anti-inflammatory role to help inhibit the development of drug-induced liver injury.

Ginseng, a precious medicinal material that has been widely used in Asian countries for thousands of years, can produce a variety of medicinal effects in the field of disease treatment, including antitumor, antidiabetic, antifatigue, antioxidation, heart protection, and immune stimulation and neuroprotective effects. Ginsenoside is the main active ingredient responsible for its pharmacological effects (Kim et al., 2013; Lee et al., 2019). Ginseng can also be used as a chemopreventive agent and adjuvant therapy (Jeon et al., 2020). Previous research results have shown that ginsenoside Rc targets mitochondrial functions to increase the ATP content, remove free radicals and return to normal oxygen consumption levels. In addition, studies have found that ginsenoside Rc can stimulate and accelerate energy metabolism and fight oxidative damage, inflammation, cancer, aging, and metabolic diseases by activating SIRT1 (Huang et al., 2021). This study can treat APAP-induced liver injury by intervening inflammation, oxidative stress, and liver regeneration, which has the characteristics of multi-pathway and multi-target, and can play a better role in liver protection and liver protection. At the same time, it was found that ginsenoside Rc had a preventive protective effect on APAP-induced liver injury, and its mechanism was related to anti-oxidative stress, anti-apoptosis of hepatocytes, inhibition of the expression of inflammation-related factors, and regulation of APAP metabolism and transport *in vivo*. And we will further study the protective effect of FXR nuclear receptor, a key target of liver metabolism regulation, on APAP-induced acute liver injury, acute hepatocyte injury, oxidative stress, and inflammatory response, identify key genes regulating antioxidant genes and explore new potential drug targets, and improve the related mechanism of FXR on liver protection. To provide ideas and basis for the efficacy study and drug development and utilization of ginsenoside Rc.

Materials and methods

Reagents

Ginsenoside Rc (CAS.No11021-14-0) (purity 98.8%) and acetaminophen (APAP) were purchased from Shanghai Yuanye Biotechnology Co., Ltd. (Shanghai, China) and Aladdin Chemical Company (Shanghai, China).

Animal experiment

Male C57BL/6 mice weighing 20–25 g and aged 6 weeks were purchased from Model Animal Research Center of Guangzhou University of Traditional Chinese Medicine (Certificate SCXK 2018-0034; Guangzhou, China) (Chen L. et al., 2019). FXR knockout (FXR^{-/-}) mice were kindly sponsored by Changhui Liu and were originally purchased from Jackson Laboratory (Bar Harbor, ME, United States) (Liu et al., 2020). All the mice were housed in individually ventilated cages and were kept on a 12-h light dark cycle at all times. All the animal experiments carried

out were submitted to and approved by the Animal Ethics Committee of Guangzhou University of Traditional Chinese Medicine. WT and FXR^{-/-} mice received daily injections of ginsenoside Rc intraperitoneally at a dose of 5 mg/kg or 10 mg/kg. The control group was given normal saline (Control). The injection cycle was 10 days. On the 11th day, all observation groups were fasted overnight, and then injected with APAP dissolved in 60°C normal saline, 300 mg/kg. The injection site was the abdominal cavity, and the control group did not undergo this operation. All mice were sacrificed 10 h after APAP injection. Fresh liver tissue from the mice was then extracted for further studies. The total glutathione/-oxidized glutathione assay kit (Jianchen Bioengineering China) was used as the measurement tool for serum ALT and AST concentrations and GSH. TNF- α (Ruixinbio, Cat.#RX-D202412M), IL-6 (Ruixinbio, Cat.#RX-D203063M) and IL-1 β (Ruixinbio, Cat.#RX-D203049M), NAPQI (Cat.#SU-B28212) were measured using an ELISA (Ruixinbio, Quanzhou, China). The One step TUNEL Apoptosis Assay Kit (MA0224-1) (meilunbio, Shanghai, China) was also used.

Mouse survival experiment

In experiments on drug-induced liver injury, 300 mg/kg of APAP was injected to mice prior to the injection of different doses of Rc. In experiments conducted to test the survival rate, the time to death of mice within 72 h was recorded.

Cell protocols

Mouse primary hepatocytes (MPHs) were isolated and cultured in RPMI-1640 medium with 10% fetal bovine serum, 0.1 mg/ml streptomycin, and 100 units/ml penicillin as described above. (Liang et al., 2021b; Yang et al., 2020). After 24 h of incubation, the hepatocytes were treated with 10 mM APAP for an additional 24 h.

CCK-8 assay

A 96-well plate was used as a culture tool for MPHs, and the concentration of 5×10^4 /ml was repeated every five wells. After 6 h of cell incubation, a new culture base was formed, that is, configure various concentrations of ginsenoside Rc were configured, and the culture time was 24 h. The medium was removed and the culture was transferred to 100 μ l of new medium containing CCK-8 (1640 medium and CCK-8 solution in a ratio of 10:1) for incubation, and then the OD value was measured at 450 nm (Liang et al., 2021b; Yang et al., 2020).

Measurement of ROS

Briefly, after incubating MPH and Rc together, they were co-incubated with APAP for 24 h. In the next step, they were placed in DCFH-DA at concentration of 10 μ M and incubated again at 37°C for half an hour while avoiding light. Finally, the cells were washed three times with PBS, and the fluorescence emissions of the cells were observed by a fluorescence microscope. Then, the reactive oxygen species in the body were analyzed (Liang et al., 2021b; Yang et al., 2020). DCFH-DA (10 mM) was injected into mice through the tail vein, and again 1 h later. After death, liver tissue was extracted. The luciferase reporter gene for ROS levels in the extracted liver was detected by Berthold technology LB983 NC100.

TUNEL assay

Liver tissue was fixed with 4% paraformaldehyde solution, further sectioned at 4 μ m, and embedded in paraffin. TUNEL levels were determined with the TUNEL Apoptosis Assay Kit (MA0224-1, meilunbio) according to the manufacturer's instructions. Imaging was achieved with the aid of a fluorescence microscope (Leica Microsystems Ltd., Wetzlar, Germany).

Histology and immunofluorescence

Liver tissue was fixed with 10% paraformaldehyde, sectioned at 5 μ m, and embedded in paraffin. After routine hematoxylin and eosin (H&E) staining, the sections were placed under a slide scanner (Panoramic MIDI 1000 \times) at the Lingnan Medical Research Center of Guangzhou University of Traditional Chinese Medicine for further observation. Immunofluorescence was performed according to current protocols. Liver sections or MPH were incubated with NFkB-p65 (Affinity, United States) or primary antibodies F4/80, CD11b at 4°C overnight. After being washed three times with PBS, sections were incubated with a secondary antibody (Abclonal, Wuhan, China) at room temperature for 40 min. After being washed 5 times with PBS, images were observed using a fluorescence microscope (Nikon 1000 \times) from the Science and Technology Innovation Center of Guangzhou University of Chinese Medicine (Liu et al., 2020; Sun et al., 2021).

Western blotting

MPHs (WT and KO) that had been infected with ginsenoside Rc were exposed to APAP (10 mM) for 24 h. Proteins were extracted from Ginsenoside Rc-treated MPH cells, and the concentrations were determined using a BCA assay kit

produced by Biyuntian Technology, Beijing, China. Equal amounts of protein (60 µg) were separated with 10% SDS-polyacrylamide gels, and the fractions were transferred to PVDF membranes. The antibodies used were specific for rabbit anti-Bax (#T-40051, abmart) and rabbit anti-Bcl2 (#T-40056, abmart), rabbit anti-FXR (25055-1-AP, Proteintech), and rabbit anti-β-actin (AC026, abclonal).

Quantitative PCR

Total mRNA from MPH or liver tissue was extracted using TRIzol reagent. Reverse transcription was accomplished using a high-capacity cDNA reverse transcription kit produced by Applied Biomaterials Canada. qPCR analysis of cDNA was performed with the help of PowerUp™ SYBRTM Green Master Mix from Aibotech Biotech, Wuhan, China. The normalization of all genes was completed using β-actin, and the specific primer sequences are shown in [Supplementary Table S1](#).

Statistical analysis

The results for all the figures and text are presented as the mean ± SEM. Data were evaluated by using Student's t-test and one-way analysis of variance (ANOVA) to identify statistical differences between groups. This was followed by an analysis with GraphPad Prism (version 8.0) to determine statistical differences between groups. The post-hoc Tukey's test was performed on the results after multiple group comparisons. Survival was repeatedly measured by means of a two-way ANOVA and plotted accordingly. *p*-values < 0.05 were deemed significant.

Results

Ginsenoside Rc attenuates APAP overdose-induced ALI by restraining oxidative stress, and inflammation apoptosis in MPHs

To investigate whether Ginsenoside Rc can attenuate APAP overdose-induced ALI in MPHs, we established the APAP (10 mM)-incubated MPH model. As shown in [Figure 1A](#), Ginsenoside Rc dose-dependently alleviated APAP-induced hepatocyte damage, with a maximal effect at 50 µM (h). Next, we tested Bcl2 and Bax expression in MPHs using Western immunoblotting. After APAP-induced injury in MPHs, as can be seen in ([Figure 1B](#)), the expression of the antiapoptotic gene Bcl2 was inhibited to a certain extent, and the expression of the related apoptosis gene Bax was inhibited to a greater extent,

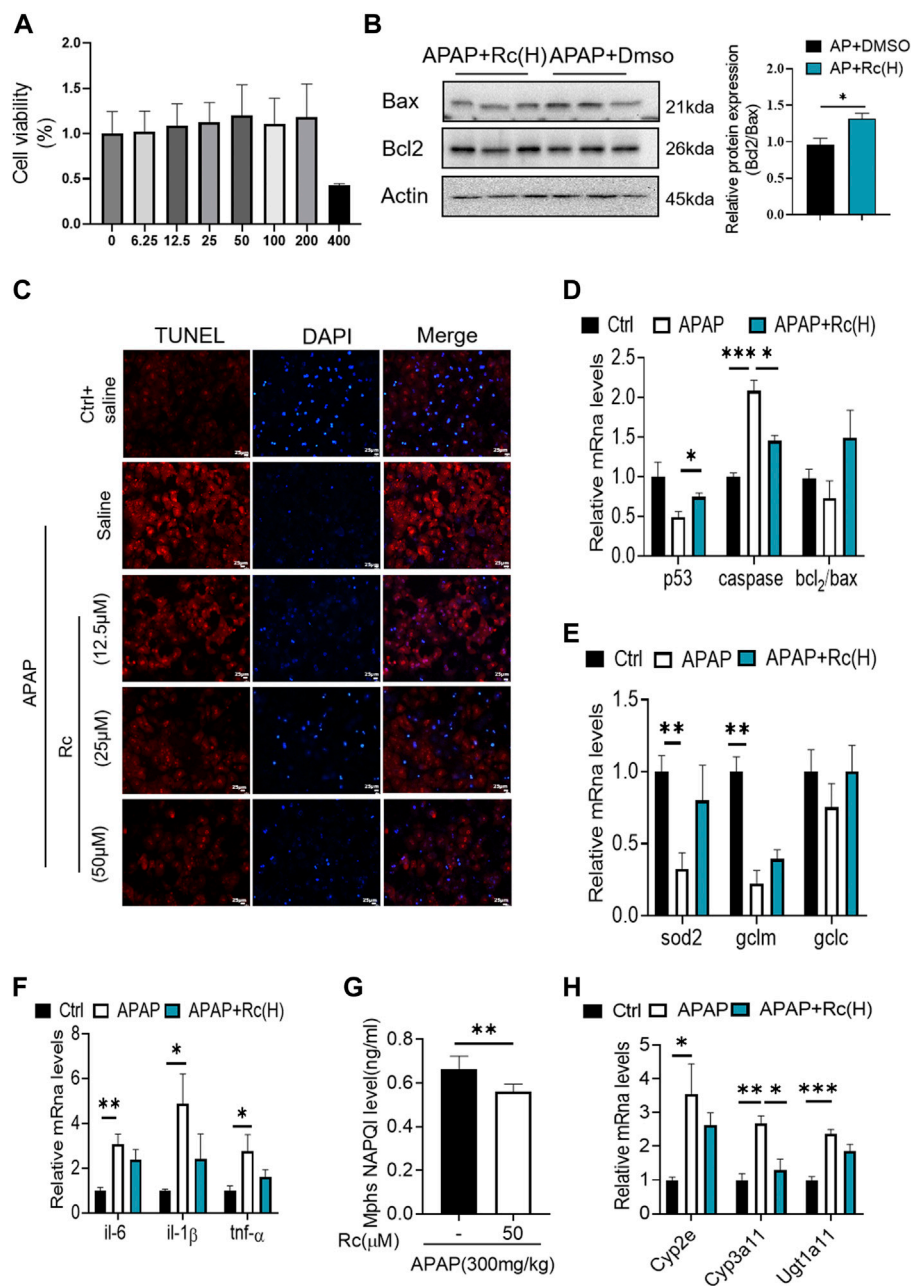
thereby significantly reducing the relative mRNA transcription level of Bcl2/Bax. However, Ginsenoside Rc treatment can reverse the downregulation of the mRNA relative expression level of Bcl2/Bax ([Figures 1C,D](#)). Moreover, TUNEL staining after high-dose Ginsenoside Rc treatment compared the number of red fluorescent label-positive apoptotic cells was the injury model group, showing a significant decrease.

In order to further analyze the oxidative stress effect of ginsenoside Rc on APAP-induced liver injury, we further explored the expression of Sod2, Gclc and Gclm at the mRNA level. These are key factors of antioxidant defense, APAP treatment decreased the mRNA transcription level of Sod2 ([Figure 1E](#)). This indicated that Ginsenoside Rc could significantly improve the antioxidant defense system function of the damaged liver, alleviating oxidative stress injury. In addition, Ginsenoside Rc administration significantly reduced NF-κB levels in APAP-induced MPHs ([Supplementary Figure S1](#)). Additionally, genes involved in inflammation such as IL-6, TNF-α, and IL-1β were significantly decreased after Ginsenoside Rc treatment ([Figure 1F](#)).

Since excess APAP needs to be metabolized by cytochrome P450 (CYP) CYP2E1 and CYP3A4 to the highly reactive metabolite N-acetyl-p-benzoquinoneimine (NAPQI), we further evaluated the expression levels of NAPQI and CYP in the liver, including CYP2E1, CYP3A11, and Ugt1a11 in MPHs. We found that, after Ginsenoside Rc treatment, the level of NAPQI decreased ([Figure 1G](#)), and the gene expression levels of these enzymes were significantly lower in the MPHs with ALI than in the MPHs without APAP treatment ([Figure 1H](#)). Interestingly, treatment with Ginsenoside Rc further significantly decreased the expression levels of these genes. In conclusion, it can be seen from these data that ginsenoside Rc can reduce ALI caused by excessive APAP by inhibiting oxidative stress, and inflammation apoptosis in MPHs.

Ginsenoside Rc alleviated hepatic damage in ALI mice by regulating oxidative stress and drug metabolism

Since ginsenoside Rc can significantly contribute to oxidative stress in MPH, it was hypothesized that ginsenoside Rc may be ameliorated in ALI mice. Therefore, mice were injected with different doses of ginsenoside Rc daily for 10 days. As shown in [Figures 2A–C](#), after the mice received ginsenoside Rc treatment, and then received APAP treatment, they were fully protected, and at the same time, the serum ALT and AST levels were significantly reduced, and lethality was significantly lower. The improved survival rate could be validated by the APAP dose (300 mg/kg). In addition, after receiving ginsenoside Rc treatment, the rate and extent of necrosis of the centrilobular liver induced by APAP excess were significantly reduced, as shown by the hematoxylin and

**FIGURE 1**

Ginsenoside Rc suppressed APAP-induced hepatocellular damage by reducing oxidative stress, and inflammation in MPHs. **(A)** CCK8 assay; **(B)** Ginsenoside Rc treatment inhibits the expression of Bcl2 protein and restrains the expression of bax in MPHs. **(C)** The TUNEL assay was performed to measure the apoptosis effect in MPHs. **(D)** Relative expression of mRNA associated with antiapoptosis (P53, Caspase, Bcl2/Bax); **(E)** Relative expression of mRNA associated with oxidative stress (Sod2, Gclm, Gclc); **(F)** Relative expressions of mRNA associated with inflammation (Il-6, Il-1β, TNF-α); **(G)** The ELISA assay showed that Ginsenoside Rc treatment decreased NAPQI levels in MPHs; **(H)** Relative expression of RNA associated with APAP-metabolizing enzymes (Cyp3a11, Cyp2E, Ugt1a11); Data are means ± SEM; n = 3-6/group. *, $p < 0.05$, **, $p < 0.01$, ***, $p < 0.001$.

eosin (H&E) staining results in [Figure 2D](#). Additionally, from the graph above, we can see that Ginsenoside Rc treatment enhanced GSH ([Figure 2E](#)) and increased the antioxidant gene expression, while the hepatic NAPQI levels were notably reduced ([Figure 2I](#)). Furthermore, Ginsenoside Rc

significantly mitigated the otherwise APAP-induced hepatic ROS overproduction ([Figure 2G](#)) and induced changes in the expression of genes involved in oxidative stress ([Figure 2F](#)), which suggests that Ginsenoside Rc can attenuate APAP excess-induced ALI by enhancing antioxidant defenses.

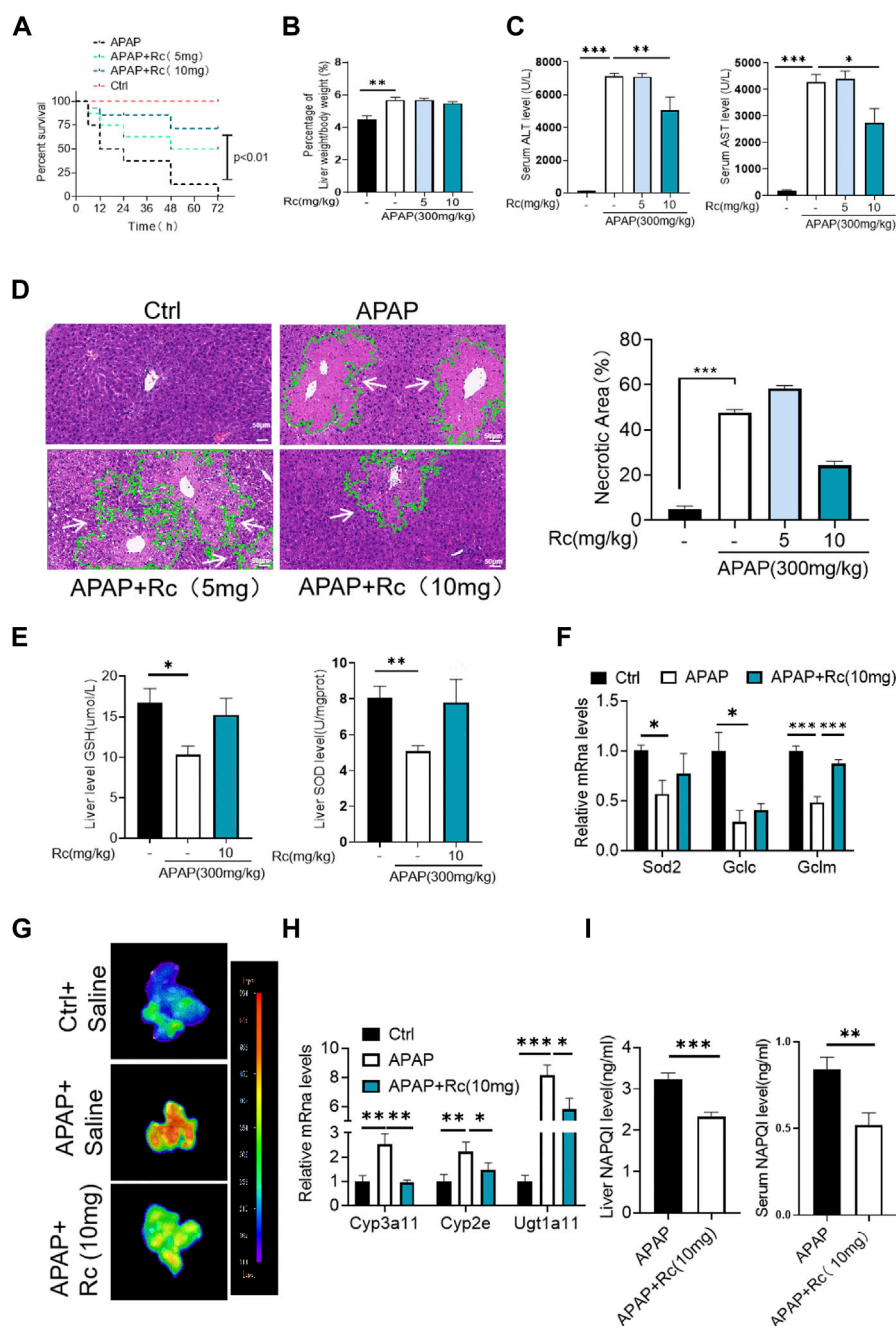
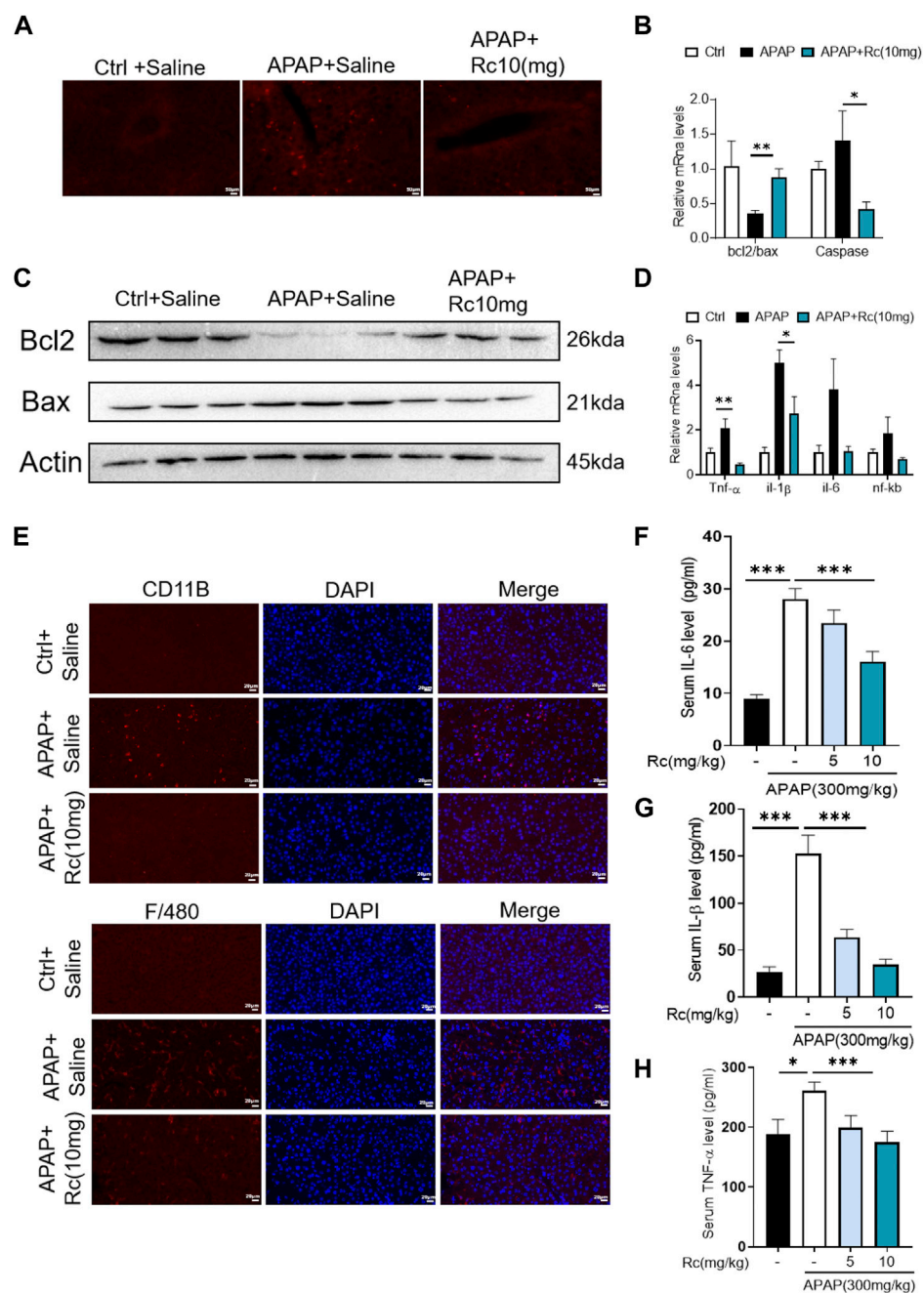


FIGURE 2

Ginsenoside Rc alleviated hepatic damage in ALI mice by regulating oxidative stress. (A) The survival rate of mice (with/without Ginsenoside Rc treatment) after intraperitoneal injection of APAP for 72 h (B) The ratio of liver weight/body weight; (C) Serum ALT and AST levels; (D) H&E staining of livers (1000x); (E) Hepatic GSH and SOD levels were reduced in APAP-induced mice after Ginsenoside Rc treatment; (F) Expression of mRNA levels of oxidative stress genes (Sod2, Gclc, Gclm); (G) Hepatic ROS levels were decreased in APAP-induced mice after Ginsenoside Rc treatment; (H) Relative expression of mRNA associated with APAP-metabolizing enzymes (Cyp3a11, Cyp2E, Ugt1a1); (I) The ELISA assay showed Ginsenoside Rc treatment decreased NAPQI levels in APAP-administrated mice. Data are means \pm SEM; n = 5-8/group. *, $p < 0.05$; **, $p < 0.01$; ***, $p < 0.001$.

**FIGURE 3**

Treatment with Ginsenoside Rc Effectively Alleviates APAP Overdose-Induced Inflammation and antiapoptosis (A) The TUNEL assay was performed to measure the apoptosis effect in APAP-induced mice; (B) Relative expression of mRNA associated with antiapoptosis (Caspase, Bcl2/Bax); (C) Ginsenoside Rc treatment inhibits the expression of the Bcl₂ protein and restrains the expression of Bax in mice; (D) Relative expression of mRNA associated with inflammation (IL-6, IL-1β, TNF-α); (E) The protein levels of F4/80 and CD11b were determined using immunofluorescence (1000X). The nuclei were stained with DAPI; (F–H) Serum pro-inflammatory cytokines, including TNF-α, IL-1β, and IL-6, were decreased in APAP-induced mice after Ginsenoside Rc treatment. Data are means ± SEM; n = 5–8/group. *, p < 0.05, **, p < 0.01, ***, p < 0.001.

Treatment with ginsenoside Rc effectively alleviates APAP overdose-induced inflammation and apoptosis

APAP overdose generates adducts with proteins in hepatocytes, which can lead to cell apoptosis. In the control injury model group, high-dose ginsenoside Rc treatment could significantly reduced the level of positive cell apoptosis marked by red fluorescence in TUNEL staining (Figure 3A). As shown in Figures 3B,C, APAP upregulates Bax and significantly reduces Bcl-2 expression at the mRNA level and in protein in liver tissue; however, ginsenoside Rc treatment can significantly protect mice from apoptosis induced by APAP excess, as TUNEL levels in liver were significantly reduced.

Acute liver injury can cause severe oxidative stress and trigger the liver's innate immune system, promoting the recognition and presentation of antigens by various immune and non-immune cells in liver tissue, thereby inducing persistent inflammatory responses and hepatocyte damage. We next analyzed serum levels of the proinflammatory cytokines TNF- α , IL-1 β , and IL-6 and hepatic mRNA levels of TNF- α , IL-1 β , and IL-6 in APAP-induced liver injury mice. We found that the markers of inflammatory monocytes F4/80 and CD11b showed significant increases. As shown in Figure 3E, mice with liver injury due to APAP showed higher levels of the serum, liver inflammatory factors TNF- α , IL-1 β , and IL-6 at the mRNA transcription level compared with the control group (Figures 3D,F–H). However, ginsenoside Rc treatment effectively suppressed the elevation of these inflammatory factors in the serum, and treatment with ginsenoside Rc significantly reduced hepatic transcription levels of TNF- α , IL-1 β , and IL-6. It can be seen that ginsenoside Rc can effectively inhibit the inflammatory response induced by APAP-induced acute liver injury in mice.

FXR serves as a candidate target for ginsenoside Rc against ALI

In order to further analyze the antagonism mechanism of ginsenoside Rc against ALI, we carried out a transcriptional analysis of liver tissue. Consistent with the above research conclusions, mice treated with APAP showed significant inhibition of the expression of FXR and its target genes SHP (NROB2) and BSEP (ABCB11). Genes involved in the antioxidation pathway, such as INOS(nos2) and genes related to APAP-metabolizing enzymes, such as UGT1(Slc35a2) and the CYP2E1 gene had decreased concentrations after exposure to Ginsenoside Rc, which has been shown to act by modulating hepatic metabolic enzymes and oxidative stress in ALI induced by APAP (Figures 4A,B). In addition, we carried out a more in-depth docking analysis of ginsenoside Rc and FXR, and the data show that the hydrophobic interaction can lead to a greater binding affinity (Figure 4C). In conclusion, this study concludes

that FXR is likely to be a new candidate target for altered expression.

After qPCR and the immunofluorescence analysis, it was again confirmed that Ginsenoside Rc can significantly increase the expression of FXR *in vivo* and *in vitro* (Figures 4D,E,H). As expected, Ginsenoside Rc increased FXR *via* inhibition of the expression levels of SHP (Supplementary Figure S2) and BSEP. APAP significantly reduced FXR expression at the protein and mRNA levels in liver tissue (Figures 4F, Supplementary Figure S6). However, mice treated with ginsenoside Rc can effectively reduce the damage caused by excessive APAP. We verified the knockout of FXR using qPCR and genotyping (Figures 4G, Supplementary Figure S3).

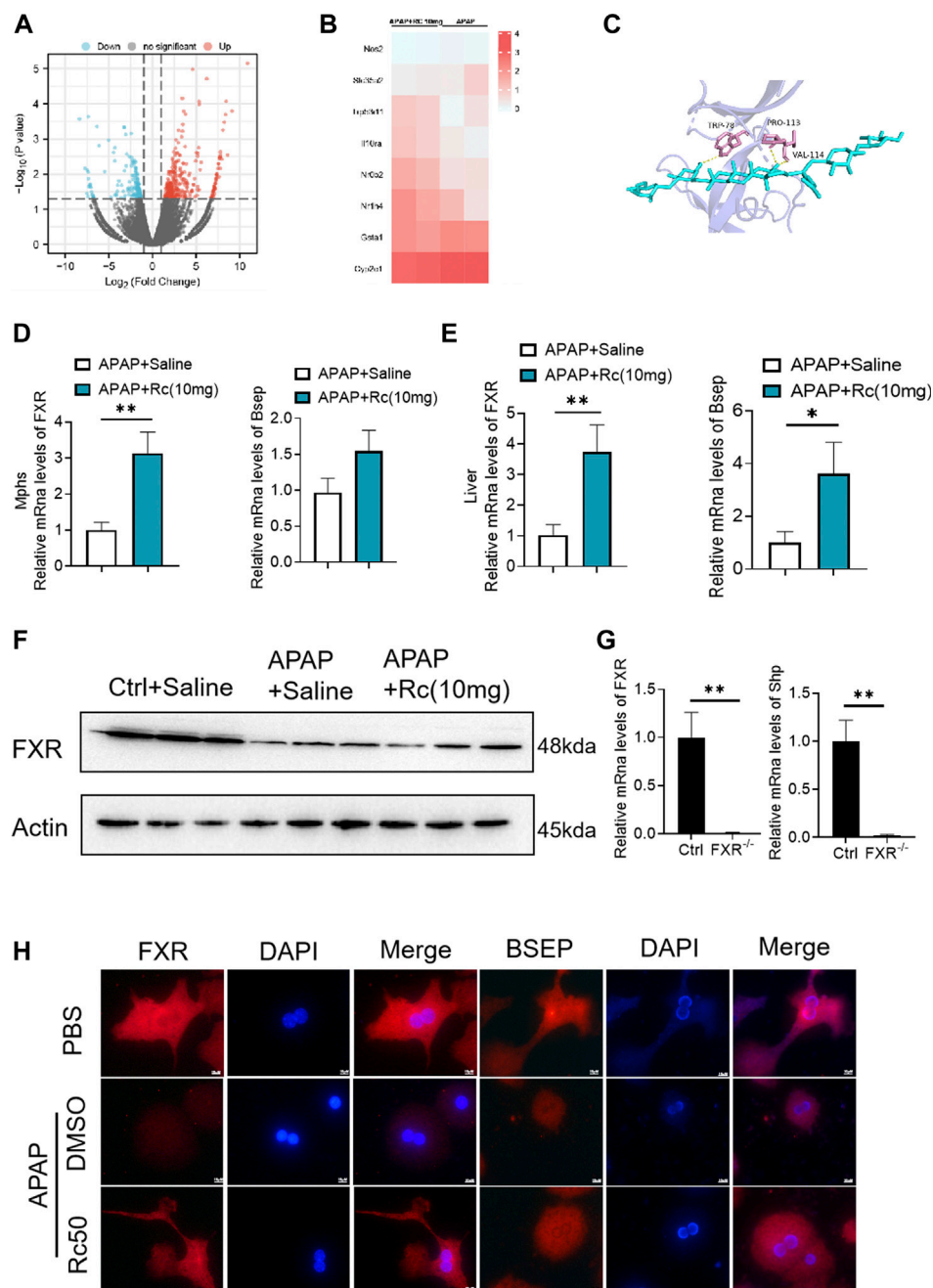
The absence of FXR abrogated the hepatoprotective effects of ginsenoside Rc against APAP overdose-induced ALI in MPHs

As can be seen from Figure 5A, the TUNEL levels in FXR^{-/-} MPH were not significantly changed after ginsenoside Rc treatment with or without APAP overdose. Furthermore, ginsenoside Rc was unable to remodel the expression of Bcl-2 and Bax in FXR^{-/-} MPHs (Figure 5B). However, in the absence of the FXR gene, the ROS-suppressive effect of ginsenoside Rc production was reduced with APAP exposure (Figure 5C), and even ginsenoside Rc treatment did not alter the antioxidant-determining effect of the FXR^{-/-} MPHs ability genes (Figure 5D). In FXR^{-/-} MPHs, although ginsenoside Rc also inhibited liver inflammation induced by APAP excess (Figure 5E), the effect was significantly weakened. APAP excess does not significantly alter the FXR^{-/-} MPH of TNF- α , IL-1 β , and IL-6 (Figure 5F). The level of NAPQI and its related genes also indicated that there are no differences in APAP-metabolizing enzymes (Figures 5G,H).

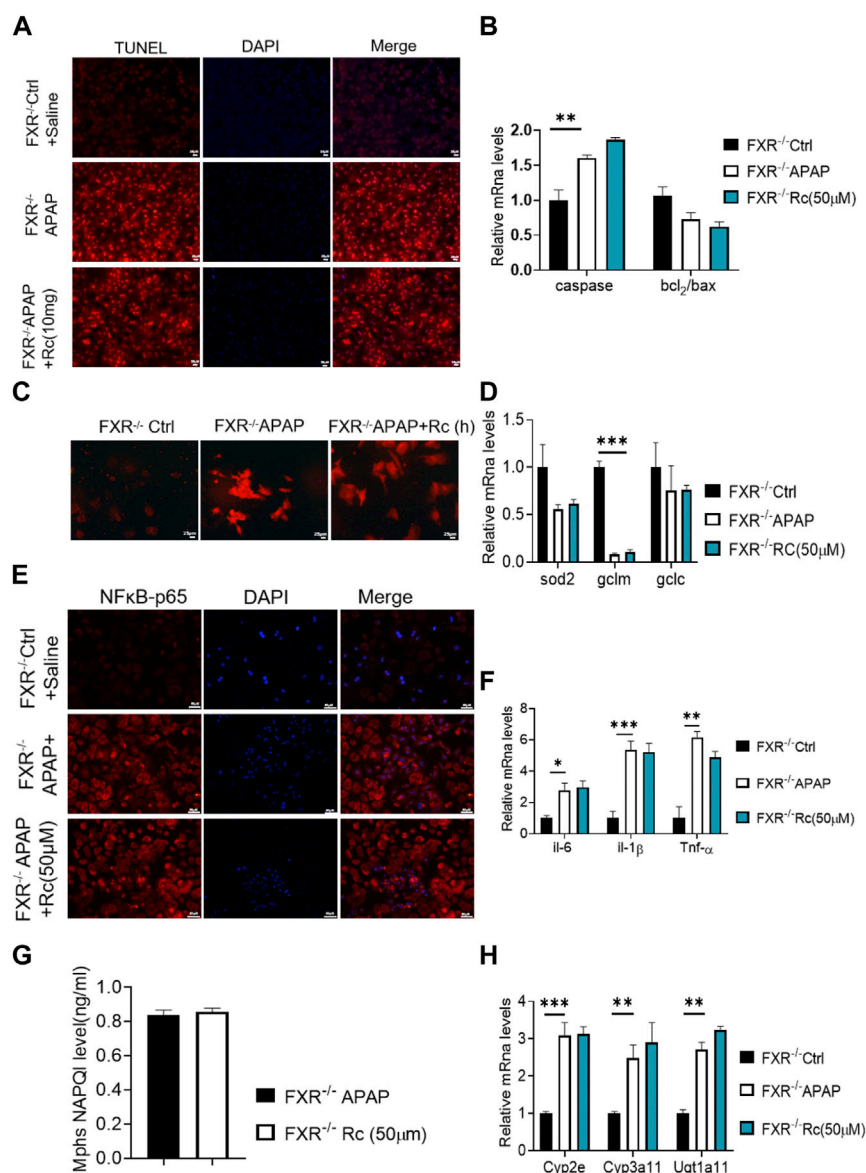
In summary, treatment with ginsenoside Rc did not alter liver genes involved in beta oxidation or APAP-metabolizing enzymes in FXR^{-/-} MPHs. Taken together, these data suggest that, in APAP-induced MPH injury, FXR is clearly dependent on ginsenoside Rc.

Ginsenoside Rc failed to alter the APAP-induced ROS burden in FXR-deficient mice

Similar to the elimination of APAP-induced production in KO MPHs by ginsenoside Rc, there was no significant difference in the survival rate of FXR^{-/-} mice (Figure 6A), and Ginsenoside Rc treatment failed to alter the ratio of liver tissue to body weight in FXR-deficient mice (Figure 6B). Additionally, in the absence of

**FIGURE 4**

FXR Serves as a Candidate Target for Ginsenoside Rc against ALI. (A,B) Heatmap of RNAseq on the liver from Ginsenoside Rc (10 mg/kg) - or saline-treated APAP-induced mice showing the changes in FXR and genes associated with APAP-metabolizing enzymes and antioxidant activity. (C) Ginsenoside Rc and FXR are bonded by hydrogen bonds; (D,E) Treatment of Ginsenoside Rc reduced the impairment in mRNA expression of FXR and FXR-dependent downstream target genes in liver tissue and MPHs. The mRNA levels of FXR were determined by qRT-PCR. (F) Treatment of Ginsenoside Rc reversed the downregulation of the protein levels of FXR in the liver tissue induced by APAP. (G) Relative expression of FXR mRNA in Fxr^{-/-} and Fxr^{+/+} mice. (H) The immunofluorescence data indicate that the protein levels of FXR and BSEP were increased in APAP-induced mice after Ginsenoside Rc treatment. (magnification: 1000x). The nucleus was stained with DAPI. Data are means \pm SEM; n = 5-8/group. *, $p < 0.05$; **, $p < 0.01$; ***, $p < 0.001$.

**FIGURE 5**

The absence of FXR abrogated the hepatoprotective effects of Ginsenoside Rc against APAP overdose-induced ALI in MPHs. (A) The TUNEL assay was performed to measure the apoptosis effect in FXR^{-/-} MPHs; (B) Ginsenoside Rc administration did not alter the genes involved in apoptosis in FXR^{-/-} MPHs; (C) ROS fluorescence in FXR^{-/-} MPHs; (D) Expression of mRNA levels of oxidative stress genes (Sod2, Gclc, Gclm) in FXR^{-/-} MPHs; (E) Immunofluorescence for NFκB- p65 (400x); (F) Ginsenoside Rc administration does not alter the genes involved in inflammation in FXR^{-/-} MPHs (Il-6, Il-1β, Tnf-α); (G) The ELISA assay showed that Ginsenoside Rc treatment does not alter the NAPQI levels in FXR^{-/-} MPHs. (H) Ginsenoside Rc administration does not alter the genes involved in APAP-metabolizing enzymes in FXR^{-/-} MPHs (Cyp3a11, Cyp2E, Ugt1a11); Data are means ± SEM; n = 5-8/group. *, $p < 0.05$, **, $p < 0.01$, ***, $p < 0.001$.

hepatic FXR, ginsenoside Rc treatment failed to alter hepatic AST and ALT levels (Figure 6C). Moreover, it could not effectively improve the necrotic area of hepatic histopathology in FXR^{-/-} mice (Figure 6D).

Moreover, hepatic antioxidants, such as SOD and GSH, were not altered by ginsenoside Rc in the absence of FXR (Figures 6E,F), as was shown for the expression levels of these

antioxidants at the mRNA level (Figure 6G). Ginsenoside Rc loses a significant protective effect against APAP-induced damage due to intrahepatic ROS production in mice with FXR (Figure 6H). Likewise, the NAPQI level and the genes related to APAP-metabolizing enzymes were not shown to be altered in FXR^{-/-} mice, even after Ginsenoside Rc treatment (Figures 6I,J).

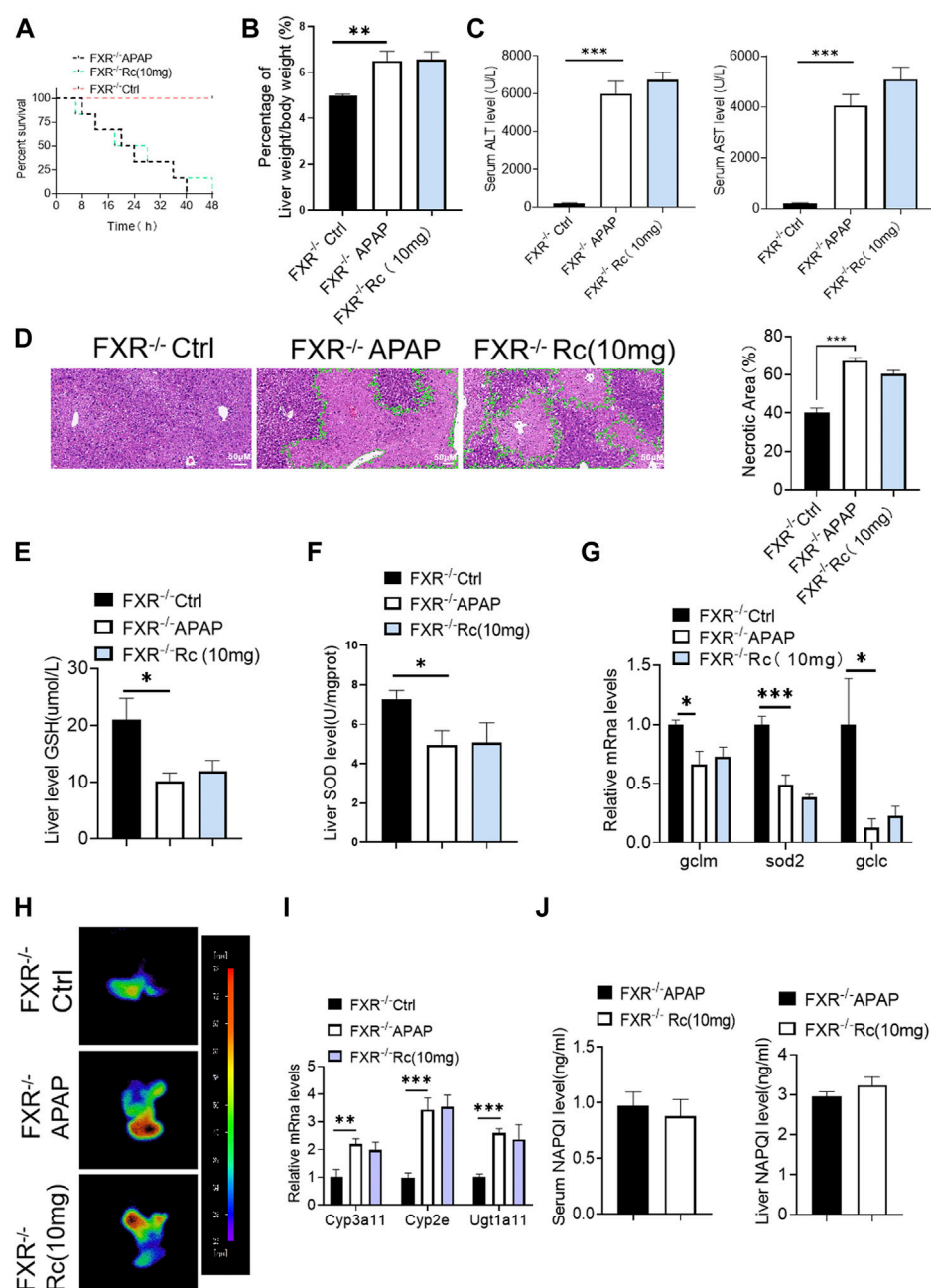


FIGURE 6

Ginsenoside Rc failed to alter the APAP-induced ROS burden in FXR^{-/-} mice. (A) The survival rate of FXR^{-/-} mice (with/without Ginsenoside Rc treatment) after intraperitoneal injection of APAP for 72 h. (B) The ratio of liver weight/body weight in FXR^{-/-} mice; (C) Serum ALT and AST levels in FXR^{-/-} mice; (D) H&E staining of FXR^{-/-} livers (1000x); (E–G) Ginsenoside Rc administration did not alter the GSH or SOD levels in FXR^{-/-} mice or the oxidative stress genes (Sod2, Gclc, Gclm); (H) ROS fluorescence in FXR^{-/-} mice; (I) Ginsenoside Rc administration did not alter the genes associated with APAP-metabolizing enzymes in FXR^{-/-} mice (Cyp3a11, Cyp2E, Ugt1a11); (J) The ELISA assay showed that Ginsenoside Rc treatment does not alter the NAPQI levels in FXR^{-/-} mice. Data are means ± SEM; n = 5–8/group. *, $p < 0.05$; **, $p < 0.01$; ***, $p < 0.001$.

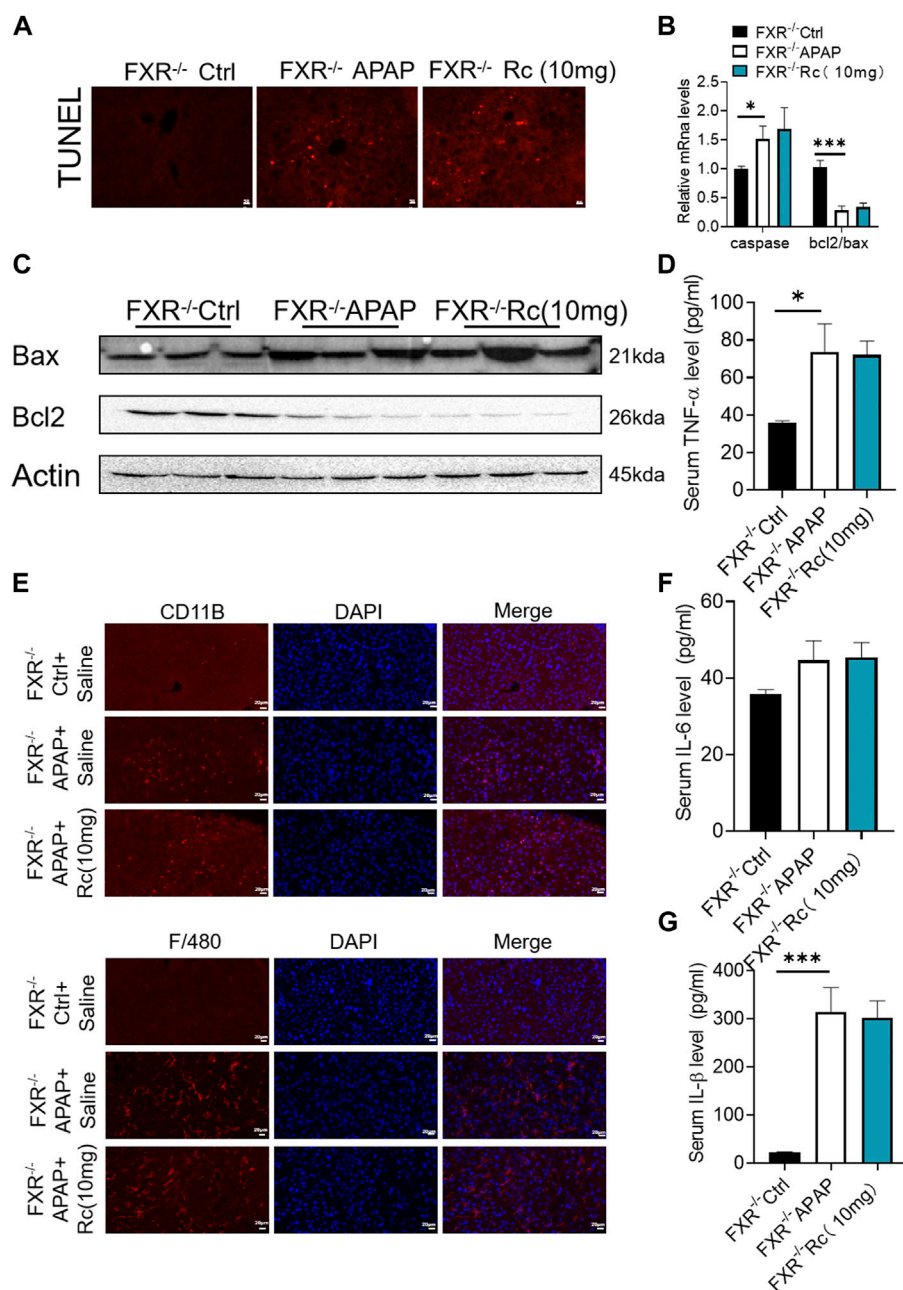


FIGURE 7

FXR^{-/-} diminished the effects of Ginsenoside Rc against APAP-induced by inflammation and antiapoptosis. (A) The TUNEL assay was performed to measure the apoptosis effect in FXR^{-/-} mice; (B,C) Ginsenoside Rc administration did not alter the genes involved in apoptosis in FXR^{-/-} mice; (D,F,G) Serum pro-inflammatory cytokines, including Tnf-α, IL-1β, and IL-6, were not altered in APAP-induced FXR^{-/-} mice after Ginsenoside Rc treatment; (E) The protein levels of F4/80 and CD11b were determined using immunofluorescence (1000X). The nuclei were stained with DAPI; Data are means ± SEM; *n* = 5–8/group. *, *p* < 0.05, **, *p* < 0.01, ***, *p* < 0.001.

Hepatic FXR deficiency diminished the effects of ginsenoside Rc against APAP-induced inflammation and antiapoptosis

In the earlier experiments, Ginsenoside Rc could not improve apoptosis and inflammation dependent on FXR under conditions of APAP-induced cellular damage in FXR^{-/-}MPHs. We further detected its effect *in vivo*. It was observed that ginsenoside Rc treatment with or without APAP overdose did not significantly alter TUNEL levels in FXR^{-/-} mice (Figure 7A). Moreover, Ginsenoside Rc was unable to alter the expression of Bcl-2 and Bax at the mRNA and protein levels (Figures 7B,C). The immunofluorescence experiments of F4/80 and CD11b showed that the improvement of hepatic inflammation with Ginsenoside Rc was abolished in FXR^{-/-} mice (Figure 7E). Moreover, for FXR^{-/-} mice, it was also difficult for ginsenoside Rc treatment to produce a significant inhibitory effect on liver inflammation caused by APAP excess. TNF- α , IL-1 β and IL-6 levels in FXR^{-/-} mice were not specifically changed after overdose of APAP (Supplementary Figure S4). The above-mentioned gene expression and Bax protein concentration were not significantly altered in FXR^{-/-} mice after ginsenoside Rc treatment (Figures 7D,F–G).

It was shown that Ginsenoside Rc lost its significant protective effect against liver damage in FXR^{-/-} mice compared with WT mice, suggesting that FXR plays an important regulatory role in the protection of ginsenoside Rc and APAP-induced acute liver injury.

Discussion

Acetaminophen (APAP), known as paracetamol, is commonly used as an analgesic, anti-inflammatory, and antipyretic drug (Cooper et al., 2017). Ingestion of APAP above the recommended dose can seriously damage liver tissue and even cause acute liver failure. According to the American acute liver failure research group, drug-induced liver injury in the US and most of Europe is largely caused by APAP overdose (Tujios and Lee, 2018). Many studies have concluded that the mechanism by which excessive APAP causes damage to hepatocytes is complicated but mainly involves oxidative stress, inflammatory cell infiltration, mitochondrial autophagy, and endoplasmic reticulum stress (Yang et al., 2017). Therefore, further exploration of the pathological mechanism associated with APAP-induced liver injury is urgently needed so that new therapeutic drugs can be developed.

Ginsenoside Rc is the main active component of ginseng and has become the main alternative for the treatment of liver diseases (Lee et al., 2019). We and others have previously confirmed the protective effects of Ginsenoside Rc against hepatitis and hepatic steatosis (Yang et al., 2020; Liang et al.,

2021b). However, whether and how Ginsenoside Rc affects acute liver injury is far from clear. Using FXR knockout (FXR^{-/-}) mice, mouse primary hepatocytes (MPHs), and RNA sequences, our current study is the first to show that the mechanism or pathway by which ginsenoside Rc reduces acetaminophen (APAP) overdose-induced hepatotoxicity involves the modulation of FXR-mediated antioxidative stress and anti-inflammatory and antiapoptotic functions.

Liver damage from APAP is likely to be caused by excessive n-acetylquinone imine (NAPQI) (Mohan et al., 2022). After a significant quantity of APAP has been ingested by the human body, it is processed through liver metabolism. APAP loses its activity by binding to sulfate and glucoside in the second stage of metabolism. A small portion of APAP is oxidized by cytochrome P450 enzymes (Glembotski et al., 2012), and converted to NAPQI, a highly active intermediate metabolite. Normally, NAPQI binds to glutathione (GSH) in the liver and is then degraded by the body. However, ingestion of a large amount of APAP bound with p-acetylphenol, sulfate, and glucosidic acid results in a significant quantity of APAP being oxidized by the P450 enzyme to produce a large quantity of NAPQI (Zhang Z. et al., 2022). Excessive NAPQI will consume a lot of glutathione in the liver. The remaining NAPQI reacts with the cell membrane, resulting in hepatocyte injury or death. Animal experiments have shown that liver glutathione consumption of greater than 70% will produce liver poisoning. With significant death of hepatocytes, oxidative stress and infectious inflammation in the liver are triggered (Cao et al., 2022). Oxidative stress and inflammation, in turn, aggravate liver damage, forming a vicious cycle (Elsayed et al., 2022). It can be seen that NAPQI is the key factor in liver injury caused by APAP. Inhibition of NAPQI synthase is also effective for treating APAP-induced liver injury. From our results, it can be found that Ginsenoside Rc can significantly reduce the synthesis of NAPQI synthase (Cyp2e, Cyp3a11, and Ugt1a11) in the liver injury model *in vivo* and *in vitro*, resulting in a decrease in the NAPQI content.

Mitochondrial protein, the key target of NAPQI, appears with excess APAP (Geib et al., 2021). Studies have shown that APAP can cause oxidative stress in the mitochondria and produce ROS through the percolation of electrons from the transport chain (Wang et al., 2021). Glutathione peroxidase (Glutathione Peroxidase, GSH-Px) and ATP synthase in mitochondria have been proven to bind to NAPQI (Kanno et al., 2017). When ATP synthase binds to NAPQI, GSH Px activity will decrease, resulting in the destruction of ATP synthesis and function. Mitochondrial complex I is a key target for ROS synthesis (Shi et al., 2021). In mice given APAP, the activity of mitochondrial complex I was found to increase accordingly (Barbier-Torres et al., 2017). There is an obvious positive relationship between the activity level of complex I and the degree of liver injury. Mitochondrial oxidative stress caused by APAP inevitably triggers cell death,

which in turn produces an inflammatory response (Geib et al., 2021). Oxidative stress in the mitochondria during the metabolic phase increases their permeability while releasing mitochondrial proteins which causing apoptosis of the factor AIF (Shi et al., 2021). Mitochondrial proteins undergo nuclear translocation, which results in cell death and nuclear DNA fragmentation. In the current research, Ginsenoside Rc was shown to significantly reduce the level of NAPQI (Geib et al., 2021). Low levels of NAPQI promote the alleviation of liver cell apoptosis, oxidative stress, and the inflammatory response.

In the process of APAP-induced acute liver injury, superoxide free radicals are formed (Ullah et al., 2021). Once formed, they decompose into hydrogen peroxide (HO) and oxygen in mitochondria or are converted to peroxynitrite (ONOO-) through a reaction mechanism with endogenous nitric oxide (NO) (Ogino et al., 2021). Subsequently, HO can be cleared by GSH, catalase (CAT), glutathione peroxidase (GPX), peroxide reductase (PRX), and other antioxidant enzymes in hepatocytes (Li et al., 2022). At the same time, ONOO- formed in mitochondria reacts with GSH and is eliminated. These excess free radicals lead to GSH depletion, cause the accumulation of ONOO-, and form nitrotyrosine protein adducts, which eventually leads to mitochondrial DNA damage and hepatotoxicity (Chau et al., 2022). At this stage, N-acetylcysteine (NAC) a glutathione supplement, is the only antidote in clinical use for the treatment of APAP-induced DILI. It mainly enhances the detoxification effect of NAQPI by supplementing GSH. However, the drug still has some defects, such as a narrow treatment window (Lewis et al., 2022). Generally speaking, the adverse reactions of NAC are not life-threatening, but they include nausea, vomiting and allergic reactions. The detoxification effect of NAC is mainly effective 8 h before APAP poisoning, and then the treatment effect begins to decline obviously. Therefore, further research is needed on new drugs and potential targets that can treat APAP liver injury, especially for those patients who appear in the late stage of liver damage. Many studies on natural products extracted from foods have revealed a great deal of molecules that can be used to resist APAP hepatotoxicity (Subramanya et al., 2018). This study found that Ginsenoside Rc significantly increased the mRNA level of GSH synthase (Sod2, Gclm, Gclc), thus increasing the content of GSH. GSH can participate in a variety of key biochemical reactions, and its function is to protect the sulfhydryl groups of key enzymatic proteins from oxidation and loss of activity, so that they can be utilized by cells and maintain normal energy metabolism. At the same time, the combination of sulfhydryl and free radicals in the body can promote the reduction of free radicals, and then convert them into acidic substances, thereby increasing the excretion rate of free radicals and reducing the damage done to key organs by free radicals. The early signal of apoptosis is often a decrease in the GSH content, and subsequent oxygen free radicals will accelerate apoptosis.

Both chronic and acute liver disease are characterized by inflammation. However, the role of inflammation in liver disease is two-sided. On the one hand, inflammation can promote the removal of cell debris, which is conducive to the proliferation and repair of liver cells (Chen et al., 2018). On the other hand, when numerous hepatocytes die, inflammation is produced, resulting in liver injury (Fernandez-Checa et al., 2021). As the inflammatory reaction continues, cytokines are released to mediate the infiltration of inflammatory cells. The collected inflammatory cells can further kill hepatocytes over a short period of time, while long-term inflammation will induce the formation of liver fibrosis. (Chayanupatkul and Schiano, 2020). Ultimately, a variety of inflammatory factors participate in the injury of liver tissue, either directly or indirectly. As a key inflammatory factor, TNF- α not only accompanies the occurrence and development of DILI but also its content is also positively correlated with the severity of DILI (Navaei-Alipour et al., 2021). At the same time, TNF- α can induce hepatocyte apoptosis directly by mediating TNF-R1, or indirectly by inducing the production of a variety of cytokines, to form a complex inflammatory factor network that aggravates the progression of liver injury (Navaei-Alipour et al., 2021). In addition, interleukin-1 (IL-1) is also a strong pro-inflammatory factor. It can induce neutrophils and vascular endothelial cells to express adhesion molecules, trigger the secretion of other inflammatory factors, and participate in inflammatory responses (Navaei-Alipour et al., 2021). Secondly, IL-6 has a wide range of biological activities, which can promote the proliferation and differentiation of B cells, leading to the production of antibodies, increasing the formation of immune complexes as well as causing an inflammatory reaction (Navaei-Alipour et al., 2021). In conclusion, the excessive production of these inflammatory factors aggravates the damage done to liver pathological tissue. Many research results have described the activation of signaling molecules, such as NF- κ B, MAPK and TXNIP/NLRP3, which participate in the inflammatory response and play important roles in liver injury. The levels of IL-1 β , TNF α and NF- κ B in hepatocytes are significantly and transiently increased following an overdose of APAP (Zhang C. et al., 2022). These elevated inflammatory factors promote the progression of the disease. In the current study, the levels of NAPQI, ROS, and inflammatory factors after APAP modeling differed from those of the normal group, which means the modeling was successful. After treatment with Ginsenoside Rc, the concentrations of ROS, and inflammatory factors (IL-1 β , TNF α , and NF- κ B) decreased significantly, resulting in decreased liver apoptosis (Bax, Bcl2, and p53) and enhanced liver repair.

FXR not only balances bile acids, but also has significant regulatory effects on lipid metabolism, glucose metabolism and other related links in the liver (Molinaro and Marschall, 2022). It plays an important role in the development of chronic liver disease. Moreover, FXR forms a complex regulatory network through

multiple signal pathways mediated by a cascade reaction signal pathway, G protein coupled receptor, cell surface receptor, and antigen receptor to protect the liver from damage due to pathogenic factors (Chiang et al., 2022). It was also confirmed that FXR can ensure that intestinal barrier function is maintained, preventing the formation of gallstones and reducing liver cholestasis, which may be based on the regulation of related genes affecting bile acid detoxification and drug metabolism by FXR (Norona et al., 2020). These genes mainly include phase I oxidases such as CYP3A4, phase II binding enzymes such as UGT2B4 and SULT2A1, and the phase I transporters MRP2 and ABCB4, which also affect the synthesis of NAPQI. From the above results, it can be seen that FXR may also affect the metabolic pathways of xenobiotics. At present, the FXR agonist 6-ECDCA, a therapeutic drug for primary biliary cirrhosis, has entered the clinical trial stage (Ho and Steinman, 2016). Similarly, another FXR agonist way-362450 is intended to treat nonalcoholic fatty liver and has also entered the clinical trial phase (Zhang et al., 2009). In a nutshell, FXR can enhance the synthesis of NAPQI, and reduce hepatic oxidative stress and the inflammatory response caused by DILI. Consistent with reports in the literature reports, our findings show that FXR can be used in the treatment of DILI. On the other hand, we also confirmed that Ginsenoside Rc, as an FXR agonist, plays a role in alleviating DILI. The detailed experimental evidence is as follows: 1) Molecular docking results showed that Ginsenoside Rc and FXR are well docked. 2) This study found that APAP leads to decreased expression of FXR and BSEP in the liver, but Ginsenoside Rc reverses this trend. BSEP can reduce the solubility of bile acids and eventually lead to cholestasis and liver injury. Some research suggests that BSEP is regulated by FXR. Activation of the FXR/BSEP signal axis can reduce oxidative stress and the inflammatory response in liver diseases such as cholestasis and liver cirrhosis. 3) The inhibition of APAP on SHP mRNA and protein expression can be reversed by ginsenoside Rc. The FXR-SHP axis can effectively regulate the metabolism of hepatic bile acids and lipids, liver immune inflammation, and tumor development. The efficacy of many FXR-SHP axis regulators has also been verified by clinical experiments. 4) We used FXR knockout mice and primary liver cells to clarify the therapeutic mechanism of ginsenoside Rc on APAP-induced liver injury using the APAP liver damage model *in vivo* and *in vitro*. The most compelling finding is that Ginsenoside Rc did not significantly reduce the APAP-metabolic enzymes, oxidative stress, and inflammatory response when FXR was knocked out *in vivo* or *in vitro*.

Ginseng is used as a medicine and food worldwide. Many studies have confirmed that ginseng has pharmacological effects such as reducing the oxidative stress response, improving atherosclerosis, improving the osteoblast survival rate, and inhibiting tumor cell growth (Sarhene et al., 2021). Furthermore, many studies have shown that ginseng can promote glucose and lipid metabolism and improve liver function (Hou et al., 2022). Ginsenoside is the main effective substance contained in ginseng. Additionally, our research group has done a lot of work on ginsenoside's effect on liver metabolism. Our previous works showed that Ginsenoside Rc can treat NAFLD by

activating the SIRT6 protein (Yang et al., 2020); Ginsenoside Rb1 and Ginsenoside Rb3 can alleviate the liver glycolipid model. Those mechanisms are related to the reduction of oxidative stress and inflammatory response. The experiment also showed that ginsenoside Rc could improve the transcription level of SIRT1 (Supplementary Figure S5), and based on our research group, we added the KLF16 experiment. KLF16 is also a protein closely related to liver damage. The use of KLF16^{-/-} MPHs suggested that the transcription level of SIRT1 by ginsenoside Rc was not obvious, indicating that KLF16 may be the upstream target of ginsenoside Rc acting on SIRT1, which provides ideas for further study of ginsenoside Rc on liver damage in the future.

In conclusion, our study presents for the first time reported that Ginsenoside Rc could act as an effective FXR activator and treatment of acetaminophen (APAP) overdose-induced liver injury by modulating FXR to produce anti-oxidative stress, anti-inflammatory, and anti-apoptotic functions. However, in this study, the in-depth mechanism of Ginsenoside Rc treating liver damage through FXR has not been further discussed such as APAP adduct protein, mitochondrial autophagy and oxidative stress, and a detailed molecular mechanism experiment will be carried out in the future.

Conclusion

In conclusion, our results provide direct evidence that Ginsenoside Rc can be considered a new FXR agonist that protects against APAP overdose-induced ALI in mice *via* the activation of FXR signaling. It works mainly by producing anti-inflammatory, antioxidant, and antiapoptotic effects. Our studies also confirmed that Ginsenoside Rc may be a promising compound for the treatment or relief of liver injury induced by APAP overdose.

Data availability statement

The original contributions presented in the study are included in the article/Supplementary Material, further inquiries can be directed to the corresponding authors.

Ethics statement

The animal study was reviewed and approved by the Animal Ethics Committee of Guangzhou University of Traditional Chinese Medicine.

Author contributions

YZ contributed to the project management and experimental design. ZP contributed to the study design and acquisition and

analysis of data. KT and YC contributed to the analysis and interpretation of data. GZ wrote the manuscript. TC, TL, and SD performed the experiments. XY, DZ, QW, and YG contributed to the study design and performed a critical revision of the manuscript. All the authors critically revised the manuscript and approved the final version. YG is the guarantor of this work.

Funding

This study was supported by the following funding sources: The Natural Science Foundation of China (81800738 and 82070891), the Science and Technology Key Program of Guangzhou (202002020032), and the science and innovation project of Guangzhou University of Chinese Medicine (A1-2606-21-429-001Z32).

Acknowledgments

We are grateful to Changhui Liu for providing the FXR knockout mice.

References

- Anakk, S., Watanabe, M., Ochsner, S. A., McKenna, N. J., Finegold, M. J., and Moore, D. D. J. T. J. o. c. i. (2011). Combined deletion of Fxr and Shp in mice induces Cyp17a1 and results in juvenile onset cholestasis. *J. Clin. Invest.* 121 (1), 86–95. doi:10.1172/JCI42846
- Baghdasaryan, A., Claudel, T., Gumhold, J., Silbert, D., Adorini, L., Roda, A., et al. (2011). Dual farnesoid X receptor/TGR5 agonist INT-767 reduces liver injury in the Mdr2-/- (Abcb4-/-) mouse cholangiopathy model by promoting biliary HCO output. *Hepatology* 54 (4), 1303–1312. doi:10.1002/hep.24537
- Barbier-Torres, L., Iruzubieta, P., Fernández-Ramos, D., Delgado, T. C., Taibo, D., Gutiérrez-de-Juan, V., et al. (2017). The mitochondrial negative regulator MCJ is a therapeutic target for acetaminophen-induced liver injury. *Nat. Commun.* 8 (1), 2068–2111. doi:10.1038/s41467-017-01970-x
- Bechmann, L. P., Kocabayoglu, P., Sowa, J. P., Sydor, S., Best, J., Schlattjan, M., et al. (2013). Free fatty acids repress small heterodimer partner (SHP) activation and adiponectin counteracts bile acid-induced liver injury in superobese patients with nonalcoholic steatohepatitis. *Hepatology* 57 (4), 1394–1406. doi:10.1002/hep.26225
- Cao, Y. -J., Huang, Z. -R., You, S. -Z., Guo, W. -L., Zhang, F., Liu, B., et al. (2022). The Protective Effects of Ganoderic Acids from *Ganoderma lucidum* Fruiting Body on Alcoholic Liver Injury and Intestinal Microflora Disturbance in Mice with Excessive Alcohol Intake. *Foods* 11 (7), 949.
- Chau, J. H., Zhang, R., Lee, M. M., Lam, K. W., Eric, Y. Y., Lam, J. W. Y., et al. (2022). A ratiometric theranostic system for visualization of ONOO-species and reduction of drug-induced hepatotoxicity. *Biomater. Sci.* 10, 1083–1089. doi:10.1039/d1bm01675j
- Chayanupatkul, M., and Schiano, T. D. J. C. i. L. D. (2020). Acute liver failure secondary to drug-induced liver injury. *Clin. Liver Dis.* 24 (1), 75–87. doi:10.1016/j.cld.2019.09.005
- Chen, D., Ni, H. M., Wang, L., Ma, X., Yu, J., Ding, W. X., et al. (2019a). p53 up-regulated modulator of apoptosis induction mediates acetaminophen-induced necrosis and liver injury in mice. *Hepatology* 69 (5), 2164–2179. doi:10.1002/hep.30422
- Chen, L., Deng, H., Cui, H., Fang, J., Zuo, Z., Deng, J., et al. (2018). Inflammatory responses and inflammation-associated diseases in organs. *Oncotarget* 9 (6), 7204–7218. doi:10.18632/oncotarget.23208
- Chen, L., Liu, Q., Tang, Q., Kuang, J., Li, H., Pu, S., et al. (2019b). Hepatocyte-specific Sirt6 deficiency impairs ketogenesis. *J. Biol. Chem.* 294 (5), 1579–1589. doi:10.1074/jbc.RA118.005309

Conflict of interest

The authors declare that the research was conducted in the absence of any commercial or financial relationships that could be construed as a potential conflict of interest.

Publisher's note

All claims expressed in this article are solely those of the authors and do not necessarily represent those of their affiliated organizations, or those of the publisher, the editors and the reviewers. Any product that may be evaluated in this article, or claim that may be made by its manufacturer, is not guaranteed or endorsed by the publisher.

Supplementary material

The Supplementary Material for this article can be found online at: <https://www.frontiersin.org/articles/10.3389/fphar.2022.1027731/full#supplementary-material>

- Chen, Y., Liu, K., Zhang, J., Hai, Y., Wang, P., Wang, H., et al. (2020). c-Jun NH2-terminal protein kinase phosphorylates the nrf2-ECH homology 6 domain of nuclear factor erythroid 2-related factor 2 and downregulates cytoprotective genes in acetaminophen-induced liver injury in mice. *Hepatology* 71 (5), 1787–1801. doi:10.1002/hep.31116
- Chiang, J. Y., Ferrell, J. M. J. M., and Endocrinology, C. (2022). Discovery of farnesoid X receptor and its role in bile acid metabolism. *Mol. Cell. Endocrinol.* 548, 111618. doi:10.1016/j.mce.2022.111618
- Cooper, T. E., Fisher, E., Anderson, B., Wilkinson, N. M., Williams, D. G., and Eccleston, C. J. C. D. o. S. R. (2017). Paracetamol (acetaminophen) for chronic non-cancer pain in children and adolescents. *Cochrane Database Syst. Rev.* 2017 (8), CD012539. doi:10.1002/14651858.CD012539.pub2
- Elsayed, H. E., Ebrahim, H. Y., Mady, M. S., Khattab, M. A., El-Sayed, E. K., and Moharram, F. A. J. o. E. (2022). Ethnopharmacological impact of *Melaleuca rugulosa* (Link) Craven leaves extract on liver inflammation. *J. Ethnopharmacol.* 292, 115215.
- Fernandez-Checa, J. C., Bagnaninchi, P., Ye, H., Sancho-Bru, P., Falcon-Perez, J. M., Royo, F., et al. (2021). Advanced preclinical models for evaluation of drug-induced liver injury—consensus statement by the European Drug-Induced Liver Injury. *Netw. [PRO-EURO-DILI-NET]* 75 (4), 935–959. doi:10.1016/j.jhep.2021.06.021
- Fiorucci, S., Distrutti, E., Bifulco, G., D'Auria, M. V., and Zampella, A. J. T. i. P. S. (2012). Marine sponge steroids as nuclear receptor ligands. *Trends Pharmacol. Sci.* 33 (11), 591–601. doi:10.1016/j.tips.2012.08.004
- Gao, R. Y., Wang, M., Liu, Q., Feng, D., Wen, Y., Xia, Y., et al. (2020a). Hypoxia-inducible factor-2α reprograms liver macrophages to protect against acute liver injury through the production of interleukin-6. *Hepatology* 71 (6), 2105–2117. doi:10.1002/hep.30954
- Gao, Z., Zhang, J., Wei, L., Yang, X., Zhang, Y., Cheng, B., et al. (2020b). The protective effects of imperatorin on acetaminophen overdose-induced acute liver injury. *Oxid. Med. Cell. Longev.* 2020, 8026838. doi:10.1155/2020/8026838
- Geib, T., Moghaddam, G., Supinski, A., Golizeh, M., and Sleno, L. J. F. i. C. (2021). Protein targets of acetaminophen covalent binding in rat and mouse liver studied by LC-MS/MS. *Front. Chem.* 9, 736788. doi:10.3389/fchem.2021.736788
- Glembotski, C. C., Thuerauf, D. J., Huang, C., Vekich, J. A., Gottlieb, R. A., and Doroudgar, S. J. J. o. B. C. (2012). Mesencephalic astrocyte-derived neurotrophic factor protects the heart from ischemic damage and is selectively secreted upon

- sarco/endoplasmic reticulum calcium depletion. *J Biol Chem.* 287 (31), 25893–25904.
- Hartmann, P., Hochrath, K., Horvath, A., Chen, P., Seebauer, C. T., Llorente, C., et al. (2018). Modulation of the intestinal bile acid/farnesoid X receptor/fibroblast growth factor 15 axis improves alcoholic liver disease in mice. *Hepatology* 67 (6), 2150–2166. doi:10.1002/hep.29676
- Ho, P. P., and Steinman, L. J. P. o. t. N. A. o. S. (2016). Obeticholic acid, a synthetic bile acid agonist of the farnesoid X receptor, attenuates experimental autoimmune encephalomyelitis. *Proc. Natl. Acad. Sci. U. S. A.* 113 (6), 1600–1605. doi:10.1073/pnas.1524890113
- Hou, Z., Song, F., Xing, J., Zheng, Z., Liu, S., and Liu, Z. J. J. o. E. (2022). Comprehensive fecal metabolomics and gut microbiota for the evaluation of the mechanism of Panax Ginseng in the treatment of Qi-deficiency liver cancer. *J. Ethnopharmacol.* 292, 115222. doi:10.1016/j.jep.2022.115222
- Huang, Q., Su, H., Qi, B., Wang, Y., Yan, K., Wang, X., et al. (2021). A SIRT1 activator, ginsenoside Rc, promotes energy metabolism in cardiomyocytes and neurons. *J. Am. Chem. Soc.* 143 (3), 1416–1427. doi:10.1021/jacs.0c10836
- Jeon, J.-H., Lee, S., Lee, W., Jin, S., Kwon, M., Shin, C. H., et al. (2020). Herb–Drug interaction of red ginseng extract and ginsenoside Rc with valsartan in rats. *Molecules* 25 (3), 622. doi:10.3390/molecules25030622
- Kanno, S.-I., Tomizawa, A., Yomogida, S., and Hara, A. J. I. J. o. M. M. (2017). Glutathione peroxidase 3 is a protective factor against acetaminophen-induced hepatotoxicity *in vivo* and *in vitro*. *Int. J. Mol. Med.* 40 (3), 748–754. doi:10.3892/ijmm.2017.3049
- Kim, J.-K., Cui, C.-H., Liu, Q., Yoon, M.-H., Kim, S.-C., and Im, W.-T. J. F. c. (2013). Mass production of the ginsenoside Rg3 (S) through the combinative use of two glycoside hydrolases. *Food Chem.* 141 (2), 1369–1377. doi:10.1016/j.foodchem.2013.04.012
- Lee, H., Heo, J.-K., Lee, G.-H., Park, S.-Y., Jang, S.-N., Kim, H.-J., et al. (2019). Ginsenoside Rc is a new selective UGT1A9 inhibitor in human liver microsomes and recombinant human UGT isoforms. *Drug Metab. Dispos.* 47 (12), 1372–1379. doi:10.1124/dmd.119.087965
- Lewis, J., Lim, M., Lai, L., Mendoza, E., Albertson, T., and Chenoweth, J. J. C. T. (2021). Evaluation of N-acetylcysteine dose for the treatment of massive acetaminophen ingestion. *Clin. Toxicol.* 60 (4), 507–513. doi:10.1080/15563650.2021.1984503
- Li, J., Gao, Y., Cui, L., He, H., Zheng, J., Mo, S., et al. (2022). Combination of monoammonium glycyrrhizinate and cysteine hydrochloride protects mice against acetaminophen-induced liver injury via Keap1/Nrf2/ARE pathway. *J. Pharm. Pharmacol.* 74, 730. doi:10.1093/jpp/rgab180
- Liang, W., Zhou, K., Jian, P., Chang, Z., Zhang, Q., Liu, Y., et al. (2021b). Ginsenosides improve nonalcoholic fatty liver disease *via* integrated regulation of gut microbiota, inflammation and energy homeostasis. *Front. Pharmacol.* 12, 622841. doi:10.3389/fphar.2021.622841
- Liu, M., Zhang, G., Song, M., Wang, J., Shen, C., Chen, Z., et al. (2020). Activation of farnesoid X receptor by sphaetoside ameliorates acetaminophen-induced hepatotoxicity by modulating oxidative stress and inflammation. *Antioxid. Redox Signal.* 33 (2), 87–116. doi:10.1089/ars.2019.7791
- Mohan, S., Koziatke, C., Swartz, J., Howland, M. A., and Su, M. K. J. C. T. (2022). Thromboelastography in the setting of acetaminophen-induced hepatotoxicity. *Clin. Toxicol. (Phila)* 60, 651. doi:10.1080/15563650.2021.2016797
- Molinaro, A., and Marschall, H.-U. J. B. S. T. (2022). Bile acid metabolism and FXR-mediated effects in human cholestatic liver disorders. *Biochem. Soc. Trans.* 50 (1), 361–373. doi:10.1042/BST20210658
- Navaei-Alipour, N., Mastali, M., Ferns, G. A., Saberi-Karimian, M., and Ghayour-Mobarhan, M. J. P. R. (2021). The effects of honey on pro- and anti-inflammatory cytokines: A narrative review. *Phytother. Res.* 35 (7), 3690–3701. doi:10.1002/ptr.7066
- Norona, L. M., Fullerton, A., Lawson, C., Leung, L., Brumm, J., Kiyota, T., et al. (2020). *In vitro* assessment of farnesoid X receptor antagonism to predict drug-induced liver injury risk. *Arch. Toxicol.* 94 (9), 3185–3200. doi:10.1007/s00204-020-02804-4
- Ogino, N., Nagaoka, K., Tomizuka, K., Matsuura-Harada, Y., Eitoku, M., Suganuma, N., et al. (2021). Compromised glutathione synthesis results in high susceptibility to acetaminophen hepatotoxicity in acatalasemic mice. *Food Chem Toxicol.* 156, 112509
- Sarhene, M., Ni, J. Y., Duncan, E. S., Liu, Z., Li, S., Zhang, J., et al. (2021). Ginsenosides for cardiovascular diseases; update on pre-clinical and clinical evidence, pharmacological effects and the mechanisms of action. *Pharmacol. Res.* 166, 105481. doi:10.1016/j.phrs.2021.105481
- Shi, L., Wang, Y., Zhang, C., Zhao, Y., Lu, C., Yin, B., et al. (2021). An acidity-unlocked magnetic nanoplatfrom enables self-boosting ROS generation through upregulation of lactate for imaging-guided highly specific chemodynamic therapy. *Angew. Chem. Int. Ed. Engl.* 60 (17), 9562–9572. doi:10.1002/anie.202014415
- Soeda, J., Mouralidarane, A., Ray, S., Novelli, M., Thomas, S., Roskams, T., et al. (2014). The beta adrenoceptor agonist isoproterenol rescues acetaminophen injured livers through increasing progenitor numbers by Wnt in mice. *Hepatology* 60 (3), 1023–1034.
- Subramanya, S. B., Venkataraman, B., Meeran, M. F. N., Goyal, S. N., Patil, C. R., and Ojha, S. J. I. J. o. M. S. (2018). Therapeutic potential of plants and plant derived phytochemicals against acetaminophen-induced liver injury. *Int. J. Mol. Sci.* 19 (12), 3776. doi:10.3390/ijms19123776
- Sun, N., Shen, C., Zhang, L., Wu, X., Yu, Y., Yang, X., et al. (2021). Hepatic Krüppel-like factor 16 (KLF16) targets PPARα to improve steatohepatitis and insulin resistance. *Gut* 70 (11), 2183–2195. doi:10.1136/gutjnl-2020-321774
- Tsai, M.-S., Chien, C.-C., Lin, T.-H., Liu, C.-C., Liu, R. H., Su, H.-L., et al. (2015). Galangin prevents acute hepatorenal toxicity in novel propacetamol-induced acetaminophen-overdosed mice. *J. Med. Food* 18 (11), 1187–1197. doi:10.1089/jmf.2014.3328
- Tujios, S. R., and Lee, W. M. J. L. I. (2018). Acute liver failure induced by idiosyncratic reaction to drugs: Challenges in diagnosis and therapy. *Liver Int.* 38 (1), 6–14. doi:10.1111/liv.13535
- Ullah, H., Lee, Y. Y., Kim, M., Kim, T.-W., Saba, E., Kwak, Y.-S., et al. (2021). Red ginseng oil attenuates oxidative stress and offers protection against ultraviolet-induced photo toxicity. *Oxid. Med. Cell Longev.* 2021, 5538470. doi:10.1155/2021/5538470
- Wang, Y., Zhao, Y., Wang, Z., Sun, R., Zou, B., Li, R., et al. (2021). Peroxiredoxin 3 inhibits acetaminophen-induced liver pyroptosis through the regulation of mitochondrial ROS. *Front. Immunol.* 12, 652782. doi:10.3389/fimmu.2021.652782
- Yang, G., Zhang, L., Ma, L., Jiang, R., Kuang, G., Li, K., et al. (2017). Glycyrrhetic acid prevents acetaminophen-induced acute liver injury via the inhibition of CYP2E1 expression and HMGB1-TLR4 signal activation in mice. *Int. Immunopharmacol.* 50, 186–193. doi:10.1016/j.intimp.2017.06.027
- Yang, Z., Yu, Y., Sun, N., Zhou, L., Zhang, D., Chen, H., et al. (2020). Ginsenosides Rc, as a novel SIRT6 activator, protects mice against high fat diet induced NAFLD. *J. Ginseng Res.* doi:10.1016/j.jgr.2020.07.005
- Yin, H., Cheng, L., Holt, M., Hail, N., Jr, MacLaren, R., and Ju, C. J. H. (2010). Lactoferrin protects against acetaminophen-induced liver injury in mice. *Hepatology* 51 (3), 1007–1016. doi:10.1002/hep.23476
- Zhang, C., Lin, J., Zhen, C., Wang, F., Sun, X., Kong, X., et al. (2022a). Amygdalin protects against acetaminophen-induced acute liver failure by reducing inflammatory response and inhibiting hepatocyte death. *Biochem. Biophys. Res. Commun.* 602, 105–112. doi:10.1016/j.bbrc.2022.03.011
- Zhang, S., Wang, J., Liu, Q., and Harnish, D. C. J. J. o. h. (2009). Farnesoid X receptor agonist WAY-362450 attenuates liver inflammation and fibrosis in murine model of non-alcoholic steatohepatitis. *J. Hepatol.* 51 (2), 380–388. doi:10.1016/j.jhep.2009.03.025
- Zhang, Z., Yao, T., Zhao, N., Liu, H., Cheng, H., Gonzalez, F. J., et al. (2022b). Disruption of peroxisome proliferator-activated receptor α in hepatocytes protects against acetaminophen-induced liver injury by activating the IL-6/STAT3 pathway. *Int. J. Biol. Sci.* 18 (6), 2317–2328. doi:10.7150/ijbs.69609



OPEN ACCESS

EDITED BY

Shuai Wang,
Guangzhou University of Chinese
Medicine, China

REVIEWED BY

Daijie Wang,
Qilu University of Technology, China
Xiang Luo,
Guangzhou University of Chinese
Medicine, China

*CORRESPONDENCE

Denglang Zou,
dlangzou@foxmail.com
Yulin Li,
liyulin@nwipb.cas.cn
Liangliang He,
heliangliang5878@163.com
Duojie Longzhu,
850002632@qq.com

[†]These authors have contributed equally
to this work

SPECIALTY SECTION

This article was submitted to
Inflammation Pharmacology,
a section of the journal
Frontiers in Pharmacology

RECEIVED 14 September 2022

ACCEPTED 10 October 2022

PUBLISHED 19 October 2022

CITATION

Zou D, Wang Q, Chen T, Sang D, Yang T,
Wang Y, Gao M, He F, Li Y, He L and
Longzhu D (2022), Bufadienolides
originated from toad source and their
anti-inflammatory activity.
Front. Pharmacol. 13:1044027.
doi: 10.3389/fphar.2022.1044027

COPYRIGHT

© 2022 Zou, Wang, Chen, Sang, Yang,
Wang, Gao, He, Li, He and Longzhu. This
is an open-access article distributed
under the terms of the [Creative
Commons Attribution License \(CC BY\)](#).
The use, distribution or reproduction in
other forums is permitted, provided the
original author(s) and the copyright
owner(s) are credited and that the
original publication in this journal is
cited, in accordance with accepted
academic practice. No use, distribution
or reproduction is permitted which does
not comply with these terms.

Bufadienolides originated from toad source and their anti-inflammatory activity

Denglang Zou^{1,2,3†*}, Qiqi Wang^{2†}, Tao Chen³, Duocheng Sang¹,
Tingqin Yang¹, Yuhan Wang¹, Mengze Gao¹, Fangfang He¹,
Yulin Li^{3*}, Liangliang He^{2*} and Duojie Longzhu^{1*}

¹School of Life Science, Qinghai Normal University, Xining, China, ²College of Pharmacy, Jinan University, Guangzhou, China, ³Northwest Institute of Plateau Biology, Chinese Academy of Sciences, Xining, China

Bufadienolide, an essential member of the C-24 steroid family, is characterized by an α -pyrone positioned at C-17. As the predominantly active constituent in traditional Chinese medicine of Chansu, bufadienolide has been prescribed in the treatment of numerous ailments. It is a specifically potent inhibitor of Na^+/K^+ ATPase with excellent anti-inflammatory activity. However, the severe side effects triggered by unbiased inhibition of the whole-body cells distributed $\alpha 1$ -subtype of Na^+/K^+ ATPase, restrict its future applicability. Thus, researchers have paved the road for the structural alteration of desirable bufadienolide derivatives with minimal adverse effects via biotransformation. In this review, we give priority to the present evidence for structural diversity, MS fragmentation principles, anti-inflammatory efficacy, and structure modification of bufadienolides derived from toads to offer a scientific foundation for future in-depth investigations and views.

KEYWORDS

toad sourced bufadienolide, structure diversity, MS fragmentation principles, anti-inflammatory activity, structure modification

Introduction

Bufadienolide, an essential member of the C-24 steroid family, is characterized by an α -pyrone (six-membered lactone) ring positioned at C-17 (Gao et al., 2011). In 1933, the first bufadienolide, namely Scillaren A, was isolated and identified from Egyptian squill (Stoll et al., 1933). Since then, this class of steroid has become a research hotspot, piquing the interest of researchers worldwide, to promote the isolation and identification of bufadienolide with structural diversity (Steyn and van Heerden 1998). Currently, an increasing number of bufadienolides were originally characterized from the traditional Chinese medicine of ChanSu which is one of the richest sources of bufadienolides (Rodríguez et al., 2017; Wei et al., 2019; Pearson and Tarvin 2022). Another notable source is venom from toads (Bufonidae), such as *Bufo bufo gargarizans* Cantor (Zhan et al., 2020), *Rhinella marina* (Hayes et al., 2009), and *Bufo melanostictus* Schneider (Verpoorte and Svendsen 1979; Verpoorte and Svendsen 1980).

Remarkable progress, in terms of pharmacology and the potential of bufadienolide as a therapeutic agent, has been achieved in recent years. Importantly, bufadienolide exhibited significant antitumor and anti-inflammatory activity (Ogawa et al., 2009; Kanai et al., 2013). The pharmacological mechanism behind bufadienolide was the alteration of intracellular calcium concentration, which was triggered by its potent inhibition of Na^+/K^+ ATPase (Holmgren et al., 2000). When calcium ion accumulates within the appropriate concentration range in the body, bufadienolide displays the desired biological properties, such as anticancer and anti-inflammatory activity. However, if the calcium ion accumulates in a manner far beyond the threshold concentration, it might result in rather severe toxicity. Brilliantly, some creatures utilized the toxic bufadienolide as chemical defense weapons to highlight its ecological value, which was given by its powerful Na^+/K^+ ATPase inhibitory activity. Unarmed animals, such as fireflies and Asian snakes, have been found to sequester and store numerous bufadienolides for defensive purposes (Dobler et al., 2012; Petschenka and Agrawal 2015; Ujvari et al., 2015; Mohammadi et al., 2016; Smedley et al., 2017; Bókonyi et al., 2018).

Promisingly, an increasing number of researchers have concentrated on the anti-inflammatory properties of bufadienolide in recent years. In the 1960s, the anti-inflammatory activity of bufadienolide was firstly documented (Lancaster and Vega 1967). After that, numerous investigations have verified the anti-inflammatory effect of bufadienolide, as demonstrated by a reduction in inflammatory symptoms in various animal models of acute and chronic inflammation (Esposito 1985; de Vasconcelos et al., 2011; Fürst et al., 2017). To discover the underlying mechanisms, the majority of studies have focused on leukocytes. It was found that bufadienolide exhibited anti-inflammation activity by primarily inhibiting cell proliferation and the secretion of proinflammatory cytokines (Forshammar et al., 2011; Forshammar et al., 2013).

However, some nonnegligible drawbacks, including high toxicity, low bioavailability, and poor water solubility of bufadienolide, severely restrict its further applications (Deng et al., 2017; Fu et al., 2019; Shao et al., 2021). Hence, it is particularly essential to find effective ways for structural modification of bufadienolide with the potential to both lower toxicity and increase or at least keep activity. Although chemical synthesis is usually the go-to option (Michalak et al., 2017; Shimizu et al., 2020; Wu et al., 2020), it is severely hindered by factors beyond the control, such as chemical waste, tedious protection and deprotection steps, unsatisfied synthesis yield accompanied with undesired by-products. Biosynthesis, on the other hand, has been emerged and recognized as an outstanding alternative to conquer these obstacles due to its eco-friendly and cost-effective qualities (Heasley 2012; Huang et al., 2019; Hoshino and Gaucher 2021; Pavesi et al., 2021). In the field of biosynthesis, glycosylation may be a mainstream method for

bufadienolide structure modification (Thorson and Vogt 2003; Zhou et al., 2012). Bufadienolide glycosylation generally refers to the enzyme catalysis process to attach glycans at their C-3 position. It was not until 2007 that Thorson performed the first successful enzyme catalytic glycosylation of cardiac steroids (Williams et al., 2007; Gantt et al., 2008). An actinomycete-sourced glycosyltransferase OleD and its practical mutant ASP with substrate heterogeneity were discovered through high-throughput screening to perform cardiac steroid glycosylation. Accordingly, Wen et al. further discovered that C-3 glycosylation of bufadienolide could be accomplished by a glycosyltransferase called UGT74AN1 in an environmentally friendly and highly effective manner (Wen et al., 2018).

The characters, in terms of attractive structure diversity and promising biological activity, make bufadienolide a hot research topic. In the present review, we primarily analyzed and reviewed the current evidence for structure diversity, MS fragmentation principles, anti-inflammatory activity and structure modification of bufadienolides originated from toad source to provide a scientific basis for future in-depth studies and perspectives of potential drug candidates discovery.

Structure diversity

Structurally, toad-sourced bufadienolide could be classified into two groups: free bufadienolide and conjugated bufadienolide. The steroid core of free bufadienolide is replaced with a variable amount of hydroxyl groups. For conjugated bufadienolide, it is defined by esterification of hydroxyl group at C-3 position with specific groups, including argininy side chain, lactic acid and sulfonic acid. The typical structures of free bufadienolide and conjugated bufadienolide were shown in Figure 1A.

Free bufadienolide

Unsubstituted α or β hydroxyl groups at the C-3 position are the distinguishing features of free bufadienolide. Depending on whether the C-14 position is substituted by a β -OH or the C-14, 15 positions form a β -epoxy structure, free bufadienolide could be divided into two categories (Group 1 and Group 2 in Figure 1B), which could be further classified into five sub-categories based on the contained function groups (hydroxy, aldehyde, carbonyl, etc.) (Figure 1B). It was reported that at least 75 free bufadienolides (**I**–**75**) have been identified (Li et al., 2015; Rodríguez et al., 2017; Wei et al., 2019; Zhan et al., 2020), whose chemical structures were shown in Figure 2.

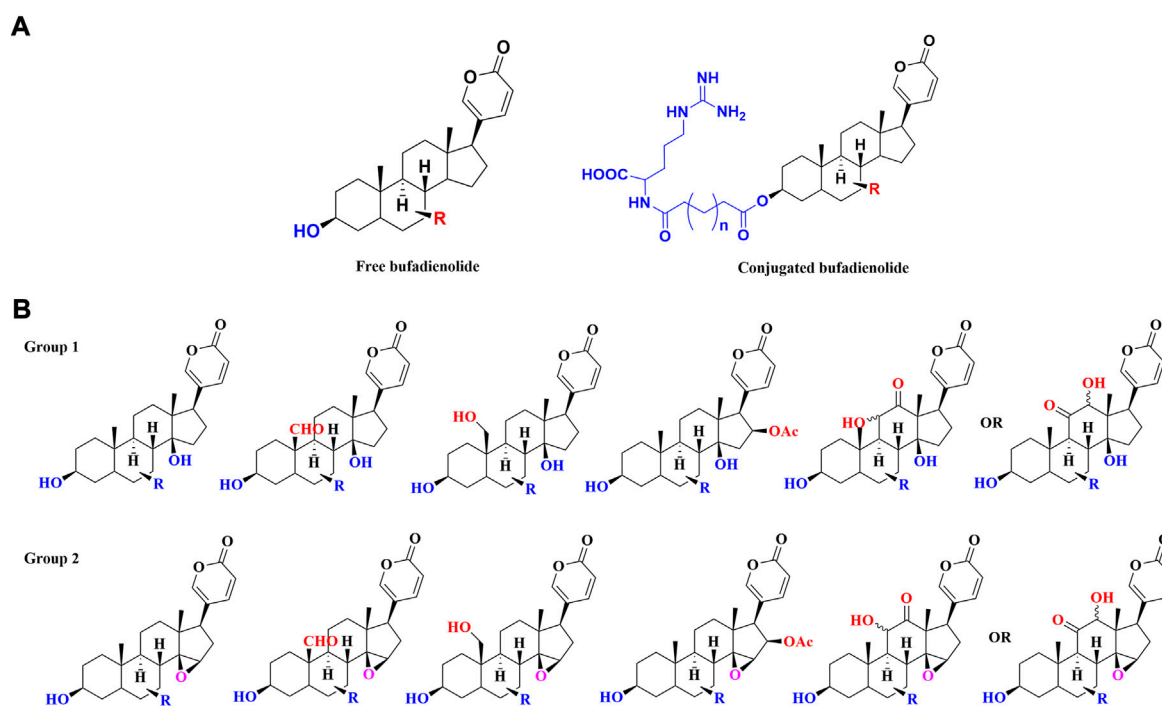


FIGURE 1

The classification of toad-sourced bufadienolide: (A) The typical structures of free bufadienolide and conjugated bufadienolide; (B) The typical structures of five sub-categories of free bufadienolide according to the contained substituents.

In recent years, the finding of free bufadienolide with 3 α -OH configuration in toad bile, the epimer of the ubiquitously disseminated free bufadienolides with 3 β -OH configuration, has merited our attention (Zou et al., 2018). Generally, free bufadienolide with 3 α -OH configuration originated from microbial transformation or animal metabolism (Zhang et al., 2011; Bhatti and Khera 2012; Hegazy et al., 2015; Wei et al., 2022), whose natural occurrence is quite rare. Our group isolated and identified eleven free bufadienolides (76–86) with 3 α -OH configuration from the bile of *Bufo gargarizans* (unpublished data) (Figure 2).

With the development of chromatography technology and unremitting efforts of researchers (Guillarme et al., 2010), novel structures or new backbone type of free bufadienolide have continued to be discovered. Specifically, six free bufadienolides of new backbone type (Matsukawa et al., 1996; Matsukawa et al., 1997; Tian et al., 2010; Tian et al., 2017), namely Bufogargarizins A, Bufogargarizins B, Bufogargarizins C, Bufospirostenin A, Marinosin and Marinosin acid (87–92), were discovered and isolated from *Bufo sinensis* and Cane toad. Meanwhile, a rare series of 20, 21-epoxybufenolides (Nogawa et al., 2001; Kamano et al., 2002; Chen et al., 2015; Chen et al., 2018), namely 20S, 21-epoxyresibufogenin, 20R, 21-epoxyresibufogenin and 20S,

21R-epoxymarinobufagin (93–95), were discovered and isolated from the Brazilian toad *Rhinella schneideri* (Figure 2).

Conjugated bufadienolide

The substitution of C-3 hydroxyl group is the defining property of conjugated bufadienolide, which often appears in a form of ester (Figure 3), including sulfonic acid, amino acid, fatty acid and arginine diacyl chain esterification (Gao et al., 2010; Zhou et al., 2017; Zhou et al., 2021).

Eight conjugated bufadienolides that C-3 position esterized with fatty acid from the egg of *Bufo bufo gargarizans* were isolated and identified by Zhang et al. (96–103) (Zhang et al., 2016). Besides, three unusual conjugated bufadienolides were separated from the ovaries of *Bufo marinus* (104–106) (Matsukawa et al., 1998). Zhou et al. isolated and identified three pairs of epimers in which the C-3 hydroxyl groups were substituted by lactic acid from the egg of *Bufo bufo gargarizans* (107–112) (Zhou et al., 2017). It was the first time to reveal the racemization of lactate in amphibians.

Gao et al. isolated and identified five sulfonated bufadienolides from the venom of *Bufo Melanostictus* by the joint use of LC-DAD-MSⁿ and LC-SPE-NMR (113–117) (Gao

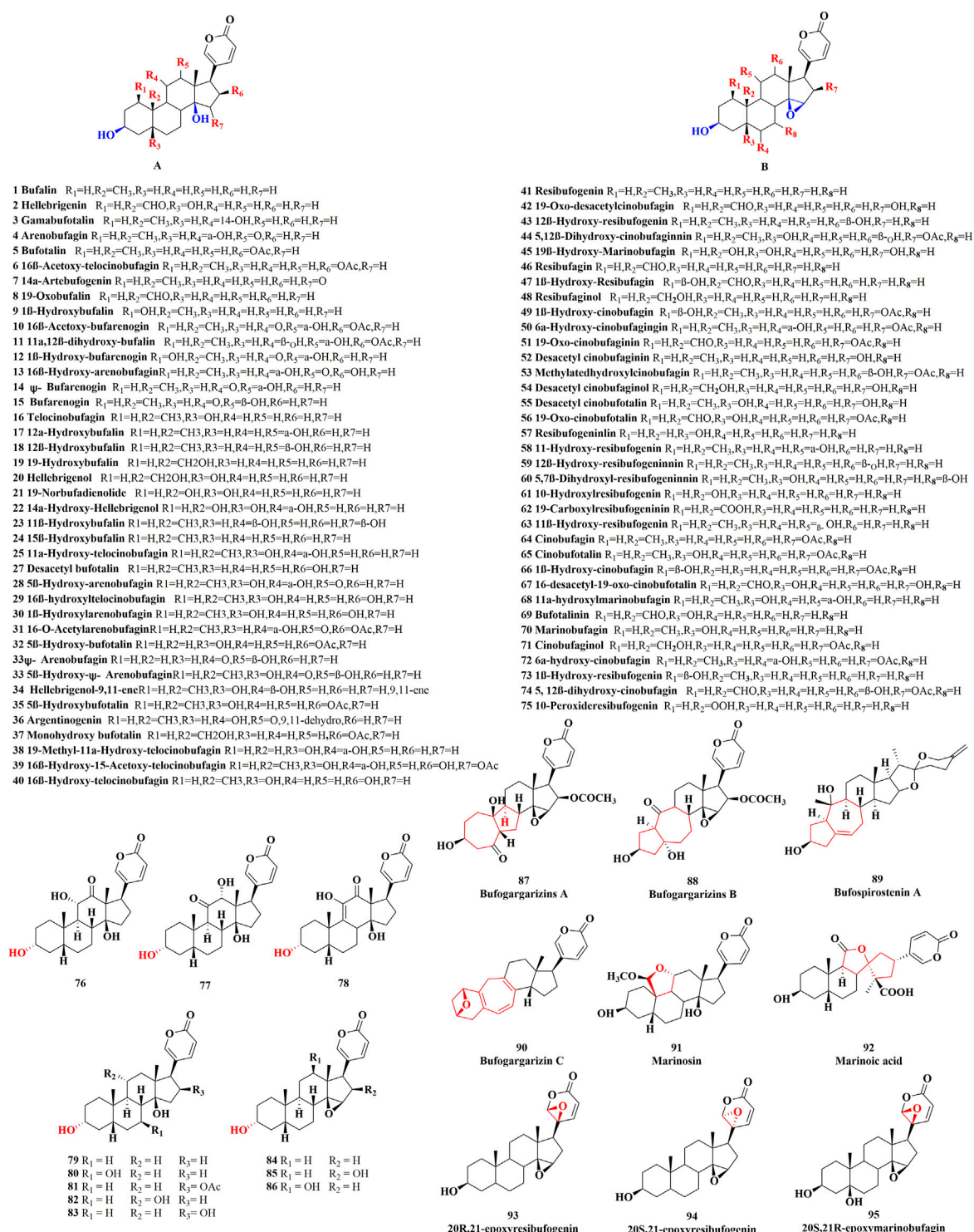


FIGURE 2

The chemical structures of reported free bufadienolide.

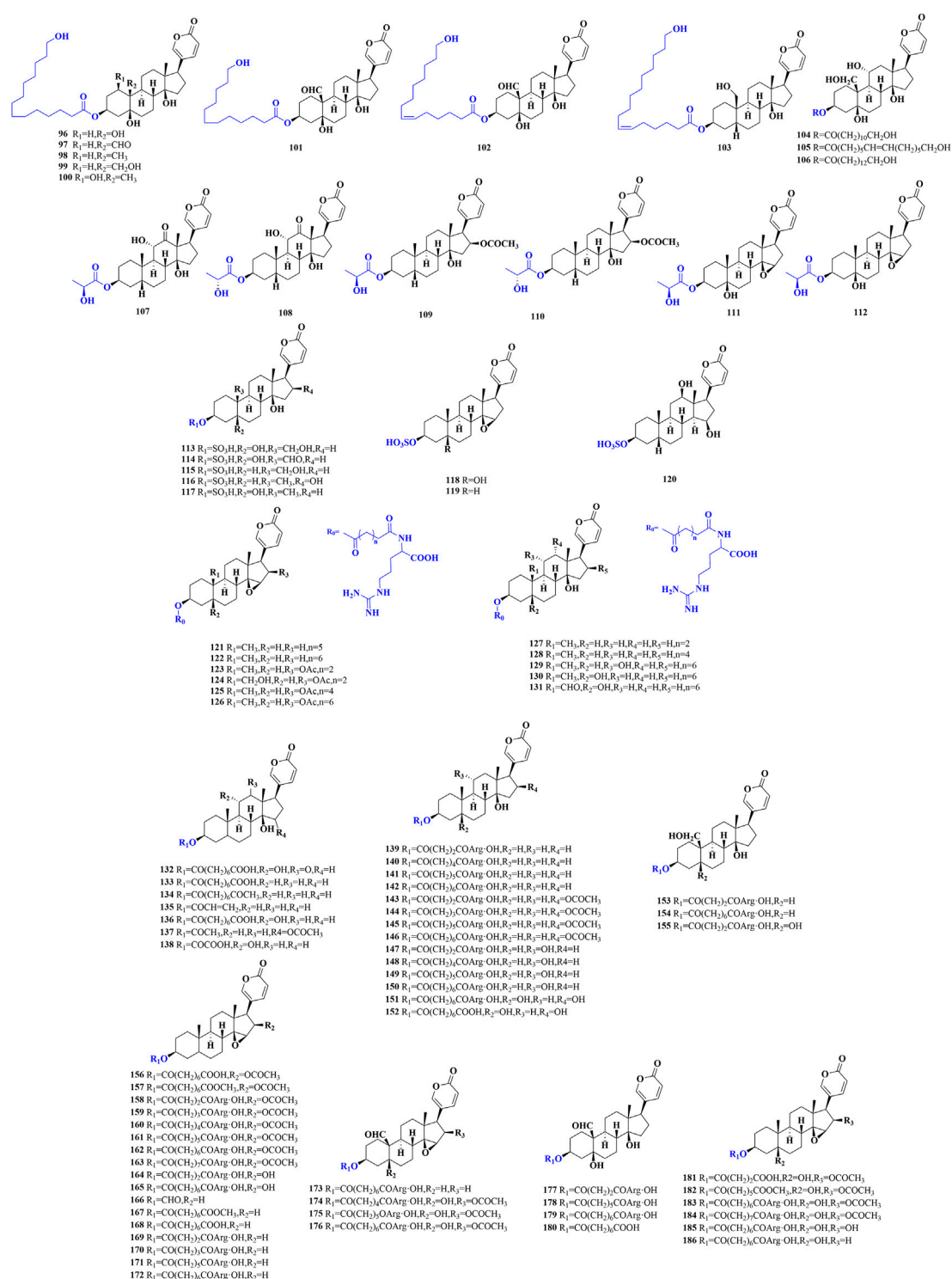


FIGURE 3

The chemical structures of reported conjugated bufadienolide.

TABLE 1 Conjugated bufadienolide detected in Argentine Toad venom by MALDI-MS.

No.	<i>m/z</i>	Adduct	Tentative structure assigned
187	657	[M + H] ⁺	3-(<i>N</i> -glutaryl argininy)-bufalin
188	669	[M + H] ⁺	3(<i>N</i> -adipoyl argininy)-resibufogenin
189	671	[M + H] ⁺	3-(<i>N</i> -adipoyl argininy)-bufalin
190	683	[M + H] ⁺	3-(<i>N</i> -pimeloyl argininy)-resibufogenin
191	685	[M + H] ⁺	3-(<i>N</i> -pimeloyl argininy)-bufalin/3-(<i>N</i> -adipoyl argininy)-marinobufagin
192	691	[M + Na] ⁺	3-(<i>N</i> -adipoyl argininy)-resibufogenin
193	693	[M + Na] ⁺	3-(<i>N</i> -adipoyl argininy)-bufalin
194	696	[M + Na] ⁺	3-(<i>N</i> -glutaryl argininy)-telocinobufagin
195	699	[M + H] ⁺	3-(<i>N</i> -suberoyl argininy)-bufalin (bufalitoxin)/3-(<i>N</i> -pimeloyl argininy)-marinobufagin/3-(<i>N</i> -adipoyl)-bufotalinin
196	701	[M + H] ⁺	3-(<i>N</i> -pimeloyl argininy)-telocinobufagin, 3-(<i>N</i> -adipoyl argininy)-bufarenogin or arenobufagin or hellebrigenin
197	707	[M + Na] ⁺	3-(<i>N</i> -pimeloyl argininy)-bufalin/3-(<i>N</i> -adipoyl argininy)-marinobufagin
198	710	[M + Na] ⁺	3-(<i>N</i> -adipoyl argininy)-telocinobufagin
199	713	[M + H] ⁺	3-(<i>N</i> -azelayl argininy)-bufalin/3-(<i>N</i> -suberoyl argininy)-marinobufagin (marinobufotoxin)/3-(<i>N</i> -pimeloyl argininy)-bufotalinin
200	715	[M + H] ⁺	3-(<i>N</i> -suberoyl argininy)-telocinobufagin (telocinobufatoxin), 3-(<i>N</i> -pimeloyl argininy)-bufarenogin or arenobufagin or hellebrigenin
201	721	[M + Na] ⁺	3-(<i>N</i> -suberoyl argininy)-bufalin (bufalitoxin)/3-(<i>N</i> -pimeloyl argininy)- marinobufagin//3-(<i>N</i> -adipoyl)-bufotalinin
202	724	[M + Na] ⁺	3-(<i>N</i> -pimeloyl argininy)-telocinobufagin, 3-(<i>N</i> -adipoyl argininy)- bufarenogin or arenobufagin or hellebrigenin
203	727	[M + H] ⁺	3-(<i>N</i> -sebacyl argininy)-bufalin/3-(<i>N</i> -azelayl argininy)-marinobufagin/3-(<i>N</i> -suberoyl argininy)-bufotalinin
204	729	[M + H] ⁺	3-(<i>N</i> -adipoyl argininy)-bufotalin/3-(<i>N</i> -suberoyl argininy)-bufarenogin or arenobufagin or hellebrigenin
205	736	[M + Na] ⁺	3-(<i>N</i> -azelayl argininy)-bufalin/3-(<i>N</i> -suberoyl argininy)-marinobufagin (marinobufotoxin)/3-(<i>N</i> -pimeloyl argininy)-bufotalinin
206	738	[M + Na] ⁺	3-(<i>N</i> -suberoyl argininy)-telocinobufagin (telocinobufatoxin)/3-(<i>N</i> -pimeloyl argininy)-bufarenogin or arenobufagin or hellebrigenin
207	752	[M + Na] ⁺	3-(<i>N</i> -suberoyl argininy)-bufarenogin or arenobufagin or hellebrigenin
208	757	[M + H] ⁺	3-(<i>N</i> -suberoyl argininy)-bufotalin (bufotoxin)/3-(<i>N</i> -undecadienoyl argininy)-telocinobufagin/3-(<i>N</i> -sebacyl argininy)-bufarenogin or arenobufagin or hellebrigenin
209	1339	[M + H] ⁺	3-(<i>N</i> - adipoyl argininy)-resibufogenin dimer
210	1355	[M + H] ⁺	[3-(<i>N</i> - adipoyl argininy)-resibufogenin]-[3-(<i>N</i> - adipoyl argininy)-marinobufagin] dimer
211	1371	[M + H] ⁺	[3-(<i>N</i> - adipoyl argininy)-marinobufagin] dimer
212	1367	[M + H] ⁺	[3-(<i>N</i> - adipoyl argininy)-resibufogenin]-[3-(<i>N</i> -suberoyl argininy)-bufalin] dimer
213	1369	[M + H] ⁺	[3-(<i>N</i> - adipoyl argininy)-resibufogenin]-[3-(<i>N</i> - adipoyl)-bufotalinin] dimer
214	1369	[M + H] ⁺	3-(<i>N</i> - adipoyl argininy)-resibufogenin and 3-(<i>N</i> - adipoyl argininy)-bufarenogin or arenobufagin or hellebrigenin dimer
215	1367	[M + H] ⁺	[3-(<i>N</i> - adipoyl argininy)-bufalin]-[3-(<i>N</i> -suberoyl argininy)-bufalin] dimer
216	1369	[M + H] ⁺	[3-(<i>N</i> - adipoyl argininy)-bufalin]-[3-(<i>N</i> - adipoyl)-bufotalinin] dimer
217	1383	[M + H] ⁺	[3-(<i>N</i> - adipoyl argininy)-resibufogenin]-[3-(<i>N</i> -suberoyl argininy)-telocinobufagin] dimer
218	1383	[M + H] ⁺	3-(<i>N</i> - adipoyl argininy)-resibufogenin and 3-(<i>N</i> -pimeloyl argininy)-bufarenogin or arenobufagin or hellebrigenin dimer
219	1383	[M + H] ⁺	[3-(<i>N</i> - adipoyl argininy)-bufalin]-[3-(<i>N</i> -suberoyl argininy)-telocinobufagin] dimer
220	1383	[M + H] ⁺	3-(<i>N</i> - adipoyl argininy)-bufalin and 3-(<i>N</i> -pimeloyl argininy)-bufarenogin or arenobufagin or hellebrigenin dimer
221	1383	[M + H] ⁺	[3-(<i>N</i> -pimeloyl argininy)-telocinobufagin]-[3-(<i>N</i> - pimeloyl argininy)-bufalin] dimer
222	1385	[M + H] ⁺	[3-(<i>N</i> -pimeloyl argininy)-telocinobufagin]-[3-(<i>N</i> - adipoyl argininy)-marinobufagin] dimer
223	1383	[M + H] ⁺	3-(<i>N</i> - adipoyl argininy)-bufarenogin or arenobufagin or hellebrigenin and 3-(<i>N</i> - pimeloyl argininy)-bufalin dimer
224	1385	[M + H] ⁺	3-(<i>N</i> - adipoyl argininy)-bufarenogin or arenobufagin or hellebrigenin and 3-(<i>N</i> - adipoyl argininy)-marinobufagin dimer
225	1381	[M + H] ⁺	[3-(<i>N</i> -suberoyl argininy)-bufalin]-[3-(<i>N</i> - pimeloyl argininy)-bufalin] dimer
226	1383	[M + H] ⁺	[3-(<i>N</i> -suberoyl argininy)-bufalin]-[3-(<i>N</i> - adipoyl argininy)-marinobufagin] dimer
227	1383	[M + H] ⁺	[3-(<i>N</i> - pimeloyl argininy)-marinobufagin]-[3-(<i>N</i> - pimeloyl argininy)-bufalin] dimer
228	1385	[M + H] ⁺	[3-(<i>N</i> - pimeloyl argininy)-marinobufagin]-[3-(<i>N</i> - adipoyl argininy)-marinobufagin] dimer
229	1383	[M + H] ⁺	[3-(<i>N</i> - adipoyl)-bufotalinin]-[3-(<i>N</i> - pimeloyl argininy)-bufalin] dimer
230	1385	[M + H] ⁺	[3-(<i>N</i> - adipoyl)-bufotalinin]-[3-(<i>N</i> - adipoyl argininy)-marinobufagin] dimer
231	1397	[M + H] ⁺	[3-(<i>N</i> - adipoyl argininy)-resibufogenin]-[3-(<i>N</i> - adipoyl argininy)-bufotalin] dimer
232	1397	[M + H] ⁺	3-(<i>N</i> - adipoyl argininy)-resibufogenin and 3-(<i>N</i> - suberoyl argininy)-bufarenogin or arenobufagin or hellebrigenin dimer

(Continued on following page)

TABLE 1 (Continued) Conjugated bufadienolide detected in Argentine Toad venom by MALDI-MS.

No.	m/z	Adduct	Tentative structure assigned
233	1399	[M + H] ⁺	[3-(N- adipoyl argininy)-bufalin]-[3-(N- adipoyl argininy)-bufotalin] dimer
234	1397	[M + H] ⁺	3-(N- adipoyl argininy)-bufalin and 3-(N- suberoyl argininy)-bufarenogin or arenobufagin or hellebrigenin dimer
235	1397	[M + H] ⁺	[3-(N-suberoyl argininy)-telocinobufagin]-[3-(N- pimeloyl argininy)-bufalin] dimer
236	1399	[M + H] ⁺	[3-(N-suberoyl argininy)-telocinobufagin]-[3-(N- adipoyl argininy)-marinobufagin] dimer
237	1397	[M + H] ⁺	3-(N-pimeloyl argininy)-bufarenogin or arenobufagin or hellebrigenin and 3-(N- pimeloyl argininy)-bufalin dimer
238	1399	[M + H] ⁺	3-(N-pimeloyl argininy)-bufarenogin or arenobufagin or hellebrigenin and 3-(N- adipoyl argininy)-marinobufagin dimer
239	1395	[M + H] ⁺	[3-(N-suberoyl argininy)-bufalin] dimer
240	1397	[M + H] ⁺	[3-(N- adipoyl)-bufotalinin] dimer
241	1397	[M + H] ⁺	[3-(N- pimeloyl argininy)-marinobufagin]dimer
242	1411	[M + H] ⁺	[3-(N- adipoyl argininy)-bufotalin]-[3-(N- pimeloyl argininy)-bufalin] dimer
243	1413	[M + H] ⁺	[3-(N- adipoyl argininy)-bufotalin]-[3-(N- adipoyl argininy)-marinobufagin] dimer
244	1411	[M + H] ⁺	3-(N- suberoyl argininy)-bufarenogin or arenobufagin or hellebrigenin and 3-(N- pimeloyl argininy)-bufalin dimer
245	1413	[M + H] ⁺	3-(N- suberoyl argininy)-bufarenogin or arenobufagin or hellebrigenin and 3-(N- adipoyl argininy)-marinobufagin dimer
246	1411	[M + H] ⁺	[3-(N- suberoyl argininy)-marinobufagin]-[3-(N-suberoyl argininy)-bufalin] dimer
247	1411	[M + H] ⁺	[3-(N- suberoyl argininy)-marinobufagin]-[3-(N- pimeloyl argininy)-marinobufagin] dimer
248	1411	[M + H] ⁺	[3-(N- suberoyl argininy)-marinobufagin]-[3-(N- adipoyl)-bufotalinin] dimer
249	1411	[M + H] ⁺	3-(N-pimeloyl argininy)-bufotalinin and 3-(N-suberoyl argininy)-bufalin dimer
250	1411	[M + H] ⁺	3-(N-pimeloyl argininy)-bufotalinin and 3-(N- pimeloyl argininy)-marinobufagin dimer
251	1411	[M + H] ⁺	3-(N-pimeloyl argininy)-bufotalinin and 3-(N- adipoyl)-bufotalinin dimer
252	1427	[M + H] ⁺	3-(N-suberoyl argininy)-telocinobufagin dimer
253	1427	[M + H] ⁺	3-(N-suberoyl argininy)-telocinobufagin and 3-(N-pimeloyl argininy)-bufarenogin or arenobufagin or hellebrigenin dimer
254	1427	[M + H] ⁺	3-(N-pimeloyl argininy)-bufarenogin or arenobufagin or hellebrigenin dimer
255	1427	[M + H] ⁺	3-(N-suberoyl argininy)-telocinobufagin and 3-(N- suberoyl argininy)-marinobufagin dimer
256	1427	[M + H] ⁺	3-(N-suberoyl argininy)-telocinobufagin and 3-(N-pimeloyl argininy)-bufotalinin dimer
257	1427	[M + H] ⁺	3-(N-pimeloyl argininy)-bufarenogin or arenobufagin or hellebrigenin and 3-(N- suberoyl argininy)-marinobufagin dimer
258	1427	[M + H] ⁺	3-(N-pimeloyl argininy)-bufarenogin or arenobufagin or hellebrigenin and 3-(N-pimeloyl argininy)-bufotalinin dimer
259	1427	[M + H] ⁺	3-(N- suberoyl argininy)-bufarenogin or arenobufagin or hellebrigenin and 3-(N-pimeloyl argininy)-telocinobufagin dimer
260	1427	[M + H] ⁺	3-(N- suberoyl argininy)-bufarenogin or arenobufagin or hellebrigenin and 3-(N- adipoyl argininy)-bufarenogin or arenobufagin or hellebrigenin dimer
261	1427	[M + H] ⁺	[3-(N- adipoyl argininy)-bufotalin]-[3-(N-pimeloyl argininy)-telocinobufagin] dimer
262	1427	[M + H] ⁺	3-(N- adipoyl argininy)-bufotalin and 3-(N- adipoyl argininy)-bufarenogin or arenobufagin or hellebrigenin dimer
263	1425	[M + H] ⁺	3-(N- suberoyl argininy)-bufarenogin or arenobufagin or hellebrigenin and 3-(N-suberoyl argininy)-bufalin dimer
264	1427	[M + H] ⁺	3-(N- suberoyl argininy)-bufarenogin or arenobufagin or hellebrigenin and 3-(N- pimeloyl argininy)-marinobufagin dimer
265	1427	[M + H] ⁺	3-(N- suberoyl argininy)-bufarenogin or arenobufagin or hellebrigenin and 3-(N- adipoyl)-bufotalinin dimer
266	1425	[M + H] ⁺	[3-(N- adipoyl argininy)-bufotalin]-[3-(N-suberoyl argininy)-bufalin] dimer
267	1427	[M + H] ⁺	[3-(N- adipoyl argininy)-bufotalin]-[3-(N- pimeloyl argininy)-marinobufagin] dimer
268	1427	[M + H] ⁺	[3-(N- adipoyl argininy)-bufotalin]-[3-(N- adipoyl)-bufotalinin] dimer
269	1439	[M + H] ⁺	[3-(N- adipoyl argininy)-bufotalin]-[3-(N- suberoyl argininy)-marinobufagin] dimer
270	1441	[M + H] ⁺	[3-(N- adipoyl argininy)-bufotalin]-[3-(N-pimeloyl argininy)-bufotalinin] dimer
271	1439	[M + H] ⁺	3-(N- suberoyl argininy)-bufarenogin or arenobufagin or hellebrigenin and 3-(N- suberoyl argininy)-marinobufagin dimer
272	1441	[M + H] ⁺	3-(N- suberoyl argininy)-bufarenogin or arenobufagin or hellebrigenin and 3-(N-pimeloyl argininy)-bufotalinin dimer
273	1441	[M + H] ⁺	[3-(N- adipoyl argininy)-bufotalin]-[3-(N-suberoyl argininy)-telocinobufagin] dimer
274	1441	[M + H] ⁺	[3-(N- adipoyl argininy)-bufotalin and 3-(N-pimeloyl argininy)-bufarenogin or arenobufagin or hellebrigenin dimer
275	1441	[M + H] ⁺	3-(N- suberoyl argininy)-bufarenogin or arenobufagin or hellebrigenin and 3-(N-suberoyl argininy)-telocinobufagin dimer
276	1441	[M + H] ⁺	3-(N- suberoyl argininy)-bufarenogin or arenobufagin or hellebrigenin and 3-(N-pimeloyl argininy)-bufarenogin or arenobufagin or hellebrigenin dimer

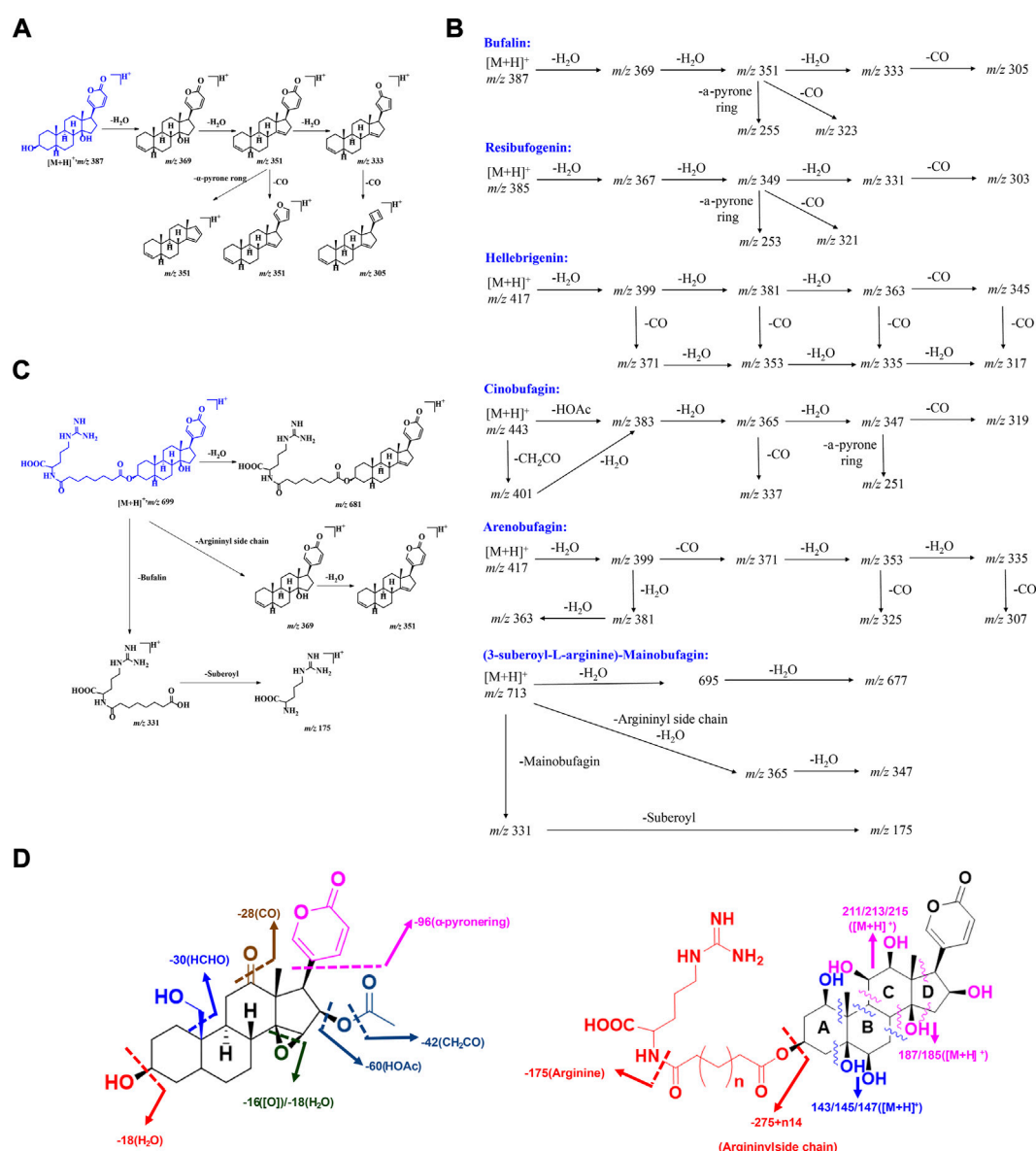


FIGURE 4

The MS fragmentation principles of bufadienolide: (A–C) The typical fragmentation pathways of free and conjugated bufadienolide; (D) The summarized fragmentation patterns of free and conjugated bufadienolide.

et al., 2010). From the bile of the Cane toad, three sulfonated bufadienolides (**118–120**) were also characterized by Lee et al. (Lee et al., 1994). The sulfonated bufadienolide exhibited better water solubility compared to the corresponding free bufadienolide. Bufadienolide sulfonation may be one of the metabolism and detoxification mechanisms of bufadienolide in animals and it may also indicate that the toxicity of sulfonated bufadienolide could be significantly reduced.

In addition to fatty acid and sulfonic acid conjugated bufadienolide, arginine diacyl ester is the predominant form of conjugated bufadienolide. It is characterized by the

esterification of C-3 hydroxyl group with an arginine diacyl group, and the variable length of the arginine diacyl chain leads to the structure diversity of this kind of conjugated bufadienolide. Zhou et al. identified a series of arginine diacyl chain conjugated bufadienolides from *Bufo Bufoni* by UPLC-QQQ-MS analysis (**121–131**) (Zhou et al., 2015). Furthermore, at least 55 arginine diacyl chain conjugated bufadienolides have been isolated and identified from Chansu (**132–186**) (Gao et al., 2011; Wei et al., 2019; Zhan et al., 2020; Li et al., 2021), and their chemical structures were shown in Figure 3.

It was worth mentioning that Argentine researchers discovered a high concentration of arginine diacyl chain conjugated bufadienolides (**187–276**) in the venom of Argentine toad by MALDI-MS analysis (Table 1) (Petroselli et al., 2018). Furthermore, the characteristic fragment ions indicated that there may still exist numerous arginine diacyl chain conjugated bufadienolides polymerized as dimers or multimers remained to be discovered.

Bufadienolide MS fragmentation principles

In the realm of natural products, the ion response of bufadienolide is more sensitive in the positive ion mode of electrospray ionization (ESI) than in the negative ion mode. The MS/MS spectra of bufadienolide could be divided into two regions: the steroid core region is located at m/z 50–250, while the functional group region spans m/z 250–500. In the functional group region, it is common to observe the fragment ions resulting from the loss of a series of neutral molecules, such as H_2O and CO , which correspond to the fragmentation of certain functional groups including hydroxyl, aldehyde, and carbonyl et al. For the steroidal core region, the fragment ions are acquired primarily by the Retro-Diels-Alder (RDA) reaction, induced cleavage, and hydrogenation rearrangement (Tureček and Hanuš 1984; Silva and Lopes 2015). Based on the MS/MS fragmentation of bufadienolide standards and literature reports (Han et al., 2016; Meng et al., 2016; Han et al., 2017), the general MS/MS fragmentation principles for bufadienolide are summarized as follows (Figure 4).

Bufalin and its polyhydroxy derivatives

Bufalin produced an obvious $[M + H]^+$ ion at m/z 387.2515. After Collision-Induced Dissociation (CID), a series of MS/MS ions, including $[M + H-18]^+$ (m/z , 369.2414), $[M + H-36]^+$ (m/z , 351.2309), $[M + H-54]^+$ (m/z , 333.2214) and $[M + H-36-96]^+$ (m/z , 255.2100), were produced, which were evoked by successive losses of H_2O and CO . Meanwhile, a strong intensity ion at m/z 255.2100 (a neutral loss of 96 Da) was observed, and it was initiated by the elimination of α -pyrone ring at C-17 position. The possible fragmentation pathway of bufalin is shown in Figures 4A,B. The polyhydroxy derivatives of bufalin showed similar fragmentation patterns to bufalin: successive losses of H_2O and CO , which are evoked by the elimination of specific functional groups. They are followed by a neutral loss of 96 Da triggered by the elimination of α -pyrone ring at the C-17 position.

Resibufogenin and its polyhydroxy derivatives

The MS/MS spectrum of resibufogenin exhibited very similar patterns to those of bufalin. Obvious fragment ions, including $[M + H-18]^+$ (m/z , 367.2263), $[M + H-36]^+$ (m/z , 349.2155), $[M + H-18-28]^+$ (m/z , 339.2310) and $[M + H-36-96]^+$ (m/z , 253.1948), were abundant in the MS/MS spectrum. The above ions were given by successive losses of H_2O and CO by elimination of hydroxyl groups, C-14/15 epoxy ring, and α -pyrone ring fragmentation (Figure 4B). Their MS/MS fragment ions generally could be correlated with the number of equipped hydroxyl groups. The whole hydroxyl groups, including C-14/15 epoxy ring, tended to be eliminated to give a stable fragment ion.

Bufadienolide with aldehyde substituent

This group of bufadienolide is characterized by an aldehyde group positioned at C-10. Hellebrigenin is a typical bufadienolide with acetoxyl substituent. It produced an obvious $[M + H]^+$ ion at m/z 417.2257. After CID, hellebrigenin gave a series of MS/MS ions including $[M + H-18]^+$ (m/z , 399.2165), $[M + H-36]^+$ (m/z , 381.2068), $[M + H-54]^+$ (m/z , 363.1952), $[M + H-18-28]^+$ (m/z , 371.2221), $[M + H-36-28]^+$ (m/z , 353.2109), $[M + H-54-28]^+$ (m/z , 335.1996) and $[M + H-54-28-96]^+$ (m/z , 239.1793). Obviously, a series of MS/MS ions characterized by the loss of 28 (CO) were clearly more abundant for bufadienolide with aldehyde substituent than other types of bufadienolide. These ions presumably resulted from the elimination of CO from aldehyde group positioned at C-10 (Figure 4B).

Bufadienolide with acetoxyl substituent

Bufadienolide with acetoxyl substituent is usually equipped with an acetoxyl group at the C-16 position, giving a characteristic fragmentation pattern. The obvious and abundant MS/MS fragment ions of Cinobufalin, a typical bufadienolide with acetoxyl substituent, usually included $[M + H-42]^+$ (m/z , 417.2273), $[M + H-60]^+$ (m/z , 399.2175), $[M + H-60-18]^+$ (m/z , 381.2063), $[M + H-60-36]^+$ (m/z , 363.1952), $[M + H-60-54]^+$ (m/z , 345.1855). In general, the specific ions, namely $[M + H-42]^+$ and $[M + H-60]^+$, are the characteristic ions for this kind of bufadienolide. They are produced by the elimination of acetoxyl group to trigger the initial loss of 42 (CH_2CO) or 60 ($HOAc$) Da (Figure 4B). The remaining ions are produced by consecutive losses of H_2O and CO evoked by the specific functional group fragmentation, as with the above three groups of bufadienolide.

Bufadienolide with carbonyl substituent

This group of bufadienolide contains a carbonyl group at the C-11 or C-12 position. A typical bufadienolide belonging to this group is arenobufagin, which contains a carbonyl group at the C-11 position. The MS/MS fragment ions of arenobufagin typically consisted of $[M + H - 18]^+$ (m/z , 399.2150), $[M + H - 36]^+$ (m/z , 381.2060), $[M + H - 54]^+$ (m/z , 363.1954), $[M + H - 18 - 28]^+$ (m/z , 371.2220), $[M + H - 36 - 28]^+$ (m/z , 353.2115), $[M + H - 54 - 28]^+$ (m/z , 335.2003) and $[M + H - 54 - 28 - 96]^+$ (m/z , 239.1797). Characteristically, the existence of a carbonyl group leads to the neutral loss of 28 Da (CO) to generate the corresponding diagnostic ions (Figure 4B). Importantly, the relative intensity of diagnostic ions, in terms of the ions at m/z 399 generated by the elimination of C-3 hydroxyl group and its subsequent CO eliminated ions, could be utilized to distinguish between isomers of bufadienolides with the carbonyl group substituted at C-11 and C-12 position.

Conjugated bufadienolide (substituted with arginine diacyl chain)

For conjugated bufadienolide, strong arginine diacyl chain ions and a series of fragment ions formed by the subsequent fragmentation of these diacyl chains were given due to the strong ability of N to stabilize the positive charge. Meanwhile, the bufadienolide part, giving rather weak ion peaks in MS/MS spectrum, was eliminated as a neutral molecular (Figures 4B,C). (3-suberoyl-L-arginine)-Mainobufagin is a typical conjugated bufadienolide with an obvious $[M + H]^+$ ion at m/z 713.4089 in its MS spectrum. After CID, a series of MS/MS fragment ions, including $[M + H - 18]^+$ (m/z , 695.3990), $[M + H - 36]^+$ (m/z , 677.3921), $[M + H - 382]^+$ (m/z , 331.1958), and $[M + H - 382 - 156]^+$ (m/z , 175.1188), were produced. When employing negative ion mode and increasing the induced collision voltage in MS/MS, the ion intensity of bufadienolide part could be significantly increased. However, it is still rather weak compared to that of arginine diacyl chain fragmentation.

MS fragmentation principles of bufadienolide could be primarily and briefly summarized as follows: 1) Bufadienolide containing solely hydroxyl groups can be detected by consecutive losses of H_2O and CO, and the amount of hydroxyl groups is generally associated with the resulting ion profile. Unfortunately, determination the hydroxyl substitution location solely based on MS/MS data is difficult or impossible. Meanwhile, the achievement of the 14-OH and 14/15-epoxy ring distinguishment is also impossible just by the MS/MS profile; 2) CO elimination is informative. It may indicate the presence of a C-10 aldehyde group and a carbonyl group at C-11 or C-12 position; 3) The specific loss of 30 Da (HCHO) indicates the presence of a C-19 hydroxyl group; 4) The characteristic loss of 42 Da (CH_2CO) and 60 Da (HOAc) indicates the presence of an

acetoxyl group at the C-16 position; 5) Strong arginine diacyl chain ion peaks, accompanied by a series of fragment ions formed by the subsequent elimination of these chains, indicate the presence of arginine diacyl chains for conjugated bufadienolide (Figure 4D).

Anti-inflammatory efficacy

On account of the molecular level regulatory ability and specific Na^+/K^+ ATPase inhibitory activity, bufadienolide exhibited excellent bioactivities, including cardiotonic, anti-inflammatory, anti-tumor, immunoregulatory, NO production, renal sodium excretion and blood pressure stimulating (Prassas and Diamandis 2008; de Vasconcelos et al., 2011; Gao et al., 2011; Wen et al., 2014). Of the whole activities defined for bufadienolide, anti-inflammatory activity may be one of the most promising and interesting research topics.

Specific inhibition of Na^+/K^+ -ATPase

Na^+/K^+ ATPase was discovered in 1957 by the Danish scientist Jens Christian Skou, who was awarded a Nobel Prize for this milestone discovery in 1997 (Boyer et al., 1997). The predominant function of Na^+/K^+ ATPase is to transport K^+ and Na^+ in a manner of reverse gradient using the energy fueled by ATP hydrolysis. For a detailed transport procedure, two K^+ are transported into the cell, while three Na^+ are transferred out of the cell. By cooperating with ion free diffusion, cell resting potential could be maintained to a state that electrochemical gradient keeps equal on both sides of the cell membrane (Figure 5A). This discovery marked an important step forward in the understanding of how ions get into and out of cells (Jørgensen 1982; Nyblom et al., 2013).

Structurally, three subunits (α subunit, β subunit, and FXYD subunit) compose the structure of Na^+/K^+ ATPase (Figure 5A). It is the distribution and expression difference of the three subunits in various tissue that achieves the functional diversity of Na^+/K^+ ATPase (Morth et al., 2007; Kanai et al., 2013). There exist four subtypes of α subunit, namely $\alpha 1$, $\alpha 2$, $\alpha 3$, and $\alpha 4$ subunit, that have been discovered in human beings (Sweadner 1989). Of the four subtypes of α subunit, $\alpha 1$ subtype is predominant and is found in almost all the body cells. In contrast, $\alpha 2$ subtype, $\alpha 3$ subtype, and $\alpha 4$ subtype mainly distribute in cardiomyocytes, nerve cells, and testis tissue, respectively.

The most attractive point of bufadienolide is cardiotonic activity, which is triggered by the specific inhibition of Na^+/K^+ ATPase. For a detailed action mechanism, the specific inhibition of Na^+/K^+ ATPase leads to an increase of intracellular Na^+ concentration and a decrease of the K^+ concentration. The above ions concentration change will activate Na^+/Ca^{2+} exchanger on the sarcoplasmic reticulum to regulate the Ca^{2+}

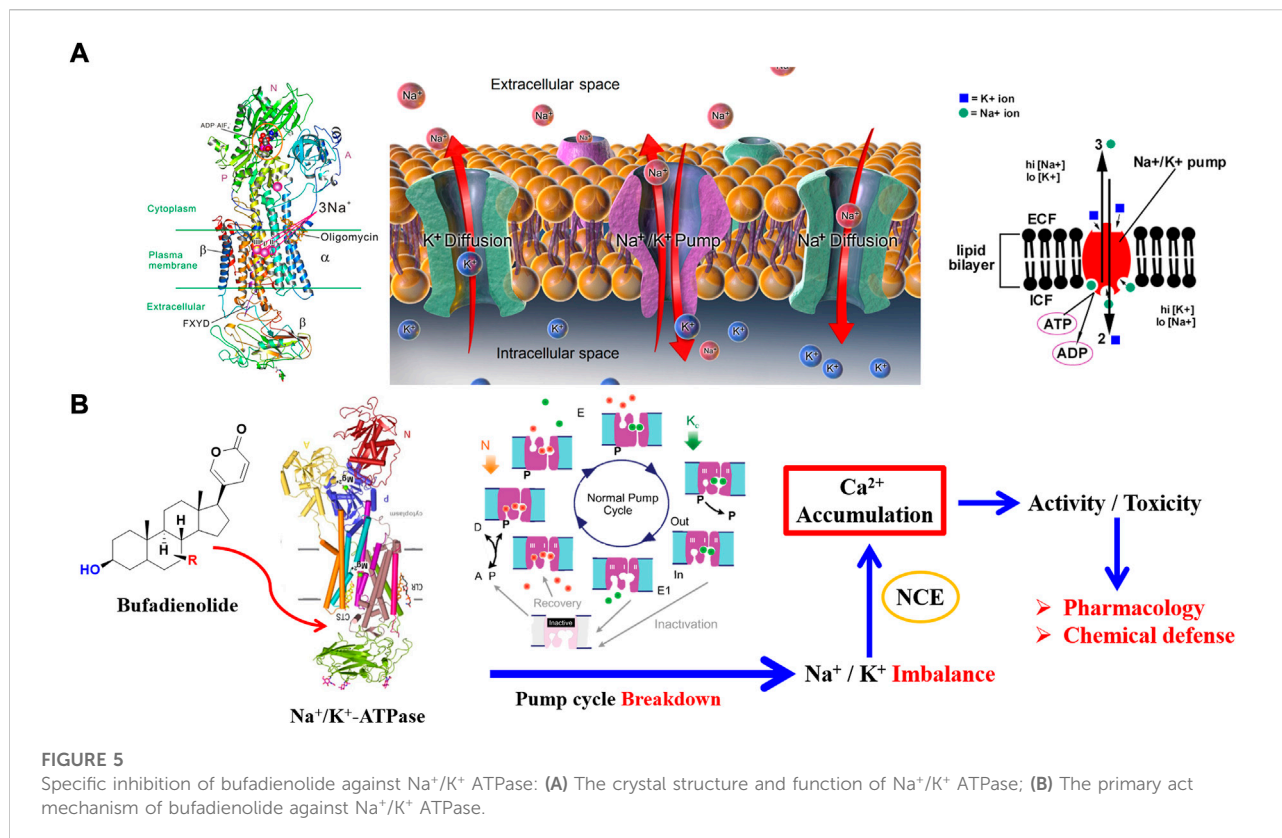


FIGURE 5

Specific inhibition of bufadienolide against Na⁺/K⁺ ATPase: (A) The crystal structure and function of Na⁺/K⁺ ATPase; (B) The primary act mechanism of bufadienolide against Na⁺/K⁺ ATPase.

concentration for a balanced cell electrochemical gradient. Eventually, a positive inotropic activity is achieved *via* promoting the contraction of troponin in cardiomyocytes triggered by the upregulated Ca²⁺ concentration (Ogawa et al., 2009; Laursen et al., 2015). However, serious toxicity would be obtained if the intracellular calcium ion is excessively accumulated (Figure 5). As mentioned above, both the cell membrane of the whole tissue in the body almost distributes the $\alpha 1$ subtype of Na⁺/K⁺ ATPase, which will result in a narrow therapeutic safety window. Consequently, the therapeutic dose has reached the level of 60% of the toxic dose due to its double-edged sword property (Huang et al., 2019). Thus, it is emergency to discover Na⁺/K⁺ ATPase inhibitors with high selectivity that can regulate the activity of specific subtypes of Na⁺/K⁺ ATPase present in targeted tissues.

Anti-inflammatory activity

Generally, anti-inflammatory activity is closely linked with anticancer activity. Bufadienolide has been comprehensively studied for its anticancer activity in diverse types of cancer, such as breast cancer, lung carcinoma, human leukemia, gastrointestinal, hepatoma et al. The underlying anticancer mechanisms were always linked with anti-inflammatory

pathway (Prassas and Diamandis 2008; Gao et al., 2011; Deng et al., 2021).

It was revealed that chronic inflammation could result in tissue damage accompanied by an increased risk of cancer development. Generally, the microenvironment with inflammation is the prerequisite for cancer progression. Cancer tissues would frequently produce inflammation without the occurrence of precancerous inflammation (Coussens and Werb 2002). For cancer-involved inflammation, the expression level of numerous inflammatory products is dramatically affected by a predominant transcription factor namely NF- κ B (Liu et al., 2017). Consequently, inflammatory diseases, such as rheumatoid arthritis, could be treated by some anticancer drugs. In turn, it provides a promising approach for cancer prevention and therapy by inflammation elimination (Todoric et al., 2016).

Bufadienolide has been long reported for anti-inflammatory activity, especially for cancer-involved inflammation (Gao et al., 2011; Qi et al., 2014; Rong et al., 2014). Ye found that bufalin exhibited anti-inflammatory activity by blocking TNF (tumor necrosis factor), which was mediated *via* the NF- κ B nuclear translocation. Jiang found that NF- κ B expression and phosphorylation could be suppressed by bufalin (Jiang et al., 2010), which supported the previous conclusion. An investigation led by Chen revealed that phosphoinositide-3-

kinase (PI3K) and phosphorylation of AKT could be attenuated by bufalin in the SK-Hep1 cell line. Importantly, this attenuation was triggered by the decreased expression level of NF- κ B (Chen et al., 2015). Furthermore, Dong demonstrated that the expression of NF- κ B p65 protein could be dramatically suppressed by cinobufagin in the HepG2 cell line (Dong et al., 2010).

Meanwhile, NO, a key inflammatory factor, was found to be a predominant signaling molecule regulated by bufadienolide in the tumorigenesis process. Bhuiyan further confirmed the NO regulatory ability of bufalin (Bhuiyan et al., 2003). Their work also showed an interesting phenomenon: NO production was significantly up-regulated by a low concentration of bufalin, while bufalin with a high concentration gave the opposite result. In another study led by Kim via the BV2 microglial cell line, it was found that the expression of two key inflammatory-related enzymes, namely iNOS and COX-2, was significantly inhibited by Chansu. At the same time, it also suppressed the production of NO and PGE2 (Kim et al., 2008). Wang further discovered the powerful anti-inflammatory activity of Huachansu. It was found that TNF- α mediated NF- κ B and COX-2 activation were inhibited, and the expression levels of two pro-inflammatory cytokines, namely IL-6 and IL-8, were decreased by bufadienolide in Huchansu (Wang et al., 2019).

Structure modification

Despite the excellent pharmacological activity of bufadienolide, (cardio)toxicity is a non-negligible drawback (Li et al., 2015). In addition, as a specific inhibitor of Na⁺/K⁺ ATPase, bufadienolide would result in serious side effects, including cardiac dysfunction, conduction block, and arrhythmia (Bagrov et al., 2009). It is this serious side effect that severely limits the further pharmacological application of bufadienolide. Therefore, researchers have lit a way to discover bufadienolide derivatives with reserved activity and reduced side effects by performing structure modification *via* biosynthesis.

Plant suspension culture cell transformation

It is a promising way to employ plant suspension culture cells to perform desired structure modification. A series of works have been reported for bufadienolide structural modification *via* plant suspension culture cells. Ye performed biotransformation of cinobufagin *via* suspension culture cells originated from *Catharanthus roseus* and *Platycodon grandiflorum*. Three cinobufagin derivatives, namely 3-*epi*-desacetylcinobufagin, desacetylcinobufagin and 1-hydroxyl desacetylcinobufagin, were obtained (Ye et al., 2003). Xue also modified

telocinobufagin by utilizing *Catharanthus roseus* suspension culture cells, and a new bufadienolide namely 3-*epi*-telocinobufagin was produced. Three bufadienolides, including bufatalin, gamabufalin and telocinobufagin, were biotransformed by Zhang *via* *Saussurea involucre* suspension culture cells. Fortunately, eleven bufadienolide derivatives were obtained, which strongly supported the practicability of plant suspension culture cell transformation for bufadienolide structure modification (Zhang et al., 2011).

Microbial transformation

Besides the plant suspension culture cell approach, microbial transformation is also a promising alternative. *Alternaria alternata* was employed by Ye et al. to perform the biotransformation of cinobufagin (Ye and Guo 2008), and six cinobufagin derivatives were obtained. After reaction condition optimization, cinobufagin could be totally converted to the major transformation product 12 β -hydroxy-cinobufagin. Importantly, Ma discovered that *Fusarium solani* could achieve an isomerization reaction for bufadienolide. In detail, it could convert bufadienolide with 3 β -hydroxyl configuration to 3 α -hydroxyl configuration, and selectively oxidize the 3 β -hydroxyl, instead of 3 α -hydroxyl, to ketone (Ma et al., 2007).

The nature of the above two approaches is to employ the corresponding enzymes therein with satisfied substrate heterogeneity for bufadienolide structure modification. The operation simplicity and mildness of reaction conditions made them effective approaches to replace chemical synthesis. Nonetheless, there existed obvious drawbacks of these transformation approaches. Of which the most annoying aspect is that these transformations did not exhibit any selectivity to the desired targets due to too many enzymes involving the transformation. This also resulted in the relatively low yield of desired products. For example, only 2% of yield was obtained for cinobufagin biotransformation *via* plant suspension cells. Therefore, both the above two approaches exhibit some limitations and could not be applied to an industrial scale (Yue et al., 2016).

Enzyme-catalyzed glycosylation

To obtain structurally modified bufadienolides with reduced toxicity, glycosylation may be the first choice with a bright future. In comparison to conventional chemical synthesis, laborious protection/deprotection processes are avoided, and the process is more eco-friendly. Meanwhile, in contrast to plant suspension cell and microbial transformation, enzyme catalytic glycosylation is more efficient and exhibits perfect regional or stereoselectivity, allowing it to be directly exploited to produce structure-modified bufadienolides with the desired property (Zhang et al., 2006).

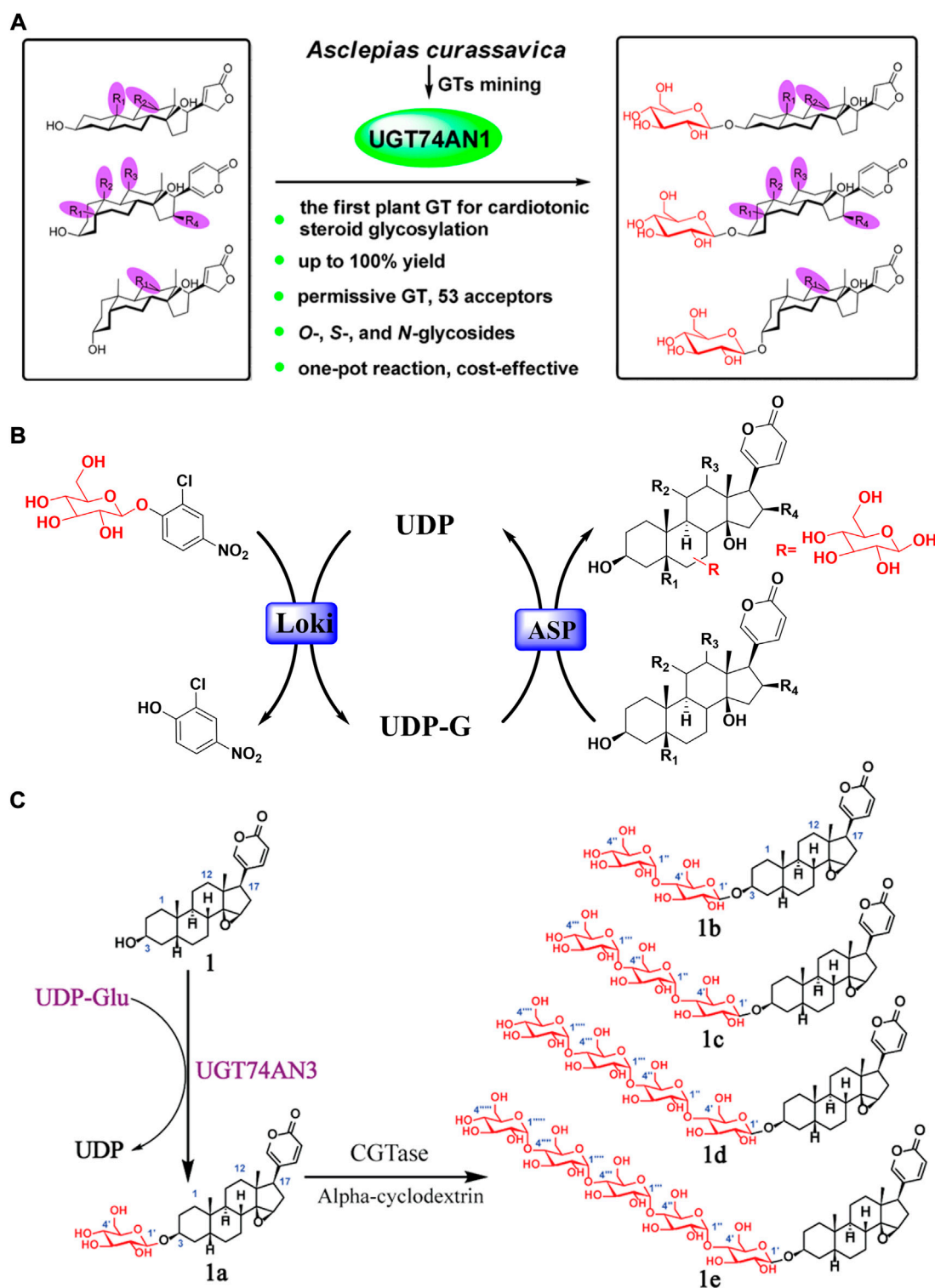


FIGURE 6

Glycosylation structure modification of bufadienolide: (A) UGT74AN1 catalyzed glycosylation of bufadienolide with regiospecificity; (B) The typical one-pot glycosylation system for bufadienolide; (C) Bufadienolide derivatives linked with sugar chains of varied length at the C-3 position obtained by enzyme catalyzed glycosylation.

Currently, enzyme catalytic glycosylation has become a focal point of study for bufadienolide structure modification (Elshahawi et al., 2015).

In 2007, Thorson completed the first enzyme catalyzed glycosylation of cardiac steroids. They discovered an actinomycete-sourced glycosyltransferase OleD. After high-throughput screening, a mutant named ASP with high substrate heterogeneity was further discovered (Williams et al., 2007). At the same time, Thorson dug the catalysis property of glycosyltransferase OleD/ASP. It was found that OleD/ASP did not exhibit steroid core site selectivity, and both C-3 and C-12 positions could be glycosylated without any differentiation. Accordingly, Zhu skillfully employed a pair of bufadienolides with different configuration of hydroxyl group at the C-3 position to further explore the stereoselectivity of OleD/ASP. It was revealed that OleD/ASP exhibited highly stereoselectivity: bufadienolide with 3 β -OH configuration could be glycosylated, while it was powerless to the bufadienolide with 3 α -OH configuration (Zhu et al., 2018).

Promisingly, Wen excavated a glycosyltransferase named UGT74AN1 from *Asclepias curassavica*, and it could conduct the glycosylation of bufadienolide specifically at C-3 position (Wen et al., 2018) (Figures 6A,B). UGT74AN1 is the first reported steroid glycosyltransferase to generate 3-O- β -D-glucoside of bufadienolide with high efficiency and regiospecificity. Furthermore, Huang developed a one-pot enzymatic system coupling UGT74AN3 and CGTase with high efficiency to generate bufadienolides linked with sugar chains of varying lengths at the C-3 position (Huang et al., 2019) (Figure 6C). Importantly, the glycosylation products displayed improved inhibitory efficacy with specificity for the Na⁺/K⁺ ATPase α 2 subunit.

In addition, Ye modified bufadienolide at the C-3 position *via* glycosyltransferase Yjic1. It gave a mono-glycoside (bufalin 3-O- β -D-glucoside) and a di-glycoside (bufalin 3-O- β -D-glucosyl (1 \rightarrow 2)- β -D-glucoside) with satisfying yields. Compared to the substrate, the solubility of corresponding glycosides was increased by 25-fold and 102-fold, respectively (Li et al., 2017). Brilliantly, Fu first reported the glycosylation of bufadienolide mixtures by glycosyltransferase Yjic1. The subsequent zebrafish embryo toxicity experiment revealed that the toxicity of glycosylated bufadienolides were much less than the corresponding aglycone (Fu et al., 2019).

Conclusion

The review has highlighted toad-sourced bufadienolides and their anti-inflammatory activity. Based on whether the C-3

hydroxyl group is substituted or not, two types of toad-derived bufadienolide (free or conjugated bufadienolide) were distinguished. And the structural diversity, as well as their MS fragmentation principles, have also been primarily summarized, laying a foundation for future analysis. In addition, the remarkable Na⁺/K⁺ ATPase inhibitory and anti-inflammatory efficacy reported for bufadienolide were also briefly highlighted. During the research process, the serious toxicity pushed the development of structural modification of bufadienolide *via* biotransformation for side effects reduction. It lighted a promising way for broadening the structural diversity and enhancing the pharmacological activity of bufadienolide. The current evidence of bufadienolide we summarized would provide a scientific basis for future in-depth studies and perspectives of potential drug candidate discovery.

Author contributions

DZ conceived, wrote and revised the article. QW, YL, LH, and DL wrote and revised the article. TC, DS, TY, YW, MG, and FH participated in the work of references selection and organization.

Funding

This work was supported by the National Natural Science Foundation of China (No. 32260129), the General Program of Natural Science Foundation of Qinghai Province (2021-ZJ-976Q), General Program of Qinghai Normal University (2020QZR016).

Conflict of interest

The authors declare that the research was conducted in the absence of any commercial or financial relationships that could be construed as a potential conflict of interest.

Publisher's note

All claims expressed in this article are solely those of the authors and do not necessarily represent those of their affiliated organizations, or those of the publisher, the editors and the reviewers. Any product that may be evaluated in this article, or claim that may be made by its manufacturer, is not guaranteed or endorsed by the publisher.

References

- Bagrov, A. Y., Shapiro, J. I., and Fedorova, O. V. (2009). Endogenous cardiotonic steroids: Physiology, pharmacology, and novel therapeutic targets. *Pharmacol. Rev.* 61 (1), 9–38. doi:10.1124/pr.108.000711
- Bhatti, H. N., and Khera, R. A. (2012). Biological transformations of steroidal compounds: A review. *Steroids* 77 (12), 1267–1290. doi:10.1016/j.steroids.2012.07.018
- Bhuiyan, M. B. A., Fant, M. E., and Dasgupta, A. (2003). Study on mechanism of action of Chinese medicine chan su: Dose-dependent biphasic production of nitric oxide in trophoblastic BeWo cells. *Clin. Chim. Acta.* 330 (1–2), 179–184. doi:10.1016/S0009-8981(03)00047-0
- Bókonyi, V., Üveges, B., Móricz, Á. M., and Hettyey, A. (2018). Competition induces increased toxin production in toad larvae without allelopathic effects on heterospecific tadpoles. *Funct. Ecol.* 32 (3), 667–675. doi:10.1111/1365-2435.12994
- Boyer, P. D., Walker, J. E., and Skou, J. C. (1997). Nobel prize in chemistry 1997. *Med. (B Aires)* 58, 107.
- Chen, H., Meng, Y.-H., Guo, D.-A., Liu, X., Liu, J.-H., and Hu, L.-H. (2015). New cytotoxic 19-norbufadienolide and bufogargarizin isolated from Chan Su. *Fitoterapia* 104, 1–6. doi:10.1016/j.fitote.2015.05.011
- Chen, Y.-L., Bian, X.-L., Guo, F.-j., Wu, Y.-c., and Li, Y.-m. (2018). Two new 19-norbufadienolides with cardiotonic activity isolated from the venom of *Bufo bufo* gargarizans. *Fitoterapia* 131, 215–220. doi:10.1016/j.fitote.2018.10.023
- Chen, Y. Y., Lu, H. F., Hsu, S. C., Kuo, C. L., Chang, S. J., Lin, J. J., et al. (2015). Bufalin inhibits migration and invasion in human hepatocellular carcinoma SK-Hep1 cells through the inhibitions of NF- κ B and matrix metalloproteinase-2/-9-signaling pathways. *Environ. Toxicol.* 30 (1), 74–82. doi:10.1002/tox.21896
- Coussens, L. M., and Werb, Z. (2002). Inflammation and cancer. *Nature* 420 (6917), 860–867. doi:10.1038/nature01322
- de Vasconcelos, D. I. B., Leite, J. A., Carneiro, L. T., Piuvezam, M. R., de Lima, M. R. V., de Moraes, L. C. L., et al. (2011). Anti-inflammatory and antinociceptive activity of ouabain in mice. *Mediat. Inflamm.* 2011, 912925. doi:10.1155/2011/912925
- Deng, L.-J., Lei, Y.-H., Quan, J.-Y., Li, B.-J., Zhang, D.-M., Tian, H.-Y., et al. (2021). 1 β -OH-arenobufagin induces mitochondrial apoptosis in hepatocellular carcinoma through the suppression of mTOR signaling pathway. *J. Ethnopharmacol.* 266, 113443. doi:10.1016/j.jep.2020.113443
- Deng, L.-J., Wang, L.-H., Peng, C.-K., Li, Y.-B., Huang, M.-H., Chen, M.-F., et al. (2017). Fibroblast activation protein α activated tripeptide bufadienolide antitumor prodrug with reduced cardiotoxicity. *J. Med. Chem.* 60 (13), 5320–5333. doi:10.1021/acs.jmedchem.6b01755
- Dobler, S., Dalla, S., Wagschal, V., and Agrawal, A. A. (2012). Community-wide convergent evolution in insect adaptation to toxic cardenolides by substitutions in the Na, K-ATPase. *Proc. Natl. Acad. Sci. U. S. A.* 109 (32), 13040–13045. doi:10.1073/pnas.1202111109
- Dong, Y., Ma, W., Gu, J., and Zheng, W. (2010). Effect of cinobufagin on nuclear factor- κ B pathway in HepG2 cells. *Nan Fang. Yi Ke Da Xue Xue Bao* 30 (1), 137–139.
- Elshahawi, S. I., Shaaban, K. A., Kharel, M. K., and Thorson, J. S. (2015). A comprehensive review of glycosylated bacterial natural products. *Chem. Soc. Rev.* 44 (21), 7591–7697. doi:10.1039/C4CS00426D
- Esposito, A. L. (1985). Digoxin disrupts the inflammatory response in experimental pneumococcal pneumonia. *J. Infect. Dis.* 152 (1), 14–23. doi:10.1093/infdis/152.1.14
- Forshammar, J., Block, L., Lundborg, C., Biber, B., and Hansson, E. (2011). Naloxone and ouabain in ultralow concentrations restore Na⁺/K⁺-ATPase and cytoskeleton in lipopolysaccharide-treated astrocytes. *J. Biol. Chem.* 286 (36), 31586–31597. doi:10.1074/jbc.M111.247767
- Forshammar, J., Jörneberg, P., Björklund, U., Westerlund, A., Lundborg, C., Biber, B., et al. (2013). Anti-inflammatory substances can influence some glial cell types but not others. *Brain Res.* 1539, 34–40. doi:10.1016/j.brainres.2013.09.052
- Fu, Z.-H., Wen, C., Ye, Q.-M., Huang, W., Liu, X.-M., and Jiang, R.-W. (2019). An efficient strategy for the glycosylation of total bufadienolides in venom bufonis. *ACS Omega* 4 (4), 6819–6825. doi:10.1021/acsomega.9b00386
- Fürst, R., Zündorf, I., and Dingermann, T. (2017). New knowledge about old drugs: The anti-inflammatory properties of cardiac glycosides. *Planta Med.* 83 (12/13), 977–984. doi:10.1055/s-0043-105390
- Gantt, R. W., Goff, R. D., Williams, G. J., and Thorson, J. S. (2008). Probing the aglycon promiscuity of an engineered glycosyltransferase. *Angew. Chem. Int. Ed. Engl.* 47 (46), 8889–8892. doi:10.1002/anie.200803508
- Gao, H., Popescu, R., Kopp, B., and Wang, Z. (2011). Bufadienolides and their antitumor activity. *Nat. Prod. Rep.* 28 (5), 953–969. doi:10.1039/C0NP00032A
- Gao, H., Zehl, M., Kaehlig, H., Schneider, P., Stuppner, H., Moreno, L., et al. (2010). Rapid structural identification of cytotoxic bufadienolide sulfates in toad venom from *Bufo melanostictus* by LC-DAD-MS n and LC-SPE-NMR. *J. Nat. Prod.* 73 (4), 603–608. doi:10.1021/np900746k
- Guillarme, D., Ruta, J., Rudaz, S., and Veuthey, J.-L. (2010). New trends in fast and high-resolution liquid chromatography: A critical comparison of existing approaches. *Anal. Bioanal. Chem.* 397 (3), 1069–1082. doi:10.1007/s00216-009-3305-8
- Han, L., Si, N., Gao, B., Wang, H., Zhou, Y., Yang, J., et al. (2017). Metabolites analysis of 4 arenobufagin structure-related bufadienolides in human liver microsomes using UHPLC-ESI-Orbitrap mass. *Int. J. Mass Spectrom.* 422, 88–93. doi:10.1016/j.ijms.2017.08.011
- Han, L., Wang, H., Si, N., Ren, W., Gao, B., Li, Y., et al. (2016). Metabolites profiling of 10 bufadienolides in human liver microsomes and their cytotoxicity variation in HepG2 cell. *Anal. Bioanal. Chem.* 408 (10), 2485–2495. doi:10.1007/s00216-016-9345-y
- Hayes, R. A., Crossland, M. R., Hagman, M., Capon, R. J., and Shine, R. (2009). Ontogenetic variation in the chemical defenses of cane toads (*Bufo marinus*): Toxin profiles and effects on predators. *J. Chem. Ecol.* 35 (4), 391–399. doi:10.1007/s10886-009-9608-6
- Heasley, B. (2012). Chemical synthesis of the cardiotonic steroid glycosides and related natural products. *Chemistry* 18 (11), 3092–3120. doi:10.1002/chem.201103733
- Hegazy, M.-E. F., Mohamed, T. A., ElShamy, A. I., Abou-El-Hamd, H. M., Mahalel, U. A., Reda, E. H., et al. (2015). Microbial biotransformation as a tool for drug development based on natural products from mevalonic acid pathway: A review. *J. Adv. Res.* 6 (1), 17–33. doi:10.1016/j.jare.2014.11.009
- Holmgren, M., Wagg, J., Bezanilla, F., Rakowski, R. F., De Weer, P., and Gadsby, D. C. (2000). Three distinct and sequential steps in the release of sodium ions by the Na⁺/K⁺-ATPase. *Nature* 403 (6772), 898–901. doi:10.1038/35002599
- Hoshino, Y., and Gaucher, E. A. (2021). Evolution of bacterial steroid biosynthesis and its impact on eukaryogenesis. *Proc. Natl. Acad. Sci. U. S. A.* 118 (25), e2101276118. doi:10.1073/pnas.2101276118
- Huang, W., Wen, C., Zhou, Z. R., Fu, Z. H., Katz, A., Plotnikov, A., et al. (2019). An efficient one-pot enzymatic synthesis of cardiac glycosides with varied sugar chain lengths. *Adv. Synth. Catal.* 361 (13), 3114–3119. doi:10.1002/adsc.201900227
- Jiang, Y., Zhang, Y., Luan, J., Duan, H., Zhang, F., Yagasaki, K., et al. (2010). Effects of bufalin on the proliferation of human lung cancer cells and its molecular mechanisms of action. *Cytotechnology* 62 (6), 573–583. doi:10.1007/s10616-010-9310-0
- Jørgensen, P. L. (1982). Mechanism of the Na⁺, K⁺ pump protein structure and conformations of the pure (Na⁺ + K⁺)-ATPase. *Biochim. Biophys. Acta* 694 (1), 27–68. doi:10.1016/0304-4157(82)90013-2
- Kamano, Y., Nogawa, T., Yamashita, A., Hayashi, M., Inoue, M., Drašar, P., et al. (2002). Isolation and structure of a 20, 21-epoxybufenolide series from “ch’an su”. *J. Nat. Prod.* 65 (7), 1001–1005. doi:10.1021/np0200360
- Kanai, R., Ogawa, H., Vilsen, B., Cornelius, F., and Toyoshima, C. (2013). Crystal structure of a Na⁺-bound Na⁺, K⁺-ATPase preceding the E1P state. *Nature* 502 (7470), 201–206. doi:10.1038/nature12578
- Kim, M.-H., Lyu, J.-H., Lyu, S., Hong, S.-H., Kim, W.-I., Yoon, H.-J., et al. (2008). Inhibitory effect of Chan-Su on the secretion of PGE2 and NO in LPS-stimulated BV2 microglial cells. *J. Physiology Pathology Korean Med.* 22 (5), 1315–1321.
- Lancaster, M., and Vegad, J. (1967). Suppression of the early inflammatory response in the sheep by strophanthin G. *Nature* 213 (5078), 840–841. doi:10.1038/213840b0
- Laursen, M., Gregersen, J. L., Yatime, L., Nissen, P., and Fedosova, N. U. (2015). Structures and characterization of digoxin- and bufalin-bound Na⁺, K⁺-ATPase compared with the ouabain-bound complex. *Proc. Natl. Acad. Sci. U. S. A.* 112 (6), 1755–1760. doi:10.1073/pnas.1422997112
- Lee, S.-S., Derguini, F., Bruening, R. C., Nakanishi, K., Wallick, E. T., Akizawa, T., et al. (1994). Digitalis-like compounds of toad bile: Sulfation and reduction of bufadienolides decrease potency of Na⁺, K⁺-ATPase inhibition. *Heterocycles* 2 (39), 669–686. doi:10.3987/com-94-s(b)59
- Li, B.-J., Tian, H.-Y., Zhang, D.-M., Lei, Y.-H., Wang, L., Jiang, R.-W., et al. (2015). Bufadienolides with cytotoxic activity from the skins of *Bufo bufo* gargarizans. *Fitoterapia* 105, 7–15. doi:10.1016/j.fitote.2015.05.013

- Li, F. J., Hu, J. H., Ren, X., Zhou, C. M., Liu, Q., and Zhang, Y. Q. (2021). Toad venom: A comprehensive review of chemical constituents, anticancer activities, and mechanisms. *Arch. Pharm.* 354 (7), 2100060. doi:10.1002/ardp.202100060
- Li, K., Feng, J., Kuang, Y., Song, W., Zhang, M., Ji, S., et al. (2017). Enzymatic synthesis of bufadienolide O-glycosides as potent antitumor agents using a microbial glycosyltransferase. *Adv. Synth. Catal.* 359 (21), 3765–3772. doi:10.1002/adsc.201700777
- Li, W., Lin, X., Yang, Z., Zhang, W., Ren, T., Qu, F., et al. (2015). A bufadienolide-loaded submicron emulsion for oral administration: Stability, antitumor efficacy and toxicity. *Int. J. Pharm.* 479 (1), 52–62. doi:10.1016/j.ijpharm.2014.12.054
- Liu, T., Zhang, L., Joo, D., and Sun, S.-C. (2017). NF- κ B signaling in inflammation. *Signal Transduct. Target. Ther.* 2 (1), 17023–17029. doi:10.1038/sigtrans.2017.23
- Ma, X.-C., Zheng, J., and Guo, D.-A. (2007). Highly selective isomerization and dehydrogenation of three major bufadienolides at 3-OH by *Fusarium solani*. *Enzyme Microb. Technol.* 40 (6), 1585–1591. doi:10.1016/j.enzmictec.2006.11.015
- Matsukawa, M., Akizawa, T., Morris, J. F., Butler, J., and Yoshioka, M. (1996). Marinoic acid, a novel bufadienolide-related substance in the skin of the giant toad, *Bufo marinus*. *Chem. Pharm. Bull.* 44 (1), 255–257. doi:10.1248/cpb.44.255
- Matsukawa, M., Akizawa, T., Ohigashi, M., Morris, J. F., Butler, J., and Yoshioka, M. (1997). A novel bufadienolide, marinosin, in the skin of the giant toad, *Bufo marinus*. *Chem. Pharm. Bull.* 45 (2), 249–254. doi:10.1248/cpb.45.249
- Matsukawa, M., Mukai, T., Akizawa, T., Miyatake, S., Yoshioka, M., Morris, J. F., et al. (1998). Isolation and characterization of novel endogenous digitalis-like factors in the ovary of the giant toad, *Bufo marinus*. *J. Nat. Prod.* 61 (12), 1476–1481. doi:10.1021/np980189g
- Meng, Q., Yau, L.-F., Lu, J.-G., Wu, Z.-Z., Zhang, B.-X., Wang, J.-R., et al. (2016). Chemical profiling and cytotoxicity assay of bufadienolides in toad venom and toad skin. *J. Ethnopharmacol.* 187, 74–82. doi:10.1016/j.jep.2016.03.062
- Michalak, M., Michalak, K., and Wicha, J. (2017). The synthesis of cardenolide and bufadienolide aglycones, and related steroids bearing a heterocyclic subunit. *Nat. Prod. Rep.* 34 (4), 361–410. doi:10.1039/C6NP00107F
- Mohammadi, S., Gompert, Z., Gonzalez, J., Takeuchi, H., Mori, A., and Savitzky, A. H. (2016). Toxin-resistant isoforms of Na⁺/K⁺-ATPase in snakes do not closely track dietary specialization on toads. *Proc. Biol. Sci.* 283 (1842), 20162111. doi:10.1098/rspb.2016.2111
- Morth, J. P., Pedersen, B. P., Toustrup-Jensen, M. S., Sørensen, T. L.-M., Petersen, J., Andersen, J. P., et al. (2007). Crystal structure of the sodium–potassium pump. *Nature* 450 (7172), 1043–1049. doi:10.1038/nature06419
- Nogawa, T., Kamano, Y., Yamashita, A., and Pettit, G. R. (2001). Isolation and structure of five new cancer cell growth inhibitory bufadienolides from the Chinese traditional drug Ch'an Su. *J. Nat. Prod.* 64 (9), 1148–1152. doi:10.1021/np0101088
- Nyblom, M., Poulsen, H., Gourdon, P., Reinhard, L., Andersson, M., Lindahl, E., et al. (2013). Crystal structure of Na⁺, K⁺-ATPase in the Na⁺-bound state. *Science* 342 (6154), 123–127. doi:10.1126/science.1243352
- Ogawa, H., Shinoda, T., Cornelius, F., and Toyoshima, C. (2009). Crystal structure of the sodium-potassium pump (Na⁺, K⁺-ATPase) with bound potassium and ouabain. *Proc. Natl. Acad. Sci. U. S. A.* 106 (33), 13742–13747. doi:10.1073/pnas.0907054106
- Pavesi, C., Flon, V., Mann, S., Leleu, S., Prado, S., and Franck, X. (2021). Biosynthesis of azaphilones: A review. *Nat. Prod. Rep.* 38 (6), 1058–1071. doi:10.1039/D0NP00080A
- Pearson, K. C., and Tarvin, R. D. (2022). A review of chemical defense in harlequin toads (Bufonidae; Atelopus). *Toxicon* X, 100092. doi:10.1016/j.toxcx.2022.100092
- Petroselli, G., Raices, M., Jungblut, L. D., Pozzi, A. G., and Erra-Balsells, R. (2018). MALDI-MS argininy bufadienolide esters fingerprint from parotid gland secretions of *Rhinella arenarum*: Age, gender, and seasonal variation. *J. Mass Spectrom.* 53 (6), 465–475. doi:10.1002/jms.4082
- Petschenka, G., and Agrawal, A. A. (2015). Milkweed butterfly resistance to plant toxins is linked to sequestration, not coping with a toxic diet. *Proc. Biol. Sci.* 282 (1818), 20151865. doi:10.1098/rspb.2015.1865
- Prassas, I., and Diamandis, E. P. (2008). Novel therapeutic applications of cardiac glycosides. *Nat. Rev. Drug Discov.* 7 (11), 926–935. doi:10.1038/nrd2682
- Qi, J., Tan, C., Hashimi, S. M., Zulfiker, A. H. M., Good, D., and Wei, M. Q. (2014). Toad glandular secretions and skin extractions as anti-inflammatory and anticancer agents. *Evid. Based. Complement. Altern. Med.* 2014, 312684. doi:10.1155/2014/312684
- Rodríguez, C., Rollins-Smith, L., Ibáñez, R., Durant-Archibold, A. A., and Gutiérrez, M. (2017). Toxins and pharmacologically active compounds from species of the family Bufonidae (Amphibia, Anura). *J. Ethnopharmacol.* 198, 235–254. doi:10.1016/j.jep.2016.12.021
- Rong, X., Ni, W., Liu, Y., Wen, J., Qian, C., Sun, L., et al. (2014). Bufalin, a bioactive component of the Chinese medicine chansu, inhibits inflammation and invasion of human rheumatoid arthritis fibroblast-like synoviocytes. *Inflammation* 37 (4), 1050–1058. doi:10.1007/s10753-014-9828-y
- Shao, H., Li, B., Li, H., Gao, L., Zhang, C., Sheng, H., et al. (2021). Novel strategies for solubility and bioavailability enhancement of bufadienolides. *Molecules* 27 (1), 51. doi:10.3390/molecules27010051
- Shimizu, S., Hagiwara, K., Itoh, H., and Inoue, M. (2020). Unified total synthesis of five bufadienolides. *Org. Lett.* 22 (21), 8652–8657. doi:10.1021/acs.orglett.0c03251
- Silva, D. B., and Lopes, N. P. (2015). MALDI-MS of flavonoids: A systematic investigation of ionization and in-source dissociation mechanisms. *J. Mass Spectrom.* 50 (1), 182–190. doi:10.1002/jms.3516
- Smedley, S. R., Risteen, R. G., Tonyai, K. K., Pitino, J. C., Hu, Y., Ahmed, Z. B., et al. (2017). Bufadienolides (lucibufagins) from an ecologically aberrant firefly (*Ellychnia corrusca*). *Chemoecology* 27 (4), 141–153. doi:10.1007/s00049-017-0240-6
- Steyn, P. S., and van Heerden, F. R. (1998). Bufadienolides of plant and animal origin. *Nat. Prod. Rep.* 15 (4), 397–413. doi:10.1039/A815397Y
- Stoll, A., Suter, E., Kreis, W., Bussemaker, B. B., and Hofmann, A. (1933). Die herzkaktiven Substanzen der Meerzwiebel. Scillaren A. *Helv. Chim. Acta* 16, 703–733. doi:10.1002/hlca.19330160198
- Sweadner, K. J. (1989). Isozymes of the Na⁺/K⁺-ATPase. *Biochim. Biophys. Acta* 988 (2), 185–220. doi:10.1016/0304-4157(89)90019-1
- Thorson, J. S., and Vogt, T. (2003). *Glycosylated natural products. Carbohydrate-based drug discovery*. New York City, NY: John Wiley&Sons, Ltd., 685–711.
- Tian, H.-Y., Ruan, L.-J., Yu, T., Zheng, Q.-F., Chen, N.-H., Wu, R.-B., et al. (2017). Bufospirostenin A and Bufogargarizin C, steroids with rearranged skeletons from the toad *Bufo bufo* gargarizans. *J. Nat. Prod.* 80 (4), 1182–1186. doi:10.1021/acs.jnatprod.6b01018
- Tian, H. Y., Wang, L., Zhang, X. Q., Wang, Y., Zhang, D. M., Jiang, R. W., et al. (2010). Bufogargarizins A and B: Two novel 19-norbufadienolides with unprecedented skeletons from the venom of *Bufo bufo* gargarizans. *Chemistry* 16 (36), 10989–10993. doi:10.1002/chem.201000847
- Todoric, J., Antonucci, L., and Karin, M. (2016). Targeting inflammation in cancer prevention and therapy. *Cancer Prev. Res.* 9 (12), 895–905. doi:10.1158/1940-6207.CAPR-16-0209
- Tureček, F., and Hanuš, V. (1984). Retro-Diels-Alder reaction in mass spectrometry. *Mass Spectrom. Rev.* 3 (1), 85–152. doi:10.1002/mas.1280030104
- Ujvari, B., Casewell, N. R., Sunagar, K., Arbuckle, K., Wüster, W., Lo, N., et al. (2015). Widespread convergence in toxin resistance by predictable molecular evolution. *Proc. Natl. Acad. Sci. U. S. A.* 112 (38), 11911–11916. doi:10.1073/pnas.1511706112
- Verpoorte, R., and Svendsen, A. B. (1979). Chemical constituents of Vietnamese toad venom collected from *Bufo melanostictus* schneider: Part I. The sterols. *J. Ethnopharmacol.* 1 (2), 197–202. doi:10.1016/0378-8741(79)90007-2
- Verpoorte, R., and Svendsen, A. B. (1980). Chemical constituents of Vietnamese toad venom, collected from *Bufo melanostictus* Schneider. Part II. The bufadienolides. *J. Nat. Prod.* 43 (3), 347–352. doi:10.1021/np50009a005
- Wang, S.-w., Bai, Y.-f., Weng, Y.-y., Fan, X.-y., Huang, H., Zheng, F., et al. (2019). Cinobufacini ameliorates dextran sulfate sodium-induced colitis in mice through inhibiting M1 macrophage polarization. *J. Pharmacol. Exp. Ther.* 368 (3), 391–400. doi:10.1124/jpet.118.254516
- Wei, W.-L., Hou, J.-J., Wang, X., Yu, Y., Li, H.-J., Li, Z.-W., et al. (2019). Venenum bufonis: An overview of its traditional use, natural product chemistry, pharmacology, pharmacokinetics and toxicology. *J. Ethnopharmacol.* 237, 215–235. doi:10.1016/j.jep.2019.03.042
- Wei, W.-L., Li, H.-J., Yang, W.-Z., Qu, H., Li, Z.-W., Yao, C.-L., et al. (2022). An integrated strategy for comprehensive characterization of metabolites and metabolic profiles of bufadienolides from Venenum Bufonis in rats. *J. Pharm. Anal.* 12 (1), 136–144. doi:10.1016/j.jpha.2021.02.003
- Wen, C., Huang, W., Zhu, X.-L., Li, X.-S., Zhang, F., and Jiang, R.-W. (2018). UGT74AN1, a permissive glycosyltransferase from *Asclepias curassavica* for the regioselective steroid 3-O-glycosylation. *Org. Lett.* 20 (3), 534–537. doi:10.1021/acs.orglett.7b03619
- Wen, L., Huang, Y., Xie, X., Huang, W., Yin, J., Lin, W., et al. (2014). Anti-inflammatory and antinociceptive activities of bufalin in rodents. *Mediat. Inflamm.* 2014, 171839. doi:10.1155/2014/171839
- Williams, G. J., Zhang, C., and Thorson, J. S. (2007). Expanding the promiscuity of a natural-product glycosyltransferase by directed evolution. *Nat. Chem. Biol.* 3 (10), 657–662. doi:10.1038/nchembio.2007.28

- Wu, W.-Y., Fan, T.-Y., Li, N.-G., Duan, J.-A., Shi, Z.-H., Chen, M., et al. (2020). Total synthesis, chemical modification and structure-activity relationship of bufadienolides. *Eur. J. Med. Chem.* 189, 112038. doi:10.1016/j.ejmech.2020.112038
- Ye, M., and Guo, D. (2008). A new bufadienolide obtained from the biotransformation of cinobufagin by *Alternaria alternata*. *Nat. Prod. Res.* 22 (1), 26–30. doi:10.1080/14786410601130141
- Ye, M., Ning, L., Zhan, J., Guo, H., and Guo, D. (2003). Biotransformation of cinobufagin by cell suspension cultures of *Catharanthus roseus* and *Platycodon grandiflorum*. *J. Mol. Catal. B Enzym.* 22 (1–2), 89–95. doi:10.1016/S1381-1177(03)00011-0
- Yue, W., Ming, Q.-L., Lin, B., Rahman, K., Zheng, C.-J., Han, T., et al. (2016). Medicinal plant cell suspension cultures: Pharmaceutical applications and high-yielding strategies for the desired secondary metabolites. *Crit. Rev. Biotechnol.* 36 (2), 215–232. doi:10.3109/07388551.2014.923986
- Zhan, X., Wu, H., Wu, H., Wang, R., Luo, C., Gao, B., et al. (2020). Metabolites from *Bufo gargarizans* (cantor, 1842): A review of traditional uses, pharmacological activity, toxicity and quality control. *J. Ethnopharmacol.* 246, 112178. doi:10.1016/j.jep.2019.112178
- Zhang, C., Griffith, B. R., Fu, Q., Albermann, C., Fu, X., Lee, I.-K., et al. (2006). Exploiting the reversibility of natural product glycosyltransferase-catalyzed reactions. *Science* 313 (5791), 1291–1294. doi:10.1126/science.1130028
- Zhang, P.-W., Tian, H.-Y., Nie, Q.-L., Wang, L., Zhou, S.-W., Ye, W.-C., et al. (2016). Structures and inhibitory activity against breast cancer cells of new bufadienolides from the eggs of toad *Bufo bufo gargarizans*. *RSC Adv.* 6 (96), 93832–93841. doi:10.1039/C6RA18676A
- Zhang, X., Ye, M., Dong, Y.-h., Hu, H.-b., Tao, S.-j., Yin, J., et al. (2011). Biotransformation of bufadienolides by cell suspension cultures of *Saussurea involucrata*. *Phytochemistry* 72 (14–15), 1779–1785. doi:10.1016/j.phytochem.2011.05.004
- Zhou, J., Gong, Y., Ma, H., Wang, H., Qian, D., Wen, H., et al. (2015). Effect of drying methods on the free and conjugated bufadienolide content in toad venom determined by ultra-performance liquid chromatography-triple quadrupole mass spectrometry coupled with a pattern recognition approach. *J. Pharm. Biomed. Anal.* 114, 482–487. doi:10.1016/j.jpba.2015.05.032
- Zhou, M., Hou, Y., Hamza, A., Zhan, C.-G., Bugni, T. S., Thorson, J. S., et al. (2012). Probing the regiospecificity of enzyme-catalyzed steroid glycosylation. *Org. Lett.* 14 (21), 5424–5427. doi:10.1021/ol3024924
- Zhou, S.-w., Quan, J.-y., Li, Z.-w., Ye, G., Shang, Z., Chen, Z.-p., et al. (2021). Bufadienolides from the eggs of the toad *Bufo bufo gargarizans* and their antimelanoma activities. *J. Nat. Prod.* 84 (5), 1425–1433. doi:10.1021/acs.jnatprod.0c00840
- Zhou, S., Zheng, Q., Huang, X., Wang, Y., Luo, S., Jiang, R., et al. (2017). Isolation and identification of l/d-lactate-conjugated bufadienolides from toad eggs revealing lactate racemization in amphibians. *Org. Biomol. Chem.* 15 (26), 5609–5615. doi:10.1039/C7OB01055A
- Zhu, X.-L., Wen, C., Ye, Q.-M., Xu, W., Zou, D.-L., Liang, G.-P., et al. (2018). Probing the stereoselectivity of OleD-catalyzed glycosylation of cardiotonic steroids. *RSC Adv.* 8 (10), 5071–5078. doi:10.1039/C7RA11979H
- Zou, D., Zhu, X., Zhang, F., Du, Y., Ma, J., and Jiang, R. (2018). An efficient strategy based on liquid–liquid extraction with three-phase solvent system and high speed counter-current chromatography for rapid enrichment and separation of epimers of minor bufadienolide from toad meat. *J. Agric. Food Chem.* 66 (4), 1008–1014. doi:10.1021/acs.jafc.7b05310



OPEN ACCESS

EDITED BY

Shuai Wang,
Guangzhou University of Chinese
Medicine, China

REVIEWED BY

Hou Wen,
Gannan Medical University, China
Yingqi Xu,
Singapore Health Services, Singapore

*CORRESPONDENCE

Xiaokang Wang,
kangtae_won@i.smu.edu.cn

SPECIALTY SECTION

This article was submitted to
Inflammation Pharmacology,
a section of the journal
Frontiers in Pharmacology

RECEIVED 14 September 2022

ACCEPTED 11 October 2022

PUBLISHED 24 October 2022

CITATION

Wang X, Rao J, Tan Z, Xun T, Zhao J and
Yang X (2022), Inflammatory signaling
on cytochrome P450-mediated drug
metabolism in hepatocytes.
Front. Pharmacol. 13:1043836.
doi: 10.3389/fphar.2022.1043836

COPYRIGHT

© 2022 Wang, Rao, Tan, Xun, Zhao and
Yang. This is an open-access article
distributed under the terms of the
[Creative Commons Attribution License](#)
(CC BY). The use, distribution or
reproduction in other forums is
permitted, provided the original
author(s) and the copyright owner(s) are
credited and that the original
publication in this journal is cited, in
accordance with accepted academic
practice. No use, distribution or
reproduction is permitted which does
not comply with these terms.

Inflammatory signaling on cytochrome P450-mediated drug metabolism in hepatocytes

Xiaokang Wang ^{1,2*}, Jiaoyu Rao¹, Zhiyi Tan³, Tianrong Xun²,
Jingqian Zhao² and Xixiao Yang²

¹Department of Pharmacy, Shenzhen Longhua District Central Hospital, Shenzhen, China,

²Department of Pharmacy, Shenzhen Hospital, Southern Medical University, Shenzhen, China,

³Guangzhou Customs Technology Center, Guangzhou, China

Cytochrome P450 (CYP450) enzymes are membrane-bound blood proteins that are vital to drug detoxification, cell metabolism, and homeostasis. CYP450s belonging to CYP families 1–3 are responsible for nearly 80% of oxidative metabolism and complete elimination of approximately 50% of all common clinical drugs in humans liver hepatocytes. CYP450s can affect the body's response to drugs by altering the reaction, safety, bioavailability, and toxicity. They can also regulate metabolic organs and the body's local action sites to produce drug resistance through altered drug metabolism. Genetic polymorphisms in the CYP gene alone do not explain ethnic and individual differences in drug efficacy in the context of complex diseases. The purpose of this review is to summarize the impact of new inflammatory-response signaling pathways on the activity and expression of CYP drug-metabolizing enzymes. Included is a summary of recent studies that have identified drugs with the potential to regulate drug-metabolizing enzyme activity. Our goal is to inspire the development of clinical drug treatment processes that consider the impact of the inflammatory environment on drug treatment, as well as provide research targets for those studying drug metabolism.

KEYWORDS

cytochrome P450, inflammatory signaling, drug metabolism, hepatocytes, clinical application

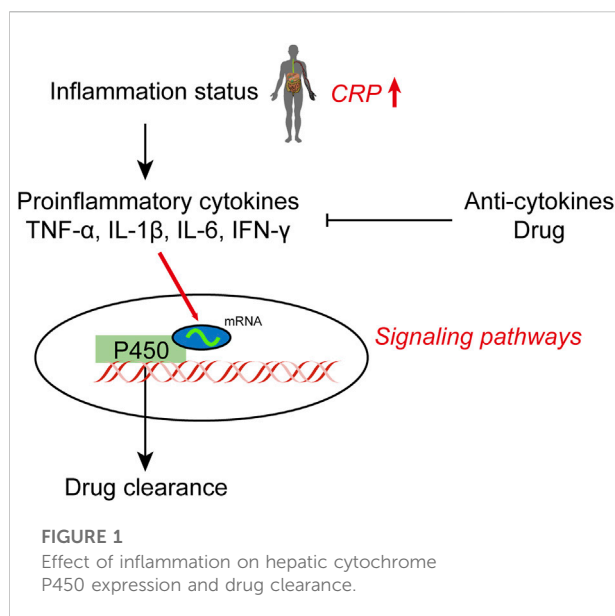
Introduction

The absorption (A), distribution (D), metabolism (M), and elimination (E) of ADME vary widely between individuals, contributing to a variety of drug-induced and environmental exposure-related toxicities, which control the fate of these compounds *in vivo* (Roberts et al., 2018). Individual responses to drugs and environmental exposures can be explained by changes in ADME processes. Many examples indicate that these differences play an important role in a genetic subpopulations' susceptibility to specific toxicities. However, the possibility of transient phenotypic transformation resulting from changes in the environment, such as inflammation and disease, is often overlooked (Morgan et al., 2020). It is becoming increasingly apparent that disease and the physiological state of the patient, as well as genetic and environmental factors, have

an impact on drug metabolism and disposition. The clinical outcome of a disease can be profoundly affected by the expression and activity of drug-metabolizing enzymes and transporters (Xie 2020).

Cytochrome P450 (CYP450) enzymes are membrane-bound, heme-containing terminal oxidases essential for human drug metabolism (M), cellular metabolism, and homeostasis. Nearly 80% of the oxidative metabolism of clinical drugs and approximately 50% of their elimination are attributed to one or more CYPs belonging to CYP families 1 through 3 (Cacabelos and Martínez-Bouza 2011; Koike et al., 2021; Zhao et al., 2021). Genetic polymorphisms may be responsible for the variation observed among races and between individuals. However, recent studies have shown that environmental factors, such as inflammatory status, chemotherapeutic drug exposure, and gut microbiota, can also provide new insights into the mechanism of individual differences in drug treatment and targets, which can be used to prevent adverse reactions (Aitken et al., 2007; Gong et al., 2018; Gomes et al., 2021). Only a handful of studies have addressed clinical problems resulting from these disease states and a systematic study, including of their effects on hepatocyte metabolism, has not been conducted. This review summarizes and highlights the most recent research on hepatic inflammation and the regulation of expression and activity of CYP enzymes during drug metabolism. Nuclear transcription factors and signaling pathways are also discussed to highlight the inflammatory signaling pathways that control the metabolism and elimination of CYP enzymes in hepatocytes, as well as to provide drug targets for future research.

Individualized drug therapy is a constant topic in modern clinical pharmacy. To achieve the most effective use of various drugs for the benefit of the patient, individualized treatment protocols are necessary (Josefsson et al., 2019). The liver is adversely affected by proinflammatory cytokines such as interleukin-1 β (IL-1 β), IL-6, and tumor necrosis factor (TNF- α); however, the impact of their adverse effect on CYP450 enzyme activity has not been systematically reported. (Renton et al., 2005; Dickmann et al., 2012). IL-6 has specifically been shown to regulate various CYPs, including CYP3A4 (Dickmann, et al., 2012). Clinical inflammatory markers, such as C-reactive protein (CRP), are associated with a variety of “negative acute phase reactions” that involve most drug metabolism enzymes and transporters, which supports the documented negative effects of inflammation on drug metabolism (Harvey and Morgan 2014; Wang et al., 2021). The mechanism leading to synergistic downregulation of drug-metabolizing enzymes and transporters (DMET) was studied in primary human hepatocytes (PHH) treated with IL-6 and selective signal transduction inhibitors (Schröder et al., 2013). MAPK and PI3K were more important for DMET regulation than JAK/STAT signaling, according to reverse-phase phosphoproteomic analysis. The RXR protein was also found to be downregulated, but not its transcript, in

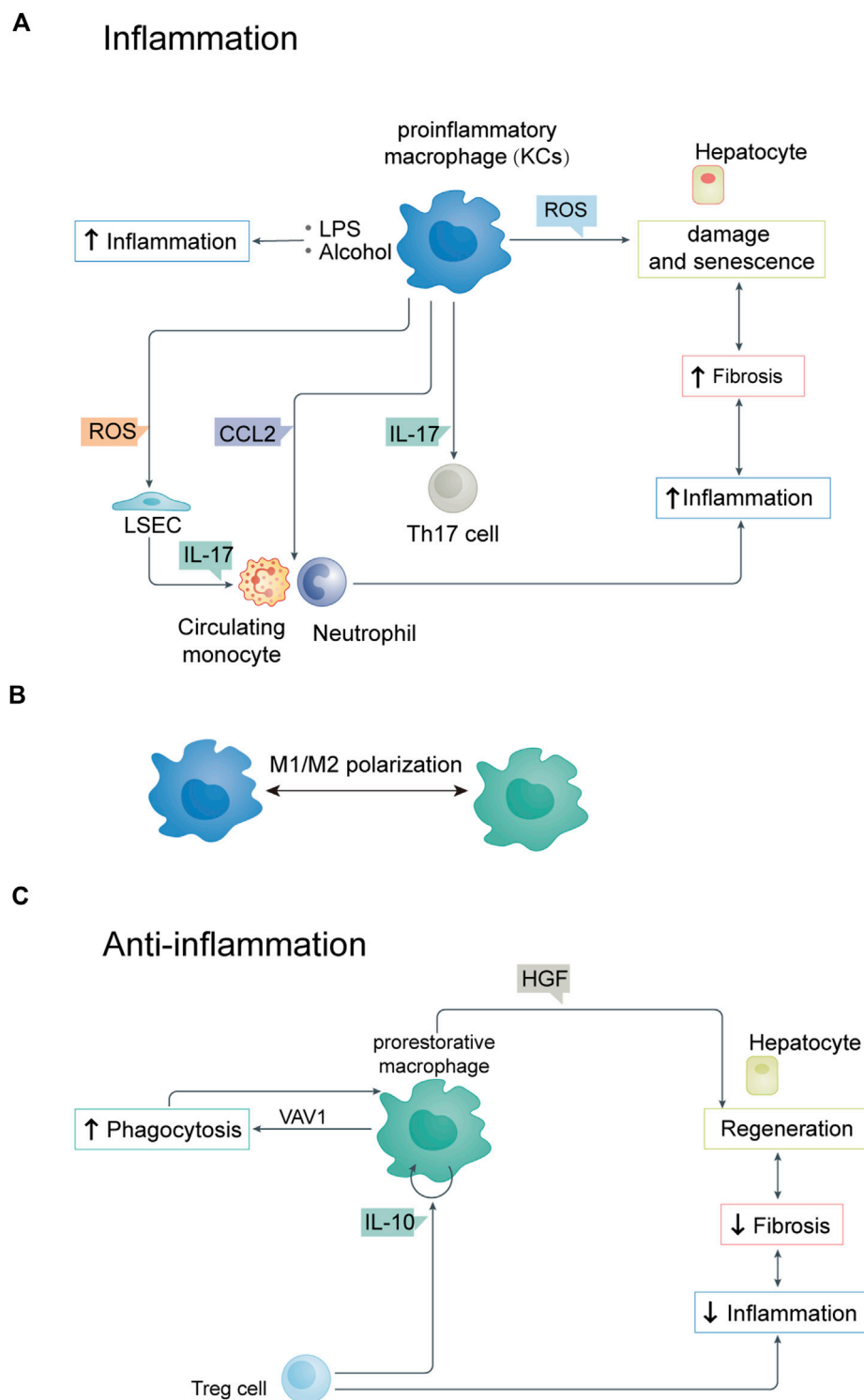


response to IL-6. Numerous miRNAs were also found to be significantly elevated in cholestatic liver, including miR-130b, which has previously been shown to suppress the activities of various cytochromes P450 enzymes during inflammation (Rieger et al., 2015). It appears that miR-130b also directly targets RXR α .

These results suggest that downregulation of DMET genes in hepatocytes during inflammation involves MAPK and PI3K signaling activation by IL-6, as well as inactivated or downregulated RXR α /nuclear receptor complexes. Lipopolysaccharide (LPS) and various cytokines, including IL-1 β , IL-2, IL-6, IFN- γ and TNF- α , also play a role in metabolism. Treatment with TNF- α results in significantly lower expression of CYP2C8 and CYP2C76 mRNA in hepatocytes. IL-1 β treatment significantly reduces the expression of CYP1A1, CYP2C8, CYP2C19, and CYP2C76 mRNA in hepatocytes, while it increases the expression of CYP3A5. Cytokines can affect the expression level of CYP450 mRNA in the liver and affect CYP450 expression in humans (Uno et al., 2020). These studies provide deeper insight into the mechanisms controlling CYP450s, specifically their activity, and provide evidence that may allow for the more effective use of clinical drugs (Figure 1).

Inflammation in hepatocytes

Hepatocytes are protected by Kupffer cells (KCs), endothelial cells, stellate cells, and the perisinusoidal space (Disse) barrier. Pathogen-associated molecular patterns (PAMPs), particularly lipopolysaccharides (LPSs) located in the outer membrane of Gram-positive bacteria, are associated with chronic liver disease, which is largely controlled by factors that contribute to its onset and progression. In chronic alcohol disease, LPS production in

**FIGURE 2**

(A) Relationship between parenchymal and non-parenchymal cells during inflammation. (B) M1/M2 polarization of KCs. (C) Relationship between parenchymal and non-parenchymal cells during anti-inflammation. LSEC, liver sinusoidal endothelial cell.

the intestine is transferred to the liver, where it combines with hepatocyte death to cause systemic inflammation, aggravating liver disease (He et al., 2021). Around 15% of the liver's cells are resident macrophages, known as KCs, which play a central role in preventing gut-derived pathogens from spreading throughout the body (Sierro et al., 2017). Around 15% of the liver's cells are resident macrophages, known as KCs, which play a central role in preventing gut-derived pathogens from spreading throughout the body. (Xu et al., 2022).

Liver macrophages, such as KCs, are activated by the convergence of alcohol and LPS. Indeed, stimulation of KCs with alcohol and LPSs can increase proinflammatory cytokines, including IL-1 β , IL-6, and TNF- α . Hepatocytes, neutrophils, and macrophages can produce reactive oxygen species more rapidly when LPS interacts with alcohol (Figure 2A) (Brenner et al., 2013). By activating NLRP3 inflammasomes, reactive oxygen species (ROS) cause hepatocyte damage and senescence, resulting in ROS production. ROS also play a role in the immune response of liver sinusoidal endothelial cells (LSECs) (Lao et al., 2018). LSECs are special capillary endothelial cells involved in maintaining metabolic and immune homeostasis and function as a structural barrier. They also participate in the liver immune response by regulating leukocyte (monocyte or neutrophil) recruitment and infiltration into tissues. If KCs are damaged by excessive BAs, they produce ROS, inflammation, and apoptotic factors that lead to LSEC dysfunction by negatively affecting viability and cell characteristics. The loss of functional LSEC may aggravate liver disease because it plays a central role in these processes (Shetty et al., 2018).

Macrophage polarization also plays an important role in the inflammation and anti-inflammatory response of hepatocytes (Figure 2B). The regulation of M1/M2 polarization of KCs is closely related to the progression of liver inflammation (Han et al., 2017). By inhibiting necroptosis-S100A9-necroinflammation, M2-like macrophages play a hepatoprotective role in acute and chronic liver failure (Bai X et al., 2021). Studies on cellular immune regulation have shown that phagocytosis is key to resolving any inflammatory reaction. The low-throughput phagocytosis that occurs during this period leads to dead cells being rapidly cleared by hepatocytes.

Macrophages are mainly responsible for clearing aging red blood cells, neutrophils, and effector CD8⁺ T lymphocytes from the liver (Uderhardt et al., 2019). Macrophages are professional phagocytes responsible for clearing dead cells from the liver after injury. Apoptotic cells respond to “eat me” signals through cell surface receptors on macrophages. During phagocytosis, liver macrophages acquire a “recovery-promoting” phenotype, contributing to liver fibrosis remodeling (Ramachandran et al., 2012). In addition to regulatory T cells, other immune cell types produce anti-inflammatory cytokines which control and terminate inflammation. These include Treg cells, which produce IL-13 that triggers macrophages to produce IL-10. IL-10 acts on macrophages in a cell autonomous manner and activates VAV1, which in turn activates RAC1. Studies have shown that hepatic RAC1 activation is necessary for phagosome

formation and phagocytosis of apoptotic cells, thus maintaining immune homeostasis (Figure 2C) (Pohlmann et al., 2018; Proto et al., 2018).

The NLRP3 inflammasome: a metabolic sensor for inflammation

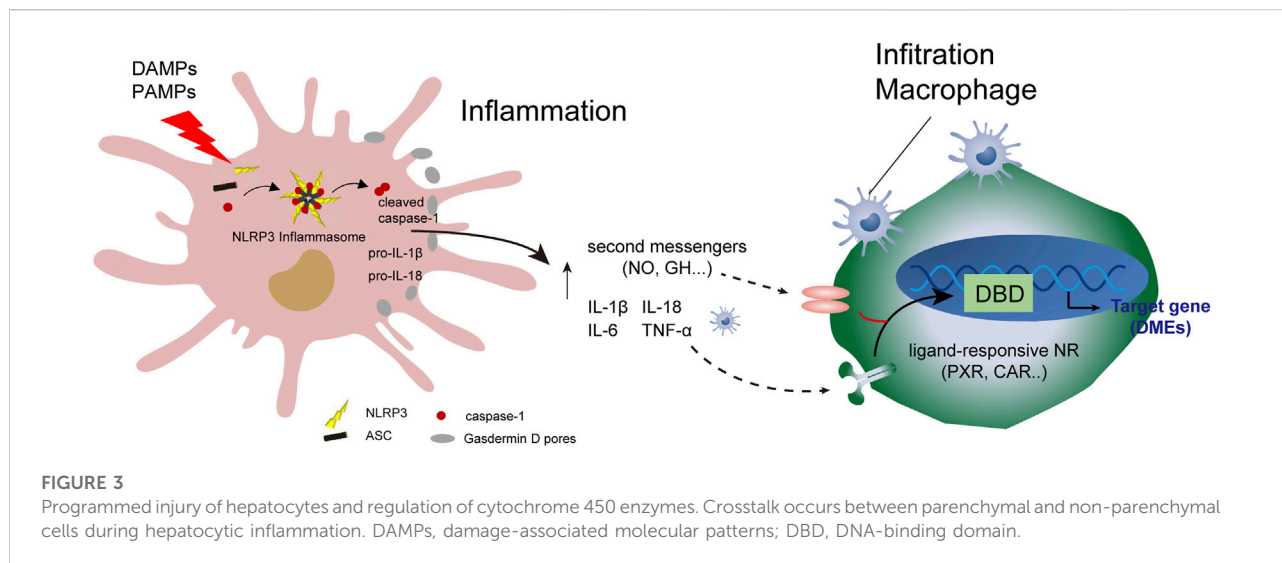
Inflammation is believed to regulate drug metabolism and transporters in a significant way (Stanke-Labesque et al., 2020). The activation of the inflammasome contributes significantly to hepatocyte damage, as well as immune cell activation and inflammation amplification. Inflammasome protein complex activation in immune cells triggers an innate immune response (Murphy 2018). Recent studies have shown that NLRP3 inflammation is involved in the regulation of multiple metabolic enzymes (Zhang et al., 2020; Zhao M et al., 2020). Research on NLRP3 inflammatory activation has become another trend, as it regulates multiple metabolic enzymes, as well as the NF- κ B signaling pathway.

Controlling inflammation by inhibiting NLRP3 inflammation is key to anti-inflammatory processes (Szabo and Petrasek 2015; Bäck et al., 2019). The endogenous metabolite bile acid can control hepatocyte inflammation and metabolic disorders by inhibiting the NLRP3 inflammasome (Guo et al., 2016). As shown in Figure 3, programmed hepatocyte injury or death (hepatocyte pyroptosis) is a response to PAMPs and danger-associated molecular patterns (DAMPs). The response is usually mediated by inflammasome sensor molecules, such as NLRP3, which is a protein 3 containing the NOD, LRR, and Pyrin domains, as well as ASC receptors and caspase-1.

A protein complex composed of ASC receptors and caspase-1 drives the pro-inflammatory cytokines IL-1 β and IL-18, and cleaves Gasdermin D to induce programmed hepatocyte death (Gaul et al., 2021). Programmed hepatocyte injury often induces the recruitment of hepatic macrophages, including KCs. A series of immune responses result in reduced hepatic drug-metabolizing enzyme activity and metabolism, such as lipid metabolism. Analysis of hepatic drug-metabolizing enzymes in disease-state environments and understanding the mechanism of action can help identify the clinical causes of drug metabolism abnormalities and develop biomarkers. These biomarkers can help determine drug-related metabolic enzyme activities, allowing for adjustment of the timing and dosage of drugs, and avoidance of drug-derived adverse reactions.

Human Hep:KC cocultures: a model of the effect of inflammation on cytochrome P450s in hepatocytes

A coculture model was developed by combining innate immune components to overcome the inherent limitations of



hepatocyte single-culture systems such as KCs. Cell cocultures can make up for the defects of monolayer cell culture and are better for observing the interaction between cells and the culture environment. Therefore, cocultures help maintain cellular function and are closer to physiological and pathological models *in vivo* and *in vitro* (Gao et al., 2020). Edward *et al.* believed that cell co-cultures simulate the physiological structure of the human body and provide conditions for cell-cell interaction. The hepatocyte and KC coculture (HKCC) model plays an important role in drug development and metabolic disease research (Rose et al., 2016). Sunman *et al.* demonstrated that a coculture system containing KCs led to IL-2 inhibition of CYP3A activity in hepatocytes for 72 h, while only 48 h of inhibition was observed in a hepatocyte monoculture (Sunman et al., 2004). Similarly, cocultures of parenchymal and non-parenchymal hepatocytes have indicated that KCs affect the upregulation and downregulation of various CYP450 isoforms and transporters (Chen et al., 2011). However, research focused on coculture systems is limited and replicating these observations is challenging. Therefore, establishing a mechanistic research model of the inflammatory state is of great significance for future exploration of CYP450 enzyme activity.

A few studies have characterized established HKCC models. A previously established system was modified to incorporate KCs, which were cultured in empirically optimized collagen micropattern domains supported by mouse 3T3-J2 fibroblasts (Wu et al., 2020). HKCC provides increased stability and allow hepatocytes to maintain their function for several weeks, thus enabling long-term studies. Receptors (i.e., IL-6 and IL-1 β) and non-receptors (i.e., IL-2 and IL-23) expressed in hepatocytes have different effects on metabolic enzymes in the Hep:KC coculture system (Nguyen et al., 2015).

Signaling pathways

Nuclear receptors (NRs)

Heme oxygenase (HO-1)

Cells are protected from oxidative damage by HO-1, which is activated by substances that cause oxidative stress, including aspirin, statins, and niacin (Abraham et al., 2016). Inflammation, diabetes, liver injury, infectious diseases, and cancer all affect HO-1 levels (Hsu et al., 2006; Abraham, et al., 2016). These diseases are often marked by oxidative stress and induction of HO-1 leads to a reduction of oxidants (heme) and the production of antioxidants, such as bilirubin and carbon monoxide (Connick et al., 2021). Anwar-Mohamed *et al.* found that that arsenite induces HO-1 expression in rat hepatocytes to mediate CYP1A1, CYP1A2, CYP3A23, and CYP3A2 inhibition (Anwar-Mohamed et al., 2012). HO-1 affects cytochrome P450 function in liver through the formation of heteromeric complex CYP1A2-HO-1 (Connick, et al., 2021). Inflammation causes cytokine levels to increase and ROS to build up, resulting in inhibition of HO-1, which depletes its cytoprotective properties. Cytochrome P450 enzymes, specifically CYP2D6, metabolize most drugs used to treat COVID-19 (Fakhouri et al., 2020). HO-1 upregulation has a potential role in the treatment and prevention of cytokine storms. Future research will determine whether inhibition of HO induces CYP2D6 at earlier stages of COVID-19 treatment.

Peroxisome proliferator activated receptor (PPAR)

PPAR, a nuclear receptor that plays a central role in metabolism, is expressed in tissues with high levels of oxidative stress (Montagner et al., 2016). It has been proposed

that inflammation induces CYP4A mRNAs; however, it is unclear if the same mechanism as chemical inducers is used, which involves PPAR activation (Lucarelli et al., 2022). PPAR δ agonists can reduce total bile acid content in patients with liver disease. Seladelpar (MBX-8025, a selective PPAR δ agonist) has been found to directly activate PPAR, repress liver expression of CYP7A1 (the rate-limiting enzyme for bile acid synthesis), and decrease plasma 7 α -hydroxy-4-cholesten-3-one (C4) levels (Jones et al., 2017). PPAR α is a ligand-activated transcription factor abundantly expressed in the liver. PPAR α activators are reported to prevent acetaminophen-induced hepatotoxicity, which involves regulation of lipid metabolism and inhibition of CYP2E1 activity (Attal et al., 2022). In two previous studies, 2-hydroxyacyl-CoA lyase levels significantly decreased while proteins associated with PPAR signaling, peroxisome proliferation, and omega oxidation, specifically CYP4A10 and CYP4A14, significantly increased in the liver proteome (Mezzar et al., 2017; Khalil et al., 2022).

Constitutive androstane receptor (CAR)

CARs are members of the nuclear receptor superfamily NR1I3, which are almost exclusively expressed in the liver. The transcription factor CAR in human hepatocytes interacts with key signaling pathways involved in drug metabolism and damage prevention in the liver (Tschuor et al., 2016; Bae et al., 2021). CAR regulates numerous genes through its function as a xenobiotic sensor in drug metabolism. By activating CAR, the polycyclic aromatic hydrocarbon pyrene induces mouse hepatotoxicity. As a moderate CYP450 inducer, metamizole has a weak inhibitory effect on CYP1A2 and acts as a moderate CYP450 inducer *via* interactions with CAR (Bachmann et al., 2021). In a previous study, wild-type mice treated with pyrene had significantly elevated levels of inflammatory cytokines, such as IL-6 and TNF- α , as well as elevated IL-6 serum levels. However, these changes were not observed in CAR KO mice (Shi et al., 2022). Therefore, the CAR nuclear transcription factor may be involved in the production of inflammatory cytokines, as well as the expression and activity of CYP450 enzymes.

Aryl hydrocarbon receptor (AhR)

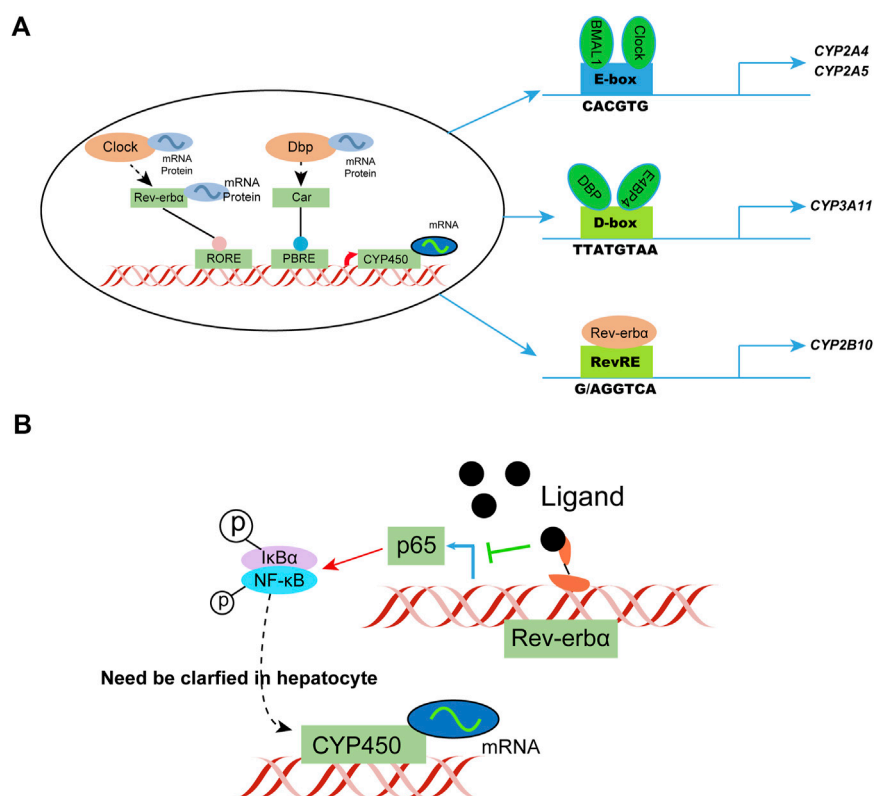
AhR recognizes heterologous and natural compounds that maintain mucosal surface homeostasis, such as tryptophan metabolites, dietary components, and microbial derived factors. As a result of AhR activation, cytochrome P450 1 (CYP1) enzymes are activated to oxidize AhR ligands, which are then metabolically cleared and detoxified (Schiering et al., 2017). CYP1 enzymes have an important feedback role by reducing AhR signals; however, their ability to regulate AhR ligands in hepatocytes is uncertain.

Polycyclic aromatic hydrocarbons and dioxins are persistent organic pollutants that damage the environment and regulate CYP1A1 expression primarily through the transcription factor AhR (Mescher and Haarmann-Stemann 2018). CYP1A1 activity analysis has been incorporated into modern toxicology concepts and testing guidelines, emphasizing the importance of this enzyme for chemical risk assessment and regulation. The development of CYP1A1 as a molecular target for preventing chemical carcinogenesis is hindered by limitations in the current research process. The main limitation is reduced metabolism of endogenous AhR ligands often observed in various human cancers, which frequently leads to downregulation of CYP1A1 (Al-Dhfyar et al., 2017). Therefore, the endogenous AhR signaling pathway is beneficial for the functional expression of CYP450 and promotes the development of therapeutic drugs.

Circadian regulation

Diurnal rhythmicity is observed in mice with coumarin hepatotoxicity, with more severe toxicity at ZT2 *versus* ZT14 (ZT, zeitgeber time; ZT2 represents lights on, and ZT14 represents lights off) (Zhao G et al., 2020). The circadian rhythm of drug-metabolizing enzyme expression is considered a key factor affecting circadian metabolism. In general, circadian clock genes regulate the circadian clock by targeting three *cis* elements, specifically the E-box, D-box, and Rev-erba. The response element or rar-related orphan receptor response element generates and regulates the circadian rhythm of drug-metabolizing enzymes. The clock-controlled nuclear receptors hepatocyte nuclear factor 4 α and PPAR γ play an important role in circadian enzyme expression. Circadian genes targeted by drugs, such as Rev-erba, provide an explanation of the genetic variability associated with drug efficacy. BMAL1 and Clock activate the transcription of CYP2A4/5 by directly binding to the E-box C element in the promoter. Knockdown of Clock or Bmal1 downregulates the expression of CYP2A4/5, which are key coumarin-metabolizing enzymes in mice.

Physiological processes, such as inflammation, are coordinated by the biological clock in mammals and recent studies indicate these two pathways interfere with each other. The pro-inflammatory transcription factor κ B in the human U2OS cell model was found to regulate the clock by inhibiting the amplitude and duration of the cycle, leading to the phenotype (Shen et al., 2021). Changes in NF- κ B also affect the circadian rhythm and motor activity of the suprachiasmatic nucleus depending on the light/dark conditions. The transcriptional activity of circadian E-box transcription factor BMAL1/clock is inhibited by RelA, much like the clock regulator CRY1. The transactivation domain of BMAL1 binds to RelA. NF- κ B competes with CRY1 and the coactivator CBP/P300 for BMAL1, thus affecting circadian transcription.

**FIGURE 4**

Circadian clock-controlled drug metabolism. **(A)** Molecular mechanisms of circadian clock regulation of CYP450; **(B)** Possible circadian clock regulation of CYP450 in hepatocytes in a state of inflammation. IκBα, I kappa B alpha.

NF-κB assumes a key role in regulating the circadian clock directly and highlights the reciprocal regulation of circadian rhythm and inflammation. Study of the transcriptional effect of NF-κB on BMAL1/Clock in a hepatocyte model, as well as the subsequent effect on CYP450 metabolizing enzyme phenotype, is a new research direction. Additional studies have shown that circadian regulation can alleviate inflammatory responses under physiological and pathological conditions, such as limiting hepatocyte inflammation by daily regulation of oxidative phosphorylation (Bai L et al., 2021). Rev-erba, a transcriptional repressor regulated by a ligand, is expected to be developed as a therapeutic agent for NASH and other liver diseases (Sato et al., 2020; Griffett et al., 2022). Such studies help predict the circadian pattern of drug metabolism genes in patients with inflammatory conditions (Figure 4).

Long non-coding RNAs (lncRNAs)

lncRNAs are a special subclass of ncRNAs that make up most of the mammalian genome and are composed of more than 200 nucleotides. They become the main regulators of

transcription *via* physical interactions with DNA, other RNAs, and proteins (Long et al., 2017). Numerous lncRNAs are associated with the development of liver disease, as well as inflammation and immune regulation (Chen et al., 2019). Indeed, the chemokine CXCL5 may contribute to the development of NAFLD fibrosis through *MALAT1* lncRNA (Leti et al., 2017). The circadian clock may also regulate lncRNA activity, in addition to the potential effects on circadian biology. Circadian NLRP3 inflammasome activity and steatohepatitis, an NLRP3-related disease, may be regulated by non-oscillatory lncRNAs.

The pluripotency-related transcript (*PLATR*) family is composed of 32 members (*PLATR* 1–32) and has been identified in embryonic stem cells (ESCs), it maintains the gene expression profile of ESCs. In one study, a 4-fold increase in *PLATR4* expression was observed in the MMTV-neu NDL breast cancer model, suggesting that *PLATR4* may be involved in tumor progression in this model (Diermeier et al., 2016). *PLATR4* is an oscillating lncRNA that is deregulated in murine steatohepatitis. Its oscillation is determined by the diurnal clock component Rev-erba drive. *PLATR4* acts as a circadian inhibitor of NLRP3 inflammasome activity by inhibiting the transcription and expression of the inflammasome components NLRP3 and ASC. The deletion of *PLATR4* sensitizes mice to

experimental steatohepatitis, whereas expression of *PLATR3* improves the pathological conditions. Mechanistically, *PLATR4* prevents NF- κ B/Rxra formation and the κ B site, thereby inhibiting the transcriptional activation of NLRP3 and ASC by NF- κ B. Therefore, *PLATR4* appears to be an attractive target for the treatment of liver inflammation.

The regulation of inflammation is achieved *via* the main components of the circadian clock, such as Clock, Rev-erba, and Cry1/2. This explains the circadian rhythm of symptom severity in inflammatory diseases, such as colitis and rheumatoid arthritis, as well as the increased susceptibility to inflammatory-related diseases, such as obesity and NAFLD (Sookoian et al., 2008). *PLATR4* is associated with the NF- κ B/NLRP3 inflammasome axis that acts as a circadian clock and an integrating factor of inflammation (Lin et al., 2021). Defining the integrative role of *PLATR4* enhances our understanding of the crosstalk between the circadian clock and inflammation and highlights the complexity of key regulators of inflammation.

The Ub-proteasome system (UPS)

UPS is an important pathway for selective degradation of intracellular proteins, along with the lysosomal pathway and Ca²⁺-dependent protease pathway. This discovery was recognized with the Nobel Prize in chemistry in 2004. This pathway is composed of ubiquitin, proteasome, and a series of related ubiquitin activating enzymes E1, ubiquitin binding enzyme E2, and ubiquitin ligase E3 (Heo et al., 2022).

In recent years, it has been found that the use of the exogenous NO donor drug NOC18 can also reduce the expression of CYP2B1 protein in primary hepatocytes of rats. However, this degradation process is slower than CYP2B1 reduction induced by IL-1, which induces proteolytic activity (Zheng et al., 2013). Therefore, we speculate that IL-1 may accelerate the protein degradation of CYP2B1 by directly enhancing the activity or expression of the proteasome in the primary hepatocytes of rats. Indeed, Jan *et al.* measured the effect of IL-1 on proteasome activity in such hepatocytes using specific fluorescent polypeptide substrates and found that it improved the chymotrypsin-like activity of the proteasome (Wu et al., 2013). In addition, it can induce the expression of low-molecular-weight polypeptide 2 (LMP2), an important proteolytic subunit of the proteasome, thus revealing the mechanism by which inflammatory cytokines reduce CYP2B1 activity through the proteasome pathway.

Second messengers

Nitric oxide

The *in vivo* synthesis of nitric oxide by nitric oxide synthase (NOS) utilizes the amino acid L-arginine and molecular oxygen.

NOSs in the body are divided into three types: neuronal (nNOS), endothelial (eNOS), and inducible synthases (iNOS) (Leo et al., 2021). Infection and inflammation are the main factors that increase the expression of iNOS (Simpson et al., 2022). By reacting with superoxide, peroxynitrite can be produced by NO, which decays into highly toxic hydroxyl radicals. In response to inflammatory stimuli, iNOS is expressed primarily in macrophages, including KCs, and hepatocytes (Navarro et al., 2015). Supernatants from LPS-activated KCs and a specific combination of cytokines and LPS induce iNOS the most in hepatocytes. Glucocorticoids inhibit IL-1 and TNF-induced iNOS induction by hepatocytes, while acute-phase proteins in the liver are differentially regulated by hepatocyte iNOS. In response to iNOS or exposure to eNOS, hepatocyte protein synthesis is reduced and mitochondrial enzymes are partially inhibited (Cho et al., 2018; Wang et al., 2022). The binding of NO to hemoproteins makes it capable of inhibiting the catalytic activity of CYP450 enzymes. Adding NO to liver microsomes from rats reduces CYP450 activity through a partially reversible process (Dey and Cederbaum 2007). The irreversible inhibition is caused by the reaction of NO species with critical amino acid residues. CYP2B1/2 activity is inhibited *in vitro* by NO derived from the NO-generating compound SIN-1, which correlates with the formation of a heme-NO adduct (Yao et al., 2019).

NO derived from induced hepatocytes and KCs has the potential to inhibit hepatic cytochrome P450s and contributes significantly to inflammation-induced reductions in CYP450 catalytic activity. NO may not be necessary for suppressing all CYP450 proteins and mRNAs, as the effects depend on the CYP450 and model of inflammation or infection being studied. It may have greater relevance in endotoxemia, where hepatic iNOS is most induced, *versus* models of remote localized inflammation, where CYP450 is downregulated and iNOS is not induced (Martínez et al., 2018). The contribution of NO to CYP450 activity reduction varies depending on the kinetics of NOS induction relative to CYP450 mRNA suppression during the inflammatory response phase.

Nicotinamide and N1-methylnicotinamide (MNAM)

Diabetes mellitus type 2 (T2DM) has become a major global public health concern (Lu et al., 2020). Insulin-resistant states, such as obesity and T2DM, are often associated with chronic, unresolved tissue inflammation (Ying et al., 2020). NASH is closely related to inflammatory changes in the liver and is caused by an endocrine disorder through a mechanism that can affect CYP17A1 (Loria et al., 2009). An endocrine disorder known as polycystic ovary syndrome (PCOS) is associated with hyperandrogenism, insulin resistance, infertility, and ovulation problems. Off-label medicines, such as metformin, are used to

treat specific problems caused by PCOS, such as insulin resistance and hyperandrogenism. As a substrate for visfatin and nicotinamide N-methyltransferase (NNMT), nicotinamide produces nicotinamide adenine dinucleotide (NAD) and MNAM, which is an anti-inflammatory, anti-thrombosis, and anti-diabetic agent (Nejabati et al., 2020). In a study that evaluated the effects of MNAM and nicotinamide on metabolic and endocrine abnormalities in a letrozol-induced rat model of PCOS (Nejabati et al., 2020), the combined effects of MNAM and nicotinamide reversed abnormal estrous cycles and reduced serum levels of testosterone, as well as CYP17A1 gene expression. All of the therapeutic factors improved homeostatic model assessment of insulin resistance scores after treatment, with nicotinamide significantly increasing GLUT4 expression and decreasing visfatin expression. These results indicate that nicotinamide and MNAM have beneficial effects, some of which may be due to the role of AMPK in CYP17A1 expression.

Growth hormone (GH)

GH is the most important physiological regulator of cytochrome P450 gene expression in rodents. GH receptors belong to a superfamily that includes receptors for a variety of cytokines, such as IL-6. RXR α is an important signaling component recently reported to participate in the sex-dependent effect of GH on CYP3A expression (Li et al., 2015). CYP2C12 accounts for more than 40% of total hepatic cytochrome P450 content in the liver of rats. Octreotide is a potent somatostatin analog and its use increases the level of hepatic ubiquitin-CYP2C12 and significantly inhibits the production of CYP2C12 protein. Therefore, GH can restrict the expression of CYP450 enzyme (Banerjee et al., 2013).

STAT5a and *STAT5b* help regulate the activity of the CYP3A10 hydroxylase promoter in response to GH (Subramanian et al., 1998). Cytokines, such as IL-6, affect the ability of GH to control expression of CYP450 by altering the properties of *STAT* heterodimers that bind DNA and activate transcription. The activation of phospholipase A affects the physiological and pathophysiological pathways (cytokines) regulated by CYP450, which is required for the regulation of *CYP2C12* genes by GH. Additional research is needed to understand the regulation of cytochrome P450 gene expression by GH.

Potential drugs for cytochrome P450

Geniposide (GP) is an iridoid glycoside derived from gardenia fruit that may have profound anti-inflammatory properties against chronic and acute inflammation. Wan et al. studied the protective effects and potential mechanism of GP on acetaminophen (APAP) hepatotoxicity. (Li et al., 2016; Yang

et al., 2019). GP inhibited CYP2E1 expression and attenuated GSH depletion and MDA accumulation in the liver. Inflammatory cell infiltration was significantly inhibited by GP, as well as the expression and activation of TLR4 and NF- κ B, which are receptors for pain signaling. These data suggest that GP downregulates expression of CYP2E1 and the NF- κ B signaling pathway to effectively protect hepatocytes from APAP hepatotoxicity (Yang et al., 2019).

In vivo and *in vitro* analyses of curcumin have shown that it inhibits the cytochrome P450 family, including CYP1A2, CYP2C, and CYP3A4. Similarly, experimental data have shown that curcumin significantly reduces HgCl₂-induced upregulation of CYP450 (Li et al., 2021). These results may reflect the ability of curcumin to act as a chelating agent by directly binding inorganic mercury, which attenuates the biotransformation process of foreign compounds. Curcumin may also inhibit the activation of AhR, which then reduces the expression of CYP1A. CYP450 may therefore play a key role in the protective effects of curcumin in the liver.

Silybin is a flavonoid lignan extracted from the seed coat of *silymarin*, a medicinal plant in the family *Compositae*. It is a CYP3A inhibitor and is extensively used as a hepatoprotective agent in many liver disease therapies. It can inhibit the reduction of CYP3A expression and the activity of conditioned medium (CM) in palmitate-treated KCs (Zhang et al., 2021). It inhibits liver inflammation in mice fed a high-fat diet by increasing *SIRT2* expression and promoting *p65* deacetylation. It also inhibits nuclear factor κ B translocation into the nucleus and restores CYP3A transcription affected by CM.

Tripterygium wilfordii contains an active compound called triptolide that has antitumor and immunomodulatory properties (Noel et al., 2019). *In vivo* and *in vitro* experiments have indicated that CYP2E1 can mediate oxidative stress and induce hepatotoxicity through a mechanism that promotes oxidative stress, inflammation, and NF- κ B (p65) by CYP2E1 (Jiang et al., 2021). Therefore, understanding the CYP2E1 mechanism, its association with NF- κ B, and the relationship with the NF- κ B (p65) signaling pathway is crucial and meaningful work, which could provide new ideas and effective means for the treatment of hepatotoxic diseases.

Besides natural plant extracts that stimulate CYP450 enzymes, metabolites from human intestinal commensal microbes also participate in hepatocyte metabolic enzyme activity (Zimmermann et al., 2019). Polysaccharide products from intestinal commensal bacteria circulate to the liver along the gut-liver axis and play a regulatory role in drug metabolism in the liver. (Bajaj 2019). *Bacteroides fragilis* polysaccharide A circulates to the liver through hepatic veins and also plays an anti-inflammatory role in the liver. It inhibits proinflammatory factors IL-1 β and TNF- α , and upregulates the expression and activity of metabolic enzymes CYP3A4 and CYP2C19, thereby promoting the metabolism of voriconazole and reducing liver toxicity (Wang et al., 2021).

HepG2 cells treated with rifamycin show elevated PXR transcriptional activity and induced expression of CYP3A4 and P-gp, which are directly responsible for detoxification and are regulated by PXR. Rifamycin also antagonizes TNF- α - and LPS-induced NF- κ B activity and inhibits IL-1 β -induced synthesis of the inflammatory chemokine IL-8. Although the mutual regulation of PXR and NF- κ B by rifamycin has not been directly analyzed, the data indicate that in the absence of PXR, the inhibition of NF- κ B by rifamycin is independent of PXR stimulation. Therefore, rifamycin effectively displays anti-inflammatory activity, which is characterized by PXR activation and concomitant induction of CYP3A4 and P-gp *in vitro*, while also inhibiting NF- κ B and IL-8 (Rosette et al., 2019).

Certain cytokine-regulated therapeutic proteins, such as gevokizumab, can act by binding to a specific epitope (IL-1 β) located close to the receptor interface without completely overtaking the interface. This action may reduce the binding of IL-1 β to the IL-1 receptor type I signaling receptor, and the subsequent recruitment of IL-1 helper proteins, primarily through a reduction in the association rate of these interactions. Gevokizumab is thought to be a regulator, rather than a blocker, of IL-1 β signaling. Therefore, it may reverse inflammation-mediated inhibition of CYP3A4 and transporters. Fardel *et al.* used primary cultures of human inflammatory hepatocytes, specifically cytokine-treated hepatocytes, to characterize the potential effects of anti-inflammatory drugs on the detoxification pathway of drugs in the liver. Gevokizumab significantly regulates CYP450 and transporter activities (Moreau et al., 2017). The exploration of this *in vitro* mechanism using primary hepatocytes may be the preclinical step needed to predict interactions between gevokizumab and other drugs and may provide an experimental basis for rational drug use in clinics.

The inflammatory cytokine IL-6 activates the Janus kinase (JAK) activation of signal transduction and transcription (STAT) signaling pathway, which inhibits expression of hepatocyte cytochrome P450s and transporters. Therapeutic proteins, such as monoclonal antibodies against IL-6 or its receptors, have been shown to restore the complete detoxification capacity of the liver, leading to inflammatory disease-related drug–drug interactions. Fardel *et al.* found that ruxolitinib, a low-dose JAK1/2 inhibitor currently used for the treatment of myeloproliferative tumors, can inhibit the inhibitory effect of IL-6 on the liver detoxification system (Febvre-James et al., 2018).

IL-6-mediated expression of CYP1A2, CYP2B6, and CYP3A4, as well as transporters NTCP, OATP1B1, and Oct1 mRNA levels, are completely inhibited in primary human hepatocytes and differentiated hepatoma HepaRG cells. These results are in line with the simultaneous recovery of CYP450 and drug transport activities in IL-6-exposed HepaRG cells. Ruxolitinib does not moderate the inhibition of drug

detoxification protein mRNA levels by IL-1 β . The JAK inhibitor and anti-rheumatoid arthritis complex tofacitinib reverses IL-6-mediated inhibition of CYP450 and transporter mRNA expression. These results indicate that small drugs such as the JAK inhibitor ruxolitinib can specifically counteract the IL-6-mediated inhibition of drug-metabolizing enzymes and drug transporters in cultured human hepatocytes.

Cholesterol 7-hydroxylase (CYP7A1) encodes the rate-limiting step of cholesterol conversion to bile acids in the liver. In one study, acute cholesterol feeding of mice upregulated CYP7A1 by stimulating liver X receptor (Janowski et al., 1996). In that same study, a chronic diet high in cholesterol inhibited the expression of CYP7A1 in the liver of mice by >60% and was associated with 2-fold elevation of cholesterol. However, acute feeding increased liver CYP7A1 expression by > 3-fold. Chronic non-acute cholesterol feeding increased the expression of infectious cytokines TNF- α and IL-1 β , which inhibited the expression of CYP7A1 in the liver. It has also been found that chronic feeding of cholesterol activates mitochondrial activated protein kinase (MAP), c-Jun N-terminal kinase (JNK), and extracellular signal-regulated kinase (ERK). *In vitro* studies have indicated that inflammatory cytokines TNF- α and IL-1 β have a JNK and ERK pathway-dependent inhibitory effect on CYP7A1. Therefore, chronic feeding of a hypercholesterolemic diet induces inflammatory cytokine activation and liver injury, leading to the inhibition of CYP450 through activation of JNK and ERK signaling pathways (Henkel et al., 2011).

People with chronic kidney disease can also experience changes in drug metabolism in the liver due to uremic toxin accumulation. We have investigated the role of advanced oxidation protein products (AOPPs) in the downregulation of CYP1A2 and CYP3A4. In a rat CKD model, the accumulation of AOPPs in plasma was associated with reduced CYP1A2 and CYP3A4 protein levels. Paracetamol and 6- β -hydroxytestosterone are CYP1A2 and CYP3A4 metabolites and were also found to be significantly reduced in liver microsomes. Hepatocytes treated with AOPPs displayed significant reductions in CYP1A2 and CYP3A4 protein and activity levels.

The effects of AOPPs on p-IKK α / β , p-I κ B α , and p-NF- κ B on the upregulation of inflammatory cytokine protein levels have been investigated. NF- κ B pathway inhibitors BAY-117082 and PDTC abolish the downregulation of AOPPs. These findings suggest that human endogenous metabolite AOPPs stimulate NF- κ B by increasing the production of inflammatory cytokines and NF- κ B-mediated signaling to downregulate the expression and activity of CYP1A2 and CYP3A4. AOPPs may also alter the clearance of non-renal drugs in CKD patients by affecting metabolic enzymes (Xun et al., 2021).

Screening for potential drug–drug interactions can be accomplished using cytokines released in response to

TABLE 1 Repots of drug treatment on the expression of cytochrome P450.

No.	Agents	Cytochromes P450	Trends	Related cytokines	Signaling route	Experimental model
1	Geniposide (GP)	CYP 2E1	↑	IL-1 β , TNF- α	TLR4/NF- κ B	Male C57 mice
2	<i>B. fragilis</i> Polysaccharide A	CYP2C19	↑	IL-1 β , TNF- α	TLR4/NF- κ B	Rats
3	Curcumin	CYP1B1	↓	IL-1 β , TNF- α	Nrf2/HO-1	Male Kunming mice
		CYP3A1	↓			
		CYP1A2	↓			
		CYP3A11	↓			
4	Gevokizumab	CYP3A4	↓	IL-1 β	(NA)	<i>In vitro</i>
5	Triptolide	CYP2E1	↑	IL-6, TNF- α	NF- κ B (p65)	Mice
6	Silybin	CYP3A	Restore	(NA)	NAD+/sirtuin 2	(NA)
7	Ruxolitinib	CYP1A2	↑	IL-6	(NA)	HepaRG cells
		CYP2B6	↑			
		CYP3A4	↑			
8	Rifamycin SV	CYP3A4	↑	IL-1 β	PXR	HepG2 cells
9	Cholesterol	CYP7A1	↓	TNF α , IL-1 β	JNK, ERK	FVB/NJ mice
10	Advanced oxidation protein products (AOPP)	CYP1A2	↓	IL-6, TNF- α	NF- κ B	Rats
		CYP3A4	↓			
11	Monocyte chemoattractant protein-1 (MCP-1)	CYP1A2	↓	(NA)	(NA)	Human hepatocytes, Kupffer cells
		CYP2B6	↓			
		CYP3A4	↓			
12	INF- α 2a (2.0 ng/ml)	CYP1A2	↑	(NA)	STAT1	Human hepatocytes, Kupffer cells
		CYP2B6	↓			
13	LncRNA <i>Platr4</i>	CYP1/2	↑	IL-1 β , IL-6, TNF- α and IL-18	NLRP3/NF- κ B signaling	Mice

(NA), Not available.

immunomodulators in the blood *ex vivo*. The investigational agonist tilsotolimod stimulates the release of macrophage chemoattractant protein-1 (MCP-1), macrophage inflammatory protein-1 α (MIP-1 α), and interferon- α 2a (INF- α 2a) in blood from healthy donors, which stimulates macrophage migration. CYP1A2, CYP2B6, and CYP3A4 enzyme expression and activity are not affected when human hepatocytes are cultured with tilsotolimod. However, cytokines stimulated *via* treatment with tilsotolimod reduce CYP1A2 and CYP2B6 activities. The indirect effects of cytokines induced by tilsotolimod on CYP450 enzymes has been investigated *in vitro*. In one study, the presence of the recombinant human chemokines MCP-1 and MIP-1 did not alter CYP1A2, CYP2B6, CYP2C8, CYP2C9, CYP3A4, or *STAT1* mRNA expression, or CYP1A2, CYP2B6, or CYP3A4/5 enzyme activity, in the Hep:KCs model. However, tilsotolimod increased CYP1A2 and CYP2B6 mRNA levels by 2- and 5-fold, respectively, at concentrations over 2.5 ng/ml, and reduced CYP2B6 enzyme activity by 46%. That study established that while INF-2 α is inactivated in human liver cells, it mediates the effects of tilsotolimod on CYP1A2 and CYP2B6 expression (Czerwiński et al., 2019).

Future research

Different inflammatory models require the characterization of individual CYP450 responses, which makes it clear that not all CYP450s are affected equally. Culturing and stably expanding hepatocytes have been challenging, and as of now, liver organoids can only be generated from biliary epithelial cells and tumoroids formed in primary liver cancer cells (Peng et al., 2018). Simulating organ function with hepatocytes through metabolic function is not yet mature. Sources of inflammatory stimuli should also be considered. In addition to the LPS directed stimulating in the hepatocytes, environmental LPS indirect stimulating are also responsive to hepatocytes *in vivo*. Markowicz study has shown that smoke contains 10–40 ng LPS per cigarette, with cigarettes containing 20 pg (Markowicz et al., 2014). Dust contaminated with LPS is also inhaled by agricultural workers (Gras et al., 2013). Culturing primary hepatocytes in three-dimensional (3D) environments is currently one of the most popular methods (Hu et al., 2018). A multicellular 3D human primary liver cell culture treated with LPS has been shown to potentiate or inhibit hepatic CYP1A1 induction (Esch et al., 2015), which allows an *in vitro* human disease state model to be established. We have only begun to understand the mechanism of CYP450 regulation. Current research

focuses more on stimulating individual hepatocytes, which ignores the interaction between different functional cells in human tissues and organs. There is still much work to be done to clarify the mechanisms that regulate CYP450, including NO, sphingomyelin, and cytokine response elements.

Cytokines and interferons are widely believed to mediate inflammation-induced CYP450 inhibition; other causes of CYP450 downregulation, such as trauma (Cui et al., 2021), acute liver injury (Brown and Merad 2015), and partial hepatectomy (Hu, et al., 2018), need to be studied further. This review only describes the Hep:KCs model, which is commonly used to explore the impact of an inflammatory response on the functional activity of hepatocytes. The application of this technology has great potential and further exploration of the expression of CYP450 through the knockdown or overexpression of the above transcription factors is expected in the future. This will allow for a clearer understanding of the regulatory role of the inflammatory response in the metabolic activity of hepatocytes.

It is important to understand how inflammation affects the activity of CYP450 when using CYP450-substrate drugs to treat patients in a rational and safe manner. Inflammation significantly reduces the activity of CYP450 at the post-transcriptional level. A number of factors contribute to this change, including the lack of production and modification of proteins. By monitoring and studying the role and mechanism of inflammation in CYP450 activity, CYP450-substrate drugs can be correctly used in clinicopathological settings based on theoretical and experimental information.

Conclusion

Infectious and inflammatory stimuli profoundly affect hepatic CYP450 activity, as well as clinical and toxicological outcomes. While it is possible to induce some CYP450s, most are suppressed in the liver. *In vitro* and *in vivo* studies have continuously reported that traditional Chinese medicine, natural products, and monoclonal antibodies can prevent the inhibition of inflammatory cytokines and upregulate the expression of metabolic enzymes. Metabolites, such as endotoxins LPS and AOPPs, can promote the activity of inflammatory cytokines, downregulate the expression of metabolic enzymes, and regulate the metabolic phenotype (Table 1). Therefore, inflammation models may affect the quality and quantity of CYP450 populations around hepatocytes differently, depending on cytokine profiles and concentrations.

Hepatocyte membrane receptors, transcription factors, small-molecule RNAs, and other primary and secondary signaling factors may be involved in regulating the expression and activity of CYP450 in the inflammatory environment. Metabolic enzyme activity is usually reduced through the downregulation of CYP450 gene transcription and inhibition of enzyme expression. This makes it possible to determine the impact of the inflammatory environment or abnormal lipid

metabolism, such as insulin resistance, on the metabolic enzyme activity of corresponding sensitive drugs. It also provides a reference for the selection of corresponding metabolic enzyme drugs for patients in the clinic. The ultimate goal is to predict the clinical or toxic response of humans and other animals to a given drug or toxin in cases of ongoing infection or inflammation. This review highlights all factors that can affect drug-metabolizing enzymes in the liver that are associated with the inflammatory response signaling pathways.

Author contributions

XW and JR reviewed the literature and drafted the manuscript. XY and TX participated in the conception and interpretation of the relevant literature for the manuscript. ZT, QD, and JR performed a critical revision of the manuscript. The final version of this review has been edited, revised critically, and approved by all authors

Funding

This work was supported by research grants from the Project of Guangdong Administration of Traditional Chinese Medicine (No. 20221273), Shenzhen Longhua District Science and Technology Innovation Fund Projects (Nos. 2022045, 2020036, and 2020152).

Acknowledgments

We would like to give our sincere gratitude to Danyi Lu's suggestions in the whole manuscript and also appreciate all the reviewers for their helpful comments on this paper.

Conflict of interest

The authors declare that the research was conducted in the absence of any commercial or financial relationships that could be construed as a potential conflict of interest.

Publisher's note

All claims expressed in this article are solely those of the authors and do not necessarily represent those of their affiliated organizations, or those of the publisher, the editors and the reviewers. Any product that may be evaluated in this article, or claim that may be made by its manufacturer, is not guaranteed or endorsed by the publisher.

References

- Abraham, N. G., Junge, J. M., and Drummond, G. S. (2016). Translational significance of heme oxygenase in obesity and metabolic syndrome. *Trends Pharmacol. Sci.* 1, 17–36. doi:10.1016/j.tips.2015.09.003
- Aitken, A. E., and Morgan, E. T. (2007). Gene-specific effects of inflammatory cytokines on cytochrome P450 2C, 2B6 and 3A4 mRNA levels in human hepatocytes. *Drug Metab. Dispos.* 9, 1687–1693. doi:10.1124/dmd.107.015511
- Al-Dhfyhan, A., Alhoshani, A., and Korashy, H. (2017). Aryl hydrocarbon receptor/cytochrome P450 1A1 pathway mediates breast cancer stem cells expansion through PTEN inhibition and β -Catenin and Akt activation. *Mol. Cancer* 1, 14. doi:10.1186/s12943-016-0570-y
- Anwar-Mohamed, A., Klotz, L., and El-Kadi, A. (2012). Inhibition of heme oxygenase-1 partially reverses the arsenite-mediated decrease of CYP1A1, CYP1A2, CYP3A23, and CYP3A2 catalytic activity in isolated rat hepatocytes. *Drug Metab. Dispos.* 3, 504–514. doi:10.1124/dmd.111.042564
- Attal, N., Marrero, E., Thompson, K., and McKillop, I. (2022). Cytochrome P450 2E1-dependent hepatic ethanol metabolism induces fatty acid-binding protein 4 and steatosis. *Alcohol. Clin. Exp. Res.* 6, 928–940. doi:10.1111/acer.14828
- Bachmann, F., Duthaler, U., Meyer, Z., Schwabedissen, H. E., Puchkov, M., Huwyler, J., et al. (2021). Metamizole is a moderate cytochrome P450 inducer via the constitutive androstane receptor and a weak inhibitor of CYP1A2. *Clin. Pharmacol. Ther.* 6, 1505–1516. doi:10.1002/cpt.2141
- Bäck, M., Yurdagül, A., Tabas, I., Öörni, K., and Kovanen, P. T. (2019). Inflammation and its resolution in atherosclerosis: Mediators and therapeutic opportunities. *Nat. Rev. Cardiol.* 7, 389–406. doi:10.1038/s41569-019-0169-2
- Bae, S. D. W., Nguyen, R., Qiao, L., and George, J. (2021). Role of the constitutive androstane receptor (CAR) in human liver cancer. *Biochim. Biophys. Acta. Rev. Cancer* 2, 188516. doi:10.1016/j.bbcan.2021.188516
- Bai, L., Kong, M., Duan, Z., Liu, S., Zheng, S., and Chen, Y. (2021). M2-like macrophages exert hepatoprotection in acute-on-chronic liver failure through inhibiting necroptosis-S100A9-necroinflammation axis. *Cell. Death Dis.* 1, 93. doi:10.1038/s41419-020-03378-w
- Bai, X., Liao, Y., Sun, F., Xiao, X., and Fu, S. (2021). Diurnal regulation of oxidative phosphorylation restricts hepatocyte proliferation and inflammation. *Cell. Rep.* 10, 109659. doi:10.1016/j.celrep.2021.109659
- Bajaj, J. S. (2019). Alcohol, liver disease and the gut microbiota. *Nat. Rev. Gastroenterol. Hepatol.* 4, 235–246. doi:10.1038/s41575-018-0099-1
- Banerjee, S., Das, R. K., and Shapiro, B. H. (2013). Growth hormone-independent suppression of growth hormone-dependent female isoforms of cytochrome P450 by the somatostatin analog octreotide. *Eur. J. Pharmacol.* 1–3, 256–261. doi:10.1016/j.ejphar.2013.05.013
- Brenner, C., Galluzzi, L., Kepp, O., and Kroemer, G. (2013). Decoding cell death signals in liver inflammation. *J. Hepatol.* 3, 583–594. doi:10.1016/j.jhep.2013.03.033
- Brown, B. D., and Merad, M. (2015). Authorship: Archives and citation miss equal authors. *Nature* 7582, 333. doi:10.1038/528333a
- Cacabelos, R., and Martínez-Bouza, R. (2011). Genomics and pharmacogenomics of dementia. *CNS Neurosci. Ther.* 5, 566–576. doi:10.1111/j.1755-5949.2010.00189.x
- Chen, J., Ao, L., and Yang, J. (2019). Long non-coding RNAs in diseases related to inflammation and immunity. *Ann. Transl. Med.* 18, 494. doi:10.21037/atm.2019.08.37
- Chen, Q., Zhang, T., Wang, J-F., and Wei, D-Q. (2011). Advances in human cytochrome p450 and personalized medicine. *Curr. Drug Metab.* 5, 436–444. doi:10.2174/138920011795495259
- Cho, Y., Yu, L., Abdelmegeed, M., Yoo, S., and Song, B. (2018). Apoptosis of enterocytes and nitration of junctional complex proteins promote alcohol-induced gut leakiness and liver injury. *J. Hepatol.* 1, 142–153. doi:10.1016/j.jhep.2018.02.005
- Connick, J. P., Reed, J. R., Cawley, G. F., and Backes, W. L. (2021). Heme oxygenase-1 affects cytochrome P450 function through the formation of heteromeric complexes: Interactions between CYP1A2 and heme oxygenase-1. *J. Biol. Chem.* 100030, 100030. doi:10.1074/jbc.RA120.015911
- Cui, W., Wu, X., Shi, Y., Guo, W., Luo, J., Liu, H., et al. (2021). 20-HETE synthesis inhibition attenuates traumatic brain injury-induced mitochondrial dysfunction and neuronal apoptosis via the SIRT1/PGC-1 α pathway: A translational study. *Cell. Prolif.* 2, e12964. doi:10.1111/cpr.12964
- Czerwinski, M., Gilligan, K., Westland, K., and Ogilvie, B. W. (2019). Effects of monocyte chemoattractant protein-1, macrophage inflammatory protein-1 α , and interferon- α 2a on P450 enzymes in human hepatocytes in vitro. *Pharmacol. Res. Perspect.* 6, e00551. doi:10.1002/prp.2551
- Dey, A., and Cederbaum, A. (2007). Induction of cytochrome P450 2E1 [corrected] promotes liver injury in ob/ob mice. *Hepatology* 6, 1355–1365. doi:10.1002/hep.21603
- Dickmann, L. J., McBride, H. J., Patel, S. K., Miner, K., Wienkers, L. C., and Slatter, J. G. (2012). Murine collagen antibody induced arthritis (CAIA) and primary mouse hepatocyte culture as models to study cytochrome P450 suppression. *Biochem. Pharmacol.* 12, 1682–1689. doi:10.1016/j.bcp.2012.03.001
- Diermeier, S. D., Chang, K-C., Freier, S. M., Song, J., El Demerdash, O., Krasnitz, A., et al. (2016). Mammary tumor-associated RNAs impact tumor cell proliferation, invasion, and migration. *Cell. Rep.* 1, 261–274. doi:10.1016/j.celrep.2016.08.081
- Esch, M. B., Prot, J-M., Wang, Y. L., Miller, P., Llamas-Vidales, J. R., Naughton, B. A., et al. (2015). Multi-cellular 3D human primary liver cell culture elevates metabolic activity under fluidic flow. *Lab. Chip* 10, 2269–2277. doi:10.1039/c5lc00237k
- Fakhouri, E. W., Peterson, S. J., Kothari, J., Alex, R., Shapiro, J. L., and Abraham, N. G. (2020). Genetic polymorphisms complicate COVID-19 therapy: Pivotal role of HO-1 in cytokine storm. *Antioxidants* 7, E636. doi:10.3390/antiox9070636
- Febvre-James, M., Bruyère, A., Le Vée, M., and Fardel, O. (2018). The JAK1/2 inhibitor ruxolitinib reverses interleukin-6-mediated suppression of drug-detoxifying proteins in cultured human hepatocytes. *Drug Metab. Dispos.* 2, 131–140. doi:10.1124/dmd.117.078048
- Gao, C., Yang, Y., Zhang, Y., Qian, M., and Yang, J. (2020). HGF gene delivering alginate/galactosylated chitosan sponge scaffold for three-dimensional coculture of hepatocytes/3T3 cells. *DNA Cell. Biol.* 3, 451–458. doi:10.1089/dna.2019.5136
- Gaul, S., Leszczynska, A., Alegre, F., Kaufmann, B., Johnson, C. D., Adams, L. A., et al. (2021). Hepatocyte pyroptosis and release of inflammasome particles induce stellate cell activation and liver fibrosis. *J. Hepatol.* 1, 156–167. doi:10.1016/j.jhep.2020.07.041
- Gomes, J. V. D., Herz, C., Helmig, S., Förster, N., Mewis, L., and Lamy, E. (2021). Drug-drug interaction potential, cytotoxicity, and reactive oxygen species production of *salix* cortex extracts using human hepatocyte-like HepaRG cells. *Front. Pharmacol.* 779801, 779801. doi:10.3389/fphar.2021.779801
- Gong, S., Lan, T., Zeng, L., Luo, H., Yang, X., Li, N., et al. (2018). Gut microbiota mediates diurnal variation of acetaminophen induced acute liver injury in mice. *J. Hepatol.* 1, 51–59. doi:10.1016/j.jhep.2018.02.024
- Gras, D., Chanez, P., Vachier, I., Petit, A., and Bourdin, A. (2013). Bronchial epithelium as a target for innovative treatments in asthma. *Pharmacol. Ther.* 3, 290–305. doi:10.1016/j.pharmthera.2013.07.008
- Griffett, K., Hayes, M., Boeckman, M., and Burris, T. (2022). The role of REV-ERB in NASH. *Acta Pharmacol. Sin.* 5, 1133–1140. doi:10.1038/s41401-022-00883-w
- Guo, C., Xie, S., Chi, Z., Zhang, J., Liu, Y., Zhang, L., et al. (2016). Bile acids control inflammation and metabolic disorder through inhibition of NLRP3 inflammasome. *Immunity* 4, 802–816. doi:10.1016/j.immuni.2016.09.008
- Han, Y., Kim, H., Na, H., Nam, M., Kim, J., Kim, J., et al. (2017). ROR α induces KLF4-mediated M2 polarization in the liver macrophages that protect against nonalcoholic steatohepatitis. *Cell. Rep.* 1, 124–135. doi:10.1016/j.celrep.2017.06.017
- Harvey, R. D., and Morgan, E. T. (2014). Cancer, inflammation, and therapy: Effects on cytochrome p450-mediated drug metabolism and implications for novel immunotherapeutic agents. *Clin. Pharmacol. Ther.* 4, 449–457. doi:10.1038/clpt.2014.143
- He, Y., Guo, X., Lan, T., Xia, J., Wang, J., Li, B., et al. (2021). Human umbilical cord-derived mesenchymal stem cells improve the function of liver in rats with acute-on-chronic liver failure via downregulating Notch and Stat1/Stat3 signaling. *Stem Cell. Res. Ther.* 1, 396. doi:10.1186/s13287-021-02468-6
- Henkel, A. S., Anderson, K. A., Dewey, A. M., Kavesh, M. H., and Green, R. M. (2011). A chronic high-cholesterol diet paradoxically suppresses hepatic CYP7A1 expression in FVB/NJ mice. *J. Lipid Res.* 2, 289–298. doi:10.1194/jlr.M012781
- Heo, A., Ji, C., and Kwon, Y. (2022). The Cys/N-degron pathway in the ubiquitin-proteasome system and autophagy. *Trends Cell. Biol.* doi:10.1016/j.tcb.2022.07.005
- Hsu, M., Muchova, L., Morioka, I., Wong, R. J., Schröder, H., and Stevenson, D. K. (2006). Tissue-specific effects of statins on the expression of heme oxygenase-1 in vivo. *Biochem. Biophys. Res. Commun.* 3, 738–744. doi:10.1016/j.bbrc.2006.03.036
- Hu, H., Gehart, H., Artegiani, B., López-Iglesias, C., Dekkers, F., Basak, O., et al. (2018). Long-term expansion of functional mouse and human hepatocytes as 3D organoids. *Cell.* 6, 1591–1606. doi:10.1016/j.cell.2018.11.013
- Janowski, B. A., Willy, P. J., Devi, T. R., Falck, J. R., and Mangelsdorf, D. J. (1996). An oxysterol signalling pathway mediated by the nuclear receptor LXR α . *Nature* 6602, 728–731. doi:10.1038/383728a0
- Jiang, H-Y., Bao, Y-N., Lin, F-M., and Jin, Y. (2021). Triptolide regulates oxidative stress and inflammation leading to hepatotoxicity via inducing CYP2E1. *Hum. Exp. Toxicol.* 12_suppl, S775–S787. doi:10.1177/09603271211056330

- Jones, D., Boudes, P. F., Swain, M. G., Bowlus, C. L., Galambos, M. R., Bacon, B. R., et al. (2017). Seladelpar (MBX-8025), a selective PPAR- δ agonist, in patients with primary biliary cholangitis with an inadequate response to ursodeoxycholic acid: A double-blind, randomised, placebo-controlled, phase 2, proof-of-concept study. *Lancet. Gastroenterol. Hepatol.* 10, 716–726. doi:10.1016/S2468-1253(17)30246-7
- Josefsson, A., Larsson, K., Freyhult, E., Damber, J., and Welén, K. (2019). Gene expression alterations during development of castration-resistant prostate cancer are detected in circulating tumor cells. *Cancers* 1, E39. doi:10.3390/cancers12010039
- Khalil, Y., Carrino, S., Lin, F., Ferlin, A., Lad, H., Mazzacua, F., et al. (2022). Tissue proteome of 2-hydroxyacyl-CoA lyase deficient mice reveals peroxisome proliferation and activation of ω -oxidation. *Int. J. Mol. Sci.* 2, 987. doi:10.3390/ijms23020987
- Koike, T., Yoshikawa, M., Ando, H. K., Farnaby, W., Nishi, T., Watanabe, E., et al. (2021). Discovery of soticlestat, a potent and selective inhibitor for cholesterol 24-hydroxylase (CH24H). *J. Med. Chem.* 16, 12228–12244. doi:10.1021/acs.jmedchem.1c00864
- Lao, Y., Li, Y., Zhang, P., Shao, Q., Lin, W., Qiu, B., et al. (2018). Targeting endothelial erk1/2-akt Axis as a regeneration strategy to bypass fibrosis during chronic liver injury in mice. *Mol. Ther.* 12, 2779–2797. doi:10.1016/j.ymthe.2018.08.016
- Leo, F., Suvorava, T., Heuser, S., Li, J., LoBue, A., Barbarino, F., et al. (2021). Red blood cell and endothelial eNOS independently regulate circulating nitric oxide metabolites and blood pressure. *Circulation* 11, 870–889. doi:10.1161/circulationaha.120.049606
- Leti, F., Legendre, C., Still, C. D., Chu, X., Petrick, A., Gerhard, G. S., et al. (2017). Altered expression of MALAT1 lncRNA in nonalcoholic steatohepatitis fibrosis regulates CXCL5 in hepatic stellate cells. *Transl. Res.* 190, 25–39. doi:10.1016/j.trsl.2017.09.001
- Li, F., Li, W., Li, X., Li, F., Zhang, L., Wang, B., et al. (2016). Geniposide attenuates inflammatory response by suppressing P2Y₁₄ receptor and downstream ERK1/2 signaling pathway in oxygen and glucose deprivation-induced brain microvascular endothelial cells. *J. Ethnopharmacol.* 185, 77–86. doi:10.1016/j.jep.2016.03.025
- Li, J., Wan, Y., Na, S., Liu, X., Dong, G., Yang, Z., et al. (2015). Sex-dependent regulation of hepatic CYP3A by growth hormone: Roles of HNF6, C/EBP α , and RXR α . *Biochem. Pharmacol.* 1, 92–103. doi:10.1016/j.bcp.2014.10.010
- Li, S., Wang, X., Xiao, Y., Wang, Y., Wan, Y., Li, X., et al. (2021). Curcumin ameliorates mercuric chloride-induced liver injury via modulating cytochrome P450 signaling and Nrf2/HO-1 pathway. *Ecotoxicol. Environ. Saf.* 111426, 111426. doi:10.1016/j.ecoenv.2020.111426
- Lin, Y., Wang, S., Gao, L., Zhou, Z., Yang, Z., Lin, J., et al. (2021). Oscillating lncRNA *Platr4* regulates NLRP3 inflammasome to ameliorate nonalcoholic steatohepatitis in mice. *Theranostics* 1, 426–444. doi:10.7150/thno.50281
- Long, Y., Wang, X., Youmans, D. T., and Cech, T. R. (2017). How do lncRNAs regulate transcription? *Sci. Adv.* 9, eaao2110. doi:10.1126/sciadv.aao2110
- Loria, P., Carulli, L., Bertolotti, M., and Lonardo, A. (2009). Endocrine and liver interaction: The role of endocrine pathways in NASH. *Nat. Rev. Gastroenterol. Hepatol.* 4, 236–247. doi:10.1038/nrgastro.2009.33
- Lu, Y., Wang, E., Chen, Y., Zhou, B., Zhao, J., Xiang, L., et al. (2020). Obesity-induced excess of 17-hydroxyprogesterone promotes hyperglycemia through activation of glucocorticoid receptor. *J. Clin. Invest.* 7, 3791–3804. doi:10.1172/JCI134485
- Lucarelli, R., Gorrochategui-Escalante, N., Taddeo, J., Buttaro, B., Beld, J., and Tam, V. (2022). Eicosanoid-activated PPAR α inhibits nf κ b-dependent bacterial clearance during post-influenza superinfection. *Front. Cell. Infect. Microbiol.* 881462, 881462. doi:10.3389/fcimb.2022.881462
- Markowicz, P., Löndahl, J., Wierzbicka, A., Suleiman, R., Shihadeh, A., and Larsson, L. (2014). A study on particles and some microbial markers in waterpipe tobacco smoke. *Sci. Total Environ.* 107, 107–113. doi:10.1016/j.scitotenv.2014.08.055
- Martínez, M., Ares, I., Rodríguez, J., Martínez, M., Roura-Martínez, D., Castellano, V., et al. (2018). Pyrethroid insecticide lambda-cyhalothrin induces hepatic cytochrome P450 enzymes, oxidative stress and apoptosis in rats. *Sci. Total Environ.* 1371, 1371–1382. doi:10.1016/j.scitotenv.2018.03.030
- Mescher, M., and Haarmann-Stemmann, T. (2018). Modulation of CYP1A1 metabolism: From adverse health effects to chemoprevention and therapeutic options. *Pharmacol. Ther.* 71, 71–87. doi:10.1016/j.pharmthera.2018.02.012
- Mezzar, S., De Schryver, E., Asselberghs, S., Meyhi, E., Morvay, P. L., Baes, M., et al. (2017). Phytol-induced pathology in 2-hydroxyacyl-CoA lyase (HACL1) deficient mice. Evidence for a second non-HACL1-related lyase. *Biochim. Biophys. Acta. Mol. Cell. Biol. Lipids* 9, 972–990. doi:10.1016/j.bbalip.2017.06.004
- Montagner, A., Polizzi, A., Fouché, E., Ducheix, S., Lippi, Y., Lasserre, F., et al. (2016). Liver PPAR α is crucial for whole-body fatty acid homeostasis and is protective against NAFLD. *Gut* 7, 1202–1214. doi:10.1136/gutjnl-2015-310798
- Moreau, A., Le Vée, M., Jouan, E., Denizot, C., Parmentier, Y., and Fardel, O. (2017). Effect of gevokizumab on interleukin-1 β -mediated cytochrome P450 3A4 and drug transporter repression in cultured human hepatocytes. *Eur. J. Drug Metab. Pharmacokinet.* 5, 871–878. doi:10.1007/s13318-017-0406-1
- Morgan, E. T., Skubic, C., Lee, C.-M., Cokan, K. B., and Rozman, D. (2020). Regulation of cytochrome P450 enzyme activity and expression by nitric oxide in the context of inflammatory disease. *Drug Metab. Rev.* 4, 455–471. doi:10.1080/03602532.2020.1817061
- Murphy, M. P. (2018). Newly made mitochondrial DNA drives inflammation. *Nature* 7717, 176–177. doi:10.1038/d41586-018-05764-z
- Navarro, L., Wree, A., Povero, D., Berk, M., Eguchi, A., Ghosh, S., et al. (2015). Arginase 2 deficiency results in spontaneous steatohepatitis: A novel link between innate immune activation and hepatic de novo lipogenesis. *J. Hepatol.* 2, 412–420. doi:10.1016/j.jhep.2014.09.015
- Nejabati, H. R., Samadi, N., Shahnazi, V., Mihanfar, A., Fattahi, A., Latifi, Z., et al. (2020). Nicotinamide and its metabolite N1-Methylnicotinamide alleviate endocrine and metabolic abnormalities in adipose and ovarian tissues in rat model of Polycystic Ovary Syndrome. *Chem. Biol. Interact.* 324, 109093. doi:10.1016/j.cbi.2020.109093
- Nguyen, T. V., Ukairo, O., Khetani, S. R., McVay, M., Kanchagar, C., Seghezzi, W., et al. (2015). Establishment of a hepatocyte-kupffer cell coculture model for assessment of proinflammatory cytokine effects on metabolizing enzymes and drug transporters. *Drug Metab. Dispos.* 5, 774–785. doi:10.1124/dmd.114.061317
- Noel, P., Von Hoff, D. D., Saluja, A. K., Velagapudi, M., Borazanci, E., and Han, H. (2019). Triptolide and its derivatives as cancer therapies. *Trends Pharmacol. Sci.* 5, 327–341. doi:10.1016/j.tips.2019.03.002
- Peng, W. C., Logan, C. Y., Fish, M., Anbarchian, T., Aguisanda, F., Álvarez-Varela, A., et al. (2018). Inflammatory cytokine TNF α promotes the long-term expansion of primary hepatocytes in 3D culture. *Cell* 6, 1607–1619. doi:10.1016/j.cell.2018.11.012
- Pohlmann, S., Scheu, S., Ziegler, V., Schupp, N., Henninger, C., and Fritz, G. (2018). Hepatic Rac1 GTPase contributes to liver-mediated basal immune homeostasis and LPS-induced endotoxemia. *Biochim. Biophys. Acta. Mol. Cell. Res.* 9, 1277–1292. doi:10.1016/j.bbamcr.2018.06.007
- Proto, J. D., Doran, A. C., Gusarova, G., Yurdagül, A., Sozen, E., Subramanian, M., et al. (2018). Regulatory T cells promote macrophage efferocytosis during inflammation resolution. *Immunity* 4, 666–677. doi:10.1016/j.immuni.2018.07.015
- Ramachandran, P., Pellicoro, A., Vernon, M. A., Boulter, L., Aucott, R. L., Ali, A., et al. (2012). Differential Ly-6C expression identifies the recruited macrophage phenotype, which orchestrates the regression of murine liver fibrosis. *Proc. Natl. Acad. Sci. U. S. A.* 46, E3186–E3195. doi:10.1073/pnas.1119964109
- Renton, K. W. (2005). Regulation of drug metabolism and disposition during inflammation and infection. *Expert Opin. Drug Metab. Toxicol.* 4, 629–640. doi:10.1517/17425255.1.4.629
- Rieger, J. K., Reutter, S., Hofmann, U., Schwab, M., and Zanger, U. M. (2015). Inflammation-associated microRNA-130b down-regulates cytochrome P450 activities and directly targets CYP2C9. *Drug Metab. Dispos.* 6, 884–888. doi:10.1124/dmd.114.062844
- Roberts, D. M., Sevestos, J., Carland, J. E., Stocker, S. L., and Lea-Henry, T. N. (2018). Clinical pharmacokinetics in kidney disease: Application to rational design of dosing regimens. *Clin. J. Am. Soc. Nephrol.* 8, 1254–1263. doi:10.2215/CJN.05150418
- Rose, K. A., Holman, N. S., Green, A. M., Andersen, M. E., and LeCluyse, E. L. (2016). Co-Culture of hepatocytes and kupffer cells as an in vitro model of inflammation and drug-induced hepatotoxicity. *J. Pharm. Sci.* 2, 950–964. doi:10.1016/S0022-3549(15)00192-6
- Rosette, C., Agan, F. J., Rosette, N., Moro, L., Mazzetti, A., Hassan, C., et al. (2019). Rifamycin SV exhibits strong anti-inflammatory in vitro activity through pregnane X receptor stimulation and NF κ B inhibition. *Drug Metab. Pharmacokinet.* 3, 172–180. doi:10.1016/j.dmpk.2019.01.002
- Sato, K., Meng, F., Francis, H., Wu, N., Chen, L., Kennedy, L., et al. (2020). Melatonin and circadian rhythms in liver diseases: Functional roles and potential therapies. *J. Pineal Res.* 3, e12639. doi:10.1111/jpi.12639
- Schiering, C., Wincent, E., Metidji, A., Iseppon, A., Li, Y., Potocnik, A., et al. (2017). Feedback control of AHR signalling regulates intestinal immunity. *Nature* 7640, 242–245. doi:10.1038/nature21080

- Schröder, A., Klein, K., Winter, S., Schwab, M., Bonin, M., Zell, A., et al. (2013). Genomics of ADME gene expression: Mapping expression quantitative trait loci relevant for absorption, distribution, metabolism and excretion of drugs in human liver. *Pharmacogenomics J.* 1, 12–20. doi:10.1038/tpj.2011.44
- Shen, Y., Endale, M., Wang, W., Morris, A., Francey, L., Harold, R., et al. (2021). NF- κ B modifies the mammalian circadian clock through interaction with the core clock protein BMAL1. *PLoS Genet.* 11, e1009933. doi:10.1371/journal.pgen.1009933
- Shetty, S., Lalor, P. F., and Adams, D. H. (2018). Liver sinusoidal endothelial cells - gatekeepers of hepatic immunity. *Nat. Rev. Gastroenterol. Hepatol.* 9, 555–567. doi:10.1038/s41575-018-0020-y
- Shi, Z., Li, X., Zhang, Y., Zhou, Y., Gan, X., Fan, Q., et al. (2022). Constitutive androstane receptor (CAR) mediates pyrene-induced inflammatory responses in mouse liver, with increased serum amyloid A proteins and Th17 cells. *Br. J. Pharmacol.* doi:10.1111/bph.15934
- Sierro, F., Evrard, M., Rizzetto, S., Melino, M., Mitchell, A. J., Florido, M., et al. (2017). A liver capsular network of monocyte-derived macrophages restricts hepatic dissemination of intraperitoneal bacteria by neutrophil recruitment. *Immunity* 2, 374–388. doi:10.1016/j.immuni.2017.07.018
- Simpson, D., Pang, J., Weir, A., Kong, I., Fritsch, M., Rashidi, M., et al. (2022). Interferon- γ primes macrophages for pathogen ligand-induced killing via a caspase-8 and mitochondrial cell death pathway. *Immunity* 3, 423–441.e9. e429. doi:10.1016/j.immuni.2022.01.003
- Sookoian, S., Gemma, C., Gianotti, T. F., Burgueño, A., Castaño, G., and Pirola, C. J. (2008). Genetic variants of Clock transcription factor are associated with individual susceptibility to obesity. *Am. J. Clin. Nutr.* 6, 1606–1615. doi:10.1093/ajcn/87.6.1606
- Stanke-Labesque, F., Gautier-Veyret, E., Chhun, S., and Guilhaumou, R. (2020). Inflammation is a major regulator of drug metabolizing enzymes and transporters: Consequences for the personalization of drug treatment. *Pharmacol. Ther.* 215, 107627. doi:10.1016/j.pharmthera.2020.107627
- Subramanian, A., Wang, J., and Gil, G. (1998). STAT 5 and NF- κ B are involved in expression and growth hormone-mediated sexually dimorphic regulation of cytochrome P450 3A10/lithocholic acid 6 β -hydroxylase. *Nucleic Acids Res.* 9, 2173–2178. doi:10.1093/nar/26.9.2173
- Sunman, J. A., Hawke, R. L., LeCluyse, E. L., and Kashuba, A. D. M. (2004). Kupffer cell-mediated IL-2 suppression of CYP3A activity in human hepatocytes. *Drug Metab. Dispos.* 3, 359–363. doi:10.1124/dmd.32.3.359
- Szabo, G., and Petrasek, J. (2015). Inflammasome activation and function in liver disease. *Nat. Rev. Gastroenterol. Hepatol.* 7, 387–400. doi:10.1038/nrgastro.2015.94
- Tschuor, C., Kachaylo, E., Limani, P., Raptis, D. A., Linecker, M., Tian, Y., et al. (2016). Constitutive androstane receptor (Car)-driven regeneration protects liver from failure following tissue loss. *J. Hepatol.* 1, 66–74. doi:10.1016/j.jhep.2016.02.040
- Uderhardt, S., Martins, A. J., Tsang, J. S., Lämmermann, T., and Germain, R. N. (2019). Resident macrophages cloak tissue microlesions to prevent neutrophil-driven inflammatory damage. *Cell* 3, 541–555. doi:10.1016/j.cell.2019.02.028
- Uno, Y., Murayama, N., and Yamazaki, H. (2020). Interleukin-1 β and tumor necrosis factor- α affect cytochrome P450 expression in cynomolgus macaque hepatocytes. *Drug Metab. Pharmacokinet.* 3, 341–343. doi:10.1016/j.dmpk.2020.02.001
- Wang, X., Wu, T., Ma, H., Huang, X., Huang, K., Ye, C., et al. (2022). VX-765 ameliorates inflammation and extracellular matrix accumulation by inhibiting the NOX1/ROS/NF- κ B pathway in diabetic nephropathy. *J. Pharm. Pharmacol.* 3, 377–386. doi:10.1093/jpp/rgab112
- Wang, X., Ye, C., Xun, T., Mo, L., Tong, Y., Ni, W., et al. (2021). *Bacteroides fragilis* polysaccharide A ameliorates abnormal voriconazole metabolism accompanied with the inhibition of TLR4/NF- κ B pathway. *Front. Pharmacol.* 663325, 663325. doi:10.3389/fphar.2021.663325
- Wu, H., Chung, M., Wang, C., Huang, C., Liang, H., and Jan, T. (2013). Iron oxide nanoparticles suppress the production of IL-1 β via the secretory lysosomal pathway in murine microglial cells. *Part. Fibre Toxicol.* 46, 46. doi:10.1186/1743-8977-10-46
- Wu, X., Wang, S., Li, M., Li, J., Shen, J., Zhao, Y., et al. (2020). Conditional reprogramming: Next generation cell culture. *Acta Pharm. Sin. B* 8, 1360–1381. doi:10.1016/j.apsb.2020.01.011
- Xie, W. (2020). Editorial of special issue on drug metabolism and disposition in diseases. *Acta Pharm. Sin. B* 1, 2. doi:10.1016/j.apsb.2019.12.016
- Xu, Y., Chen, J., Jiang, W., Zhao, Y., Yang, C., Wu, Y., et al. (2022). Multiplexing nanodrug ameliorates liver fibrosis via ROS elimination and inflammation suppression. *Small* 3, e2102848. doi:10.1002/smll.202102848
- Xun, T., Lin, Z., Wang, X., Zhan, X., Feng, H., Gan, D., et al. (2021). Advanced oxidation protein products downregulate CYP1A2 and CYP3A4 expression and activity via the NF- κ B-mediated signaling pathway in vitro and in vivo. *Lab. Invest.* 9, 1197–1209. doi:10.1038/s41374-021-00610-9
- Yang, S., Kuang, G., Jiang, R., Wu, S., Zeng, T., Wang, Y., et al. (2019). Geniposide protected hepatocytes from acetaminophen hepatotoxicity by down-regulating CYP 2E1 expression and inhibiting TLR 4/NF- κ B signaling pathway. *Int. Immunopharmacol.* 105625, 105625. doi:10.1016/j.intimp.2019.05.010
- Yao, H., Bai, R., Ren, T., Wang, Y., Gu, J., and Guo, Y. (2019). Enhanced platelet response to clopidogrel in Zucker diabetic fatty rats due to impaired clopidogrel inactivation by carboxylesterase 1 and increased exposure to active metabolite. *Drug Metab. Dispos.* 8, 794–801. doi:10.1124/dmd.118.085126
- Ying, W., Fu, W., Lee, Y. S., and Olefsky, J. M. (2020). The role of macrophages in obesity-associated islet inflammation and β -cell abnormalities. *Nat. Rev. Endocrinol.* 2, 81–90. doi:10.1038/s41574-019-0286-3
- Zhang, R., Xu, D., Zhang, Y., Wang, R., Yang, N., Lou, Y., et al. (2021). Silybin restored CYP3A expression through the sirtuin 2/nuclear factor κ -B pathway in mouse nonalcoholic fatty liver disease. *Drug Metab. Dispos.* 9, 770–779. doi:10.1124/dmd.121.000438
- Zhang, X., Kuang, G., Wan, J., Jiang, R., Ma, L., Gong, X., et al. (2020). Salidroside protects mice against CCl₄-induced acute liver injury via down-regulating CYP2E1 expression and inhibiting NLRP3 inflammasome activation. *Int. Immunopharmacol.* 106662, 106662. doi:10.1016/j.intimp.2020.106662
- Zhao, G., Wang, X., Edwards, S., Dai, M., Li, J., Wu, L., et al. (2020). NLRX1 knockout aggravates lipopolysaccharide (LPS)-induced heart injury and attenuates the anti-LPS cardioprotective effect of CYP2J2/11, 12-EET by enhancing activation of NF- κ B and NLRP3 inflammasome. *Eur. J. Pharmacol.* 881, 173276. doi:10.1016/j.ejphar.2020.173276
- Zhao, M., Ma, J., Li, M., Zhang, Y., Jiang, B., Zhao, X., et al. (2021). Cytochrome P450 enzymes and drug metabolism in humans. *Int. J. Mol. Sci.* 23, 12808. doi:10.3390/ijms222312808
- Zhao, M., Xing, H., Chen, M., Dong, D., and Wu, B. (2020). Circadian clock-controlled drug metabolism and transport. *Xenobiotica* 5, 495–505. doi:10.1080/00498254.2019.1672120
- Zheng, Y., Humphry, M., Maguire, J., Bennett, M., and Clarke, M. (2013). Intracellular interleukin-1 receptor 2 binding prevents cleavage and activity of interleukin-1 α , controlling necrosis-induced sterile inflammation. *Immunity* 2, 285–295. doi:10.1016/j.immuni.2013.01.008
- Zimmermann, M., Zimmermann-Kogadeeva, M., Wegmann, R., and Goodman, A. L. (2019). Mapping human microbiome drug metabolism by gut bacteria and their genes. *Nature* 7762, 462–467. doi:10.1038/s41586-019-1291-3



OPEN ACCESS

EDITED BY

Xiaojuan Chao,
The First Affiliated Hospital of Sun
Yat-sen University, China

REVIEWED BY

Rui Han,
Yale University, United States
Mingshui Chen,
Fujian Provincial Cancer Hospital, China

*CORRESPONDENCE

Ying Tang,
tangying@gzucm.edu.cn
Wenyi Gu,
w.gu@uq.edu.au

SPECIALTY SECTION

This article was submitted to
Inflammation Pharmacology,
a section of the journal
Frontiers in Pharmacology

RECEIVED 17 July 2022

ACCEPTED 13 October 2022

PUBLISHED 28 October 2022

CITATION

Qi Y, Zou H, Zhao X, Kapeleris J,
Monteiro M, Li F, Xu ZP, Deng Y, Wu Y,
Tang Y and Gu W (2022), Inhibition of
colon cancer K-Ras^{G13D} mutation
reduces cancer cell proliferation but
promotes stemness and inflammation
via RAS/ERK pathway.
Front. Pharmacol. 13:996053.
doi: 10.3389/fphar.2022.996053

COPYRIGHT

© 2022 Qi, Zou, Zhao, Kapeleris,
Monteiro, Li, Xu, Deng, Wu, Tang and
Gu. This is an open-access article
distributed under the terms of the
[Creative Commons Attribution License](#)
(CC BY). The use, distribution or
reproduction in other forums is
permitted, provided the original
author(s) and the copyright owner(s) are
credited and that the original
publication in this journal is cited, in
accordance with accepted academic
practice. No use, distribution or
reproduction is permitted which does
not comply with these terms.

Inhibition of colon cancer K-Ras^{G13D} mutation reduces cancer cell proliferation but promotes stemness and inflammation *via* RAS/ERK pathway

Yan Qi^{1,2}, Hong Zou^{2,3}, XiaoHui Zhao², Joanna Kapeleris²,
Michael Monteiro², Feng Li⁴, Zhi Ping Xu², Yizhen Deng⁵,
Yanheng Wu⁵, Ying Tang^{6*} and Wenyi Gu^{2,5*}

¹Department of Pathology, Central People's Hospital of Zhanjiang and Zhanjiang Central Hospital, Guangdong Medical University, Zhanjiang, China, ²Australian Institute for Bioengineering and Nanotechnology (AIBN), University of Queensland (UQ), Brisbane, QLD, Australia, ³Department of Pathology, The Second Affiliated Hospital of Zhejiang University School of Medicine, Hangzhou, China, ⁴Department of Pathology, Beijing Chaoyang Hospital, Capital Medical University, Beijing, China, ⁵Gillion Biotherapeutics Ltd., Guangzhou Huangpu Industrial Zoon, Guangzhou, China, ⁶Science and Technology Innovation Center, Guangzhou University of Chinese Medicine, Guangzhou, China

K-Ras is a well-studied oncogene, and its mutation is frequently found in epithelial cancers like pancreas, lung, and colorectal cancers. Cancer cells harboring K-Ras mutations are difficult to treat due to the drug resistance and metastasis properties. Cancer stem cells (CSCs) are believed the major cause of chemotherapeutic resistance and responsible for tumor recurrence and metastasis. But how K-Ras mutation affects CSCs and inflammation is not clear. Here, we compared two colon cancer cell lines, HCT-116 and HT-29, with the former being K-Ras^{G13D} mutant and the latter being wildtype. We found that HCT-116 cells treated with a K-Ras mutation inhibitor S7333 formed significantly more tumor spheroids than the untreated control, while the wild type of HT-29 cells remained unchanged. However, the size of tumor spheroids was smaller than the untreated controls, indicating their proliferation was suppressed after S7333 treatment. Consistent with this, the expressions of stem genes Lgr5 and CD133 significantly increased and the expression of self-renewal gene TGF- β 1 also increased. The flow cytometry analysis indicated that the expression of stem surface marker CD133 increased in the treated HCT-116 cells. To understand the pathway through which the G13D mutation induced the effects, we studied both RAS/ERK and PI3K/Akt pathways using specific inhibitors SCH772984 and BEZ235. The results indicated that RAS/ERK rather than PI3K/Akt pathway was involved. As CSCs play the initial role in cancer development and the inflammation is a vital step during tumor initiation, we analyzed the correlation between increased stemness and inflammation. We found a close correlation of increased Lgr5 and CD133 with proinflammatory factors like IL-17, IL-22, and IL-23. Together, our findings suggest that K-Ras^{G13D} mutation promotes cancer cell growth but decreases cancer stemness and

inflammation thus tumorigenesis and metastasis potential in colon cancer. Inhibition of this mutation reverses the process. Therefore, care needs be taken when employing targeted therapies to K-Ras^{G13D} mutations in clinics.

KEYWORDS

K-Ras^{G13D} mutation, colon cancer, cancer stem cells, tumor spheroid, ERK pathway, PI3K/Akt pathway, inflammation

Introduction

Gene mutation is frequently observed in tumor development and is one of the most common reasons for tumor aggressiveness and poor prognosis (Chen et al., 2021), which is also known as tumor mutation burden (TMB). High TMB tumors are usually correlated with the deficiency of DNA repair, microsatellite instability, and a high possibility of drug resistance though they may attract more immune cell infiltration (Chen et al., 2021; Xiao et al., 2021). K-Ras gene is one of the most popular and well-defined oncogene that mutates in a broad range of solid tumors (Der et al., 1982), including lung adenocarcinoma (~30%) (Siegfried et al., 1997), pancreatic adenocarcinoma (~70%–90%) (Visani et al., 2013), stomach cancer (~10%) (Lee et al., 2003), and colorectal cancer (~30%–50%) (Andreyev et al., 1998; Downward, 2003). K-Ras mutations are generally associated with poor overall survival and resistance to therapies (Downward, 2003) and these mutations often occur at codons 12, 13, and 61, with codon 12 being the most frequently mutated (Addeo et al., 2021). The mutations at codons 12 and 13 can lead to wild-type glycine (G) being replaced by cysteine (C), valine (V), aspartic acid (D), arginine (R), alanine (A), or serine (S) (Cox et al., 2014). These mutations are usually accompanied with alternations of signaling pathways and thus change cancer cells in proliferation, drug resistance, and tumor recurrence. Therefore, in clinical settings, detection of these mutations becomes an important tool for prognosis and guides for targeted cancer therapies.

Colon cancer is a top lethal cancer for men and women worldwide (Selvam et al., 2019; Lichtenstern et al., 2020) and K-Ras mutation is one of the most frequently activated oncogenes observed in around 40% of colorectal carcinomas (Morkel et al., 2015). In clinical settings, once K-Ras gene mutations are detected, the inhibitor treatment of the gene mutation (targeted therapy) will be applied together with first line chemotherapeutics (Reck et al., 2021; Serna-Blasco et al., 2021). However, even with the targeted therapy, concerns still exist regarding the effectiveness of such therapies *in vivo* given the possibilities of existing intratumor heterogeneity or *de novo* mutation leading to treatment resistance (Cannataro et al., 2018) and the 5-year overall survival rate of colon cancer is still low around 10% (Davies and Goldberg, 2011). Consequently, K-Ras-specific drugs have rarely been approved in clinics (Christensen et al., 2020), suggesting whether the use of

mutation inhibitors will benefit the long-term outcome of treatment and the deep mechanism of K-Ras mutations needs further investigations.

Cancer stem cells (CSCs) are a small population of cancer cells with multi-potency and self-renewing abilities. They are the “seeds” of tumors, responsible for the initiation, growth, and development of tumors *in vivo* (Gu et al., 2011; Gu et al., 2015). From this concept, the gene mutation may firstly occur in CSCs and then heritate to the daughter cells. Therefore, understanding the effect of oncogene mutation such as K-Ras in colon CSCs is very important for the future development of more effective approaches for targeted therapies. Meanwhile, understanding the relationship between oncogene mutation and cancer stemness, especially how stemness will be changed after the inhibition of the effect of a gene mutation, is an interesting and open question to answer. For CSCs, there is no unique biomarker to identify them, for instance, in colon cancer, the most popular biomarkers are some surface adhesion molecules like CD24, CD44, and CD133 (Chen et al., 2015; Lee et al., 2015). In addition, some typical stem genes like CD133 and Lgr5, and self-renewing genes like TGF- β are also used to characterize colon CSCs (Gu et al., 2011; Chen et al., 2015).

It has been reported that K-Ras mutation can activate different pathways and thus affect cancer cell proliferation and development. For example, about 40% of colorectal cancers have mutations in K-Ras accompanied by the downstream activation of mitogen-activated protein kinase (MAPK) signalling, which promotes tumour invasion and progression since tumour cells with high MAPK activity resided specifically at the leading tumour edge, ceased to proliferate, underwent epithelial-mesenchymal transition (EMT), and expressed markers related to colon CSCs (Blaj et al., 2017). These results imply that differential MAPK signalling balances EMT, cancer stem cell potential, and tumour growth in colorectal cancer (Blaj et al., 2017).

Compared with other K-Ras mutations, G12 mutation is the most frequent and well-studied, which was also shown to relate to drug resistance in non-small-lung carcinoma (Adachi et al., 2020). Recently, an inhibitor, sotorasib, has been approved by the Food and Drug Administration as a fast track designation for the treatment of metastatic non-small-cell lung carcinoma with the G12C KRAS mutation (FDA website: published on Fri 28 May 2021). A study analysed tissues from colorectal (CRC) patients ($n = 49$) to determine whether K-Ras mutations contributed to CSC activation during colorectal tumorigenesis.

K-Ras wild-type DLD-1-K-Ras-WT and K-Ras mutated DLD-1-K-Ras-MT cells were cultured and evaluated for their ability to differentiate, form spheroids *in vitro*, and form tumours *in vivo*. Interaction between APC (Adenomatous polyposis coli) and K-Ras mutations in colorectal tumorigenesis was evaluated using APC (Min/+)/K-Ras (LA2) mice and DLD-1-K-Ras-WT and DLD-1-K-Ras-MT cell xenografts. The results showed that the sphere-forming capability of DLD-1-K-Ras-MT cells was significantly higher than that of DLD-1-K-Ras-WT cells (DLD-1-K-Ras-MT mean = 86.661 pixel, DLD-1-K-Ras-WT mean = 42.367 pixels, $p = 0.003$). Moreover, both the size and weight of tumours from DLD-1-K-Ras-MT xenografts were markedly increased compared with tumours from DLD-1-K-Ras-WT cells. Expression of the CSC markers CD44, CD133, and CD166 was induced in intestinal tumours from APC (Min/+)/K-Ras (LA2) mice, but not K-Ras (LA2) mice, indicating that K-Ras mutated cells are more tumorigenic and that APC mutation is required for CSC activation by oncogenic K-Ras mutation (Moon et al., 2014).

Unlike 12C, K-Ras G13 mutation is much less studied and whether K-Ras G13 point mutation is also related to cancer stemness, especially when the mutation is targeted, whether the signal pathway change will alter the stemness in colon cancer has not been reported before. In this research, we aimed to study the relation of K-Ras G13 mutation with cancer stemness. HCT-116 and HT-29 cells are two well-established colon cancer cell lines and reported to be K-Ras G13D mutated and wild type, respectively (Ahmed et al., 2013). We, therefore, employ an inhibitor of K-Ras G12C, which could also block G13 mutation at a higher dose or long-term treatment, to study if suppressing the mutation will affect the stemness of colon HCT-116 cells. We found that suppressing this mutation can reduce colon cancer cell proliferation but increase their stemness, including sphere formation and stem surface and gene marker expressions. We further prove that this effect is through the RAS/ERK pathway. To further confirm the increased stemness will affect tumor recurrence and metastasis, we analyzed their relations to inflammation, we found a good correlation with pro-inflammatory factors like IL-17, IL-22, and IL-23, which are reported as important factors for tumor initiation (Grivennikov et al., 2012; Zhao et al., 2021). These results indicate that when using targeted therapies for K-Ras G13 mutation, we may need to consider its effects on promoting cancer stemness and inflammation.

Materials and methods

Cell lines and tumor spheroid culture

The colon cancer cell lines HCT-116 (K-Ras mutated at G13D) and HT-29 (wild type) were purchased from America Tissue Collection Centre (ATCC) as we reported before (Zou et al., 2016) and were maintained in Dulbecco's Modified Eagles

Medium (DMEM, Invitrogen, Australia) supplemented with 10% fetal calf serum, 1% penicillin, and 1% streptomycin in 75 ml flasks at 37°C and with 5% CO₂. Sphere culture medium and method were as previously reported (Gu et al., 2011). Briefly, HCT-116 or HT-29 cells were suspended in sphere cultural media (Dulbecco's Modified Eagle's Medium F-12, 0.4% BSA, 0.2% epidermal growth factor and 0.2% insulin, Sigma) at a cell concentration of 4000 cells/mL in upright T25 flasks. The sphere culture was maintained in a humidified incubator at 37°C under 5% CO₂. And fed every 2 days with 20% of the original culture volume of sphere media until day 7–8. Spheroids were collected by centrifugation at 100× g for 5 min and resuspended in a sphere culture medium for counting (a cutoff size 50 µm) or trypsinized for 5 min to separate individual spherical cells by multiple pipetting and passing through 40 µm cell strainers. Isolated and purified spherical cells were further cultured in a sphere cultural medium for second generation culture or used for characterization and other assays. For counting or imaging the spheres, a small aliquot (eg, 50 µL) was transferred to a well of 96-well plate. After setting for 2 min, the spheroids in each well were counted and imaged. The total spheroid number was calculated by multiplying the count/well with the total volume (µL)/50 µL. The sphere size was calculated by total spherical cell numbers divided by spheroid numbers.

Inhibitor treatment in cell culture

To evaluate the inhibitor effect on the number and size of tumor sphere formation, tumor cells (HCT-116 and HT-29) were cultured with or without S7333 inhibitor (4 µM, K-Ras (G12C) inhibitor 6, Cat No: S7333, Jomar Life Research, Australia) for 72 h, SCH772984 inhibitor (25, 50, 100, 200 nM, R & D Systems, Inc., Minneapolis, MN, United States) for 48 h, and BEZ235 inhibitor (50, 100, 200, 300, 400 nM, Jomar Life Research, Australia) for 48 h in completed DMEM medium. After each treatment, cells were directly counted (trypan blue assay), used for MTT assay, and collected for real-time qRT-PCR tests and tumor spheroid culture as above. For combinational treatment, the cells were firstly treated with 4 µM S7333 for 72 h and then collected and set for further culture with the SCH772984 inhibitor (200 nM) or BEZ235 inhibitor (50 nM) for 48 h for gene testing or tumor spheroid culture for testing sphere formation and stemness surface markers.

Flow cytometry analysis for colon cancer stemness surface markers

The spherical cells isolated from tumor spheroids of HCT-116 and HT-29 cell cultures without any treatment were firstly verified by their surface markers as we reported before (Wu et al., 2017). This was to ensure the colon CSCs have been enriched after the sphere culture. For the tumor spheroid culture after each treatment, 1×10^5

spherical cells were used for staining with rabbit anti-human CD133 (prominin-1) antibody (Sigma-Aldrich); mouse anti-human CD44 conjugated with FITC (Invitrogen, Australia); and mouse anti-human CD24 antibody conjugated with RPE (Invitrogen, Australia). For CD133 staining, mouse anti-rabbit IgG-FITC (Sigma-Aldrich) was used as the secondary antibody. After 3 washes with 2% FCS/PBS, the cells were fixed in 2% paraformaldehyde (PFA)/PBS and analyzed by flow-cytometry (Accuri, BD) and CFlow Sampler software. Three biological repeats were performed.

Real-time RT-PCR for stemness gene expression

Total RNA extraction from tumor cells was prepared as instructed by the manufacturer using TRIzol[®] reagent (Invitrogen, Australia). Reverse transcription reactions were performed with oligo-dT primer using the High-Capacity cDNA RT Kit (Applied Biosystems). Real-time PCR was carried out with SYBR green master mixture (Promega) on a Rotor-Gene RG-3000 (Corbett Research, Australia) with the program pre-heating 95°C 5 min; then 40 cycles of 94°C 15 s; 60°C 15 s; and 72°C 20 s. The primers are: GAPDH, Forward: 5'-CTTTTGCCTCGCCAG-3', Reverse: 5'-TTGATG GCAACAATATCCAC-3'; CD133, Forward 5'-CACCAAGCA CAGAGGGTCAT-3', Reverse 5'-CACTACCAAGGACAAGGC GT-3'; TGF- β 1, Forward 5'-CAACAATTCTGGCGATACC-3', Reverse 5'-GAACCCGTTGATGTCCACTT-3'; Lgr5, Forward 5'-GATGTTGCTCAGGGTGGACT-3', Reverse 5'-GGGAGCAGC TGACTGATGTT-3'; K-Ras, Forward 5'-TGT CAAGCTCAG CACAATCTG, Reverse 5'-GGTAGGGAGGCAAGATGACA; Ki-67: Forward 5'-AATTCAGACTCCATGTGCCTGAG-3', and Reverse 5'-CTTGACACACACATTGTCCTCAGC-3'. The GAPDH primers were used as the internal control to normalize other gene expressions. The normalized expressions of treated samples were then used to calculate fold changes by dividing the expression of the control sample.

MTT 3-(4,5-dimethylthiazol-2-yl)-2,5-diphenyltetrazolium bromide) assay

For cell survival assay, 1×10^4 treated or untreated colon cancer cells in 100 μ L of medium were seeded to each well in a 96-well plate and treated with various concentrations of BEZ235. After 24 h treatment, the MTT assay was used to measure cell viability as instructed by the manufacturer (Sigma-Aldrich). Briefly, after cells were incubated with 10 μ L of MTT (5 mg/ml) for 4 h at 37°C under light-blocking conditions, the medium was then removed and 100 μ L of DMSO was added into each well. The absorbance of each well was measured at 570/630 nm using the INFINITE M PLEX reader (Tecan). The 100% viable rates were cells with a complete DMEM medium.

Western blotting analysis

Treated or untreated cells from the cultures were lysed in RIPA buffer (Cell Signal Technology) containing 2 μ L/ml protease inhibitor cocktail (Sigma-Aldrich). Protein samples were separated by electrophoresis using pre-casted mini-PAGE (Bio-Rad) at 120 V for 1.5 h. The separated proteins were transferred onto the PVDF membrane at 100 V for 1 h. The membrane was blocked at room temperature with 5% bovine serum albumin in Tris-Buffered Saline and 0.5% Tween 20 (TBST) buffer for 1 h and washed three times with TBST with each wash being 5 min. The membranes then were incubated overnight with anti-human ERK1/ERK2 antibodies (Phospho-ERK1/ERK2 (Thr185, Tyr187) antibody (44-680G) and ERK1/ERK2 monoclonal antibody (ERK-7D8), ThermoFisher Scientific) at 1:1000 dilutions. After washing three times with TBST, the membrane was incubated for 2 h at room temperature with horseradish peroxidase conjugated goat anti-rabbit antibody (Cell Signal Technology) at a dilution of 1:2500. All the incubation was performed with a constant shaking. Then the membrane was rinsed 3 times with TBST, and merged in 2 mL Clarity ECL blotting substrate (Bio-Rad Laboratories, Inc., Hercules, CA) for 1 min. The blot image of antibody signals was acquired using Geldoc (Bio-Rad Laboratories, Inc., Hercules, CA). Densitometry analysis of protein bands was conducted by ImageJ software.

Database analysis

The correlation of K-Ras expression with RAF, PI3K, AKT, MAPK, and IL-17 in the TCGA-COAD cohort was analyzed using Spearman's correlation analysis. To analyze the K-Ras expression with stemness, the expression matrix was directly obtained through the GEO (<http://www.ncbi.nlm.nih.gov/geo>) Query package. After downloading and installing the Gene Set Enrichment Analysis Database (GSEA) software (<http://software.broadinstitute.org/gsea/msigdb/index.jsp>), the expression file, the description file, and the target cluster of the selected research need to be prepared and the parameters need to be set up to run GSEA. The enrichment analysis is performed based on the expression of K-Ras in the selected sample, and the result is all the enrichment of expressed genes in various metabolic pathways. It is generally believed that the absolute value of $NES \geq 1.0$, $p\text{-val} \leq 0.05$, and $p\text{-ajust} \leq 0.05$ are meaningful gene sets. The K-Ras mRNA expression data were extracted from The Cancer Genome Atlas (TCGA) database (<https://portal.gdc.cancer.gov/repository>). The inclusion criteria are: 1) colon cancer; 2) complete RNA-seq data. A total of 480 colon cancer cases and 41 normal cases were included in the present study, and the workflow type was HTSeq-FPKM. To explore the correlation of expression of CD133 and IL-7, IL-17, IL-22, and IL-23 in the TCGA-COAD cohort was analyzed using Spearman's correlation analysis. To explore the correlation of expression of LGR5 and IL-11, IL-17, IL-22, and IL-23 in the TCGA-COAD cohort was analyzed using Spearman's correlation analysis.

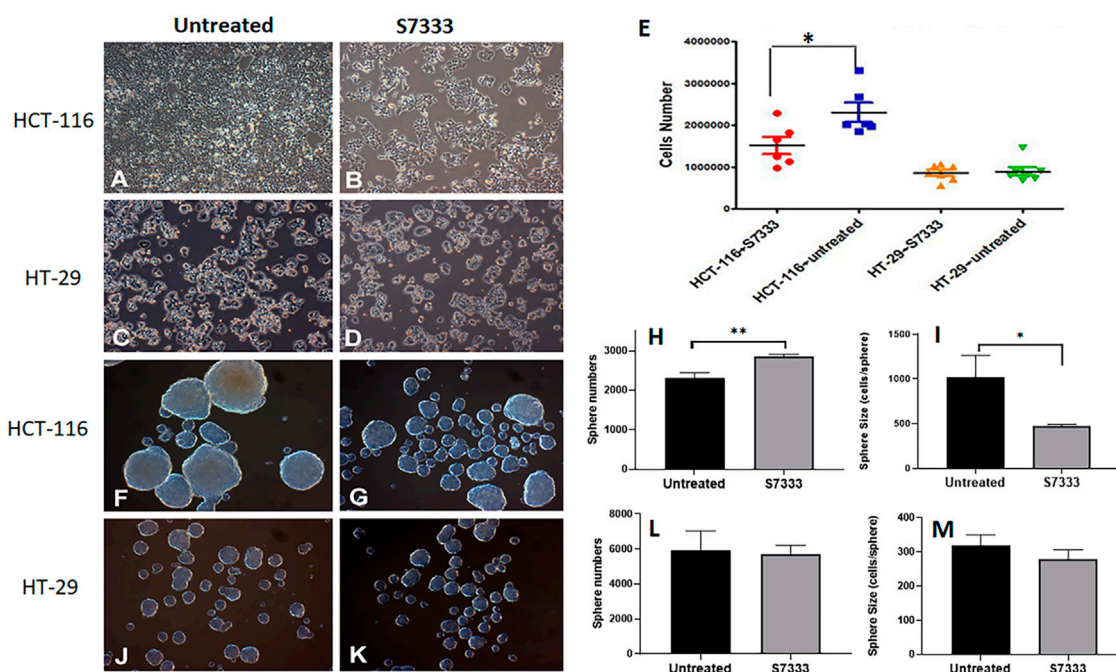


FIGURE 1

The comparison of cell growth and spheroid formation between HCT-116 and HT-29 cells after S7333 treatment. Cell morphology and density changes under light microscope of HCT-116 (A,B) and HT-29 cells (C,D) before and after treatment with S7333 for 72 h at 4 μ M. (E), the comparison of live cell numbers between HCT-116 and HT-29 cells before and after the treatment with S7333. (F,G) show the morphology and numbers of tumor spheroids from HCT-116 cells before (F) and after (G) treatment. The number of spheroids significantly increased (H) while the size of spheroids (average cell numbers/spheroid) significantly decreased (I) after S7333 treatment in HCT-116 cells. In HT-29 cells, no morphology (J,K), number (L), and size (M) changes were seen before and after S7333 treatment. *: $p < 0.05$; **: $p < 0.01$.

Data presentation and statistical analysis

Data collected from experimental and control groups were expressed as mean \pm SD and these assays were repeated 2–3 times. The one-way analysis of variance and Turkey's multiple comparisons or the unpaired Student's *t*-test (GraphPad Prism 9.1 program) were used to analyze the differences between groups and discriminate the significant differences (two-tail, $p < 0.05$) between experimental and control groups.

Results

Inhibition of K-Ras^{G13D} mutation decreases HCT-116 cell proliferation but increases their sphere formation

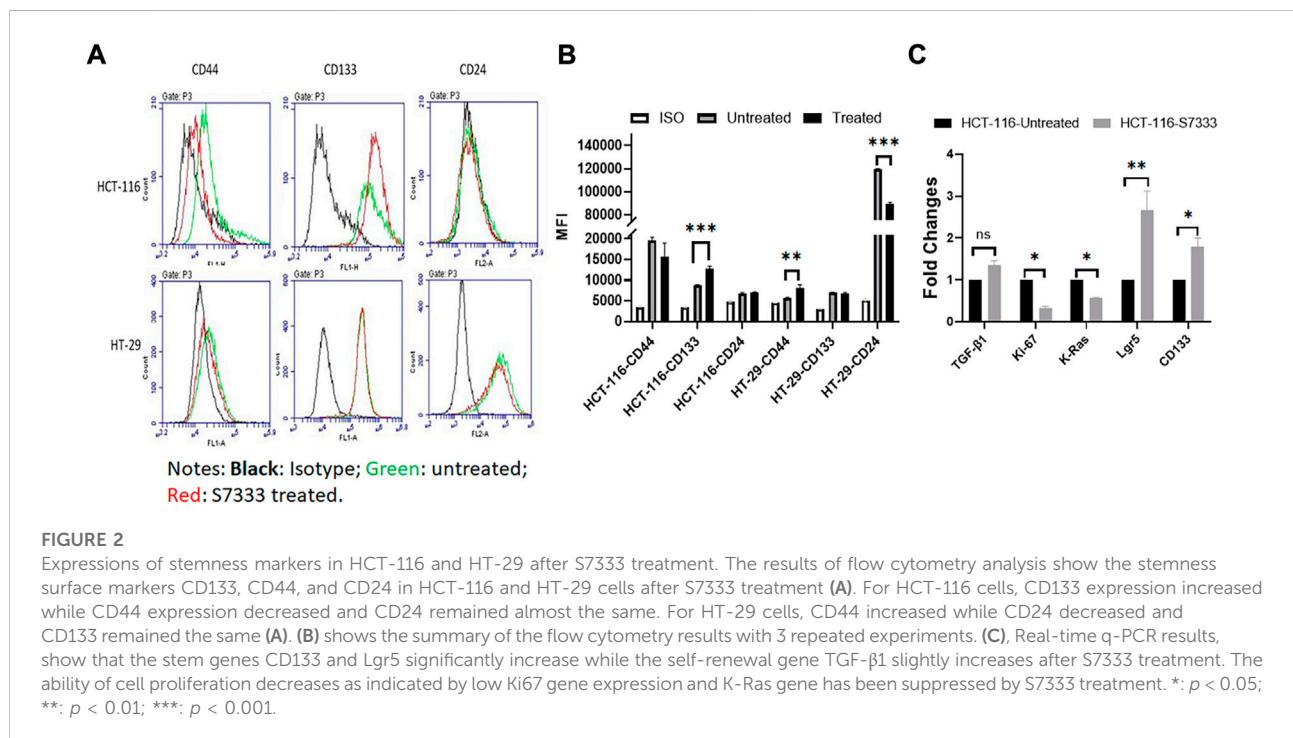
The K-Ras (G12C) inhibitor 6-S7333 (named S7333 afterward) was employed according to the manufacturers' instruction, in which, the treatment lasted for 3 days (72 h) would inhibit the activity of G12/G13 mutations. Therefore, both cell lines of HCT-116 (K-Ras G13D mutated, K-Ras^{G13D}) and HT-29 (wide type, K-Ras^{WT}) were treated with

S7333 for 72 h at 4 μ M concentration in DMEM complete culture medium before other assays were conducted. The first observation after treatment was that the cell number significantly decreased in HCT-116 cells (Figure 1A vs. 1B), whereas no such change was seen in HT-29 cells (Figure 1C vs. 1D).

This result suggests that S7333 treatment has a specific effect on HCT-116 cells but not on HT-29 cells (Figure 1E). Both cells were then set for tumor spheroid formation after S7333 treatment. Interestingly, the result showed that the number of tumor spheroids was obviously increased after the treatment in HCT-116 but the sphere size was greatly decreased under the microscope, compared to the untreated controls (Figures 1F vs. 1G). The quantitative determination of the total spheroid number (Figure 1H) and size (in terms of average cells/spheroid, Figure 1I) was statistical significance ($p < 0.001$ and $p < 0.05$, respectively). In contrast, there were no such changes observed in HT-29 K-Ras^{WT} cells after S7333 treatment both in spheroid number and size (Figures 1J vs. 1K, and Figures 1L,M). These data collectively suggest that S7333 can effectively inhibit HCT-116 cells that leads to the decrease of their cell proliferation but increase the spheroid formation, an important indicator of cancer stemness.

TABLE 1 Comparison of the positive rate of cancer stem surface makers between HCT-116 and HT-29 cells before and after S7333 treatment.

	CD44 ⁺ cells (mean \pm SD %)		CD133 ⁺ cells (mean \pm SD %)		CD24 ⁺ cells (mean \pm SD %)	
	HCT-116	HT-29	HCT-116	HT-29	HCT-116	HT-29
Un-treated	38.8 \pm 1.4	0.4 \pm 0.1	46.4 \pm 1.4	10.9 \pm 1.1	3.8 \pm 0.1	89.2 \pm 0.7
S7333 treated	18.4 \pm 0.9	0.6 \pm 0.1	59.2 \pm 1.2	9.8 \pm 1.7	3.9 \pm 0.1	84.3 \pm 2.2



Inhibition of K-Ras^{G13D} mutation increases cancer stemness in HCT-116 cells

To further investigate the increased stemness in HCT-116 cells after S7333 treatment, we examined signatural stem markers of colon CSCs, including the cell surface markers like CD133, CD44, and CD24 and gene markers like Lgr5, CD133, and TGF- β 1 before and after S7333 treatment. Ki-67 gene expression was also measured to confirm cell proliferation and K-Ras gene was included to verify the effect of S7333 treatment. The results showed that after the treatment in mutant HCT-116 cells, cell surface CD133 expressions significantly increased in terms of positive cell percentage (Table 1) and mean fluorescent intensity (MFI, Figures 2A,B).

The surface level of CD24 expression also increased slightly but CD44 expression decreased (Figures 2A,B). The CD133 positive cells increased from 46.4% to 59.2%, and

CD44 positive cells decreased from 38.8% to 18.4% (Table 1). As a control, HT-29 cells were also assayed for stem markers. As shown in Figure 2A and Table 1, the expressions of these surface markers in K-Ras^{WT} cells were different from HCT-116 cells where significant increase of CD44 and significant decrease of CD24 between the treated and untreated cells were observed (Figure 2B).

Real-time qPCR results further proved that the stem genes of CD133 and Lgr5 expressions significantly increased in treated HCT-116 cells while Ki-67 was decreased after S7333 treatment (Figure 2C). The self-renew gene TGF- β 1 expression was also higher after S7333 treatment in HCT-116 cells though did not reach the statistical significance (Figure 2C). As expected, the K-Ras gene expression was significantly down-regulated after S7333 treatment, indicating the inhibitor specifically acted on K-Ras gene of HCT-116 but not HT-29 cells (Figure 2C). Together, all above data suggest that the major cancer stem

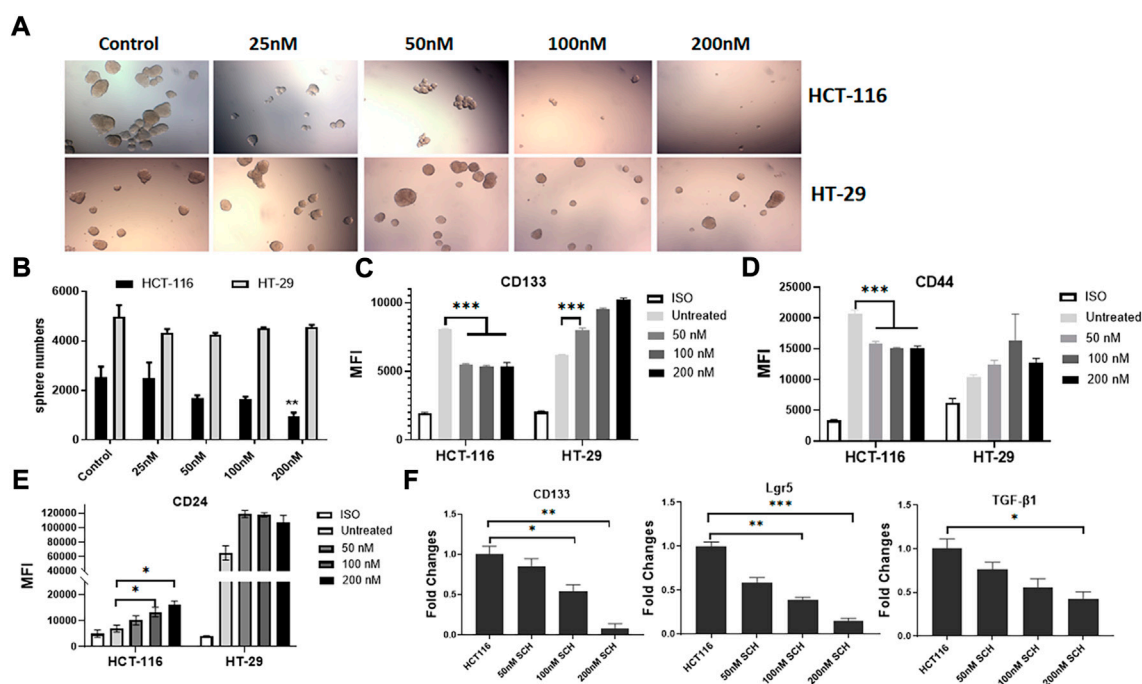


FIGURE 3

Inhibition of ERK by SCH772984 suppresses the spheroid formation and stemness in HCT-116 but not in HT-29 cells. The photos show the morphology and numbers of tumor spheroids from HCT-116 and HT-29 cells after SCH772984 (SCH) treatment at different doses (A). A dose-dependent inhibition of sphere formation and growth in HCT-116 cells can be seen, comparing to that in HT-29 cells. (B), the number of spheroids was significantly decreased in HCT-116 cells at the 200 nM dose, but not in HT-29 cells. Flow cytometry analysis showed surface marker expressions of CD133 (C) and CD44 (D) decreased in dose-dependent manners at the doses of 50, 100, and 200 nM in HCT-116, though there was a slight increase for CD24 (E). Inversely, the expressions of these markers increased (C, D, E) in HT-29 cells after SCH772984 treatment. (F), the stem gene expressions of CD133, Lgr5, and TGF- β 1 in HCT-116 cells, they all displayed a dose-dependent decrease after SCH772984 treatment. *: $p < 0.05$; **: $p < 0.01$; ***: $p < 0.001$.

markers increase but the cell proliferation decreases when K-Ras^{G13D} mutation is suppressed by S7333 treatment.

Inhibition of RAS/ERK pathway suppresses the spheroid formation and stemness profile in HCT-116 rather than HT-29 cells

To understand the signaling pathway through which the mutated K-Ras^{G13D} affects the stemness in HCT-116 cells, we analyzed the downstream signal pathways of K-Ras in the cell line and used HT-29 cells as the control. Based on the literature search, there are two typical and well-studied pathways under K-Ras regulation; RAS/ERK and PI3K/Akt pathways (Thein et al., 2021). We firstly tested if ERK pathway inhibitor SCH772984 alone could inhibit the spheroid formation of the two cell lines at the doses from 25 to 200 nM. We found a dose dependent inhibition of spheroid formation in HCT-116 cells but not in HT-29 cells after 48 h treatment (Figure 3A). The spheroid number counts reached statistical significance at the dose of 200 nM (Figure 3B). These data suggest that K-Ras^{G13D} mutated

cells are more sensitive to SCH772984 treatment than the wildtype HT-29 cells. In another word, the ERK pathway may be more actively involved in spheroid formation in K-Ras^{G13D} mutated colon cancer cells.

Next, we assessed the expression of surface markers in different dose groups of HCT-116 and HT-29 cells by FACS analysis. In HCT-116 cells, the expression of CD133 and CD44 were remarkably decreased after inhibition of ERK activity by SCH772984 treatment in both positive cell rates (decreased from 52.8% to 35.3% for CD133, and from 74.3% to 29.8% for CD44) and MFI (Table 2 and Figures 3C,D). However, the treatment increased CD24 expression in terms of MFI (Figure 3E) and positive cell rates (Table 2). Differently, in HT-29 cells, the treatment increased MFI of CD133 as the dose increases (Figure 3C), while MFI of CD44 (Figure 3D) and CD24 (Figure 3E) slightly increased with the positive cell rates basically remaining unchanged (Table 2). These findings suggest that in colon cancer, except CD24 expression, ERK pathway differently regulates stemness properties between mutant K-Ras^{G13D} and K-Ras^{WT} cells, which may relate to the mutation.

TABLE 2 Comparison of positive cells (%) of cancer stem surface makers between HCT-116 and HT-29 cells after S7333 or SCH or combined treatment.

	CD44 ⁺ cells (%)		CD133 ⁺ cells (%)		CD24 ⁺ cells (%)	
	HCT-116	HT-29	HCT-116	HT-29	HCT-116	HT-29
Untreated cells (Control)	74.3 ± 9.8	22.6 ± 1.9	52.8 ± 4.8	41.5 ± 6.5	4.8 ± 1.3	94.4 ± 8.3
S7333 treated	78.0 ± 7.7	19.0 ± 2.3	59.3 ± 7.5	42.7 ± 5.6	2.4 ± 1.1	96.1 ± 9.5
SCH treated	29.8 ± 5.4	19.7 ± 3.1	35.3 ± 2.9	73.5 ± 7.9	16.8 ± 3.2	99.0 ± 11.9
S7333+SCH	24.8 ± 3.6	20.5 ± 2.3	34.9 ± 3.3	77.9 ± 7.3	18.6 ± 2.9	97.5 ± 10.7

To further confirm the effect of ERK pathway on the stemness in mutant HCT-116 cells, we measured stem gene expressions after SCH772984 treatment. The results demonstrated that the inhibitor could effectively suppress all stem gene expressions including CD133, Lgr5, and TGF- β 1 in HCT-116 cancer cells and in dose-dependent manners (Figure 3F). Among them, CD133 and Lgr5 were more significant than TGF- β (Figure 3F). These data collectively suggest that the inhibition of ERK pathway can decrease the cancer stemness profile in HCT-116 cells more sensitively than in HT-29 cells.

Blocking K-Ras^{G13D} mutation attenuates the suppressive effect of ERK inhibitor SCH772984

To confirm that the significant inhibition of stemness properties by ERK inhibitor SCH772984 in HCT-116 cells is relevant to K-Ras^{G13D} mutation, we firstly treated HCT-116 with S7333 for 72 h to block the effect of mutation followed by the treatment with the ERK inhibitor SCH772984 at the dose of 200 nM. The results showed that after S7333 treatment the spheroid number increased but their sizes decreased compared to controls (Figure 4A), which are consistent with our above results in Figure 1, suggesting the treatment was effective. However, compared to SCH772984 treatment alone that was shown in the above section to significantly inhibit spheroid formation, did not show such inhibition in both sphere number (in fact significantly increased) and size (slightly increased, Figure 4A). In contrast, no significant changes were seen in spheroid numbers of K-Ras^{WT} cell line HT-29 (Figures 4A,B). For tumor spheroid sizes, in terms of average cell numbers per spheroid, both SCH772984 alone and S7333 + SCH772984 combination treatment decreased (Figure 4C). Notably, same as the spheroid number.

The size did not decrease in the combination treatment group, compared to SCH772984 alone group (Figure 4C). To further prove that S7333 and SCH772984 treatment had effect on the targeted proteins, we conducted Western-blot analysis. As

shown in Figure 4D, the expression of phosphorylated ERK (pERK) decreased in HCT-116 cells after S7333 treatment, compared to the control. SCH772984 treatment alone remarkably decreased pERK expression in the cell line harboring K-Ras^{G13D} mutation. The combination treatment with S7333 and SCH772984 further decreased the level of pERK expression. Compared to HCT-116 cells, we observed less inhibitory effects of pERK levels in the cell line with HT-29^{WT} cells (Figure 4D) either with SCH772984 treatment alone or S7333 and SCH772984 combination treatment. These data suggest that the inhibitor treatments can affect both cell lines but more sensitively affect the K-Ras^{G13D} mutated HCT-116 cells.

To further verify ERK pathway involvement in the regulation of cancer stemness, we analysed the stem surface markers of CD133 (Figures 5A,D), CD44 (Figures 5B,E), and CD24 (Figures 5C,F). The results showed that after the treatment of S7333, CD133 level increased whereas SCH772984 treatment decreased the level. After blocking the K-Ras^{G13D} mutation, the SCH772984 treatment significantly increased CD133 expression (Figure 5D). For CD44, S7333, and SCH772984 treatment alone decreased the expression but SCH772984 treatment after S7333 blocking the mutation slightly increased the expression levels (Figure 5E). For CD24, either treatment alone with S7333 and SCH772984 or the combination treatment increased the expression levels (Figure 5F). In contrast, in HT-29 cells, the CD133, CD44, and CD24 expressions were different from HCT-116 cells in either treatment alone with S7333 and SCH772984 or combination treatment with both (Figures 5A–F). These results suggest even after blocking K-Ras^{G13D} mutation, there was a difference in signalling pathways in the two cell lines.

To further verify the stemness in HCT-116 cells, we measured the stem gene expression. The results showed that after blocking K-Ras^{G13D} mutation in HCT-116 cells, SCH772984 treatment did not decrease but increase stem gene profiles including CD133 (Figure 5G) and Lgr5 (Figure 5H) expressions. However, TGF- β 1 (Figure 5I) expression decreased after the combination treatment. Consistent with the results in Figure 2, after S7333 treatment, CD133, Lgr5, and TGF- β 1 gene expression all increased, compared to the control (all $p < 0.05$,

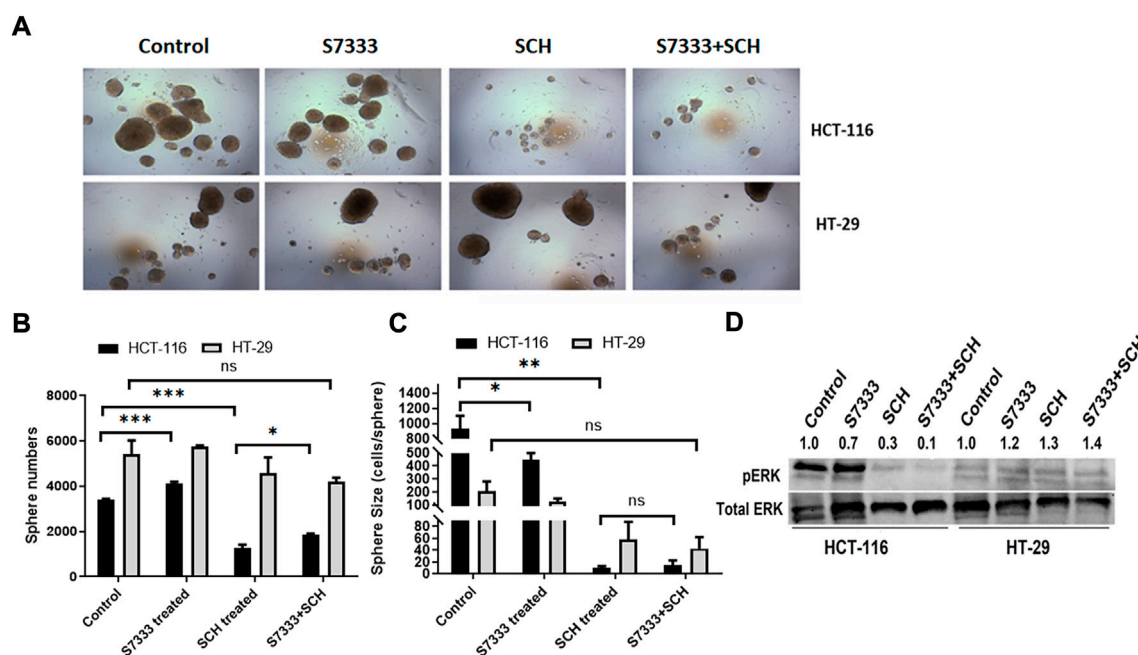


FIGURE 4

After blocking K-Ras^{G13D} mutation, the sensitivity to ERK pathway inhibitor SCH772984 reduced in HCT-116 but not HT-29 cells. The images show the sphere formation rates and numbers after the S7333 (4 μM for 72 h) or SCH772984 (200 nM for 48 h) alone and the combination treatment in HCT-116 and HT-29 cells (A). The sphere number counts show the significant increase after S7333 treatment and decrease after SCH772984 treatment, compared with the control (B). However, there is a significant increase of spheroids by SCH772984 treatment after blocking the K-Ras mutation with S7333 (B). The sphere size was obviously decreased after both S7333 and SCH772984 treatment alone (C). However, after blocking K-Ras mutation, SCH772984 treatment slightly increases the size (C). The Western blotting results show the protein levels of phosphorylated ERK (pERK) and total ERK protein (total ERK) in HCT-116 and HT-29 cells after S7333, SCH772984, and combination treatment. The numbers on the protein bands represent densitometry analysis results (D). *: $p < 0.05$; **: $p < 0.001$; ***: $p < 0.0001$; ns: $p > 0.05$.

Figures 5G–I). Taken together, all above data indicate that after blocking K-Ras^{G13D} mutation, ERK inhibitor has attenuated its suppressive effect on HCT-116 cells but not much in HT-29 cells, that implies that K-Ras^{G13D} mutation works *via* the ERK pathway to promote major cancer stemness in HCT-116 cells.

PI3K/Akt/mTOR pathway inhibition equally suppresses spheroid formation in both cell lines

Another axis under K-Ras regulation is PI3K/Akt/mTOR pathway. To investigate if this pathway was also involved in K-Ras^{G13D} regulation, we used a dual inhibitor of this pathway BEZ235 that targets both PI3K and mTOR (Chen et al., 2014). We treated HCT-116 and HT-29 cells with BEZ235 at different doses and measured cell viability using the MTT assay. The results showed that both cells exhibited a dose-dependent decrease of cell viability and there was no difference between the two cell lines at the doses ranged from 50 to 400 nM (Figure 6A). We also measured their cell viability after S7333 treatment, the results showed that both cells exhibited a

similar dose-dependent decrease of cell viability with HT-29 cells being slightly more sensitive than HCT-116 to the treatment (Figure 6B). However, there was no significant difference between the two cell lines. In addition, BEZ235 treatment significantly suppressed the sphere formation in both cell lines no matter they were treated with S7333 or not (Figures 6C,D). These data suggest that BEZ235 is effective at suppressing PI3K/Akt pathway in colon cancer cells with or without K-Ras^{G13D} mutation. This implicates that, unlike the ERK pathway, PI3K/Akt pathway is independent of the regulation of K-Ras^{G13D} mutation.

To further explore if the increased stemness in colon cancer will relate to tumor recurrence and metastasis, we employed the public database to analyze the correlation between CD133 and Lgr5 and other relevant gene expressions. Interestingly, we found that both stem genes were associated with gene expressions of some pro-inflammatory cytokines like IL-17, IL-22, and IL-23 (Figures 7A,B). These cytokines have been confirmed for the roles in tumor development “inflammation and tumor transformation”, and they mostly play a promotive role in tumor initiation and progression (Grivennikov et al., 2012). This analysis indicates that cancer stemness may involve in

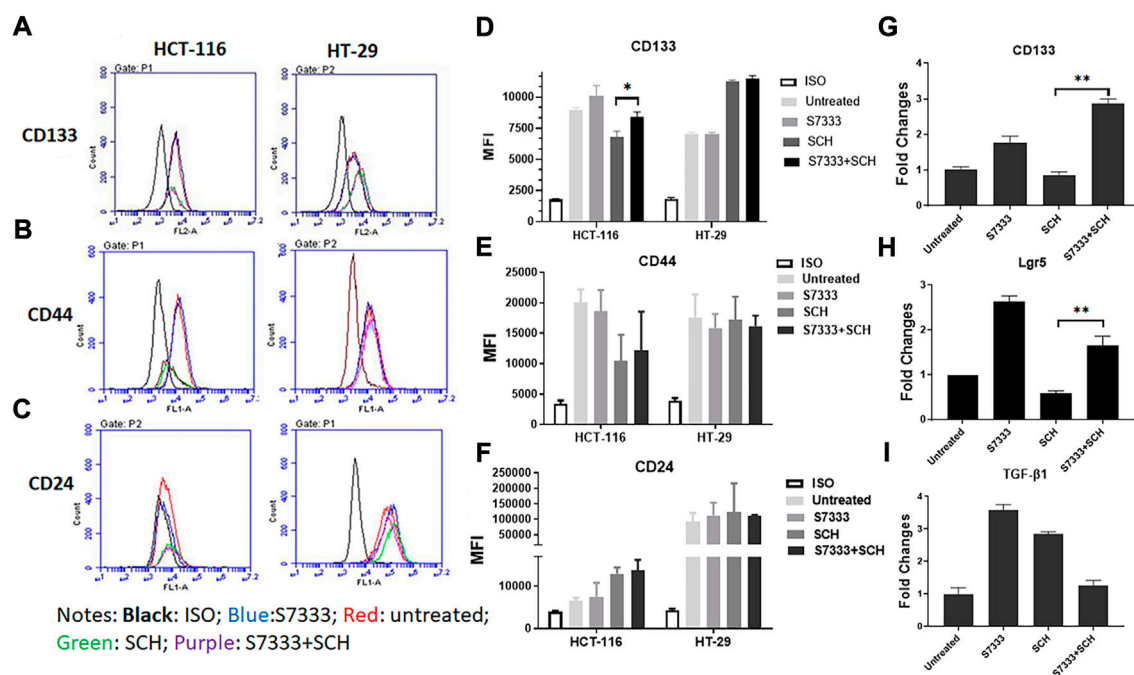


FIGURE 5

Blocking K-Ras mutation reduced the suppressive effect of SCH772984 treatment on cancer stemness markers in HCT-116 cells. The flow cytometry analysis of the expressions of surface stem markers CD133 (A), CD44 (B), and CD24 (C) in HCT-116 and HT-29 spheroids following the SCH772984 treatment after the K-Ras^{G13D} mutation has been blocked. CD133 and CD44 expressions are increased after the combination treatment whereas the expression of CD133, CD44, and CD24 did not increase after the same treatment in HT-29 spheroids (D–F). Real-time qPCR results show the stem gene CD133 (G), Lgr5 (H), and TGF- β 1 (I) expressions for HCT-116 cells. *: $p < 0.05$; **: $p < 0.01$.

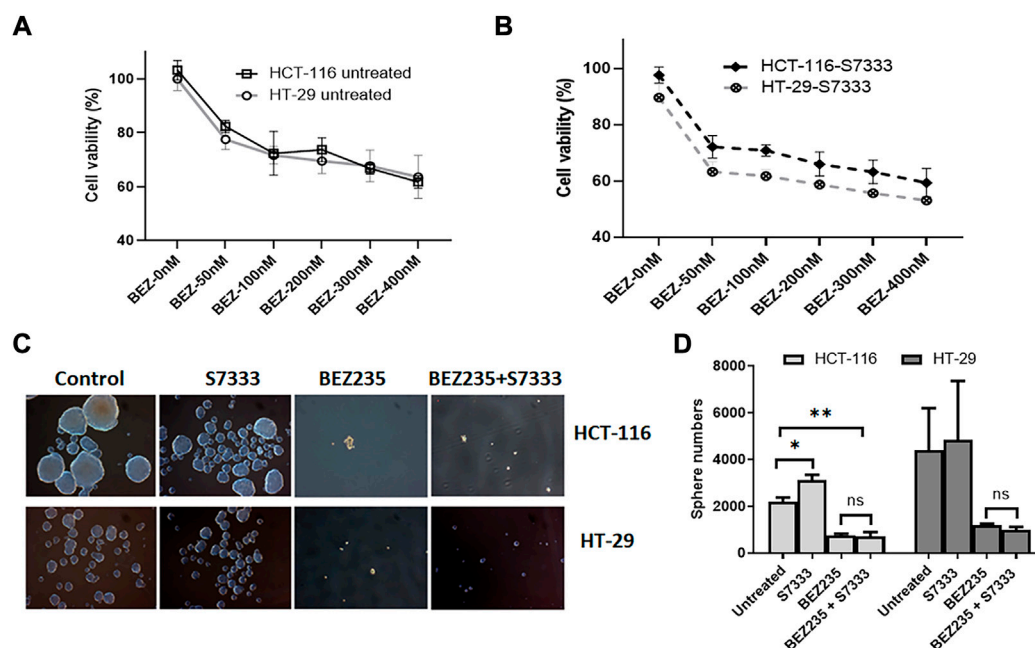
the regulation of inflammation potential that helps CSCs to start tumor initiation and “inflammation and tumor transformation”.

We then analyzed the expression of K-Ras with possible signaling pathways, it was found that it positively correlated with RAF1, PIK3CA, PIK3C3, AKT3, and MAPK1, and negatively correlated with AKT1, AKT2, and IL-17RC (Figure 7C). These pathways are mostly related to cell survival and inflammation (Zhao et al., 2021). We also analyzed K-Ras mRNA expression in normal and cancer samples of colon cancer patients (Figure 7D) and found that K-Ras mRNA expression in cancer tissues was significantly lower than in normal tissues, suggesting that K-Ras itself (without mutation) may be not a promotive factor for inflammation. However, when it mutates (at least G13 mutation) it will regulate cancer stemness. If the mutation has being suppressed, it will increase the stemness like CD133 and Lgr5 levels and subsequently promote inflammation potential. To further prove this, we analyzed K-Ras and its relationship with cancer stemness by conducting the gene set enrichment analysis (GSEA) from the publicly available GEO database (for colon cancer). The result showed a positive correlation ($p < 0.05$) between K-Ras expression and stemness-related gene signatures (Figure 7E). This analysis

supports a possible link between K-Ras expression and cancer stemness.

Discussion

K-Ras, a GTPase, has a high frequency (~30%) of mutants occurred in all human cancers, and the association with the cancer aggressiveness and resistance to existing therapies. In colorectal cancer, around 40% of cancer cases harbor a K-Ras mutation that dictates the resistance to therapies and poor prognosis (Morkel et al., 2015; Blaj et al., 2017). Consequently, inhibitors targeting K-Ras mutations, especially the K-Ras G12C mutation, have been developed and proceeded to phase I/II clinical trials with promising results (Seton-Rogers, 2020). However, available information indicates that each K-Ras mutation (including codons 12 and 13) has a distinct gene/protein profile and is very different in signal pathway activations (Hammond et al., 2015), suggesting a deep understanding of the molecular mechanism of each mutation is essential for guiding more precise and effective treatments of K-Ras mutated colon cancer patients in clinic. To achieve this, in this study we attempted to understand the relation between K-Ras^{G13D} mutation and cancer stemness, as CSCs are majorly

**FIGURE 6**

BEZ235 can equally inhibit the cancer stemness in HCT-116 and HT-29 cells. Cell viability assay of MTT shows that both HCT-116 and HT-29 cells exhibit a similar dose-dependent decrease as BEZ235 dose increases (A). After S7333 treatment, they still exhibit the dose-dependent decrease of cell viability though HT-29 cells are slightly more sensitive than HCT-116 (B), but there are no statistical differences between these two cell lines at any doses. The sphere numbers were remarkably decreased after BEZ235 treatment with or without S7333 blocking the K-Ras^{G13D} mutation in both HCT-116 and HT-29 cells (C,D). *: $p < 0.05$; **: $p < 0.01$.

responsible for tumor initiation, development, drug-resistance, and metastasis. Our data indicate that suppressing K-Ras^{G13D} mutation in colon cancer cells with a pre-clinical G12C inhibitor S7333 can reduce the cell proliferation but promote their stemness including spheroid formation, stem marker CD133, K-Ras, and stem gene *Lgr5* expressions. In contrast, no such increases are seen in K-Ras wildtype cells after the same treatment, confirming that S7333 treatment in HCT-116 is not an off-target effect on K-Ras gene and that K-Ras^{G13D} mutation plays a role in increasing cancer cell proliferation and suppressing cancer stemness in colon cancer. These findings thus prove that K-Ras^{G13D} mutation can regulate cancer stemness and therefore contribute to tumorigenesis of colon cancer. Our database analysis reveals that compared to normal tissues, colon cancer samples express less K-Ras mRNA (Figure 7D), suggesting that mutation could be the mechanism that the K-Ras gene promotes colon cancer growth.

According to the manufacturer, S7333 is a K-Ras G12C selective inhibitor. However, in our study, we treated the cells with S7333 over 72 h at a dose of 4 μ M to ensure G13D mutation has been blocked. Our data have confirmed this though more detailed data on G13D mutation detection or employing HCT-116 wildtype control cells will provide further confirmations.

Specific point mutation usually links to certain signaling pathway alterations. Of the two major pathways positively related to K-Ras, we have shown that K-Ras^{G13D} mutation mainly associates with RAS/ERK rather than the PI3K/Akt pathway (Figure 8). As more and more inhibitors for K-Ras mutation proceed to pre-clinical studies or clinical trials, the importance of this study becomes more obvious and is necessary to consider in clinical practice. That is, the K-Ras targeted therapy (with inhibitors), though can inhibit the cancer cell growth, may promote cancer stemness thus maintain CSCs and inflammation potential that will lead to tumor recurrence and metastasis. In this case, according to our results, for K-Ras^{G13D} mutant colon cancer, PI3K/Akt/mTOR or RAS/ERK pathway inhibitor (BEZ235 or SCH772984) alone would be a better treatment option than S7333 alone. When combinational therapy is necessary, the combination of S7333 with BEZ235 may be a better choice than with SCH772984. However, these concepts need to be tested in clinical trials.

Unlike G12C, that is, the most frequently observed and studied K-Ras mutation in colon cancer, G13D mutation is much less studied and no specific inhibitor has been reported. We therefore used the S7333 inhibitor to investigate its effect on cancer stemness. Our data suggest

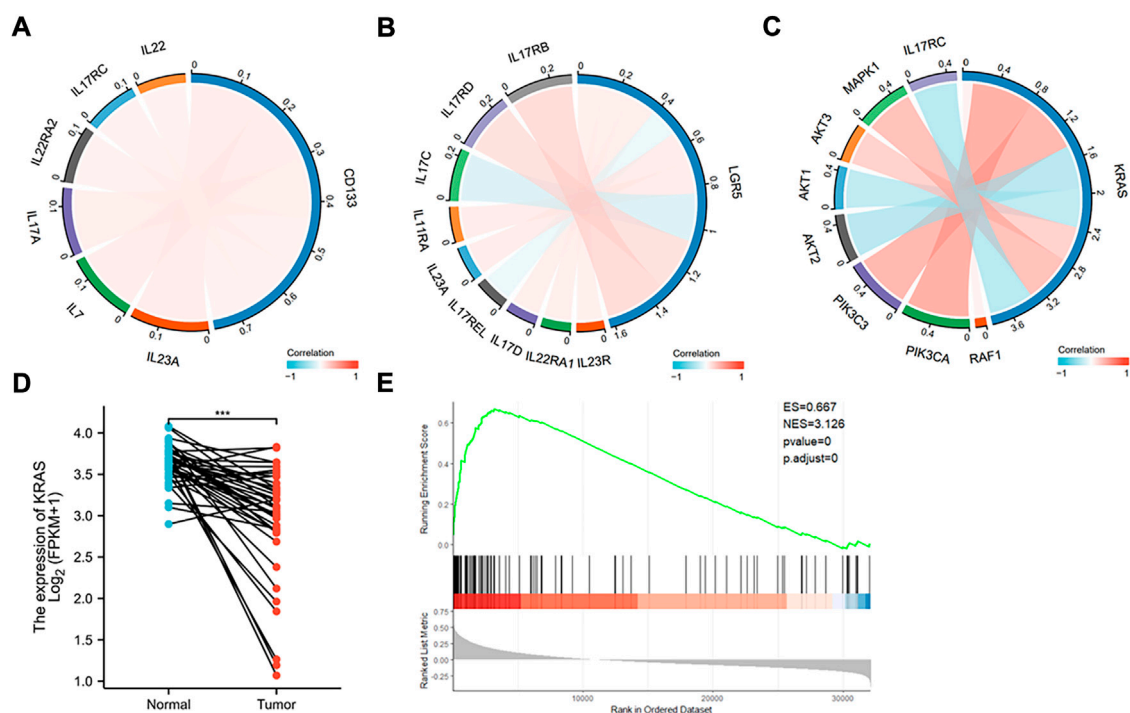


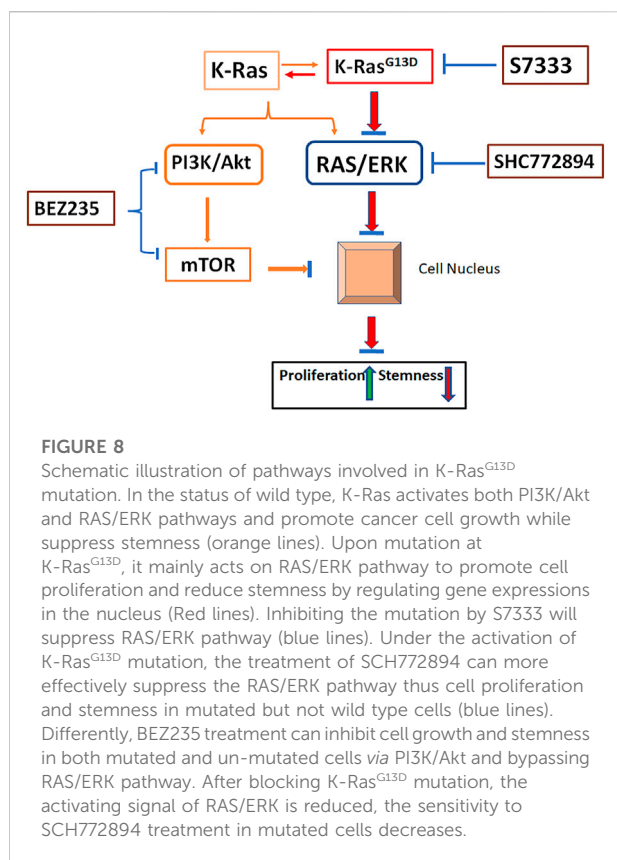
FIGURE 7

Database analysis of stem and K-Ras gene expressions in colon cancer. **(A)** Chordal graph of the correlation between the expression of CD133 and inflammatory genes. The expression of CD133 was found to positively correlate with IL-7, IL-17A, IL-17RC, IL-22RA2, IL-22, and IL-23A. **(B)** Chordal graph of the correlation between the expression of Lgr5 and inflammatory genes. The expression of LGR5 was found to positively correlate with IL-11RA, IL-17RB, IL-17RD, IL-17D, IL-22RA1, IL-23R, and IL-23A, and negatively correlate with IL-17C, and IL-17REL. **(C)** Chordal graph of the correlation between the expression of K-Ras and inflammatory genes. The expression of K-Ras was found to positively correlate with RAF1, PIK3CA, PIK3C3, AKT3, and MAPK1, and negatively correlate with AKT1, AKT2, and IL-17RC. **(D)** K-Ras gene expression based on the TCGA database analysis in normal and colon cancer tissues (***: $p < 0.001$). **(E)** GSEA analysis indicated significant correlations between K-Ras mRNA expression and stemness-related gene signatures. GSEA from the publicly available GEO database (Colon cancer) has shown positive correlation ($p < 0.05$) between K-Ras expression and stemness-related gene signatures.

that the effect on increasing cell proliferation and reducing cancer stemness was mainly *via* the RAS/ERK pathway. Although the role of RAS/ERK pathway in cell survival and proliferation has been well-described (Lavoie et al., 2020; Asl et al., 2021), there are not many studies describing its link with cancer stemness. Wang et al. (2010) reported that the upstream molecules in Akt and MAPK pathways were preferentially expressed in colon cancer CD133 (+) cells and the kinase activities of Akt and (ERK)1/2 were also significantly upregulated in CD133 (+) cells. The treatment of synovial sarcoma Fuji cells with a specific MEK/ERK inhibitor, U0126, markedly decreased CD133 expression, but there was no significant effect in colon cancer Caco-2 cells, suggesting cell type-specific regulation of CD133 expression. Instead, the side population (another hallmark of CSCs) was dramatically diminished in Caco-2 cells by U0126 (Tabu et al., 2010), which is similar to our results on the spheroid formation (Figure 3). In addition, Ras-mediated oncogenic

transformation in normal human astrocytes conferred the stem-like capability to form neurosphere-like colonies.

Neurosphere-like colonies with the increase of CD133 mRNA expression (Tabu et al., 2010). Therefore, the RAS/ERK pathway at least in part contributes to the maintenance and acquisition of stem-like hallmarks, although the extent of its contribution is varied in a cell type-specific manner. A study examined the inhibitory effect of tubulin inhibitor STK899704 on colon cancer cell migration and CSC stemness and showed that STK899704 downregulated the mRNA expression levels of the cell migration mediator focal adhesion kinase (FAK) and suppressed MAPK and ERK, which are downstream signaling molecules of FAK. Additionally, STK899704 inhibited stem gene expression and sphere formation in colon cancer stem cells (Jang et al., 2018), suggesting that ERK can involve in regulating stemness in colon cancer, which is consistent with and confirmed by our current study.



Above information suggests that RAS/ERK pathway can maintain or regulate cancer stemness in colon cancer, which is particularly true in K-Ras^{G13D} mutated colon cancer where the mutation more specifically activated on ERK. Therefore, we can see more suppressive effects on stemness (Figure 3) and pERK protein levels (Figure 4D) in HCT-116 than HT-29 cells. When the mutation was blocked by S7333, the treatment of ERK inhibitor was less effective in HCT-116 cells on their stemness (Figures 4, 5). Instead, PI3K/Akt inhibitor BEZ235 treatment was equally effective on both mutated and wildtype cell lines, reflecting the mutation mainly acts on RAS/ERK pathway. Not only in cell lines, K-Ras-ERK axis engagement in cancer stemness or stem cells is also reported in animal models. A study showed the transient expression of reprogramming factors in K-Ras mutant mice was sufficient to induce the robust and persistent activation of ERK signaling in acinar cells and rapid formation of pancreatic ductal adenocarcinoma. In contrast, the forced expression of acinar cell-related transcription factors inhibited the pancreatitis-induced activation of ERK signaling and development of precancerous lesions in K-Ras-mutated acinar cells (Shibata et al., 2018). Not only in epithelial cancers, in human hematopoietic malignancies, RAS mutations are frequently observed and related to cancer stemness. For example, when cultured on bone marrow stroma, K-Ras (G12 V)-transduced cord blood CD34 (+)

stem/progenitor cells displayed a strong proliferative advantage over control cells, which coincided with increased early cobblestone (CAFC) formation and induction of myelomonocytic differentiation. Both the ERK and p38 MAPK pathways, but not JNK, were activated by K-Ras (G12 V) and the proliferation and CAFC formation were mediated *via* ERK, while differentiation was predominantly mediated *via* p38 (Fatrai et al., 2011). Above data reveal that K-Ras and its mutations are widely involved in RAS/ERK pathway and cancer stemness.

As to K-Ras^{G13D} mutation, a study reported that the tumor suppressor NF1 was co-mutated in K-Ras G13-mutated cells. NF1 GTPase-activating protein was inactive against K-Ras G12 and Q61-mutated K-Ras but stimulated GTP hydrolysis when bound to K-Ras^{G13D}. K-Ras^{G13D} mutant cells also respond to EGFR inhibitors in a neurofibromin-dependent manner. Crystallographic analysis of wild-type and G13D K-Ras complexed with neurofibromin provides the structural basis for neurofibromin-mediated GTP hydrolysis (Rabara et al., 2019). However, this study did not report on whether this mutation is related to cancer stemness, our data thus provide the first evidence of the link. Though the suppression of K-Ras mutation can promote cancer stemness, the direct transfection of K-Ras mutation itself did not promote cancer stemness in colon cancer development. A study showed that K-Ras mutation (G12D) could promote serrated and hyperplastic morphologic features in colon epithelium, but it was not able to initiate adenoma development, perhaps in part because activated K-Ras signaling did not increase the number of presumptive stem cells in affected crypts (Feng et al., 2011). This study suggests that K-Ras mutation may initiate epithelial cell transformation through altering signaling pathways or working with other mutations in the cells. According to our results, we believe that there is another reason for this, that is, the transfected K-Ras mutations mainly promote cell proliferation and suppress major cancer stemness. Nevertheless, in our study, we found that the suppression of G13D mutation promoted major stem markers like CD133, Lgr5, and TGF- β but not others like CD44 and CD24, which were reported as common and important biomarkers for colon cancer by us (Chen et al., 2015) and others (Lee et al., 2015; Ribeiro et al., 2016). This suggests that regulation of colon cancer stemness is more complex and RAS/ERK pathway only involves major stemness regulation. Another possible reason for CD24 did not show meaningful results is that the antibody used in the current study did not stain higher cell populations in HCT-116 cells (Tables 1, 2), whereas our previous study showed a positive population about 17% (Chen et al., 2015). The reason of inconsistency is not clear but could relate to the change of antibody batches. Additionally, CD44 expression increased in HT-29 cells after S7333 treatment in comparison with the decrease in HCT-116, which could be an interesting point to follow.

Despite of CD24 and CD44, CD133 is the molecule playing an initial role in colon cancer cluster formation (Grunt et al., 2015), and is also an essential and more common stem marker of many organs and cancers (Grosse-Gehling et al., 2013; Jang et al., 2017). In this study, we showed that both mRNA and protein levels of CD133 increased after suppression of K-Ras^{G13D} mutation (Figure 2), suggesting this is an important CSC marker related to spheroid formation. Lgr5 is another stem gene for intestine epithelial cells and is often highly expressed in colon cancer patients. Lgr5 expression in the epithelium and stroma was also closely associated with tumor stage, by integrating functional experiments with Lgr5-sorted cell RNA sequencing data from adenoma and normal organoids, the correlations between Lgr5 and colorectal cancer-specific genes, indicating Lgr5 is an essential marker for studying stem cells in human tissue homeostasis and carcinogenesis (Dame et al., 2018). TGF- β is considered as an EMT and self-renewal marker (Gu et al., 2011). Though it has not reached statistical significance in our study, we showed that this growth factor increased after suppression of K-Ras^{G13D} mutation (Figure 2), and it responded to ERK inhibitor and combinational treatments, indicating the self-renewal ability of colon cancer cells was regulated by the mutation. TGF- β pathway is also involved in tumorigenesis of colon cancer, as genetic inactivation of TGF- β type 1 receptor (Tgfr1/Alk5) enhanced the ability of K-Ras (G12D/+) mutation to drive dedifferentiation and markedly accelerated tumorigenesis, which was associated with a marked activation of MAPK signaling (Cammareri et al., 2017). This suggests that more detailed study is needed for understanding its role in K-Ras^{G13D} settings. Collectively, above data suggest that though some colon cancer stem markers are not modulated by the inhibitor treatments, the major stemness profile aligns well with colon cancer stemness property, therefore supporting the conclusion that suppression of K-Ras^{G13D} mutation promotes major cancer stemness in colon cancer.

Conclusion

In this study, we used an inhibitor to suppress K-Ras^{G13D} mutation in colon cancer HCT-116 cells and found that the inhibition reduced the cell proliferation in terms of cell numbers and gene expression of Ki-67. However, this also induced an increase of stemness and potency of inflammation in treated cells. In contrast, these changes were not seen in wildtype HT-29 cells, suggesting these alterations only relate to K-Ras^{G13D}. Our further investigations indicated that these changes were through ERK but not PI3K/Akt pathway. These data imply that caution needs to be taken when using K-Ras mutation targeted therapy as it may promote cancer stemness and inflammation thus lead to tumor recurrence and metastasis.

Data availability statement

The original contributions presented in the study are included in the article/supplementary material, further inquiries can be directed to the corresponding authors.

Author contributions

Conceptualization, WG; Formal analysis, YQ and YT; Investigation, YQ, HZ, XZ, and JK; Methodology, HZ; Supervision, MM, FL, ZX, YW, and WG; Writing—original draft, YT; Writing—review and editing, YD and WG.

Funding

The study was partially funded by Australia Research Council discovery project (ID: DP120100240) to WG.

Acknowledgments

The authors would like to acknowledge the technical support of Jennifer Scorning (The University of Queensland) and Chinese Scholarship Council fellowships to HZ and YQ.

Conflict of interest

Authors YD, YW, and WG are employed by Gillion Biotherapeutics Ltd.

The remaining authors declare that the research was conducted in the absence of any commercial or financial relationships that could be construed as a potential conflict of interest.

Publisher's note

All claims expressed in this article are solely those of the authors and do not necessarily represent those of their affiliated organizations, or those of the publisher, the editors and the reviewers. Any product that may be evaluated in this article, or claim that may be made by its manufacturer, is not guaranteed or endorsed by the publisher.

Supplementary material

The Supplementary Material for this article can be found online at: <https://www.frontiersin.org/articles/10.3389/fphar.2022.996053/full#supplementary-material>

References

- Adachi, Y., Ito, K., Hayashi, Y., Kimura, R., Tan, T. Z., Yamaguchi, R., et al. (2020). Epithelial-to-Mesenchymal transition is a cause of both intrinsic and acquired resistance to KRAS G12C inhibitor in KRAS G12C-mutant non-small cell lung cancer. *Clin. Cancer Res.* 26 (22), 5962–5973. doi:10.1158/1078-0432.CCR-20-2077
- Addeo, A., Banna, G. L., and Friedlaender, A. (2021). KRAS G12C mutations in NSCLC: From target to resistance. *Cancers* 13 (11), 2541. doi:10.3390/cancers13112541
- Ahmed, D., Eide, P. W., Eilertsen, I. A., Danielsen, S. A., Eknæs, M., Hektoen, M., et al. (2013). Epigenetic and genetic features of 24 colon cancer cell lines. *Oncogenesis* 2 (9), e71. doi:10.1038/oncsis.2013.35
- Andreyev, H. J., Norman, A. R., Cunningham, D., Oates, J. R., and Clarke, P. A. (1998). Kirsten ras mutations in patients with colorectal cancer: The multicenter "RASCAL" study. *J. Natl. Cancer Inst.* 90 (9), 675–684. doi:10.1093/jnci/90.9.675
- Asl, E. R., Amini, M., Najafi, S., Mansoori, B., Mokhtarzadeh, A., Mohammadi, A., et al. (2021). Interplay between MAPK/ERK signaling pathway and MicroRNAs: A crucial mechanism regulating cancer cell metabolism and tumor progression. *Life Sci.* 278, 119499. doi:10.1016/j.lfs.2021.119499
- Blaj, C., Schmidt, E. M., Lamprecht, S., Hermeking, H., Jung, A., Kirchner, T., et al. (2017). Oncogenic effects of high MAPK activity in colorectal cancer mark progenitor cells and persist irrespective of RAS mutations. *Cancer Res.* 77 (7), 1763–1774. doi:10.1158/0008-5472.CAN-16-2821
- Cammareri, P., Vincent, D. F., Hodder, M. C., Ridgway, R. A., Murgia, C., Nobis, M., et al. (2017). TGF β pathway limits dedifferentiation following WNT and MAPK pathway activation to suppress intestinal tumorigenesis. *Cell Death Differ.* 24 (10), 1681–1693. doi:10.1038/cdd.2017.92
- Cannataro, V. L., Gaffney, S. G., Stender, C., Zhao, Z. M., Philips, M., Greenstein, A. E., et al. (2018). Heterogeneity and mutation in KRAS and associated oncogenes: Evaluating the potential for the evolution of resistance to targeting of KRAS G12C. *Oncogene* 37 (18), 2444–2455. doi:10.1038/s41388-017-0105-z
- Chen, J., Apizi, A., Wang, L., Wu, G., Zhu, Z., Yao, H., et al. (2021). TCGA database analysis of the tumor mutation burden and its clinical significance in colon cancer. *J. Gastrointest. Oncol.* 12 (5), 2244–2259. doi:10.21037/jgo-21-661
- Chen, J., Shao, R., Li, F., Monteiro, M., Liu, J. P., Xu, Z. P., et al. (2015). PI3K/Akt/mTOR pathway dual inhibitor BEZ235 suppresses the stemness of colon cancer stem cells. *Clin. Exp. Pharmacol. Physiol.* 42, 1317–1326. doi:10.1111/1440-1681.12493
- Chen, J., Shao, R., Li, L., Xu, Z. P., and Gu, W. (2014). Effective inhibition of colon cancer cell growth with MgAl-layered double hydroxide (LDH) loaded 5-FU and PI3K/mTOR dual inhibitor BEZ-235 through apoptotic pathways. *Int. J. Nanomedicine* 9, 3403–3411. doi:10.2147/IJN.S61633
- Christensen, J. G., Olson, P., Briere, T., Wiel, C., and Bergo, M. O. (2020). Targeting Krasg12c-mutant cancer with a mutation-specific inhibitor. *J. Intern. Med.* 288 (2), 183–191. doi:10.1111/joim.13057
- Cox, A. D., Fesik, S. W., Kimmelman, A. C., Luo, J., and Der, C. J. (2014). Drugging the undruggable RAS: Mission possible? *Nat. Rev. Drug Discov.* 13 (11), 828–851. doi:10.1038/nrd4389
- Dame, M. K., Attili, D., McClintock, S. D., Dedhia, P. H., Ouilllette, P., Hardt, O., et al. (2018). Identification, isolation and characterization of human LGR5-positive colon adenoma cells. *Development* 145 (6), dev153049. doi:10.1242/dev.153049
- Davies, J. M., and Goldberg, R. M. (2011). Treatment of metastatic colorectal cancer. *Semin. Oncol.* 38 (4), 552–560. doi:10.1053/j.seminoncol.2011.05.009
- Der, C. J., Krontiris, T. G., and Cooper, G. M. (1982). Transforming genes of human bladder and lung carcinoma cell lines are homologous to the ras genes of Harvey and Kirsten sarcoma viruses. *Proc. Natl. Acad. Sci. U. S. A.* 79 (11), 3637–3640. doi:10.1073/pnas.79.11.3637
- Downward, J. (2003). Targeting RAS signalling pathways in cancer therapy. *Nat. Rev. Cancer* 3 (1), 11–22. doi:10.1038/nrc969
- Fatrai, S., van Gosliga, D., Han, L., Daenen, S. M. G. J., Vellenga, E., and Schuringa, J. J. (2011). KRAS(G12V) enhances proliferation and initiates myelomonocytic differentiation in human stem/progenitor cells via intrinsic and extrinsic pathways. *J. Biol. Chem.* 286 (8), 6061–6070. doi:10.1074/jbc.M110.201848
- Feng, Y., Bommer, G. T., Zhao, J., Green, M., Sands, E., Zhai, Y., et al. (2011). Mutant KRAS promotes hyperplasia and alters differentiation in the colon epithelium but does not expand the presumptive stem cell pool. *Gastroenterology* 141 (3), 1003–1013. doi:10.1053/j.gastro.2011.05.007
- Grivennikov, S. I., Wang, K., Mucida, D., Stewart, C. A., Schnabl, B., Jauch, D., et al. (2012). Adenoma-linked barrier defects and microbial products drive IL-23/IL-17-mediated tumour growth. *Nature* 491 (7423), 254–258. doi:10.1038/nature11465
- Grosse-Gehling, P., Fargeas, C. A., Dittfeld, C., Garbe, Y., Alison, M. R., Corbeil, D., et al. (2013). CD133 as a biomarker for putative cancer stem cells in solid tumours: Limitations, problems and challenges. *J. Pathol.* 229 (3), 355–378. doi:10.1002/path.4086
- Grunt, T. W., Hebar, A., Laffer, S., Wagner, R., Peter, B., Herrmann, H., et al. (2015). Prominin-1 (CD133, AC133) and dipeptidyl-peptidase IV (CD26) are indicators of infinitive growth in colon cancer cells. *Am. J. Cancer Res.* 5 (2), 560–574.
- Gu, W., Prasad, I., Yu, M., Zhang, F., Ling, P., Xiao, Y., et al. (2015). Gamma tocotrienol targets tyrosine phosphatase SHP2 in mammospheres resulting in cell death through RAS/ERK pathway. *BMC Cancer* 15 (1), 609. doi:10.1186/s12885-015-1614-1
- Gu, W., Yeo, E., McMillan, N., and Yu, C. (2011). Silencing oncogene expression in cervical cancer stem-like cells inhibits their cell growth and self-renewal ability. *Cancer Gene Ther.* 18 (12), 897–905. doi:10.1038/cgt.2011.58
- Hammond, D. E., Magee, C. J., Rusilowicz, E. V., Wickenden, J. A., Clague, M. J., and Prior, I. A. (2015). Differential reprogramming of isogenic colorectal cancer cells by distinct activating KRAS mutations. *J. Proteome Res.* 14 (3), 1535–1546. doi:10.1021/pr501191a
- Jang, H. J., Bak, Y., Pham, T. H., Kwon, S. B., Kim, B. Y., Hong, J., et al. (2018). STK899704 inhibits stemness of cancer stem cells and migration via the FAK-MEK-ERK pathway in HT29 cells. *BMB Rep.* 51 (11), 596–601. doi:10.5483/BMBRep.2018.51.11.180
- Jang, J.-W., Song, Y., Kim, S. H., Kim, J., and Seo, H. R. (2017). Potential mechanisms of CD133 in cancer stem cells. *Life Sci.* 184, 25–29. doi:10.1016/j.lfs.2017.07.008
- Lavoie, H., Gagnon, J., and Therrien, M. (2020). ERK signalling: A master regulator of cell behaviour, life and fate. *Nat. Rev. Mol. Cell Biol.* 21 (10), 607–632. doi:10.1038/s41580-020-0255-7
- Lee, S. H., Hong, J. H., Park, H. K., Park, J. S., Kim, B. K., Lee, J. Y., et al. (2015). Colorectal cancer-derived tumor spheroids retain the characteristics of original tumors. *Cancer Lett.* 367 (1), 34–42. doi:10.1016/j.canlet.2015.06.024
- Lee, S. H., Lee, J. W., Soung, Y. H., Kim, H. S., Park, W. S., Kim, S. Y., et al. (2003). BRAF and KRAS mutations in stomach cancer. *Oncogene* 22 (44), 6942–6945. doi:10.1038/sj.onc.1206749
- Lichtenstern, C. R., Ngu, R. K., Shalpour, S., and Karin, M. (2020). Immunotherapy, inflammation and colorectal cancer. *Cells* 9 (3), 618. doi:10.3390/cells9030618
- Moon, B. S., Jeong, W. J., Park, J., Kim, T. I., Min, D. S., and Choi, K. Y. (2014). Role of oncogenic K-Ras in cancer stem cell activation by aberrant Wnt/ β -catenin signaling. *J. Natl. Cancer Inst.* 106 (2), djt373. doi:10.1093/jnci/djt373
- Morkel, M., Riemer, P., Blaker, H., and Sers, C. (2015). Similar but different: Distinct roles for KRAS and BRAF oncogenes in colorectal cancer development and therapy resistance. *Oncotarget* 6 (25), 20785–20800. doi:10.18632/oncotarget.4750
- Rabara, D., Tran, T. H., Dharmiah, S., Stephens, R. M., McCormick, F., Simanshu, D. K., et al. (2019). KRAS G13D sensitivity to neurofibromin-mediated GTP hydrolysis. *Proc. Natl. Acad. Sci. U. S. A.* 116 (44), 22122–22131. doi:10.1073/pnas.1908353116
- Reck, M., Carbone, D. P., Garassino, M., and Barlesi, F. (2021). Targeting KRAS in non-small-cell lung cancer: Recent progress and new approaches. *Ann. Oncol.* 32 (9), 1101–1110. doi:10.1016/j.annonc.2021.06.001
- Ribeiro, K. B., da Silva Zanetti, J., Ribeiro-Silva, A., Rapatoni, L., de Oliveira, H. F., da Cunha Tirapelli, D. P., et al. (2016). KRAS mutation associated with CD44/CD166 immunorepression as predictors of worse outcome in metastatic colon cancer. *Cancer Biomark.* 16 (4), 513–521. doi:10.3233/CBM-160592
- Selvam, C., Prabu, S. L., Jordan, B. C., Purushothaman, Y., Umamaheswari, A., Hosseini Zare, M. S., et al. (2019). Molecular mechanisms of curcumin and its analogs in colon cancer prevention and treatment. *Life Sci.* 239, 117032. doi:10.1016/j.lfs.2019.117032

- Serna-Blasco, R., Sanchez-Herrero, E., Sanz-Moreno, S., Rodriguez-Festa, A., Garcia-Veros, E., Casarrubios, M., et al. (2021). KRAS p.G12C mutation occurs in 1% of EGFR-mutated advanced non-small-cell lung cancer patients progressing on a first-line treatment with a tyrosine kinase inhibitor. *ESMO Open* 6 (5), 100279. doi:10.1016/j.esmoop.2021.100279
- Seton-Rogers, S. (2020). KRAS-G12C in the crosshairs. *Nat. Rev. Cancer* 20 (1), 3. doi:10.1038/s41568-019-0228-3
- Shibata, H., Komura, S., Yamada, Y., Sankoda, N., Tanaka, A., Ukai, T., et al. (2018). *In vivo* reprogramming drives Kras-induced cancer development. *Nat. Commun.* 9 (1), 2081. doi:10.1038/s41467-018-04449-5
- Siegfried, J. M., Gillespie, A. T., MeRa, R., Casey, T. J., Keohavong, P., Testa, J. R., et al. (1997). Prognostic value of specific KRAS mutations in lung adenocarcinomas. *Cancer Epidemiol. Biomarkers Prev.* 6 (10), 841–847.
- Tabu, K., Kimura, T., Sasai, K., Wang, L., Bizen, N., Nishihara, H., et al. (2010). Analysis of an alternative human CD133 promoter reveals the implication of Ras/ERK pathway in tumor stem-like hallmarks. *Mol. Cancer* 9, 39. doi:10.1186/1476-4598-9-39
- Thein, K. Z., Biter, A. B., and Hong, D. S. (2021). Therapeutics targeting mutant KRAS. *Annu. Rev. Med.* 72, 349–364. doi:10.1146/annurev-med-080819-033145
- Visani, M., de Biase, D., Baccarini, P., Fabbri, C., Polifemo, A. M., Zanini, N., et al. (2013). Multiple KRAS mutations in pancreatic adenocarcinoma: Molecular features of neoplastic clones indicate the selection of divergent populations of tumor cells. *Int. J. Surg. Pathol.* 21 (6), 546–552. doi:10.1177/1066896912475073
- Wang, Y. K., Zhu, Y. L., Qiu, F. M., Zhang, T., Chen, Z. G., Zheng, S., et al. (2010). Activation of Akt and MAPK pathways enhances the tumorigenicity of CD133+ primary colon cancer cells. *Carcinogenesis* 31 (8), 1376–1380. doi:10.1093/carcin/bgq120
- Wu, Y., Chen, M., Wu, P., Chen, C., Xu, Z. P., and Gu, W. (2017). Increased PD-L1 expression in breast and colon cancer stem cells. *Clin. Exp. Pharmacol. Physiol.* 44 (5), 602–604. doi:10.1111/1440-1681.12732
- Xiao, J., Li, W., Huang, Y., Huang, M., Li, S., Zhai, X., et al. (2021). A next-generation sequencing-based strategy combining microsatellite instability and tumor mutation burden for comprehensive molecular diagnosis of advanced colorectal cancer. *BMC Cancer* 21 (1), 282. doi:10.1186/s12885-021-07942-1
- Zhao, H., Wu, L., Yan, G., Chen, Y., Zhou, M., Wu, Y., et al. (2021). Inflammation and tumor progression: Signaling pathways and targeted intervention. *Signal Transduct. Target. Ther.* 6 (1), 263. doi:10.1038/s41392-021-00658-5
- Zou, H., Li, L., Garcia Carcedo, I., Xu, Z. P., Monteiro, M., and Gu, W. (2016). Synergistic inhibition of colon cancer cell growth with nanoemulsion-loaded paclitaxel and PI3K/mTOR dual inhibitor BEZ235 through apoptosis. *Int. J. Nanomedicine* 11, 1947–1958. doi:10.2147/IJN.S100744



OPEN ACCESS

EDITED BY

Xiaojuan Chao,
University of Kansas Medical Center,
United States

REVIEWED BY

Wei Pan,
Xuzhou Medical University, China
Xiaona Cui,
Peking University Third Hospital, China

*CORRESPONDENCE

Jiawen Huang,
huangjw0630@163.com
Yuanlin Ding,
gdmusbd@gdmu.edu.cn
Dong Zhang,
zhangdongvonhbxg@163.com
Naihua Liu,
liunaihua@gzucm.edu.cn

*These authors have contributed equally
to this work

SPECIALTY SECTION

This article was submitted to
Inflammation Pharmacology,
a section of the journal
Frontiers in Pharmacology

RECEIVED 22 July 2022

ACCEPTED 26 September 2022

PUBLISHED 28 October 2022

CITATION

Tang K, Kong D, Peng Y, Guo J, Zhong Y,
Yu H, Mai Z, Chen Y, Chen Y, Cui T,
Duan S, Li T, Liu N, Zhang D, Ding Y and
Huang J (2022), Ginsenoside Rc
attenuates DSS-induced ulcerative
colitis, intestinal inflammatory, and
barrier function by activating the
farnesoid X receptor.
Front. Pharmacol. 13:1000444.
doi: 10.3389/fphar.2022.1000444

COPYRIGHT

© 2022 Tang, Kong, Peng, Guo, Zhong,
Yu, Mai, Chen, Chen, Cui, Duan, Li, Liu,
Zhang, Ding and Huang. This is an open-
access article distributed under the
terms of the [Creative Commons
Attribution License \(CC BY\)](https://creativecommons.org/licenses/by/4.0/). The use,
distribution or reproduction in other
forums is permitted, provided the
original author(s) and the copyright
owner(s) are credited and that the
original publication in this journal is
cited, in accordance with accepted
academic practice. No use, distribution
or reproduction is permitted which does
not comply with these terms.

Ginsenoside Rc attenuates DSS-induced ulcerative colitis, intestinal inflammatory, and barrier function by activating the farnesoid X receptor

Kaijia Tang^{1†}, Danli Kong^{2†}, Yuan Peng^{3†}, Jingyi Guo^{1†},
Yadi Zhong¹, Haibing Yu², Zhenhua Mai⁴, Yanling Chen⁵,
Yingjian Chen¹, Tianqi Cui¹, Siwei Duan¹, Tianyao Li¹,
Naihua Liu^{1*}, Dong Zhang^{6*}, Yuanlin Ding^{2*} and
Jiawen Huang^{1*}

¹Science and Technology Innovation Center, Guangzhou University of Chinese Medicine, Guangzhou, China, ²Department of Epidemiology and Medical Statistics, School of Public Health, Guangdong Medical University, Dongguan, China, ³Department of Pharmacy, Affiliated Hospital of North Sichuan Medical College, Nanchong, China, ⁴Department of Critical Care Medicine, Affiliated Hospital of Guangdong Medical University, Zhanjiang, China, ⁵The First Clinical Medical College of Guangzhou University of Chinese Medicine, Guangzhou, China, ⁶The Fourth Clinical Medical College of Guangzhou University of Chinese Medicine, Shenzhen, China

Objectives: Farnesoid X receptor (FXR) activation is involved in ameliorating inflammatory bowel disease (IBD), such as ulcerative colitis (UC), and inflammatory regulation may be involved in its mechanism. Ginsenoside Rc (Rc) is a major component of *Panax ginseng*, and it plays an excellent role in the anti-inflammatory processes. Our aim is to explore the alleviative effect of Rc on dextran sulfate sodium (DSS)-induced inflammation and deficiencies in barrier function based on FXR signaling.

Materials and Methods: *In vitro*, we treated human intestinal epithelial cell lines (LS174T) with LPS to explore the anti-inflammatory effect of Rc supplementation. *In vivo*, a DSS-induced IBD mice model was established, and the changes in inflammatory and barrier function in colons after Rc treatment were measured using the disease activity index (DAI), hematoxylin and eosin (H&E) staining, immunofluorescence, ELISA, and qPCR. Molecular docking analysis, luciferase reporter gene assay, and qPCR were then used to analyze the binding targets of Rc. DSS-induced FXR-knockout (FXR^{-/-}) mice were used for further validation.

Results: Rc significantly recovered the abnormal levels of inflammation indexes (*TNF-α*, *IL-6*, *IL-1β*, and *NF-κB*) induced by LPS in LS174T. DSS-induced C57BL/6 mice exhibited a significantly decreased body weight and elevated DAI, as well as a decrease in colon weight and length. Increased inflammatory markers (*TNF-α*, *IL-6*, *IL-1β*, *ICAM1*, *NF-κB*, F4/80, and CD11b displayed an increased expression) and damaged barrier function (*Claudin-1*, *occludin*, and *ZO-1* displayed a decreased expression) were observed in DSS-induced C57BL/6 mice. Nevertheless, supplementation with Rc mitigated the increased

inflammatory and damaged barrier function associated with DSS. Further evaluation revealed an activation of FXR signaling in Rc-treated LS174T, with *FXR*, *BSEP*, and *SHP* found to be upregulated. Furthermore, molecular docking indicated that there is a clear interaction between Rc and FXR, while Rc activated transcriptional expression of FXR in luciferase reporter gene assay. However, these reversal abilities of Rc were not observed in DSS-induced *FXR*^{-/-} mice.

Conclusion: Our findings suggest that Rc may ameliorate inflammation and barrier function in the intestine, which in turn leads to the attenuation of DSS-induced UC, in which Rc may potentially activate FXR signaling to protect the intestines from DSS-induced injury.

KEYWORDS

ulcerative colitis, inflammatory bowel disease, inflammation, ginsenoside Rc, intestinal barriers

Introduction

Ulcerative colitis (UC) is a type of inflammatory bowel disease (IBD) that is often characterized by diarrhea, rectal bleeding, abdominal pain, and so on. It is also described as a chronic idiopathic inflammatory disease (Sands, 2004). In the past few decades, high morbidity and disability caused by IBD have resulted in a high cost of treatment and care management, which requires effective prevention strategies (Higgins et al., 2003; Sterne et al., 2011). Many factors can increase the risk of IBD, such as smoking, urban living, antibiotic exposure, and so on (Piovani et al., 2019). Although the exact pathogenesis of IBD is unknown, the current view holds that it is caused by disrupted homeostasis of the mucosal immune system and impaired intestinal epithelial barriers (Kiesler et al., 2015). Clinically, aminosalicylates, glucocorticoids, and immunosuppressants are commonly used in IBD treatment. However, these drugs can have significant disadvantages, such as unsatisfactory efficacy and many adverse reactions (Lim et al., 2016). Thus, immunomodulators have received increasing attention as potential therapeutics for the treatment of IBD.

Cytokines and inflammatory mediators are the products of IBD inflammatory reactions, which often lead to damage to intestinal epithelial cells, breaking of cell junctions, and finally result in dyshomeostasis of the intestinal flora (Bischoff et al., 2014; Drury et al., 2021). The Farnesoid X receptor (FXR), which is known as a nuclear bile acid receptor, can not only modulate the metabolic balance of bile acid, lipids, and glucose (Sun et al., 2021) but may also be involved in regulating the inflammatory response (Anderson and Gayer, 2021). FXR activation controls the transcriptional induction of the expression of small heterodimer protein (SHP) (Wang et al., 2002), as well as bile salt export pump (BSEP) proteins (Ananthanarayanan et al., 2001). The recruitment of NF- κ B can be directly prevented by SHP, which represses several cytokines, including IL-1 β and TNF- α (Yang et al., 2016). Both of these can be considered to be FXR targets, and their expression levels have been inversely

correlated with inflammation levels (Huang et al., 2018; Cariello et al., 2021). Interestingly, although FXR can modulate inflammatory signaling, acute inflammatory cytokines can also influence FXR expression. For instance, TNF α was able to decrease binding activity with an FXR response element in DNA and resulted in FXR downregulation (Kim et al., 2003). Recently, an increasing number of studies have focused on pharmacologic FXR agonists and FXR has received enthusiastic attention as a developing therapeutic target (Massafra et al., 2018; Badman et al., 2020).

Progressive increases in intestinal permeability have been suggested to be involved in the pathogenesis of IBD (Weber and Turner, 2007; Xavier and Podolsky, 2007). Tight junctions (TJs) are the most important components of intestinal barriers and can be affected by many factors (e.g., immune cells). For example, TJs can be interrupted by TNF α , which downregulates claudin and occludin. This results in increased intestinal permeability (Al-Sadi et al., 2013). It is known that FXR activation can not only inhibit pro-inflammatory cytokine production but can also reduce goblet cell loss and inhibit epithelial permeability (Gadaleta et al., 2011). FXR agonists have been shown to be potential candidates for IBD treatment (Stojancevic et al., 2012).

Ginsenoside Rc (Rc) is a major anti-inflammatory component of *Panax ginseng*, which exhibits anti-oxidative and anti-inflammatory activities through different mechanisms (Yu et al., 2016). A previous study has reported that Rc can reduce inflammatory levels and repair cellular damage in cardiomyocytes (Huang et al., 2021). However, it is unknown whether Rc could ameliorate IBD by reducing the inflammatory response. Furthermore, the association of Rc and FXR has not yet been reported. Here, we hypothesize that Rc may ameliorate IBD symptoms by reducing inflammation and its mechanism may involve the activation of the FXR signaling pathway as an FXR agonist. In this study, we assess the anti-inflammation activity and intestinal damage repair ability of Rc on a dextran sulfate sodium (DSS)-induced IBD mice model. Furthermore,

experimental FXR^{-/-} and wild-type (WT) mice were used to assess the key role that FXR plays in Rc treatment of IBD. We aimed to explore the anti-inflammatory effects and the functional mechanism of Rc in IBD treatment.

Materials and methods

Cell culture

Human intestinal epithelial cell lines LS174T (ATCC) were cultured in fresh DMEM with 10% FBS. Rc (purity >98%, HPLC) was purchased from Shanghai Yuanye Bio-Technology Co., Ltd. (Shanghai, China). HepG2 cells (ATCC) were also maintained in fresh DMEM with 10% FBS. To investigate the cell viability of Rc, LS174T were treated with different concentrations of Rc (0, 6.25, 12.5, 25, 50, 100, 200, and 400 μ M). Meanwhile, 24 hours later, cell viability was evaluated *via* the CCK-8 assay. Moreover, to investigate whether Rc can reduce inflammation induced by LPS, cells were pretreated with Rc for 48 h, incubated with LPS (2000 ng/ml) for 24 h, and collected for further analysis.

Animal experiments

All of the animal experimental studies were approved by the Animal Ethics Committee of Guangzhou University of Chinese Medicine. In total, 50 male C57BL/6 mice (6 weeks old, 20–25 g) were purchased from the Model Animal Research Center of Guangzhou University of Chinese Medicine (Certificate: SCXK 2018-0034; Guangzhou, China). They were housed in an SPF room (25°C, 12 h day/night cycle, free access to chow and water). After 2 weeks, the mice were randomly divided into five groups (Saline, DSS, DSS Rc 5 mg/kg, DSS Rc10 mg/kg, and DSS Rc 20 mg/kg), with 10 mice in each group. The mice were then administered different concentrations of Rc every day throughout the experimental period (11 days). On the third day, the mice were given a 4% DSS solution (w/v) until the end of the experimental period. FXR-knockout (FXR^{-/-}) mice were kindly provided by Changhui Liu, and were generated and used as previously purchased from the Jackson Laboratory (Bar Harbor, ME, United States) (Liu et al., 2020). The genotyping for FXR identification is shown in [Supplementary Figure S1](#). Similarly, 18 FXR^{-/-} mice were divided into three groups (Saline, DSS, and DSS Rc 20 mg/kg), and were treated in the same way as those mentioned above. All of the blood and tissues were collected from the mice after anesthesia on the last day.

Disease activity index

The disease activity index (DAI) was measured following the method of a previous study (DAI score = weight loss (%) + stool

consistency + rectal bleeding) (Detel et al., 2012). The weight loss, stool consistency, and rectal bleeding of each mouse were observed daily to evaluate the symptoms of colitis.

Hematoxylin and eosin staining

The entire colon was weighed and measured at the end of the experiment. Parts of colons were placed in 4% paraformaldehyde and embedded and cut for H&E staining. Images were collected from a light microscope. The remaining parts were stored for further analysis.

Immunofluorescence

Immunofluorescence was performed according to current protocols (Liu et al., 2018). In brief, colon sections were incubated with F4/80, CD11b, and ZO-1 (Affinity, United States) at 4°C overnight. After washing them three times in PBS, sections were incubated with secondary antibodies (Abclonal, Wuhan, China) for 40 min at room temperature. After washing them five times in PBS, images were observed using a fluorescence microscope (Nikon, Japan). LS174T cells were treated with Rc (25 μ M) for 24 h after treatment with adnexal LPS (2000 ng/ml), washed twice with PBS, blocked with 4% paraformaldehyde, incubated with NF-KB primary antibody (Abcam, ab16502) at 4°C overnight, followed by incubation with secondary antibody (Abmart, Alexa Fluor 488) for 1 h, washed three times with PBS, and blocked with DAPI blocker for microscopic observation.

TNF- α , IL-1 β , and IL-6 measurement of serum levels

Serum was collected for TNF- α , IL-1 β , and IL-6 measurements. In this experiment, IL-1 β and IL-6 were detected by the corresponding ELISA kits from Abclonal (Wuhan, China), while TNF- α was detected by ELISA kits from Ruixinbio (Quanzhou, China), following the manufacturer's instructions.

Quantitative PCR

The TRIzol reagent was used for the total mRNA extraction of mouse colon tissue samples. A high-capacity cDNA reverse-transcription kit (Abclonal, Wuhan, China) was used for reverse transcription. Meanwhile, cDNA was subjected to quantitative PCR (qPCR) analysis with the PowerUp™ SYBR™ Green Master Mix (Abclonal, Wuhan, China). The expression levels of

TABLE 1 Primers used in qPCR.

Gene name	Forward primer	Reverse primer
<i>FXR</i>	GCTTGATGTGCTACAAAAGCTG	CGTGGTGATGGTTGAATGTCC
<i>BSEP</i>	TCTGACTCAGTGATTCTTCGCA	CCCATAAACATCAGCCAGTTGT
<i>SHP</i>	TGGGTCCCAAGGAGTATGC	GCTCCAAGACTTCACACAGTG
<i>IL-6</i>	TAGTCCTTCCTACCCCAATTTCC	TTGGTCCTTAGCCACTCCTTC
<i>ICAM1</i>	GTGATGCTCAGGTATCCATCCA	CACAGTTCTCAAAGCACAGCG
<i>COX-2</i>	TTCAACACACTCTATCACTGGC	AGAAGCGTTTGCGGTACTCAT
<i>ZO-1</i>	GCCGCTAAGAGCACAGCAA	TCCCCACTCTGAAAATGAGGA
<i>occludin</i>	TTGAAAGTCCACCTCCTTACAGA	CCGGATAAAAAGAGTACGCTGG
<i>acludin-1</i>	GGGGACAACATCGTGACCG	AGGAGTCGAAGACTTTGCACT
h <i>FXR</i>	AACCATACTCGCAATACAGCAA	ACAGTCTATCCCCTTTGATCC
h <i>SHP</i>	GTGCCCAGCATACTCAAGAAG	TGGGGTCTGTCTGGCAGTT
h <i>BSEP</i>	TTGGCTGATGTTTGTGGGAAG	CCAAAAATGAGTAGCACGCCT
β -actin	ATGACCCAAGCCGAGAAGG	CGGCCAAGTCTTAGAGTTGTTG
h β -actin	GAATCAATGCAAGTTCGGTTCC	TCATCTCCGCTATTAGCTCCG

all the genes were standardized with β -actin and the specific primer sequences are shown in Table 1.

Molecular docking

The chemical composition collection method was as follows. The ChemDraw 14.0 software was used to draw the 2D structure of small molecule ligands (Rc), and then ChemDraw3D was used to transform the 2D structure into a 3D structure and save it as an MOL2 file. The 3D structure was imported into Discovery Studio. The Prepare Ligands module in Molecules was then used to process small molecules. The energy of small molecules was minimized and a CHARMM force field was used to obtain the prepared small molecules and save them in the MOL2 format. The structural acquisition and preprocessing of protein crystals were as follows. The PDB database (<https://www.rcsb.org/>) contains data on most of the crystals of biological macromolecules reported to date, including crystal complexes of biological macromolecules and small molecules. This docking study was mainly focused on the FXR protein. Discovery Studio software was used to preprocess the protein. We then deleted the water molecules, hydrogenated and charged them, extracted the original ligand from the structure, and used PyMol to process the protein.

Luciferase reporter gene assay

HepG2 cells were planted in 12-well plates. After 24 h, cells were transfected with 1 μ g hFXR-luc and 1 μ g Ramlila luciferase expression vector pCMV-RL-TK (Promega) for 36 h. Here, pCMV-RL-TK was used as an internal control. To measure the effect of Rc on FXR activity, cells were incubated with Rc

TABLE 2 Primers used in plasmids construction.

FXR Promoter-1838~+47 luc	5'-ATGTATCTCTAGTTGTCCTGATATA-3'
	5'-CGCTCCCGGGCTCTCCGCTAG-3'

(0, 6.25, 12, 25 μ M). After 24 h, cells were collected for luciferase activity assessment using the Dual Luciferase Reporter Assay System (Promega). Relative luciferase activity was corrected for Renilla luciferase activity of pCMV-RL-TK, and normalized to the activity of the control. The 5' end of the mouse FXR gene extending from position -1838 bp (relative to the transcription start site) to +47 was cloned into the pGL3-Basic (Promega) luciferase reporter plasmid with the MluI/XhoI sites. The primers that were used for plasmid construction are shown in Table 2.

Statistical analysis

All of the results are expressed as the means \pm SEMs. The data were evaluated and statistical differences between groups were assessed. For multiple group comparisons, we used Student's *t*-test and a one-way analysis of variance (ANOVA), followed by a post hoc Tukey test using GraphPad Prism 8.

Results

Rc reduces inflammation in LPS-induced LS174T cells

We used LPS-induced LS174T cells to establish the IBD cell model *in vitro* to observe the potential therapeutic effect of Rc on

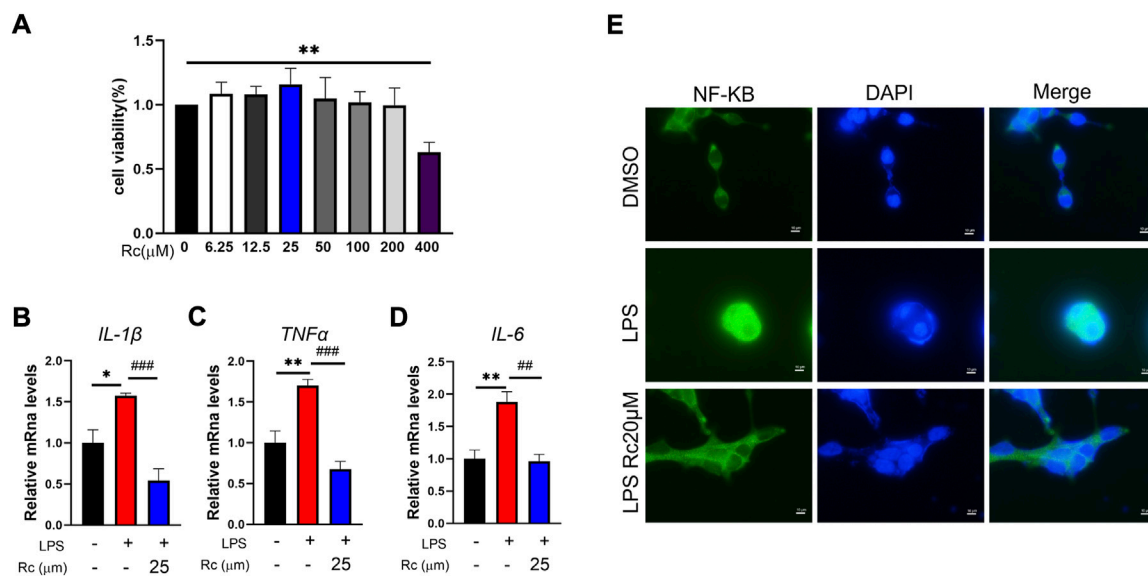


FIGURE 1

Rc attenuated inflammatory in LPS-induced LS174 cells. Cell viability (A) of Rc in LS174 cells ($n = 3$); after incubation with Rc and LPS following the protocol, the cells were collected for qPCR analysis, and the relative mRNA levels of *IL-1β*, *TNF-α* and *IL-6* (B–D) were measured ($n = 4$); representative images of immunofluorescence of NF-κB (E). Data are shown as the mean \pm SEM. * $p < 0.05$, ** $p < 0.01$, *** $p < 0.001$ vs. the DMSO group.

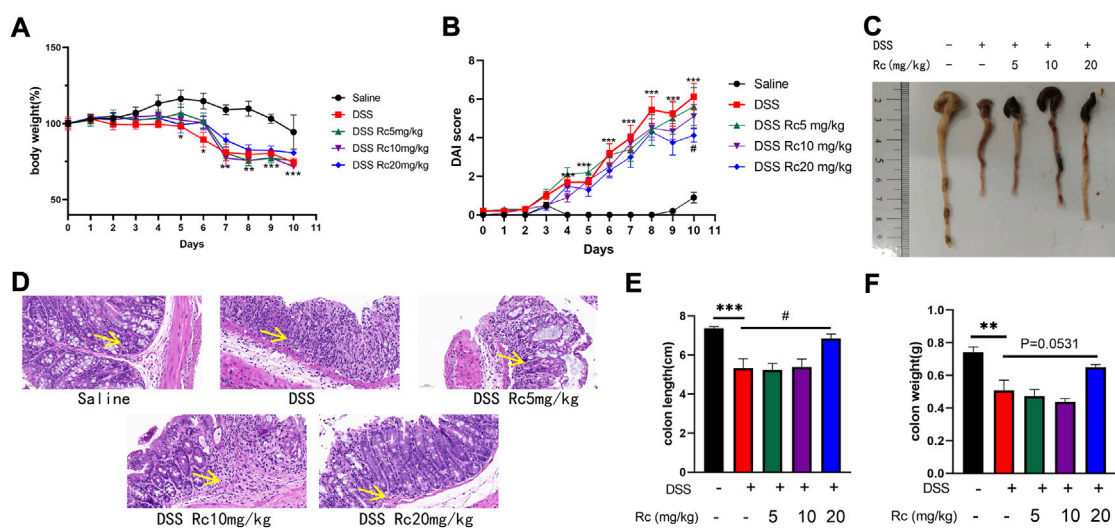


FIGURE 2

Rc ameliorated DSS-induced UC in mice. Body weight (A) changes and disease activity index (B) during the whole experiment; macroscopic observation of colon length (C); representative H&E-stained colon sections (magnification: 200 \times) (D); the statistics of colon weight (E) and colon length (F). Data are shown as the mean \pm SEM ($n = 10$). * $p < 0.05$, ** $p < 0.01$, *** $p < 0.001$ vs. the saline group; # $p < 0.05$ vs. the DSS group.

UC. In our study, Rc exhibited low cytotoxicity and Rc did not inhibit cell viability up to 400 μ M (Figure 1A). According to the result of qPCR analysis, the relative mRNA levels of inflammation, including *IL-1β*, *TNF-α*, and *IL-6* were

upregulated in the LPS-induced group. These indices were downregulated with the Rc treatment (Figures 1B–D). Immunofluorescence analysis showed that Rc could inhibit nuclear translocation of NFκB (Figure 1E). These results

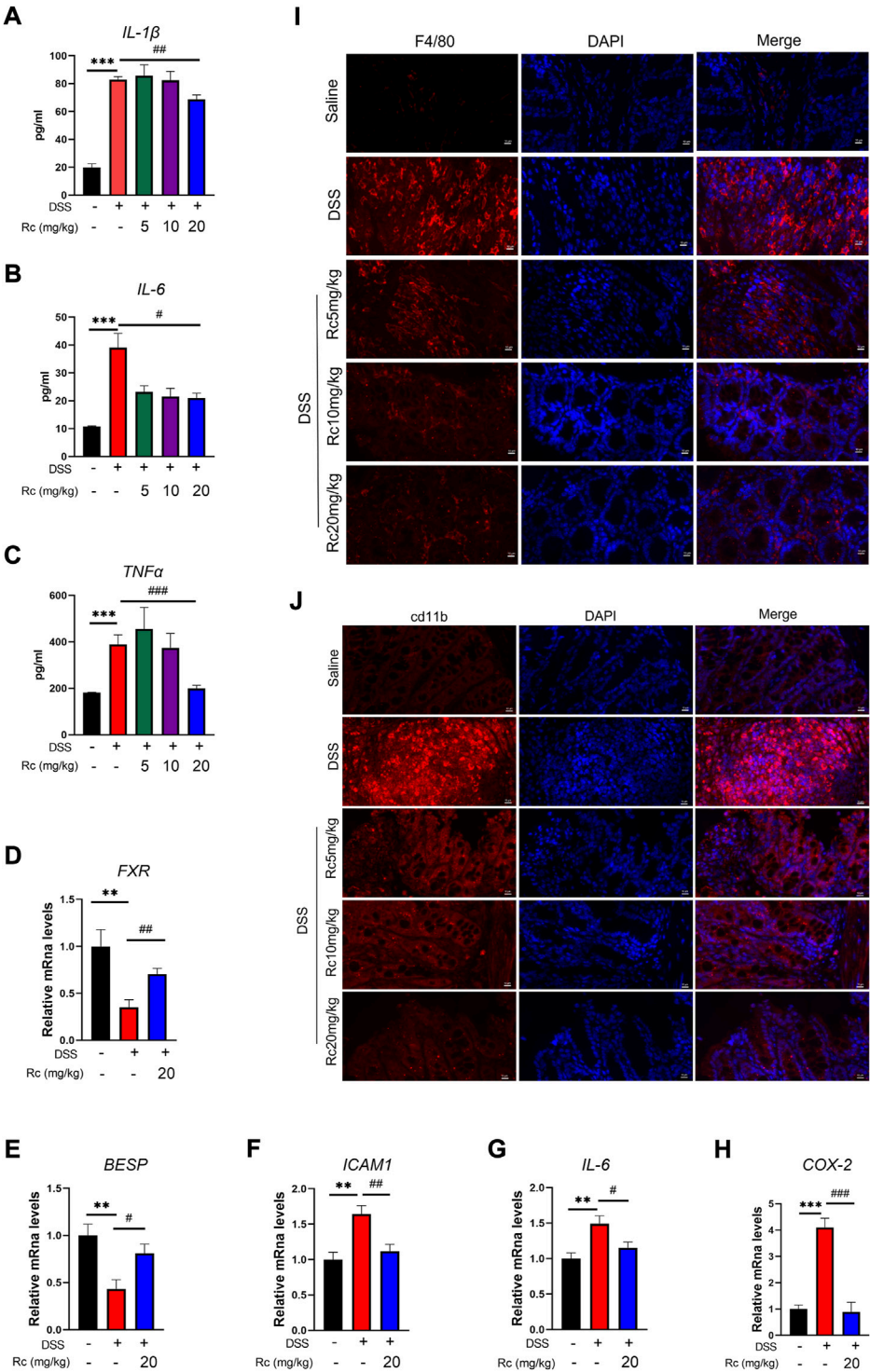


FIGURE 3 Rc suppressed inflammation by activating FXR in DSS-induced inflamed mouse colons. Serum levels of IL-1 β , IL-6 and TNF- α (A–C); the colons were collected for qPCR analysis, and the relative mRNA levels of *FXR* (D), *BSEP* (E), *ICAM1* (F), *IL-6* (G), and *COX-2* (H) were measured; representative images of immunofluorescence of F4/80 (I) and cd11b (J) in mouse colon sections (magnification: 200 \times). Data are shown as the mean \pm SEM ($n = 8$). * $p < 0.05$, ** $p < 0.01$, *** $p < 0.001$ vs. the saline group; # $p < 0.05$, ## $p < 0.01$, ### $p < 0.001$ vs. the DSS group.

indicate that Rc may have a potential effect on suppressing inflammation induced by LPS cells.

Rc treatment reduces colitis symptoms in DSS-induced mice

A DSS-induced mouse model was established to further explore the therapeutic effect of RC on UC. Compared with DSS-treated mice, Rc administration resulted in a dose-dependent weight gain (Figure 2A) and a high dose of Rc slightly reduced DAI scores (Figure 2B). DSS treatment significantly shortened colons compared to controls (Figure 2C). H&E staining analysis showed mucosal structural repair, an increased number of crypt structures, and the reduced infiltration of inflammatory cells into the mucosa and submucosa. This indicates that Rc effectively reversed the DSS-induced damage of colon tissues (Figure 2D). Meanwhile, Rc treatment reduced the length of colons and increased the weight of colons in a dose-dependent manner (Figures 2E,F). Taken together, these data suggest that Rc had a very positive impact on the treatment of UC.

Rc inhibits the inflammatory response in DSS-induced mice

To investigate whether Rc ameliorated the inflammatory response in colitis by activating FXR, we carried out some further studies. First, at the serum level, we found that IL-1 β , IL-6, and TNF- α were significantly increased in the DSS-treated model group, whereas high-dose Rc treatment was able to suppress the inflammatory response (Figures 3A–C). The mRNA expression of FXR and its downstream genes were significantly suppressed when compared with the control group, whereas Rc treatment upregulated their expression levels (Figures 3D,E). Similarly, the mRNA levels of DSS-induced pro-inflammatory factors *ICAM1*, *IL-6*, and *COX2* were significantly increased when compared with the normal group, whereas low expressions were found in the Rc-treatment group (Figures 3F–H). Similarly, immunofluorescence analysis showed that Rc reduced the expression of F4/80 and cd11b in a dose-dependent manner (Figures 3I,J). These results indicate that Rc was a potent anti-inflammatory agent, which could ameliorate or even suppress the inflammatory response and alleviate the inflammatory symptoms of UC.

Rc protects the intestinal mucosa in DSS-induced mice

Damage to intestinal barriers is a considerable feature of DSS-induced UC. In our hypothesis we predicted that Rc could

not only suppress inflammation but also repair the damage of intestinal barriers induced by DSS. Thus, we focused on TJ molecules. Our results show that Rc upregulated the mRNA expression of *ZO-1*, *claudin-1*, and *occludin* when compared with the DSS group (Figures 4A–C). Meanwhile, the results of immunofluorescence analysis showed that Rc significantly upregulated the expression of *ZO-1* in the inflammatory colon when compared with the DSS group (Figure 4D). Thus, Rc improved the reduction in intestinal permeability brought about by UC.

Rc activates the FXR signaling pathway

Molecular docking was conducted to investigate whether Rc can activate FXR. The results show that the inner part of FXR's structural domain could be bound by Rc based on hydrogen, hydrophobic interaction, and the van der Waals coefficient (Figure 5A). Luciferase reporter gene assay showed significant effect of Rc in activating transcriptional expression of FXR in a dose-dependent manner (Figure 5B). Meanwhile, qPCR results demonstrated that Rc increased the mRNA levels of *FXR*, *BSEP*, and *SHP* in a dose-dependent manner when compared with the control group (Figures 5C–E). These results indicate that Rc could activate the FXR signaling pathway *in vitro*.

FXR deficiency reduces the protective effect of Rc in DSS-induced FXR^{-/-} mice

To investigate the effect of FXR on UC, we found that the weight loss and DAI changes caused by DSS were not alleviated after optimal dose treatment with Rc in the case of the knockdown of FXR (Figures 6A,B). Furthermore, the length and weight of the colon were not improved (Figures 6C–E). HE results also showed that the mucosal structure was not repaired, with no change in the mucosa and submucosa in terms of the amount of inflammatory cell infiltration (Figure 6F). This suggests that the absence of FXR renders the treatment of Rc ineffective.

FXR deficiency deprives Rc of its anti-inflammatory effect in DSS-induced FXR^{-/-} mice

Through further studies, we found that under conditions of FXR deficiency, Rc was not able to exert an inhibitory effect on inflammation. At the ELISA level, the expression of IL-1 β , IL-6, and TNF- α was not reduced after Rc treatment when compared with the model group (Figures 7A–C). Meanwhile, the mRNA levels of *ICAM1*, *COX-2*, and *IL-6* were also not significantly inhibited (Figures 7D–F). Immunofluorescence results also

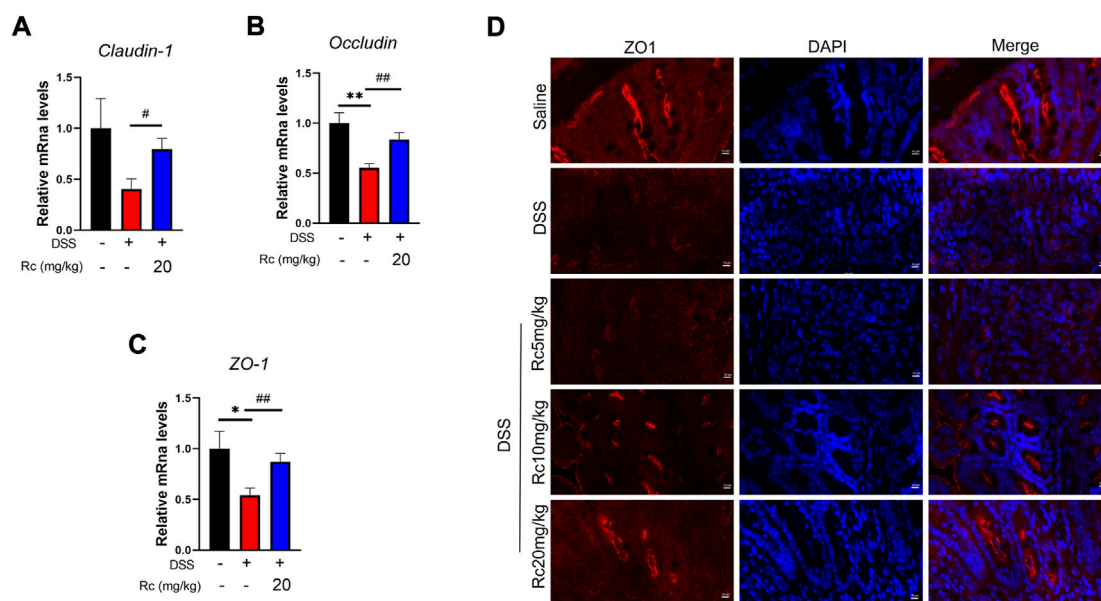


FIGURE 4

Rc maintains proper tight junctions in DSS-induced mice. The colons were collected for qPCR analysis, and the relative mRNA levels of *claudin-1* (A), *occludin* (B), and *ZO-1* (C) were measured; representative images of immunofluorescence of *ZO-1* (D) in mouse colon sections (magnification: 200 ×). Data are shown as the mean ± SEM ($n = 6$). * $p < 0.05$, ** $p < 0.01$ vs. the saline group; # $p < 0.05$, ## $p < 0.01$ vs. the DSS group.

suggested that Rc failed to produce the inhibition of inflammatory expression levels in the presence of the knockdown of FXR (Figures 7G,H). Therefore, FXR plays an important role in Rc's therapeutic process in relation to UC inflammation.

FXR deficiency does not protect intestinal barriers in DSS-induced FXR^{-/-} mice

In the absence of FXR, the mRNA expression of *claudin*, *occludin*, and *ZO-1* did not increase after Rc treatment when compared to the model group (Figures 8A–C). Immunofluorescence of *ZO-1* also showed no improvement in intestinal permeability (Figure 8D). Overall, Rc treatment could not repair the intestinal mucosal damage caused by DSS after the deletion of FXR. Therefore, FXR may play an active role in repairing the intestinal damage caused by UC and restoring the intestinal mucosa.

Discussion

Although intestinal barrier disruption is often the final factor causing IBD mortality, intestinal inflammation is often the injury that is observed at the beginning. Consequently, ameliorating inflammation by targeting the FXR signaling

pathway represents an attractive concept for combating IBD. Activating FXR might be a therapeutic strategy for treating IBD and its complications. In the present study, we assumed that Rc was an FXR activator, and we verified that Rc ameliorated DSS-induced inflammation and intestinal barrier damage by activating FXR. This therapeutic effect disappeared when FXR was absent (the mechanism diagram is shown in Supplementary Figure S2).

Rc is believed to play an anti-inflammatory role in many disease, such as gastritis, hepatitis, arthritis, and pneumonia (Yu et al., 2016; Lee et al., 2018). Based on the excellent anti-inflammatory ability of Rc, we wondered if Rc could play the same anti-inflammatory role in IBD. Pro-inflammatory cytokines—including IL-1 β , IL-6, and TNF- α —have been used to measure inflammation levels in many IBD studies (Hall et al., 2017; Breugelmans et al., 2020). As we expected, Rc reduced the mRNA levels of IL-1 β , IL-6, and TNF- α in LPS-induced LS174T *in vitro*, which indicates the potential ability of Rc to attenuate intestinal inflammation. Thus, we then explored its therapeutic effect on an IBD model *in vivo*.

DSS-induced mice are characterized by weight loss, loose stools, diarrhea, and even rectal bleeding. Thus, DSS-induced mice have often been used as an animal model of IBD, including UC and CD (Kim et al., 2012; Liu et al., 2021). Consistently, our study showed symptoms such as decreased body weight, a shortened colon, and increased DAI in DSS-induced mice. In this study, Rc-treated mice exhibited increased colonic weight

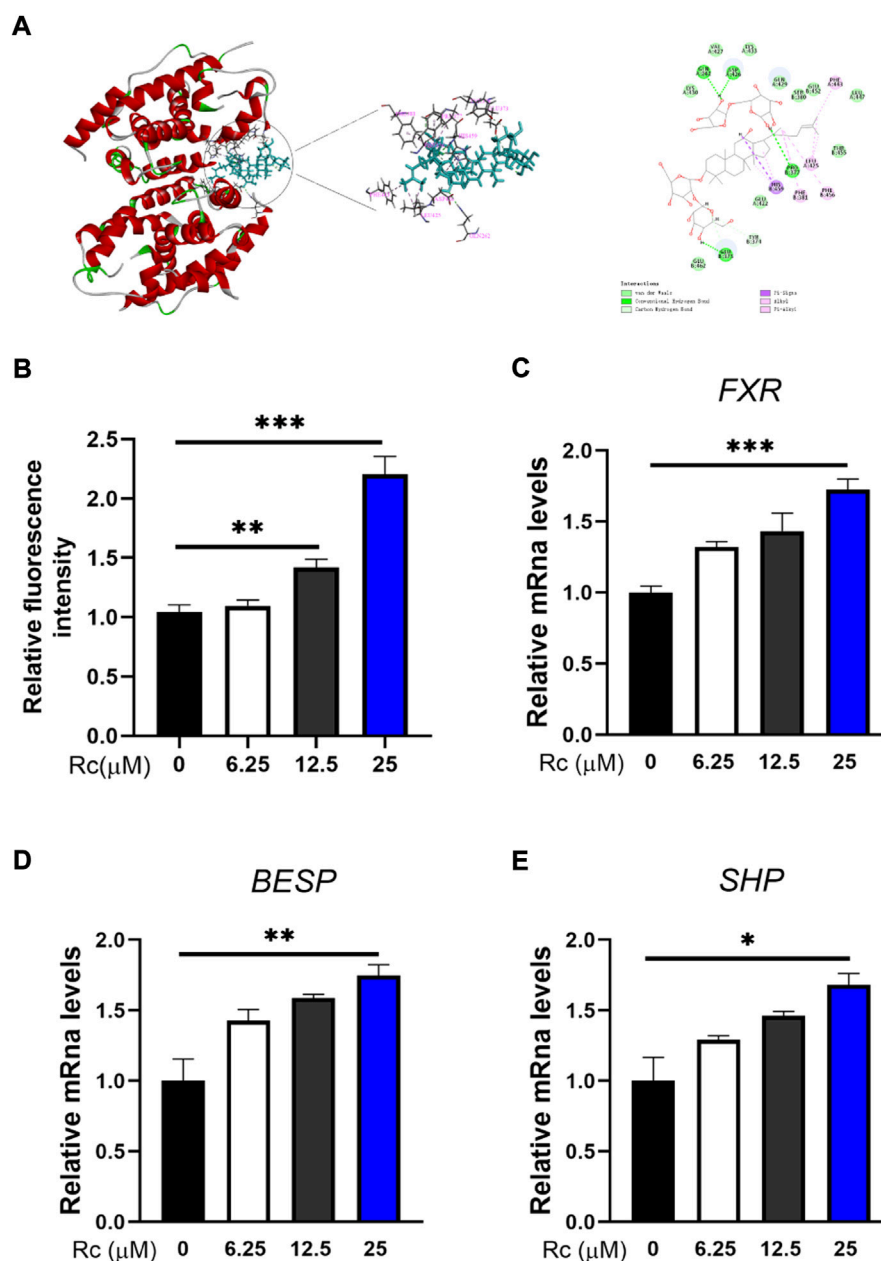


FIGURE 5

Rc activated FXR signaling pathway in LS174 cells: 3D and 2D molecular docking conformation of Rc with FXR (A); FXR reporter gene activity assay (B); the cells were collected for qPCR analysis, and the relative mRNA levels of *FXR* (C), *BSEP* (D), and *SHP* (E) were measured ($n = 4$). Data are shown as the mean \pm SEM. * $p < 0.05$, ** $p < 0.01$, *** $p < 0.001$ vs. the DMSO group.

and length when compared to DSS-induced mice. Furthermore, DSS-induced mice displayed a loss of integrity in their intestinal barriers (e.g., decreased crypt foci and increased inflammatory cell infiltration in the mucosa and submucosa), whereas Rc was able to reverse this damage induced by DSS. Here, we report for the first time that Rc can reverse these UC symptoms that are induced by DSS.

It is clear that FXR activation suppresses the inflammatory response and preserves intestinal barrier integrity in IBD (Ding et al., 2015). We thus assess the role of Rc in ameliorating inflammation and the effects of IBD on intestinal barriers *in vivo*. These pro-inflammatory cytokines can cause intestinal barrier impairment (Nunes et al., 2019). Studies have indicated that IL-1 β and TNF- α

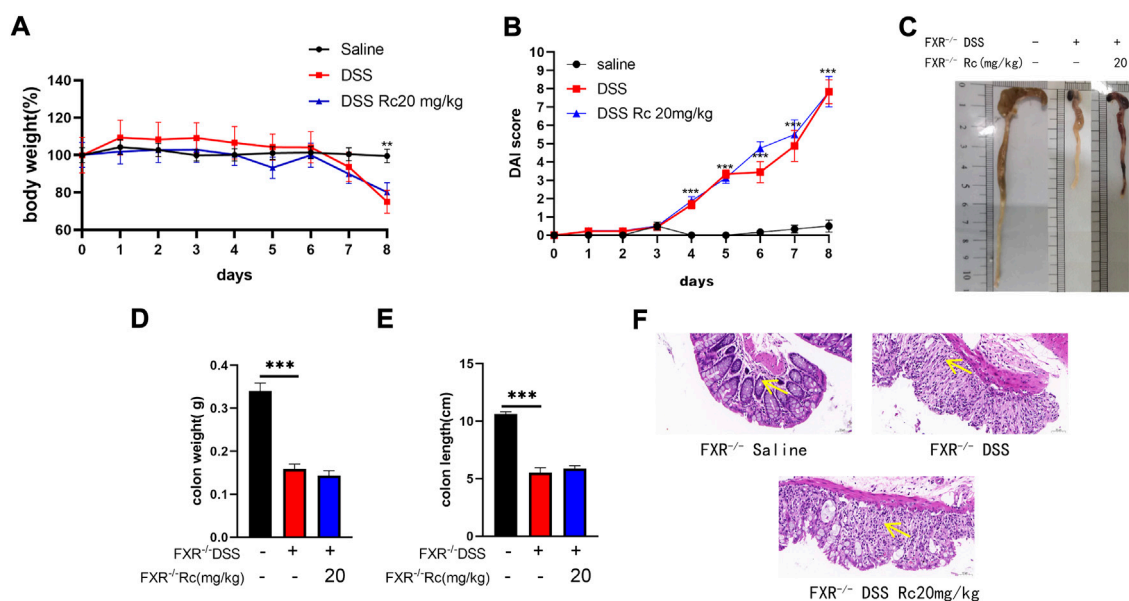


FIGURE 6

Rc did not ameliorate DSS-induced UC in FXR^{-/-} mice. Body weight (A) changes and disease activity index (B) during the whole experiment; macroscopic observation of colon length (C); the statistics of colon weight (D) and colon length (E) representative H&E-stained colon sections (magnification: 200 ×) (F). Data are shown as the mean ± SEM (n = 6). **p < 0.01, ***p < 0.001 vs. the saline group.

can cause an obvious increase in intestinal barrier permeability, depending on NF-κB activation (Haines et al., 2016; Zhong et al., 2021). According to our results, Rc suppressed the inflammatory response, which resulted in decreased serum levels of IL-1β, IL-6, and TNF-α. Furthermore, the relative mRNA levels of *ICAM1*, *NF-κB*, *IL-6*, and *COX-2* were increased by DSS but reduced by Rc in our study. These results suggest that Rc may play an anti-inflammatory role by activating the NF-κB pathway in the intestines. Further verification for this hypothesis was carried out with the use of immunofluorescence, and low levels of CD11b and F4/80 inflammatory cells in infiltration were observed in the Rc-treatment group. Intestinal macrophages are key immune cells in the maintenance of intestinal immune homeostasis in IBD, and FXR is a modulator of intestinal innate immunity (Vavassori et al., 2009; Dharmasiri et al., 2021). As we expected, the relative mRNA levels of *FXR* and its downstream target *BSEP* were increased with Rc treatment. Mutual crosstalk between FXR and NF-κB might indicate a potential pathway for the anti-inflammatory effect of FXR (Gai et al., 2018). However, more evidence is needed before we can conclude that the activation of FXR directly inhibited the NF-κB pathway. Taken together, our data show that Rc may act as an FXR agonist to reduce intestinal inflammation in DSS-induced mice.

The increasing expression of several types of pro-inflammatory mediators also impaired the intestinal

barriers (Al-Sadi et al., 2016). We found that Rc could reduce intestinal inflammation by activating FXR, resulting in NF-κB inhibition. It is known that NF-κB is also a mediator for intestinal barriers, regulating multiple cellular signaling pathways (Cuzzocrea et al., 2000). We then explored its effect on repairing intestinal barriers. As expected, our data showed that Rc improved the relative mRNA levels of *claudin-1*, *occludin*, and *ZO-1*. Further verification was carried out using immunofluorescence, which showed that Rc increased the expression of ZO-1, which indicates that Rc could improve the reduction of intestinal permeability induced by DSS.

FXR is believed to play an anti-inflammatory role and participates in a wide range of diseases of the gastrointestinal tract, such as IBD, colorectal cancer, and type 2 diabetes (Ding et al., 2015). Zhao et al. (2020) found that the downregulation of FXR promoted DSS-induced UC. Meanwhile, Gadaleta et al. (2011) and Feng et al. (2021) found that inflammation could be inhibited by activating FXR. These studies pointed out that the expression of FXR was closely related to DSS-induced UC, which indicates that the regulation of FXR may be useful for ameliorating IBD. Recently, molecular docking has become a commonly used component of the drug discovery toolbox (Luo et al., 2022). Therefore, molecular docking was conducted to explore whether Rc and FXR could interact each other. Remarkably, Rc showed a strong binding affinity to FXR,

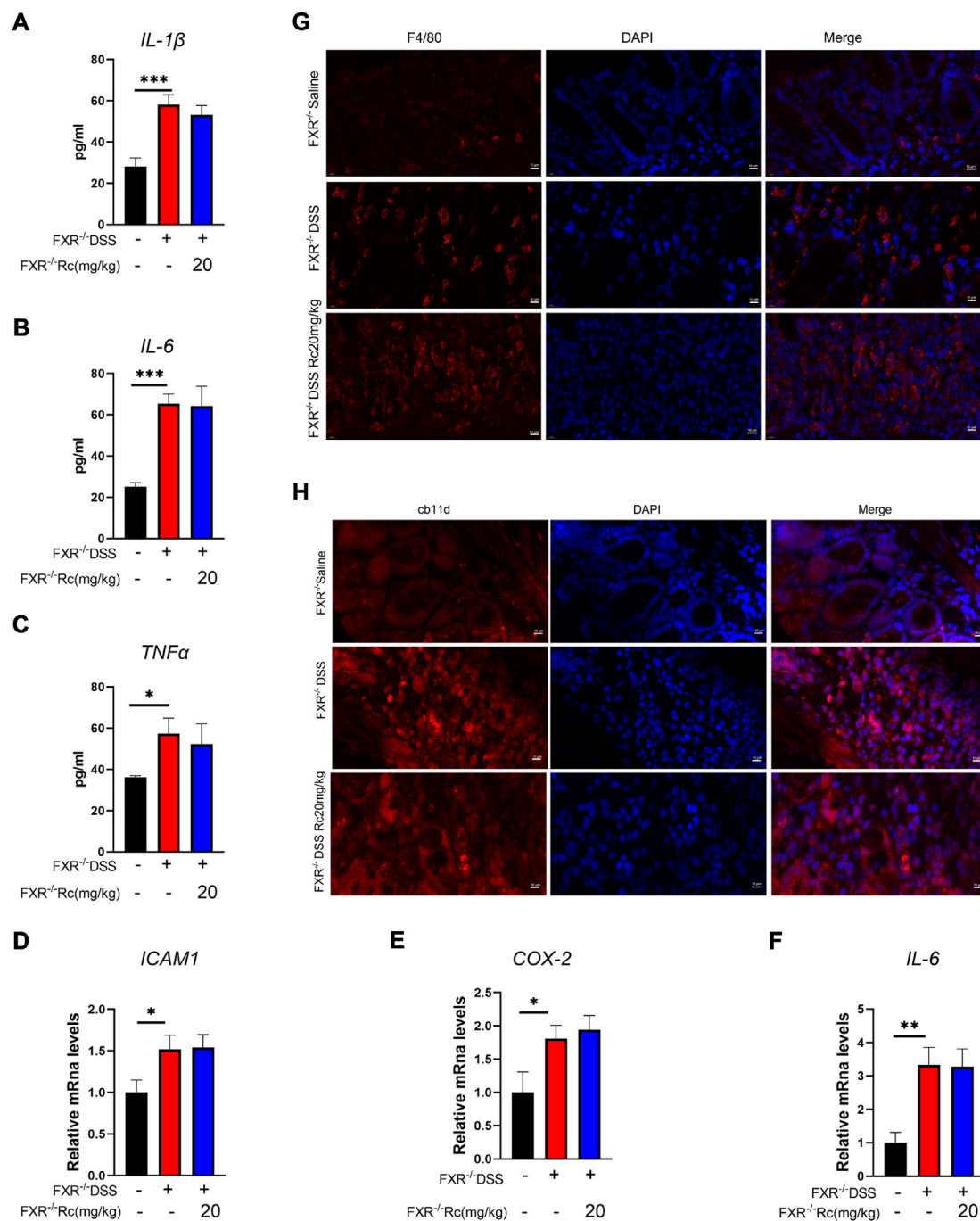


FIGURE 7

The absence of FXR blocked the effect of Rc on suppressing inflammation in DSS-induced FXR^{-/-} mice. Serum levels of IL-1 β , IL-6, and TNF- α (A–C); the colons were collected for qPCR analysis, and the relative mRNA levels of *ICAM1* (D), *COX-2* (E), and *IL-6* (F) were measured; representative images of immunofluorescence of F4/80 (G) and cd11b (H) in mouse colon sections (magnification: 200 \times). Data are shown as the mean \pm SEM ($n = 6$). * $p < 0.05$, ** $p < 0.01$, *** $p < 0.001$ vs. the saline group.

which indicates that Rc directly regulated the FXR-mediated signaling pathway. The result of the luciferase reporter gene assay further indicates that Rc regulated the transcriptional activity of FXR. Our qPCR results show that the mRNA

expressions of *FXR*, *BSEP*, and *SHP* were increased with Rc treatment. This result is in accordance with those reported for FXR activating its downstream genes *BSEP* and *SHP* (Wang et al., 2017; Fu et al., 2022). To our

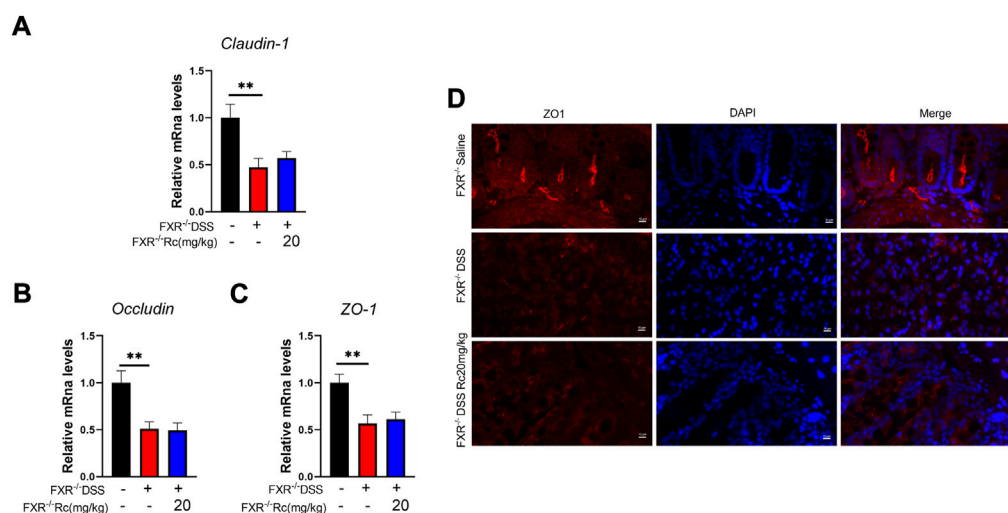


FIGURE 8

The absence of FXR blocked the effect of Rc maintaining tight junctions in DSS-induced FXR^{-/-} mice. The colons were collected for qPCR analysis, and the relative mRNA levels of *claudin-1* (A), *occludin* (B), and *ZO-1* (C) were measured; representative images of immunofluorescence of ZO-1 (D) in mouse colon sections (magnification: 200 ×). Data are shown as the mean ± SEM (*n* = 6). ***p* < 0.01 vs. the saline group.

knowledge, this is first time that Rc has been reported as an FXR regulator.

Previously, Verbeke et al. (2015) demonstrated a crucial protective role for FXR in cholestatic rats, which meant that FXR agonists could prevent gut barrier dysfunction, observing upregulated claudin-1 and occludin. Novel drugs have been reported that could improve intestinal barrier function by increasing FXR signaling, which resulted in the alleviation of colitis (Song et al., 2019; Dong et al., 2021). Knowing that the effect of Rc on anti-inflammatory and intestinal barrier repair may occur due to FXR activation, we aimed to explore whether FXR activation is essential for Rc to exert its therapeutic effect. Although FXR was lowly expressed in the intestine in DSS-induced mice, FXR-knockout (FXR^{-/-}) mice did not present high DAI scores, whereas DSS-induced FXR^{-/-} mice showed higher DAI scores, lower colon weights, and shorter colon lengths, as well as rising inflammation levels and damaged intestinal barriers. This indicates that DSS also led to UC in FXR^{-/-} mice. However, Rc did not exhibit its therapeutic effect on UC in FXR^{-/-} mice, with no change in the indexes of inflammation and intestinal barriers. Despite the multiple mechanisms behind UC treatment, here the therapeutic effect of Rc on UC appeared to only be achieved by activating FXR. Our findings explain the protective effect of Rc on UC, and they provide evidence that FXR constitutes a valid therapeutic target activated by Rc in the treatment of IBD.

Conclusion

Our study suggests that Rc may ameliorate inflammatory and barrier function in the intestines. This leads to the attenuation of DSS-induced UC, in which Rc may potentially activate FXR signaling to protect the intestines from DSS-induced injury.

Data availability statement

The original contributions presented in the study are included in the article/Supplementary Material; further inquiries can be directed to the corresponding authors.

Ethics statement

The animal study was reviewed and approved by the Animal Ethics Committee of Guangzhou University of Chinese Medicine.

Author contributions

All authors contributed to the design and conduction of experiments, data collection, and analysis. KT and JH wrote the paper draft. NL, DZ, YD, and JH revised the paper.

Funding

This work was supported by Key projects of Guangdong Provincial Department of Education (2021ZDZX 2010, China), the Basic and Applied Basic Research Foundation of Guangdong Province Regional Joint Fund Project (The Key Project, 2020B1515120021, China), the Discipline Construction Project of Guangdong Medical University (4SG21276P, 1003K20220004, China), Zhanjiang City science and technology development special fund competitive allocation project (2018A01029, China), TCM Scientific Research Project of Guangdong Provincial Bureau of Traditional Chinese Medicine (20211215, China), Characteristic Innovation Project of Guangdong Province General University (2020KTSCX042, 2019KTSCX046, China), and Dongguan City Science and Technology Correspondent Project (2022, China).

Acknowledgments

We are grateful to Changhui Liu for providing the FXR-knockout mice.

References

- Al-Sadi, R., Guo, S., Ye, D., and Ma, T. Y. (2013). TNF- α modulation of intestinal epithelial tight junction barrier is regulated by ERK1/2 activation of Elk-1. *Am. J. Pathol.* 183 (6), 1871–1884. doi:10.1016/j.ajpath.2013.09.001
- Al-Sadi, R., Guo, S., Ye, D., Rawat, M., and Ma, T. Y. (2016). TNF- α modulation of intestinal tight junction permeability is mediated by NIK/IKK- α axis activation of the canonical NF- κ B pathway. *Am. J. Pathol.* 186 (5), 1151–1165. doi:10.1016/j.ajpath.2015.12.016
- Ananthanarayanan, M., Balasubramanian, N., MakishiMaM.Mangelsdorf, D. J., and Suchy, F. J. (2001). Human bile salt export pump promoter is transactivated by the farnesoid X receptor/bile acid receptor. *J. Biol. Chem.* 276 (31), 28857–28865. doi:10.1074/jbc.M011610200
- Anderson, K. M., and Gayer, C. P. (2021). The pathophysiology of farnesoid X receptor (FXR) in the GI tract: Inflammation, barrier function and innate immunity. *Cells* 10 (11), 3206. doi:10.3390/cells10113206
- Badman, M. K., Chen, J., Desai, S., Vaidya, S., Neelakantham, S., Zhang, J., et al. (2020). Safety, tolerability, pharmacokinetics, and pharmacodynamics of the novel non-bile acid FXR agonist tropifexor (LJN452) in healthy volunteers. *Clin. Pharmacol. Drug Dev.* 9 (3), 395–410. doi:10.1002/cpdd.762
- Bischoff, S. C., Barbara, G., Buurman, W., Ockhuizen, T., Schulzke, J. D., Serino, M., et al. (2014). Intestinal permeability-a new target for disease prevention and therapy. *BMC Gastroenterol.* 14, 189. doi:10.1186/s12876-014-0189-7
- Breugelmans, T., Van Spaendonk, H., De Man, J. G., De Schepper, H. U., Jauregui-Amezaga, A., Macken, E., et al. (2020). In-depth study of transmembrane mucins in association with intestinal barrier dysfunction during the course of T cell transfer and DSS-induced colitis. *J. Crohns Colitis* 14 (7), 974–994. doi:10.1093/ecco-jcc/jjaa015
- Cariello, M., Piccinin, E., and Moschetta, A. (2021). Transcriptional regulation of metabolic pathways via lipid-sensing nuclear receptors PPARs, FXR, and LXR in NASH. *Cell. Mol. Gastroenterol. Hepatol.* 11 (5), 1519–1539. doi:10.1016/j.jcmgh.2021.01.012
- Cuzzocrea, S., Mazzon, E., De Sarro, A., and Caputi, A. P. (2000). Role of free radicals and poly(ADP-ribose) synthetase in intestinal tight junction permeability. *Mol. Med.* 6 (9), 766–778. doi:10.1007/bf03402192
- Detel, D., Pugel, E. P., Pucar, L. B., Buljevic, S., and Varljen, J. (2012). Development and resolution of colitis in mice with target deletion of dipeptidyl peptidase IV. *Exp. Physiol.* 97 (4), 486–496. doi:10.1113/expphysiol.2011.061143
- Dharmasiri, S., Garrido-Martin, E. M., Harris, R. J., Bateman, A. C., Collins, J. E., Cummings, J. R. F., et al. (2021). Human intestinal macrophages are involved in the pathology of both ulcerative colitis and crohn disease. *Inflamm. Bowel Dis.* 27 (10), 1641–1652. doi:10.1093/ibd/izab029
- Ding, L., Yang, L., Wang, Z., and Huang, W. (2015). Bile acid nuclear receptor FXR and digestive system diseases. *Acta Pharm. Sin. B* 5 (2), 135–144. doi:10.1016/j.apsb.2015.01.004
- Dong, S., Zhu, M., Wang, K., Zhao, X., Hu, L., Jing, W., et al. (2021). Dihydromyricetin improves DSS-induced colitis in mice via modulation of fecal-bacteria-related bile acid metabolism. *Pharmacol. Res.* 171, 105767. doi:10.1016/j.phrs.2021.105767
- Drury, B., Hardisty, G., Gray, R. D., and Ho, G. T. (2021). Neutrophil extracellular traps in inflammatory bowel disease: Pathogenic mechanisms and clinical translation. *Cell. Mol. Gastroenterol. Hepatol.* 12 (1), 321–333. doi:10.1016/j.jcmgh.2021.03.002
- Feng, Y., Dong, H., Sun, B., Hu, Y., Yang, Y., Jia, Y., et al. (2021). METTL3/METTL14 transactivation and m⁶A-dependent TGF- β 1 translation in activated kupffer cells. *Cell. Mol. Gastroenterol. Hepatol.* 12 (3), 839–856. doi:10.1016/j.jcmgh.2021.05.007
- Fu, Y., Feng, H., Ding, X., Meng, Q. H., Zhang, S. R., Li, J., et al. (2022). Alisol B 23-acetate adjusts bile acid metabolism via hepatic FXR-BSEP signaling activation to alleviate atherosclerosis. *Phytomedicine.* 101, 154120. doi:10.1016/j.phymed.2022.154120
- Gadaleta, R. M., van Erpecum, K. J., Oldenburg, B., Willemsen, E. C. L., Renooij, W., Murzilli, S., et al. (2011). Farnesoid X receptor activation inhibits inflammation and preserves the intestinal barrier in inflammatory bowel disease. *Gut* 60 (4), 463–472. doi:10.1136/gut.2010.212159
- Gai, Z., Visentin, M., Gui, T., Zhao, L., Thasler, W. E., Hausler, S., et al. (2018). Effects of farnesoid X receptor activation on arachidonic acid metabolism, NF- κ B signaling, and hepatic inflammation. *Mol. Pharmacol.* 94 (2), 802–811. doi:10.1124/mol.117.111047
- Haines, R. J., Beard, R. J., Chen, L., Eitnier, R. A., and Wu, M. H. (2016). Interleukin-1 β mediates β -catenin-driven downregulation of claudin-3 and barrier dysfunction in Caco2 cells. *Dig. Dis. Sci.* 61 (8), 2252–2261. doi:10.1007/s10620-016-4145-y

Conflict of interest

The authors declare that the research was conducted in the absence of any commercial or financial relationships that could be construed as a potential conflict of interest.

Publisher's note

All claims expressed in this article are solely those of the authors and do not necessarily represent those of their affiliated organizations, or those of the publisher, the editors, and the reviewers. Any product that may be evaluated in this article, or claim that may be made by its manufacturer, is not guaranteed or endorsed by the publisher.

Supplementary material

The Supplementary Material for this article can be found online at: <https://www.frontiersin.org/articles/10.3389/fphar.2022.1000444/full#supplementary-material>

- Hall, C., Campbell, E. L., and Colgan, S. P. (2017). Neutrophils as components of mucosal homeostasis. *Cell. Mol. Gastroenterol. Hepatol.* 4 (3), 329–337. doi:10.1016/j.jcmgh.2017.07.001
- Higgins, J. P., Thompson, S. G., Deeks, J. J., and Altman, D. G. (2003). Measuring inconsistency in meta-analyses. *BMJ* 327 (7414), 557–560. doi:10.1136/bmj.327.7414.557
- Huang, J., Jia, R., and Brunner, T. (2018). Local synthesis of immunosuppressive glucocorticoids in the intestinal epithelium regulates anti-viral immune responses. *Cell. Immunol.* 334, 1–10. doi:10.1016/j.cellimm.2018.08.009
- Huang, Q., Su, H., Qi, B., Wang, Y., Yan, K., Wang, X., et al. (2021). A SIRT1 activator, ginsenoside Rc, promotes energy metabolism in cardiomyocytes and neurons. *J. Am. Chem. Soc.* 143 (3), 1416–1427. doi:10.1021/jacs.0c10836
- Kiesler, P., Fuss, I. J., and Strober, W. (2015). Experimental models of inflammatory bowel diseases. *Cell. Mol. Gastroenterol. Hepatol.* 1 (2), 154–170. doi:10.1016/j.jcmgh.2015.01.006
- Kim, J. J., Shajib, M. S., Manocha, M. M., and Khan, W. I. (2012). Investigating intestinal inflammation in DSS-induced model of IBD. *J. Vis. Exp.* 60, 3678. doi:10.3791/3678
- Kim, M. S., Shigenaga, J., Moser, A., Feingold, K., and Grunfeld, C. (2003). Repression of farnesoid X receptor during the acute phase response. *J. Biol. Chem.* 278 (11), 8988–8995. doi:10.1074/jbc.M212633200
- Lee, J. H., Min, D. S., Lee, C. W., Song, K. H., Kim, Y. S., and Kim, H. P. (2018). Ginsenosides from Korean red ginseng ameliorate lung inflammatory responses: Inhibition of the MAPKs/NF- κ B/c-Fos pathways. *J. Ginseng Res.* 42 (4), 476–484. doi:10.1016/j.jgr.2017.05.005
- Lim, W. C., Wang, Y., MacDonald, J. K., and Hanauer, S. (2016). Aminosalicylates for induction of remission or response in Crohn's disease. *Cochrane Database Syst. Rev.* 7, CD008870. doi:10.1002/14651858.CD008870.pub2
- Liu, J. L., Wang, C. Y., Cheng, T. Y., Rixiati, Y., Ji, C., Deng, M., et al. (2021). Circadian clock disruption suppresses PDL1(+) intraepithelial B cells in experimental colitis and colitis-associated colorectal cancer. *Cell. Mol. Gastroenterol. Hepatol.* 12 (1), 251–276. doi:10.1016/j.jcmgh.2021.02.008
- Liu, M., Zhang, G., Song, M., Wang, J., Shen, C., Chen, Z., et al. (2020). Activation of farnesoid X receptor by schaftoside ameliorates acetaminophen-induced hepatotoxicity by modulating oxidative stress and inflammation. *Antioxid. Redox Signal.* 33 (2), 87–116. doi:10.1089/ars.2019.7791
- Liu, M., Zhang, G., Zheng, C., Song, M., Liu, F., Huang, X., et al. (2018). Activating the pregnane X receptor by imperatorin attenuates dextran sulphate sodium-induced colitis in mice. *Br. J. Pharmacol.* 175 (17), 3563–3580. doi:10.1111/bph.14424
- Luo, Z., Huang, J., Li, E., He, X., Meng, Q., Huang, X., et al. (2022). An integrated pharmacology-based strategy to investigate the potential mechanism of xiebai san in treating pediatric pneumonia. *Front. Pharmacol.* 13, 784729. doi:10.3389/fphar.2022.784729
- Massafra, V., Pellicciari, R., Gioiello, A., and van Mil, S. W. C. (2018). Progress and challenges of selective Farnesoid X Receptor modulation. *Pharmacol. Ther.* 191, 162–177. doi:10.1016/j.pharmthera.2018.06.009
- Nunes, C., Freitas, V., Almeida, L., and Laranjinha, J. (2019). Red wine extract preserves tight junctions in intestinal epithelial cells under inflammatory conditions: Implications for intestinal inflammation. *Food Funct.* 10 (3), 1364–1374. doi:10.1039/c8fo02469c
- Piovani, D., Danese, S., Peyrin-Biroulet, L., Nikolopoulos, G. K., Lytras, T., and Bonovas, S. (2019). Environmental risk factors for inflammatory bowel diseases: An umbrella review of meta-analyses. *Gastroenterology* 157 (3), 647–659. e4. doi:10.1053/j.gastro.2019.04.016
- Sands, B. E. (2004). From symptom to diagnosis: Clinical distinctions among various forms of intestinal inflammation. *Gastroenterology* 126 (6), 1518–1532. doi:10.1053/j.gastro.2004.02.072
- Song, M., Ye, J., Zhang, F., Su, H., Yang, X., He, H., et al. (2019). Chenodeoxycholic acid (CDCA) protects against the lipopolysaccharide-induced impairment of the intestinal epithelial barrier function via the FXR-MLCK pathway. *J. Agric. Food Chem.* 67 (32), 8868–8874. doi:10.1021/acs.jafc.9b03173
- Sterne, J. A., Sutton, A. J., Ioannidis, J. P. A., Terrin, N., Jones, D. R., Lau, J., et al. (2011). Recommendations for examining and interpreting funnel plot asymmetry in meta-analyses of randomised controlled trials. *BMJ* 343, d4002. doi:10.1136/bmj.d4002
- Stojancevic, M., Stankov, K., and Mikov, M. (2012). The impact of farnesoid X receptor activation on intestinal permeability in inflammatory bowel disease. *Can. J. Gastroenterol.* 26 (9), 631–637. doi:10.1155/2012/538452
- Sun, L., Cai, J., and Gonzalez, F. J. (2021). The role of farnesoid X receptor in metabolic diseases, and gastrointestinal and liver cancer. *Nat. Rev. Gastroenterol. Hepatol.* 18 (5), 335–347. doi:10.1038/s41575-020-00404-2
- Vavassori, P., Mencarelli, A., Renga, B., Distrutti, E., and Fiorucci, S. (2009). The bile acid receptor FXR is a modulator of intestinal innate immunity. *J. Immunol.* 183 (10), 6251–6261. doi:10.4049/jimmunol.0803978
- Verbeke, L., Farre, R., Verbinnen, B., Covens, K., Vanuytsel, T., Verhaegen, J., et al. (2015). The FXR agonist obeticholic acid prevents gut barrier dysfunction and bacterial translocation in cholestatic rats. *Am. J. Pathol.* 185 (2), 409–419. doi:10.1016/j.ajpath.2014.10.009
- Wang, H., Zhao, Z., Zhou, J., Guo, Y., Wang, G., Hao, H., et al. (2017). A novel intestinal-restricted FXR agonist. *Bioorg. Med. Chem. Lett.* 27 (15), 3386–3390. doi:10.1016/j.bmcl.2017.06.003
- Wang, L., Lee, Y. K., Bundman, D., Han, Y., Thevananthar, S., Kim, C. S., et al. (2002). Redundant pathways for negative feedback regulation of bile acid production. *Dev. Cell* 2 (6), 721–731. doi:10.1016/s1534-5807(02)00187-9
- Weber, C. R., and Turner, J. R. (2007). Inflammatory bowel disease: Is it really just another break in the wall? *Gut* 56 (1), 6–8. doi:10.1136/gut.2006.104182
- Xavier, R. J., and Podolsky, D. K. (2007). Unravelling the pathogenesis of inflammatory bowel disease. *Nature* 448 (7152), 427–434. doi:10.1038/nature06005
- Yang, Z., Koehler, A. N., and Wang, L. (2016). A novel small molecule activator of nuclear receptor SHP inhibits HCC cell migration via suppressing Ccl2. *Mol. Cancer Ther.* 15 (10), 2294–2301. doi:10.1158/1535-7163.MCT-16-0153
- Yu, T., Rhee, M. H., Lee, J., Kim, S. H., Yang, Y., Kim, H. G., et al. (2016). Ginsenoside Rc from Korean red ginseng (Panax ginseng C.A. Meyer) attenuates inflammatory symptoms of gastritis, hepatitis and arthritis. *Am. J. Chin. Med.* 44 (3), 595–615. doi:10.1142/S0192415X16500336
- Zhao, D., Cai, C., Chen, Q., Jin, S., Yang, B., and Li, N. (2020). High-fat diet promotes DSS-induced ulcerative colitis by downregulated FXR expression through the TGF β pathway. *Biomed. Res. Int.* 2020, 3516128. doi:10.1155/2020/3516128
- Zhong, J., Yu, R., Zhou, Q., Liu, P., Liu, Z., and Bian, Y. (2021). Naringenin prevents TNF- α -induced gut-vascular barrier disruption associated with inhibiting the NF- κ B-mediated MLCK/p-MLC and NLRP3 pathways. *Food Funct.* 12 (6), 2715–2725. doi:10.1039/d1fo00155h



OPEN ACCESS

EDITED BY

Shuai Wang,
Guangzhou University of Chinese
Medicine, China

REVIEWED BY

Xiaokang Wang,
Southern Medical University, China
Qiming MA,
Jinan University, China

*CORRESPONDENCE

Wei Wang,
nfmklysy@qq.com

[†]These authors have contributed equally
to this work

SPECIALTY SECTION

This article was submitted to
Inflammation Pharmacology,
a section of the journal
Frontiers in Pharmacology

RECEIVED 06 October 2022

ACCEPTED 27 October 2022

PUBLISHED 07 November 2022

CITATION

Huang R, Chen Y, Tu M and Wang W
(2022), Monocyte to high-density
lipoprotein and apolipoprotein A1 ratios
are associated with bone homeostasis
imbalance caused by chronic
inflammation in postmenopausal
women with type 2 diabetes mellitus.
Front. Pharmacol. 13:1062999.
doi: 10.3389/fphar.2022.1062999

COPYRIGHT

© 2022 Huang, Chen, Tu and Wang. This
is an open-access article distributed
under the terms of the [Creative
Commons Attribution License \(CC BY\)](#).
The use, distribution or reproduction in
other forums is permitted, provided the
original author(s) and the copyright
owner(s) are credited and that the
original publication in this journal is
cited, in accordance with accepted
academic practice. No use, distribution
or reproduction is permitted which does
not comply with these terms.

Monocyte to high-density lipoprotein and apolipoprotein A1 ratios are associated with bone homeostasis imbalance caused by chronic inflammation in postmenopausal women with type 2 diabetes mellitus

Rong Huang[†], Yang Chen[†], Mei Tu and Wei Wang*

Department of Endocrinology, Longyan First Affiliated Hospital of Fujian Medical University, Longyan, Fujian, China

Objective: Emerging evidences demonstrated that chronic inflammation can influence bone metabolism in type 2 diabetes mellitus (T2DM), leading to bone homeostasis imbalance. The aim of this study was to assess the correlations between novel pro-inflammatory indexes like monocyte to high-density lipoprotein (MHR), apolipoprotein A1 (MAR) ratios and bone mineral density (BMD), bone turnover markers in Chinese postmenopausal women with T2DM.

Method: In this study, a total of 619 participants with complete data were included in the final analysis. Demographic and anthropometric information was collected. Biochemical parameters and bone turnover markers were determined by standard methods. BMD was measured by dual-energy x-ray absorptiometry. Correlation analysis and regression models were conducted to assess the associations between MHR, MAR and bone turnover markers, BMD. Multiple binomial logistic regression model was used to estimate the independent variables of MHR and MAR for osteoporosis.

Results: Overall, the prevalence of osteoporosis was 38.3%. MHR and MAR were significantly correlated with C-terminal cross linking of type I collagen (β -CTX), L1-L4, femoral neck BMD and T scores. These correlations remained significant after adjustment for other confounding factors. Meanwhile, MHR and MAR were also significantly associated with higher odds of osteoporosis, the odds ratios (ORs) (95% CI) were 1.88 (1.49–2.38) and 2.30 (1.72–3.09) respectively. Furthermore, MHR and MAR seemed to have a good identifying value for osteoporosis. The area under the curve of MHR and MAR identifying osteoporosis were 0.791 (95% CI: 0.753–0.828) and 0.843 (95% CI: 0.809–0.877) respectively ($p < 0.001$). The optimal cut-off values of MHR and MAR were $4.53 \times 10^8/\text{mmol}$ (sensitivity: 60.8%, specificity: 85.9%) and $4.74 \times 10^8/\text{g}$ (sensitivity: 71.7%, specificity: 89.3%) respectively.

Conclusion: MHR and MAR were significantly associated with osteoporosis. These two novel pro-inflammatory indexes may be ideal markers to reflect

bone homeostasis imbalance caused by chronic inflammation in Chinese postmenopausal women with T2DM.

KEYWORDS

chronic inflammation, monocyte to high-density lipoprotein ratio, monocyte to apolipoprotein A1 ratio, bone homeostasis imbalance, type 2 diabetes mellitus

Introduction

Bones are important tissues belonged to dynamic and metabolically active tissues that can support the body and protect the internal organs. Bones experience a continuous cycle of bone remodeling and depend on the activity of osteoblasts and osteoclasts on the surface of the bones to keep balance between bone formation and resorption (Charles Julia and Aliprantis Antonios, 2014). This balance ensures bones can adapt to mechanical loads changes and minor damages. To our concerns, this balance can be easily upset by some diseases. Type 2 diabetes (T2DM) is a kind of metabolic and chronic inflammatory disease characterized by chronic hyperglycemia that can break the balance between bone formation and resorption. Epidemiological investigations found that T2DM can increase the risk of osteoporosis and bone fragility fractures, both of them are rapidly increasing (Bonds Denise et al., 2006; Li et al., 2019; Thong et al., 2021). Elevated advance glycation end products (AGEs), increased insulin resistance, dyslipidemia, obesity, and chronic inflammatory statuses caused by T2DM are the main underlying mechanisms for T2DM to increase the risk of osteoporosis and bone fragility fractures (McCarthy Antonio et al., 2004; Shapses Sue and Sukumar, 2012; Conte et al., 2018; Yin et al., 2019; Maruyama et al., 2020). Among these underlying mechanisms, chronic inflammation triggered by metabolic disorders plays important roles in bone metabolism, it can directly influence bone formation and resorption, leading to bone mass loss and osteoporosis (Adamopoulos Iannis, 2018).

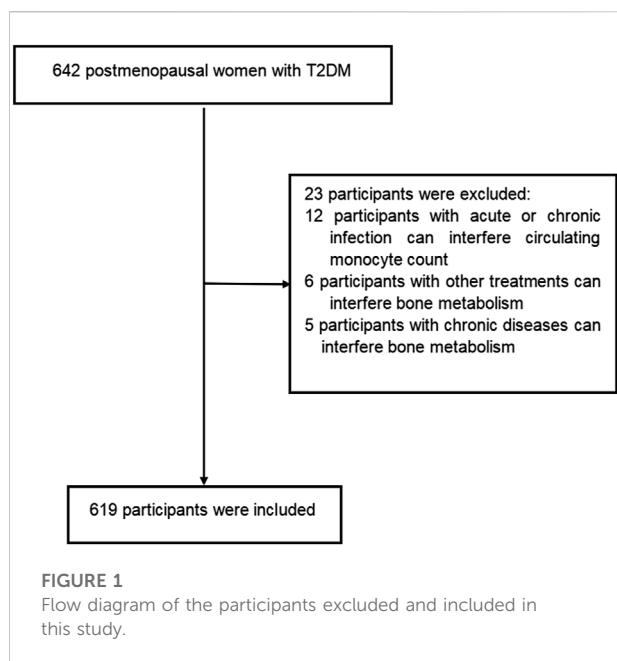
Monocyte are important innate immune cells produced in bone marrow and accumulated in circulatory system before migrating and differentiating into macrophages, it play functional roles in immune defense, chronic inflammation, and tissue remodeling (Orozco Susana et al., 2021). These biological features provide a basis for monocyte involved in the bone homeostasis imbalance caused by chronic inflammation. Besides dyslipidemia has the well recognized effects in promoting arteriosclerosis, more evidences also found that dyslipidemia was also associated with increased oxidative stress and systemic inflammation, leading to increased osteoclastic activity and decreased bone formation (Pelton et al., 2012). T2DM are often accompanied with dyslipidemia like increased low-density lipoprotein cholesterol (LDL-c) and decreased high-density lipoprotein cholesterol (HDL-c) and apolipoprotein A1 (APOA1). Recently, the ratios of monocyte to HDL-c (MHR) or APOA1 (MAR) have been

considered as pro-inflammatory indexes and were reported to have good predictive values for chronic low inflammatory diseases like peripheral artery disease (Selvaggio et al., 2020), polycystic ovarian syndrome (Kałużna et al., 2020) and nonalcoholic fatty liver disease (Wang et al., 2022). Based on the above studies, we can be hypothesized that MHR and MAR may be able to reflect bone homeostasis imbalance cause by chronic inflammation in T2DM. To prove this hypothesis, this cross-sectional study was aimed to assess the correlations between MHR, MAR and BMD, bone turnover markers in Chinese postmenopausal women with T2DM.

Study design and methods

Study design and participants

This cross-sectional study was conducted with postmenopausal women with T2DM from the Department of Endocrinology at the Longyan First Affiliated Hospital of Fujian Medical University who fulfilled the study criteria between January 2022 and June 2022. Participants were diagnosed with T2DM according to the World Health Organization criteria (2019 edition): 1) fasting plasma glucose ≥ 126 mg/dl or 2 h postprandial ≥ 200 mg/dl during oral glucose tolerance test or HbA1C $\geq 6.5\%$ or participants with classic symptoms of hyperglycemia or hyperglycemic crisis with random plasma glucose ≥ 200 mg/dl. 2) with diabetic autoimmune antibodies negative and exclude other specific types of diabetes. Participants with twelve consecutive months of amenorrhea was considered as postmenopausal women. Participants were excluded if they met the following criteria: 1) presence of acute or chronic infection, obvious liver or renal dysfunction, anemia, hemolytic diseases and bleeding that can interfere circulating monocyte count. 2) treatment with medications can interfere circulating monocyte count. 3) history of chronic diseases can interfere bone metabolism (i.e., renal, hepatic, cardiac, thyroid and rheumatic diseases). 4) current or prior use of drugs can interfere bone metabolism (i.e., glucocorticoids, anti-resorptive drugs, hormonal replacement therapy, calcium or vitamin D supplementation, anti-osteoporosis therapy, thiazolidinediones, and urate-lowering therapy). The prevalence of osteoporosis is about 30%–40% in postmenopausal women with T2DM. In present study, we estimated the sample size according to the requirement of multiple binomial logistic regression model. 12–15 variables may be put into the logistic regression



model. Based on the principle of 5–10 events per variable, we planned sample size is 500–600 participants. Overall, a total of 642 participants were screened. Among them, 619 participants met the inclusion and exclusion criteria were enrolled into this

study. The flow diagram of excluded and included participants was presented in Figure 1. All procedures were conducted in accordance with Declaration of Helsinki. This study was approved by the ethical committee of Longyan First Affiliated Hospital of Fujian Medical University (LY-2021–072). All participants provided informed consent.

Anthropometric and laboratory assessments

Demographic information was collected by trained interviewers through a standard questionnaire. A review of medical records and laboratory data were also conducted to obtain demographic information, including age, diabetes duration, history of disease, current or prior use of drugs, smoking, drinking, physic activity and menopausal status. Participants have any waking behaviors characterized by an energy expenditure ≤ 1.5 metabolic equivalents (e.g., watching television, reading, or reclining) were considered to have sedentary behavior (DiPietro et al., 2020). Participants smoke more than 4 cigarettes a week for at least 6 months continually or accumulative was considered as smoking (Organization, 1998). Participants drink more than once a year was considered as drinking (GBD 2016, 2018). Anthropometric examination was conducted by the research nurses, including height, weight and

TABLE 1 Clinical and laboratory characteristics of participants based on tertiles of MHR ($10^8/\text{mmol}$) and MAR ($10^8/\text{g}$).

Variable	Tertiles of MHR			P	Tertiles of MAR			P
	T1	T2	T3		T1	T2	T3	
Age (year)	55.7 \pm 6.3	56.4 \pm 6.8	55.4 \pm 5.1	0.230	55.1 \pm 7.1	56.1 \pm 5.3	56.3 \pm 5.8	0.123
Duration (year)	7.8 \pm 2.3	8.1 \pm 2.9	8.1 \pm 2.4	0.407	7.9 \pm 2.2	8.1 \pm 2.7	8.0 \pm 2.3	0.482
BMI(kg/m^2)	23.4 \pm 2.6 ^{ab}	24.1 \pm 2.5 ^{ac}	24.7 \pm 3.2 ^{bc}	<0.001	22.4 \pm 2.6 ^{ab}	24.2 \pm 2.4 ^{ac}	25.6 \pm 2.6 ^{bc}	<0.001
HbA1c (%)	9.0 \pm 1.3	8.8 \pm 1.2	8.9 \pm 1.0	0.218	9.0 \pm 1.2	8.8 \pm 1.2	8.9 \pm 1.1	0.392
TG (mmol/L)	1.3 \pm 0.9 ^{ab}	1.9 \pm 0.7 ^{ac}	3.3 \pm 1.5 ^{bc}	<0.001	1.3 \pm 0.7 ^{ab}	2.0 \pm 0.8 ^{ac}	3.1 \pm 1.3 ^{bc}	<0.001
TC (mmol/L)	5.1 \pm 1.2	5.0 \pm 1.2	5.1 \pm 1.1	0.408	5.1 \pm 1.3	5.1 \pm 1.2	5.0 \pm 1.1	0.503
HDL-c (mmol/L)	1.2 \pm 0.2 ^{ab}	1.1 \pm 0.2 ^{ac}	0.9 \pm 0.2 ^{bc}	<0.001	1.3 \pm 0.2 ^{ab}	1.0 \pm 0.2 ^{ac}	0.9 \pm 0.1 ^{bc}	<0.001
LDL-c (mmol/L)	3.6 \pm 1.0	3.5 \pm 1.0	3.6 \pm 1.0	0.378	3.5 \pm 1.0	3.6 \pm 0.9	3.6 \pm 1.0	0.503
APOA1 (g/L)	1.13 \pm 0.21 ^b	1.11 \pm 0.17 ^c	0.98 \pm 0.16 ^{bc}	<0.001	1.11 \pm 0.23 ^b	1.10 \pm 0.22 ^c	1.01 \pm 0.20 ^{bc}	<0.001
Monocyte ($10^8/\text{L}$)	3.5 \pm 0.7 ^{ab}	4.3 \pm 0.7 ^{ac}	4.8 \pm 0.8 ^{bc}	<0.001	3.6 \pm 0.6 ^{ab}	4.3 \pm 0.6 ^{ac}	4.7 \pm 0.7 ^{bc}	<0.001
UA (umol/L)	323 \pm 72 ^{ab}	353 \pm 77 ^{ac}	373 \pm 99 ^{bc}	<0.001	296 \pm 69 ^{ab}	369 \pm 73 ^{ac}	396 \pm 87 ^{bc}	<0.001
Creatinine (umol/L)	69.2 \pm 13.7	70.7 \pm 12.9	71.1 \pm 12.2	0.315	69.9 \pm 13.0	70.1 \pm 13.6	71.0 \pm 12.2	0.686
ALT (IU/L)	34.2 \pm 8.7	33.9 \pm 9.2	33.9 \pm 8.6	0.917	33.8 \pm 9.1	34.3 \pm 9.0	33.9 \pm 8.5	0.823
HOMA-IR	9.1 \pm 4.8 ^{ab}	10.8 \pm 5.3 ^{ac}	12.4 \pm 5.9 ^{bc}	<0.001	7.6 \pm 4.7 ^{ab}	11.2 \pm 4.7 ^{ac}	13.6 \pm 5.4 ^{bc}	<0.001
Hypertension, n (%)	61 (29.5) ^b	72 (35.0) ^c	124 (60.2) ^{bc}	<0.001	42 (20.3) ^{ab}	71 (33.8) ^{ac}	143 (70.8) ^{bc}	<0.001
Smoking, n (%)	4 (1.9)	7 (3.4)	7 (3.4)	0.592	5 (2.4)	7 (3.4)	6 (3.0)	0.854
Drinking, n (%)	35 (16.9)	33 (16.0)	33 (16.0)	0.961	32 (15.5)	40 (19.0)	29 (14.4)	0.401
Sedentary behavior, n (%)	52 (25.1)	63 (30.6)	65 (31.6)	0.300	56 (27.1)	58 (27.6)	66 (32.7)	0.388

BMI, body mass index; HbA1c, Glycated hemoglobin. UA, uric acid. TG, triglyceride. TC, total cholesterol. HDL-c, high-density lipoprotein cholesterol. LDL-c, Low density lipoprotein cholesterol. SBP: Systolic blood pressure. DBP: Diastolic blood pressure. HOMR-IR: Homeostasis model assessment insulin resistance. ^aP < 0.05; T1 vs. T2. ^bP < 0.05; T1 vs. T3. ^cP < 0.05; T2 vs. T3.

TABLE 2 Bone turnover markers and bone mineral density of participants based on tertiles of MHR ($10^8/\text{mmol}$) and MAR ($10^8/\text{g}$).

Variable	Tertiles of MHR			P	Tertiles of MAR			P
	T1	T2	T3		T1	T2	T3	
OC(ng/ml)	14.8 ± 6.9	15.6 ± 6.8	15.3 ± 7.1	0.503	15.1 ± 6.7	15.4 ± 7.0	15.4 ± 7.2	0.872
β-CTX (ng/ml)	0.42 ± 0.19 ^{ab}	0.47 ± 0.18 ^{ac}	0.52 ± 0.16 ^{bc}	<0.001	0.43 ± 0.19 ^{ab}	0.47 ± 0.18 ^{ac}	0.51 ± 0.16 ^{bc}	<0.001
25-OH-D (nmol/L)	66.6 ± 11.6	67.0 ± 12.0	68.9 ± 13.1	0.121	67.7 ± 12.3	67.3 ± 12.0	67.4 ± 12.7	0.939
iPTH(ng/L)	35.1 ± 12.9	34.0 ± 14.0	32.9 ± 10.8	0.229	33.2 ± 12.8	34.6 ± 13.0	34.2 ± 12.6	0.425
ALP(IU/L)	80.5 ± 20.9	81.1 ± 18.2	80.0 ± 17.9	0.839	79.0 ± 20.0	81.0 ± 18.2	81.6 ± 18.9	0.351
Calcium (mmol/L)	2.32 ± 0.10	2.33 ± 0.10	2.31 ± 0.12	0.365	2.32 ± 0.11	2.32 ± 0.11	2.31 ± 0.11	0.793
Phosphorous (mmol/L)	1.22 ± 0.18	1.22 ± 0.17	1.22 ± 0.17	0.951	1.23 ± 0.19	1.22 ± 0.14	1.21 ± 0.18	0.251
L1-L4 BMD(g/cm ³)	0.94 ± 0.13 ^{ab}	0.88 ± 0.10 ^{ac}	0.83 ± 0.09 ^{bc}	<0.001	0.95 ± 0.13 ^{ab}	0.88 ± 0.10 ^{ac}	0.82 ± 0.09 ^{bc}	<0.001
L1-L4 T-score	-1.3 ± 1.1 ^{ab}	-1.8 ± 0.8 ^{ac}	-2.2 ± 0.8 ^{bc}	<0.001	-1.2 ± 1.1 ^{ab}	-1.8 ± 0.7 ^{ac}	-2.3 ± 0.7 ^{bc}	<0.001
Hip BMD(g/cm ³)	0.82 ± 0.09	0.84 ± 0.10	0.83 ± 0.12	0.543	0.83 ± 0.12	0.83 ± 0.07	0.83 ± 0.13	0.876
Hip T-score	-1.2 ± 0.6	-1.1 ± 0.7	-1.2 ± 0.7	0.617	-1.2 ± 0.5	-1.2 ± 0.6	-1.2 ± 0.8	0.894
Femoral neck BMD(g/cm ³)	0.76 ± 0.24 ^{ab}	0.70 ± 0.26 ^{ac}	0.65 ± 0.13 ^{bc}	<0.001	0.77 ± 0.24 ^{ab}	0.71 ± 0.26 ^{ac}	0.63 ± 0.13 ^{bc}	<0.001
Femoral neck T-score	-0.9 ± 0.5 ^{ab}	-1.3 ± 0.7 ^{ac}	-1.6 ± 0.8 ^{bc}	<0.001	-0.8 ± 0.5 ^{ab}	-1.2 ± 0.7 ^{ac}	-1.7 ± 0.8 ^{bc}	<0.001
Osteoporosis, n (%)	23 (11.1)	68 (33.0)	146 (70.9)	<0.001	22 (10.6)	49 (23.3)	166 (82.2)	<0.001

OC, osteocalcin. β-CTX, β-cross-linked C-telopeptide of type I collagen (β-CTX). 25-OH-D: 25 hydroxyvitamin D. iPTH: intact parathyroid hormone. ALP, alkaline phosphatase. BMD, bone mineral density. ^aP<0.05: T1 vs. T2. ^bP<0.05: T1 vs. T3. ^cP<0.05: T2 vs T3.

blood pressure (BP). Participants wear hospital gowns and had bare feet. BMI was calculated as the weight divided by the square of height (kg/m²). Systolic and diastolic blood pressure (SBP and DBP) were measured by an electronic sphygmomanometer with an appropriate cuff size after the participants taking a rest for more than 5 min. Participants with anti-hypertensive therapy or three times measurements of SBP≥140 mmHg or

DBP ≥90 mmHg on different days was considered to have hypertension.

Laboratory assessments were conducted according to standard methods using fasting venous blood samples that were taken between 8 and 9 a.m. after fasting overnight. Serum levels of the following variables were determined: creatinine, alanine aminotransferase (ALT), uric acid (UA), fasting blood glucose (FBG), serum insulin, HbA1c, diabetic autoimmune antibodies (GADA, IAA, and ICA), HDL-c, low density lipoprotein (LDL-c), triglycerides (TGs), APOA1, calcium, phosphorous, alkaline phosphatase (ALP), high sensitivity C-reactive protein (hs-CRP), complete blood count, thyroid stimulating hormone (TSH) and bone turnover markers like osteocalcin (OC), β-cross-linked C-telopeptide of type I collagen (β-CTX), intact parathyroid hormone (iPTH) and 25 hydroxyvitamin D (25-OH-D). Biochemical indexes were measured by an auto-biochemical analyzer (Roche Diagnostics Corporation). ApoA1 levels were measured by the polyethylene glycol-enhanced immunoturbidimetric assay (Maker, Chengdu, China). HbA1c was evaluated by high performance liquid chromatography with a D10 set (Bio-RAD). Complete blood count were measured by Coulter LH 780 Analyzer (Beckman Coulter Ireland, Galway, Ireland). Bone turnover markers were measured by electro-chemiluminescence immunoassay method (Roche Diagnostics GmbH, Germany). Homeostasis model assessment (HOMA-IR) was calculated with the formula: fasting serum insulin (μU/ml) x fasting plasma glucose (mmol/L)/22.5 (Bonora et al., 2000). The monocyte count divided by HDL-c or APOA1 level were calculated as MHR or MAR.

TABLE 3 Correlations between MHR, MAR and bone turnover markers, bone mineral density.

Variable	MHR		MAR	
	R	P	R	P
OC(ng/ml)	0.018	0.660	0.015	0.714
β-CTX (ng/ml)	0.163	<0.001	0.186	<0.001
25-OH-D (nmol/L)	0.072	0.079	-0.044	0.271
iPTH(ng/L)	-0.073	0.072	0.025	0.533
ALP(IU/L)	0.007	0.867	0.058	0.234
Calcium (mmol/L)	0.023	0.565	0.002	0.959
Phosphorous (mmol/L)	0.043	0.283	-0.010	0.795
L1-L4 BMD(g/cm ³)	-0.285	<0.001	-0.379	<0.001
L1-L4 T-score	-0.318	<0.001	-0.415	<0.001
Hip BMD(g/cm ³)	0.016	0.692	0.005	0.911
Hip T-score	0.011	0.782	0.006	0.927
Femoral neck BMD(g/cm ³)	-0.321	<0.001	-0.298	<0.001
Femoral neck T-score	-0.343	<0.001	-0.318	<0.001

OC, osteocalcin. β-CTX, β-cross-linked C-telopeptide of type I collagen (β-CTX). 25-OH-D: 25 hydroxyvitamin D. iPTH: intact parathyroid hormone. ALP, alkaline phosphatase. BMD, bone mineral density.

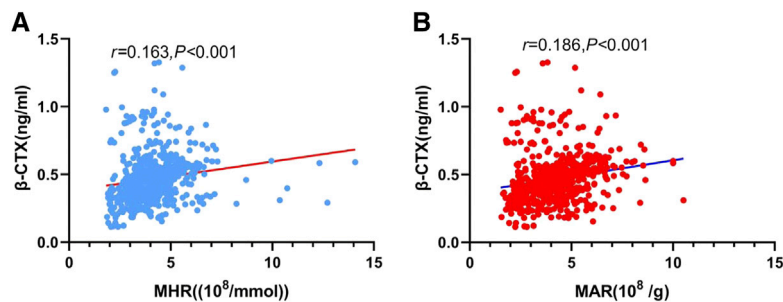


FIGURE 2
Correlation analysis showing positive correlation between β -CTX and MHR (A), MAR (B).

TABLE 4 Multivariate linear regression analysis of associations between MHR, MAR and bone turnover markers, bone mineral density.

Variable	MHR		MAR	
	β	P	β	P
β -CTX (ng/ml)				
Model 1	0.132	0.002	0.279	<0.001
Model 2	0.148	<0.001	0.275	<0.001
L1-L4 BMD(g/cm ³)				
Model 1	-0.241	<0.001	-0.394	<0.001
Model 3	-0.231	<0.001	-0.326	<0.001
L1-L4 T-score				
Model 1	-0.231	<0.001	-0.375	<0.001
Model 3	-0.220	<0.001	-0.294	<0.001
Femoral neck BMD(g/cm ³)				
Model 1	-0.196	<0.001	-0.303	<0.001
Model 3	-0.177	<0.001	-0.249	<0.001
Femoral neck T-score				
Model 1	-0.203	<0.001	-0.291	<0.001
Model 3	-0.186	<0.001	-0.256	<0.001

Model 1:Adjusted for age, diabetes duration,A1c, BMI, TG, HDL-c, LDL-c, creatinine, ALT,UA,HOMA-IR,hypertension, sedentary behavior, smoking and drinking. Model 2: Additional adjustment for bone turnover markers, such as OC,25-OH-D₃iPTH,ALP, calcium and phosphorous based on Model 1. Model 3: Additional adjustment for β -CTX based on Model 2.

TABLE 5 Binomial Logistic Regression Analysis adjusted ORs (95% CIs) for the associations between MHR, MAR and the risk of osteoporosis.

Models	MHR		MAR	
	OR (95%CI)	P	OR (95%CI)	P
Model 4	2.82 (2.28–3.49)	<0.001	3.56 (2.83–4.49)	<0.001
Model 5	1.92 (1.52–2.44)	<0.001	2.68 (2.03–3.55)	<0.001
Model 6	1.88 (1.49–2.38)	<0.001	2.30 (1.72–3.09)	<0.001

Model 4:Adjustment for age, diabetes duration, hypertension, sedentary behavior, smoking and drinking. Model5:Additionally adjustment for BMI,HbA1c, BMI, TG, HDL-c, LDL-c, creatinine, ALT,UA,HOMA-IR.Model 6:Additional adjustment for bone turnover markers, such as OC, β -CTX, 25-OH-D₃i PTH, ALP, calcium and phosphorous based on Model 5. MHR:monocyte to HDL-c ratio. MAR:monocyte to ApoA1 ratio.

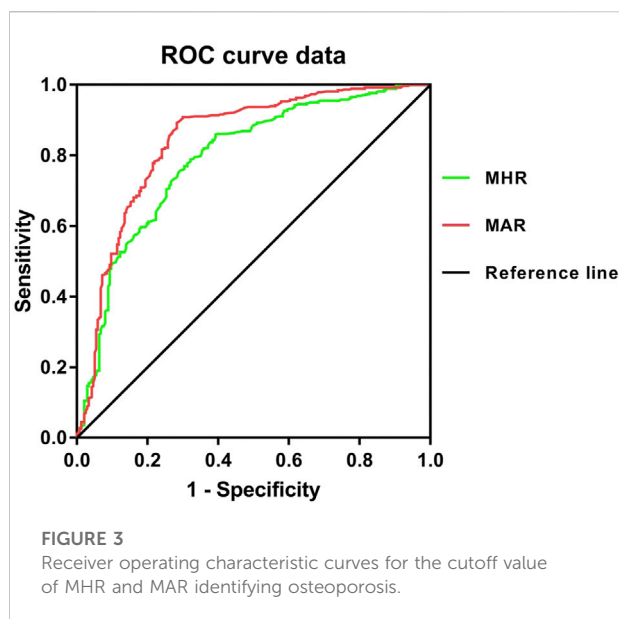
densitometry reference value. Longitudinal quality control checks were performed daily using whole-body and L1-L4 lumbar spine phantom provided by the manufacturer. Cross-calibration was performed weekly to monitor variations between the systems. The precision error was 1.0% for the BMD measurement. Postmenopausal women with T score \leq -2.5 or a history of bone fragility fractures was considered to have osteoporosis.

Statistical analysis

Data were analyzed by using the SPSS 23.0 software (SPSS Inc. IBM). Descriptive data were expressed as means \pm standard deviation (SD). Discrete variables were summarized in frequency tables (N, %). Statistical differences among groups were performed with one-way analysis of variance (ANOVA) followed by Turkey test for multiple comparisons. The chi-squared (χ^2) test or Fisher exact test were used for comparison of categorical variables. The correlations between

Assessment of bone mineral density

Participants were performed with BMD examination by dual-energy X-ray absorptiometry (Hologic, Marlborough, MA, United States) in a supine position. The BMD measurement areas consist of lumbar spine (L1-L4), total hip and femoral neck. The densitometry scanning was performed by experienced radiographers who were blinded to clinical information. T-score was calculated according to Hologic



MAR, MHR and bone turnover markers, BMD were performed by Pearson or Spearman correlation analysis. Multiple regression analysis was used to estimate independent associations between MHR, MAR and bone turnover markers, BMD after adjusting for potential confounding factors. Multiple binomial logistic regression model was used to estimate the independent variables of MHR and MAR for osteoporosis after adjusting for other covariates. The receiver operating characteristic (ROC) curves was used to assess the identifying value of MHR and MAR for osteoporosis. Optimal cut-off value was based on the greatest value of the Youden's index. A two-tailed value of $p < 0.05$ was considered statistically significant.

Results

Overall, a total of 619 participants with complete data were included in the final analysis, whose mean age was 55.8 ± 6.1 years and diabetes duration was 7.9 ± 2.4 years. Clinical and laboratory characteristics of participants based on tertiles of MHR and MAR were summarized in Table 1. There were no significant differences in level of age, diabetes duration, TC, LDL-c, creatinine, ALT and the percentage of participants with smoking, drinking and sedentary behavior across the MHR and MAR tertiles ($p > 0.05$). Increasing trends were observed in BMI, TG, UA, HOMA-IR and monocyte count across the MHR and MAR tertile ($p < 0.05$). Decreasing trends were also observed in HDL-c and APOA1 across the MHR and MAR tertile ($p < 0.05$). Furthermore, participants in higher tertile of MHR and MAR groups showed higher prevalence of hypertension ($p < 0.05$). Bone turnover markers and BMD of participants based on tertiles of MHR and MAR were presented in Table 2. The

prevalence of osteoporosis was 38.3%. As we had expected, increasing trend was observed in β -CTX. Decreasing trends were also observed in L1-L4 BMD, L1-L4 T-score, femoral neck BMD and femoral neck T-score ($p < 0.05$). In addition, participants in higher tertile of MHR and MAR groups showed higher prevalence of osteoporosis ($p < 0.05$).

The main correlations between MHR, MAR and bone turnover markers, bone mineral density were presented in Table 3. The results showed that β -CTX was positively correlated with MHR (Figure 2A) and MAR (Figure 2B). Furthermore, MHR and MAR were also negatively correlated with L1-L4 BMD, L1-L4 T-score, femoral neck BMD and femoral neck T-score ($p < 0.05$). Whereas no significant associations were observed between MHR, MAR and OC, ALP, 25-OH-D, iPTH, calcium, phosphorous, hip BMD and T-score. To determine independent variables of MHR and MAR for β -CTX, L1-L4 BMD, L1-L4 T-score, femoral neck BMD and femoral neck T-score, multiple linear regression analysis was also performed (Table 4). The results showed that MHR and MAR were positively correlated with β -CTX and were negatively correlated with L1-L4 BMD, L1-L4 T-score, femoral neck BMD and femoral neck T-score after adjustment for clinical variables like age, diabetes duration, BMI, TC, TG, LDL-c, creatinine, ALT, UA, hypertension, smoking, drinking and sedentary behavior (Model 1). Furthermore, MHR and MAR remain significantly correlated with β -CTX, L1-L4 BMD, L1-L4 T-score, femoral neck BMD and femoral neck T-score after additional adjustment for bone turnover markers like OC, 25-OH-D, ALP, iPTH, calcium, phosphorous (Model 2) and β -CTX (Model 3).

Binomial logistic regression analysis was also conducted to assess the independent variables of MHR and MAR for osteoporosis. As shown in Table 5, the MHR and MAR were shown to be independently associated with osteoporosis after adjustment for age, diabetes duration, hypertension, sedentary behavior, smoking and drinking (Model 4), the ORs (95%CI) were 2.82 (2.28–3.49) and 3.56 (2.83–4.49) respectively. Significant associations between MHR, MAR and osteoporosis were also observed after further adjustment for BMI, HbA1c, BMI, TG, HDL-c, LDL-c, creatinine, ALT, UA, HOMA-IR (Model 5), the ORs (95%CI) were 1.92 (1.52–2.44) and 2.68 (2.03–3.55) respectively. In addition, the ORs remain significant after further adjustment for bone turnover markers like OC, β -CTX, 25-OH-D, iPTH, ALP, calcium and phosphorous (Model 6), the ORs (95%CI) were 1.88 (1.49–2.38) and 2.30 (1.72–3.09) respectively.

From the ROC curve analysis, the results seemed to have a good identifying value of MHR and MAR for osteoporosis. The AUC of MHR and MAR identifying osteoporosis were 0.791 (95% CI: 0.753–0.828, $p < 0.001$) and 0.843 (95% CI: 0.809–0.877, $p < 0.001$) respectively (Figure 3). The optimal cut-off values of MHR and MAR were $4.53 \times 10^8/\text{mmol}$ (sensitivity: 60.8%,

TABLE 6 ROC Curve Analysis of MHR and MAR in identifying osteoporosis.

Variables	AUC(95% CI)	Cut-off value	Sensitivity (%)	Specificity (%)
MHR (10 ⁸ /mmol)	0.791 (0.753–0.828)	4.53	60.8	85.9
MAR (10 ⁸ /g)	0.843 (0.809–0.877)	4.74	71.7	89.3

MHR, monocyte to HDL-c ratio. MAR, monocyte to ApoA1 ratio.

specificity: 85.9%) and $4.74 \times 10^8/\text{g}$ (sensitivity: 71.7%, specificity: 89.3%) respectively (Table 6).

Discussion

Osteoporosis and T2DM have become major public health concerns in increasingly aging population, both of them are closely associated with severe morbidity and increased mortality. As the main risk factor of osteoporosis and bone fragility fractures, chronic low inflammation caused by T2DM can directly influence bone homeostasis. In this cross-sectional study, we mainly assessed the correlations between pro-inflammatory indexes of MHR, MAR and bone turnover markers, BMD in Chinese postmenopausal women with T2DM. The results in our study showed that MHR and MAR were positively associated with β -CTX and negatively associated with L1-L4 and femoral neck BMD after adjustment for other confounding factors. Moreover, MHR and MAR were also independently associated with higher odds of osteoporosis and seemed to have a good identifying value for osteoporosis.

Emerging evidences showed that chronic metabolic disorders can trigger inflammatory responses as a mechanism for coping with metabolic changes, leading to chronic inflammation occurred (Zhang et al., 2012). Clinical studies also observed a concurrent increase in circulating inflammatory cytokines in T2DM. The persistent hyperglycaemia can alter the release and functionality of inflammatory cytokines like interleukin 1 (IL-1), interleukin 6 (IL-6) and tumour necrosis factor- α (TNF- α) (Degirmenci et al., 2019), leading to an increase in T2DM. In addition, all these cytokines can increase the risk of osteoporosis and bone fragility fractures, and mediate certain aspects of bone physiology via nuclear factor kappa-light-chain enhancer of activated B cells pathway (Liu and Zhang, 2015). In the process of chronic inflammation, monocyte play an important role in initiating and up-regulating inflammatory responses. Monocyte are produced from bone marrow and accumulated in circulatory system, it can stimulate the immune system and increase inflammatory responses by releasing inflammatory cytokines like TNF- α , IL-6 and monocyte chemoattractant protein-1 (Ghanim et al., 2004; Orozco Susana et al., 2021). Clinical studies also observed that inflammatory and hyperglycemic environment caused by T2DM can increase the peripheral total monocyte counts compared with healthy

population (Tsai Jack et al., 2007; Gonzalez et al., 2012). Bala MM et al. enrolled 112 participants with obesity found that circulating monocyte count is negatively correlated with BMD in children and adolescents with obesity (Bala and Bala, 2022). These biological features and clinical findings provide a basis for monocyte to be a ideal inflammatory marker component for chronic inflammation caused by T2DM.

Dyslipidemia is another kind of metabolic disorders occurred in T2DM with increased LDL-c and decreased HDL-c and its major apolipoproteins (APOA1). The decrease of HDL-c and its major apolipoproteins (APOA1) was also reported to be associated with increased oxidative stress and systemic inflammation. HDL-c and APOA1 are clusters of “good cholesterol” can bind lipid molecules and participate in the process of cholesterol clearance. Both of them were also thought to have anti-oxidant and anti-inflammatory properties. Recent advances in lipoprotein highlighted the important roles of HDL-c in bone metabolism. HDL-c and its major apolipoproteins (APOA1) were reported to have a direct interaction effect on osteoblasts and osteoclasts in experimental mouse models (Triantaphyllidou et al., 2013). Clinical studies also found that HDL-c can directly interact with osteoblasts and osteoclasts, whereas there is no single consensus has been reached on the correlation between HDL-c and BMD, and this correlation may vary by race and hormonal status. The vast majority of studies in Asian postmenopausal women reported that HDL-c is positively associated with lumbar spine BMD (Yamaguchi et al., 2002; Jeon Yun et al., 2011; Li et al., 2015). It can be assumed that the MHR and MAR may be ideal inflammatory markers to reflect bone homeostasis imbalance caused by chronic inflammation in bone micro-environment.

β -CTX is a fragment of medium collagen degraded and released into the blood during bone remodeling, it can reflect the degree of bone resorption and bone loss, it has been considered as a marker of increased osteoclast activity. Most studies reported chronic inflammation in bone micro-environment can enhance osteoclast activity, leading to an increase in β -CTX (Eleftheriadis et al., 2008). In present study, the results confirmed our hypothesis, MHR and MAR were positively associated with β -CTX after adjustment for other confounding factors. Despite the BMD T-score may underestimate fracture risk in T2DM, while the detection of BMD by DXA does predict fracture risk in clinical practice

(Schwartz et al., 2011). Previous studies reported an increase risk of vertebral and femoral neck fractures in T2DM. In our study, we also found that MHR and MAR were negatively associated with L1-L4 and femoral neck BMD. These findings may indicate us that MHR and MAR can reflect bone homeostasis imbalance caused by chronic inflammation. Clinical studies observed MHR and MAR have good predictive values for chronic low inflammatory diseases like peripheral artery disease (Selvaggio et al., 2020), polycystic ovarian syndrome (Kałużna et al., 2020), nonalcoholic fatty liver disease (Wang et al., 2022), metabolic syndrome (Uslu Ali et al., 2018), central retinal artery occlusion (Guven and Kilic, 2021), unstable angina (Zhang et al., 2016) and parkinson's disease (Liu et al., 2021). To our surprise, the results in our study also found that MHR and MAR were not only a independent risk factor of osteoporosis, they were also seemed to have a good identifying value for osteoporosis with relatively high AUC values of 0.791 and 0.843. MHR and MAR may be potential indicators of osteoporosis for Chinese postmenopausal women with T2DM, whereas more longitudinal studies are need to further confirm these findings.

To our knowledge, our study firstly put insights into the associations between pro-inflammatory indexes (MHR and MAR) and bone turnover markers, BMD in Chinese postmenopausal women with T2DM. Meanwhile, some limitations are need to be mentioned. Despite this study adjusted several potential confounding variables in final analysis and included enough sample size can represent the Chinese newly diagnosed T2DM population, while this study was designed as a cross-sectional study without follow up, it can not directly reflect the associations between MHR, MAR and bone turnover markers, BMD. Second, due to the study population are Chinese postmenopausal women with T2DM, the associations in our studies may be not applicable to other races and hormonal status.

In conclusion, this study found that novel pro-inflammatory indexes of MHR and MAR were associated with bone resorption marker of β -CTX, L1-L4 and femoral neck BMD. In addition, MHR and MAR were also independently associated with osteoporosis and seemed to have a good identifying value for osteoporosis. These findings may indicate us MHR and MAR are ideal pro-inflammatory markers to reflect bone homeostasis imbalance caused by chronic inflammation in bone micro-environment in Chinese postmenopausal women with T2DM,

whereas more studies with enough follow-up are need to further evaluate these findings and illustrate the underlying mechanisms.

Data availability statement

The original contributions presented in the study are included in the article/Supplementary Material, further inquiries can be directed to the corresponding author.

Ethics statement

The studies involving human participants were reviewed and approved by the ethical committee of Longyan First Affiliated Hospital of Fujian Medical University. The ethics committee waived the requirement of written informed consent for participation.

Author contributions

RH took charge of the software and contributed to writing and original draft. WW, YC, and MT conducted the investigation. WW contributed to data curation and writing-editing. All authors contributed to the article and approved the submitted version.

Conflict of interest

The authors declare that the research was conducted in the absence of any commercial or financial relationships that could be construed as a potential conflict of interest.

Publisher's note

All claims expressed in this article are solely those of the authors and do not necessarily represent those of their affiliated organizations, or those of the publisher, the editors and the reviewers. Any product that may be evaluated in this article, or claim that may be made by its manufacturer, is not guaranteed or endorsed by the publisher.

References

- Adamopoulos Iannis, E. (2018). Inflammation in bone physiology and pathology. *Curr. Opin. Rheumatol.* 30, 59–64. doi:10.1097/BOR.0000000000000449
- Bala, M. M., and Bala, K. A. (2022). Bone mineral density and complete blood count ratios in children and adolescents with obesity. *Eur. Rev. Med. Pharmacol. Sci.* 26, 249–256. doi:10.26355/eurrev_202201_27775
- Bonds Denise, E., Larson Joseph, C., Schwartz Ann, V., Strotmeyer, E. S., Robbins, J., Rodriguez, B. L., et al. (2006). Risk of fracture in women with type 2 diabetes: The women's health initiative observational study. *J. Clin. Endocrinol. Metab.* 91, 3404–3410. doi:10.1210/jc.2006-0614
- Bonora, E., Targher, G., Alberiche, M., Bonadonna, R. C., Saggiani, F., Zenere, M. B., et al. (2000). Homeostasis model assessment closely mirrors

the glucose clamp technique in the assessment of insulin sensitivity: Studies in subjects with various degrees of glucose tolerance and insulin sensitivity. *Diabetes Care* 23 (1), 57–63. doi:10.2337/diacare.23.1.57

Charles Julia, F., and Aliprantis Antonios, O. (2014). Osteoclasts: More than 'bone eaters'. *Trends Mol. Med.* 20, 449–459. doi:10.1016/j.molmed.2014.06.001

Conte, C., Epstein, S., and Napoli, N. (2018). Insulin resistance and bone: A biological partnership. *Acta Diabetol.* 55, 305–314. doi:10.1007/s00592-018-1101-7

Degirmenci, I., Ozbayer, C., Kebapci Medine, N., Kurt, H., Colak, E., and Gunes, H. V. (2019). Common variants of genes encoding TLR4 and TLR4 pathway members TIRAP and IRAK1 are effective on MCP1, IL6, IL1 β , and TNF α levels in type 2 diabetes and insulin resistance. *Inflamm. Res.* 68, 801–814. doi:10.1007/s00011-019-01263-7

DiPietro, L., Al-Ansari Salih, S., Biddle Stuart, J. H., Borodulin, K., Bull, F. C., Buman, M. P., et al. (2020). Advancing the global physical activity agenda: Recommendations for future research by the 2020 WHO physical activity and sedentary behavior guidelines development group. *Int. J. Behav. Nutr. Phys. Act.* 17, 143. doi:10.1186/s12966-020-01042-2

Eleftheriadis, T., Kartsios, C., Antoniadis, G., Kazila, P., Dimitriadou, M., Sotiriadou, E., et al. (2008). The impact of chronic inflammation on bone turnover in hemodialysis patients. *Ren. Fail.* 30, 431–437. doi:10.1080/08860220801964251

GBD 2016 (2018). Alcohol use and burden for 195 countries and territories, 1990–2016: A systematic analysis for the global burden of disease study 2016. *Lancet* 392, 1015–1035. doi:10.1016/S0140-6736(18)31310-2

Ghanim, H., Aljada, A., Hofmeyer, D., Syed, T., Mohanty, P., and Dandona, P. (2004). Circulating mononuclear cells in the obese are in a proinflammatory state. *Circulation* 110, 1564–1571. doi:10.1161/01.CIR.0000142055.53122.FA

Gonzalez, Y., Herrera, M. T., Soldevila, G., Garcia-Garcia, L., Fabian, G., Perez-Armendariz, E. M., et al. (2012). High glucose concentrations induce TNF- α production through the down-regulation of CD33 in primary human monocytes. *BMC Immunol.* 13, 19. doi:10.1186/1471-2172-13-19

Guyen, S., and Kilic, D. (2021). Neutrophil to lymphocyte ratio (NLR) is a better tool rather than monocyte to high-density lipoprotein ratio (MHR) and platelet to lymphocyte ratio (PLR) in central retinal artery occlusions. *Ocul. Immunol. Inflamm.* 29, 997–1001. doi:10.1080/09273948.2020.1712433

Jeon, Y. K., Lee, J. G., Kim, S. S., Kim, B. H., Kim, Y. K., et al. (2011). Association between bone mineral density and metabolic syndrome in pre- and postmenopausal women. *Endocr. J.* 58, 87–93. doi:10.1507/endocrj.k10e-297

Kaluza, M., Czapka-Matysik, M., Wachowiak-Ochmańska, K., Moczek, J., Kaczmarek, J., Janicki, A., et al. (2020). Effect of central obesity and hyperandrogenism on selected inflammatory markers in patients with PCOS: A WHR-matched case-control study. *J. Clin. Med.* 9, E3024. doi:10.3390/jcm9093024

Li, G., Prior Jerilynn, C., Leslie William, D., Thabane, L., Papaioannou, A., Josse, R. G., et al. (2019). Frailty and risk of fractures in patients with type 2 diabetes. *Diabetes Care* 42, 507–513. doi:10.2337/dc18-1965

Li, S., Guo, H., Liu, Y., Wu, F., Zhang, H., Zhang, Z., et al. (2015). Relationships of serum lipid profiles and bone mineral density in postmenopausal Chinese women. *Clin. Endocrinol.* 82, 53–58. doi:10.1111/cen.12616

Liu, W., and Zhang, X. (2015). Receptor activator of nuclear factor- κ B ligand (RANKL)/RANK/osteoprotegerin system in bone and other tissues (review). *Mol. Med. Rep.* 11, 3212–3218. doi:10.3892/mmr.2015.3152

Liu, Z., Fan, Q., Wu, S., Wan, Y., and Lei, Y. (2021). Compared with the monocyte to high-density lipoprotein ratio (MHR) and the neutrophil to lymphocyte ratio (NLR), the neutrophil to high-density lipoprotein ratio (NHR) is more valuable for assessing the inflammatory process in Parkinson's disease. *Lipids Health Dis.* 20, 35. doi:10.1186/s12944-021-01462-4

Maruyama, M., Rhee, C., Utsunomiya, T., Zhang, N., Ueno, M., Yao, Z., et al. (2020). Modulation of the inflammatory response and bone healing. *Front. Endocrinol.* 11, 386. doi:10.3389/fendo.2020.00386

McCarthy Antonio, D., Uemura, T., Etcheverry, S. B., and Cortizo, A. M. (2004). Advanced glycation endproducts interfere with integrin-mediated osteoblastic attachment to a type-I collagen matrix. *Int. J. Biochem. Cell. Biol.* 36, 840–848. doi:10.1016/j.biocel.2003.09.006

Organization, W. H. (1998). *Guidelines for controlling and monitoring the tobacco epidemic*. Geneva, Switzerland: World Health Organization, 1–190.

Orozco Susana, L., Canny Susan, P., and Hamerman Jessica, A. (2021). Signals governing monocyte differentiation during inflammation. *Curr. Opin. Immunol.* 73, 16–24. doi:10.1016/j.coi.2021.07.007

Pelton, K., Krieder, J., Joiner, D., Freeman, M. R., Goldstein, S. A., and Solomon, K. R. (2012). Hypercholesterolemia promotes an osteoporotic phenotype. *Am. J. Pathol.* 181, 928–936. doi:10.1016/j.ajpath.2012.05.034

Schwartz, A. V., Vittinghoff, E., Bauer, D. C., Hillier, T. A., Strotmeyer, E. S., Ensrud, K. E., et al. (2011). Association of BMD and FRAX score with risk of fracture in older adults with type 2 diabetes. *JAMA* 305, 2184–2192. doi:10.1001/jama.2011.715

Selvaggio, S., Abate, A., Brugaletta, G., Musso, C., Di Guardo, M., Di Guardo, C., et al. (2020). Platelet-to-lymphocyte ratio, neutrophil-to-lymphocyte ratio and monocyte-to-HDL cholesterol ratio as markers of peripheral artery disease in elderly patients. *Int. J. Mol. Med.* 46, 1210–1216. doi:10.3892/ijmm.2020.4644

Shapses Sue, A., and Sukumar, D. (2012). Bone metabolism in obesity and weight loss. *Annu. Rev. Nutr.* 32, 287–309. doi:10.1146/annurev.nutr.012809.104655

Thong, E. P., Milat, F., Enticott, J. C., Joham, A. E., Ebeling, P. R., Mishra, G. D., et al. (2021). The diabetes-fracture association in women with type 1 and type 2 diabetes is partially mediated by falls: A 15-year longitudinal study. *Osteoporos. Int.* 32, 1175–1184. doi:10.1007/s00198-020-05771-9

Triantaphyllidou, I.-E., Kalyvioti, E., Karavia, E., Lill, I., Kypreos, K. E., and Papachristou, D. J. (2013). Perturbations in the HDL metabolic pathway predispose to the development of osteoarthritis in mice following long-term exposure to western-type diet. *Osteoarthr. Cartil.* 21, 322–330. doi:10.1016/j.joca.2012.11.003

Tsai Jack, C.-R., Sheu, S.-H., Chiu, H.-C., Chung, F. M., Chang, D. M., Chen, M. P., et al. (2007). Association of peripheral total and differential leukocyte counts with metabolic syndrome and risk of ischemic cardiovascular diseases in patients with type 2 diabetes mellitus. *Diabetes. Metab. Res. Rev.* 23, 111–118. doi:10.1002/dmrr.647

Uslu Ali, U., Sekin, Y., Tarhan, G., Canakci, N., Gunduz, M., and Karagulle, M. (2018). Evaluation of monocyte to high-density lipoprotein cholesterol ratio in the presence and severity of metabolic syndrome. *Clin. Appl. Thromb. Hemost.* 24, 828–833. doi:10.1177/1076029617741362

Wang, L., Dong, J., Xu, M., Li, L., Yang, N., and Qian, G. (2022). Association between monocyte to high-density lipoprotein cholesterol ratio and risk of non-alcoholic fatty liver disease: A cross-sectional study. *Front. Med.* 9, 898931. doi:10.3389/fmed.2022.898931

Yamaguchi, T., Sugimoto, T., Yano, S., Yamauchi, M., Sowa, H., Chen, Q., et al. (2002). Plasma lipids and osteoporosis in postmenopausal women. *Endocr. J.* 49, 211–217. doi:10.1507/endocrj.49.211

Yin, W., Li, Z., and Zhang, W. (2019). Modulation of bone and marrow niche by cholesterol. *Nutrients* 11 (6), 1394. doi:10.3390/nut11061394

Zhang, H., Dellsperger Kevin, C., and Zhang, C. (2012). The link between metabolic abnormalities and endothelial dysfunction in type 2 diabetes: An update. *Basic Res. Cardiol.* 107, 237. doi:10.1007/s00395-011-0237-1

Zhang, Y., Li, S., Guo, Y., Wu, N. Q., Zhu, C. G., Gao, Y., et al. (2016). Is monocyte to HDL ratio superior to monocyte count in predicting the cardiovascular outcomes: Evidence from a large cohort of Chinese patients undergoing coronary angiography. *Ann. Med.* 48, 305–312. doi:10.3109/07853890.2016.1168935



OPEN ACCESS

EDITED BY

Xiaojuan Chao,
The First Affiliated Hospital of Sun
Yat-sen University, China

REVIEWED BY

Jian-Fei Pei,
Chinese Academy of Medical Sciences
and Peking Union Medical College,
China
Joaquim Javary,
Institute for Research in Immunology
and Cancer, Montreal university,
Canada

*CORRESPONDENCE

Jie Wei,
weijie28@mail.sysu.edu.cn
Mianmian Liao,
lmmcsq@163.com
Chaohui Duan,
duanchh@mail.sysu.edu.cn

[†]These authors have contributed equally
to this work

SPECIALTY SECTION

This article was submitted to
Inflammation Pharmacology,
a section of the journal
Frontiers in Pharmacology

RECEIVED 08 September 2022

ACCEPTED 21 October 2022

PUBLISHED 10 November 2022

CITATION

Hu H, Sun N, Du H, He Y, Pan K, Liu X,
Lu X, Wei J, Liao M and Duan C (2022),
Mouse promyelocytic leukemia zinc
finger protein (PLZF) regulates hepatic
lipid and glucose homeostasis
dependent on SIRT1.
Front. Pharmacol. 13:1039726.
doi: 10.3389/fphar.2022.1039726

COPYRIGHT

© 2022 Hu, Sun, Du, He, Pan, Liu, Lu,
Wei, Liao and Duan. This is an open-
access article distributed under the
terms of the [Creative Commons
Attribution License \(CC BY\)](#). The use,
distribution or reproduction in other
forums is permitted, provided the
original author(s) and the copyright
owner(s) are credited and that the
original publication in this journal is
cited, in accordance with accepted
academic practice. No use, distribution
or reproduction is permitted which does
not comply with these terms.

Mouse promyelocytic leukemia zinc finger protein (PLZF) regulates hepatic lipid and glucose homeostasis dependent on SIRT1

Huiling Hu^{1,2†}, Nannan Sun^{3,4†}, Haiyan Du^{5†}, Yuqing He^{6†},
Kunyi Pan^{1,2}, Xiuli Liu^{1,2}, Xiaoxia Lu^{1,2}, Jie Wei^{1,2*},
Mianmian Liao^{5*} and Chaohui Duan^{1,2*}

¹Department of Clinical Laboratory, Sun Yat-Sen Memorial Hospital, Sun Yat-Sen University, Guangzhou, China, ²Guangdong Provincial Key Laboratory of Malignant Tumor Epigenetics and Gene Regulation, Sun Yat-Sen Memorial Hospital, Sun Yat-Sen University, Guangzhou, China, ³Department of Obstetrics and Gynecology, Guangdong Provincial Key Laboratory of Major Obstetric Diseases, The Third Affiliated Hospital of Guangzhou Medical University, Guangzhou Medical University, Guangzhou, China, ⁴State Key Laboratory of Ophthalmology, Zhongshan Ophthalmic Center, Sun Yat-sen University, Guangzhou, China, ⁵Department of Hepatology, Shenzhen Traditional Chinese Medicine Hospital, Shenzhen, China, ⁶Translational Medicine Research Center, Zhujiang Hospital, Southern Medical University, Guangzhou, China

Previous studies have demonstrated that promyelocytic leukemia zinc finger protein (PLZF) promotes the expression of gluconeogenic genes and hepatic glucose output, which leads to hyperglycemia. However, the role played by PLZF in regulating lipid metabolism is not known. In this study, we aimed to examine the function of PLZF in regulating hepatic lipid and glucose homeostasis and the underlying mechanisms. The expression of PLZF was determined in different mouse models with regard to non-alcoholic fatty liver disease (NAFLD). In the next step, adenoviruses that express PLZF (Ad-PLZF) or PLZF-specific shRNA (Ad-shPLZF) were utilized to alter PLZF expression in mouse livers and in primary hepatocytes. For the phenotype of the fatty liver, histologic and biochemical analyses of hepatic triglyceride (TG), serum TG and cholesterol levels were carried out. The underlying molecular mechanism for the regulation of lipid metabolism by PLZF was further explored using luciferase reporter gene assay and ChIP analysis. The results demonstrated that PLZF expression was upregulated in livers derived from ob/ob, db/db and diet-induced obesity (DIO) mice. Liver PLZF-overexpressing C57BL/6J mice showed fatty liver phenotype, liver inflammation, impaired glucose tolerance and insulin sensitivity. On the other hand, hepatic PLZF knockdown in db/db and DIO mice alleviated hepatic steatosis. Of note, we found that PLZF activates SREBP-1c gene transcription through binding directly to the promoter fragment of this gene, which would induce a repressor-to-activator conversion depending on its interaction with SIRT1 in the role played by PLZF in the transcription process through deacetylation. Thus, PLZF is identified as an essential regulator of hepatic lipid and glucose metabolism, where the modulation of its liver expression could open up a therapeutic path for treating NAFLD.

KEYWORDS

PLZF, SREBP-1c, SIRT1, lipid homeostasis, glucose homeostasis

Introduction

Hepatic lipogenesis dysfunction accelerates the pathogenesis of metabolic diseases, including non-alcoholic fatty liver disease (NAFLD). In NAFLD, fatty acids are ectopically accumulated in the liver (Browning and Horton, 2004). NAFLD, which is defined as a spectrum of hepatic disease ranging from hepatic steatosis to hepatic steatohepatitis, fibrosis, and cirrhosis, has expanded as a global threat, particularly in developed countries (Bedossa, 2017). Although the pathogenesis behind NAFLD is complicated, the activity modulation of a number of transcription factors responsible for regulating hepatic lipid and glucose homeostasis appears to be essential during the treatment of NAFLD. As an example of important transcription factors that take part in regulating hepatic lipid metabolism, researchers can point out the sterol regulatory element binding proteins (SREBPs) (Ahmed and Byrne, 2007).

Hepatic SREBP-1c is characterized as the primary member of the SREBP family, which constitutes major transcription factors responsible for the regulation of genes concerning cholesterol and fatty acid synthesis (Shimomura et al., 1997; Eberlé et al., 2004). Prior studies have revealed that multiple modulators regulate the expression of SREBP-1c. For example, KLF11 and Dec1 ameliorate hepatic steatosis *via* inhibition of SREBP-1c expression (Zhang et al., 2013; Shen et al., 2014). Thus, establishing the regulatory factors of SREBP-1c is crucial, because it provides novel insight into the potential therapeutic targets for the treatment of NAFLD.

The promyelocytic leukemia zinc finger (PLZF), also called ZBTB16 (zinc finger and BTB domain containing 16), is considered a transcription factor that takes part in regulating a number of different biological processes, such as spermatogenesis (Ching et al., 2010), stem cell maintenance (Liu et al., 2016), immune regulation (Xu et al., 2009) and invariant natural killer T cell (iNKT) development (Kovalovsky et al., 2008). Previous research uncovers the potential role played by PLZF in the pathogenesis of metabolic diseases. PLZF is an iNKT cells specific transcription factor that is necessary for its full functionality (Kovalovsky et al., 2008). In addition, PPAR γ 2 and PLZF synergistically promote SREBP-1c transcription to increase lipid biosynthesis in iNKT cells (Fu et al., 2020). SNP (783C>G) in the PLZF coding sequence leads to nonsynonymous amino acid substitution—serine to threonine at position 208 (T208S)—which affects total body weight, adiposity, and the insulin sensitivity of the skeletal muscles (Seda et al., 2005). Furthermore, a study conducted by Liska et al. demonstrated that PLZF deficiency ameliorates metabolic and cardiac traits in the spontaneously hypertensive rat (Liška et al., 2017). Although

a previous study has revealed that liver-overexpressed PLZF damaged glucose tolerance and insulin sensitivity *via* promoting the expression of the gluconeogenic gene and hepatic glucose output (Chen et al., 2014), the role played by PLZF in regulating lipid metabolism, including lipid synthesis, liver inflammation, and fatty acid oxidation, is still unknown.

Given what was stated above, we set out a goal to examine whether PLZF is involved in the regulation of hepatic lipogenesis *via* mediating the SREBP-1c expression. Our study demonstrated that PLZF has a crucial role in the regulation of lipogenesis. This process was dependent on its interaction with SIRT1, which allowed for a repressor-to-activator conversion in the role played by PLZF in the transcription process through deacetylation. Thus, PLZF is found to be a vital regulator of hepatic lipid metabolism, where the modulation of its liver expression may open up a therapeutic path for treating NAFLD.

Materials and methods

Animals

The experimental procedures concerning animals received approval from the Animal Care and Use Committee of Zhongshan Ophthalmic Center of Sun Yat-sen University; they were carried out in accordance with all relevant ethical regulations. Male ob/ob, db/db, db/m, and C57BL/6J mice (aged six to 8 weeks) were acquired from the Model Animal Research Center of Nanjing University (Nanjing, China) and were kept in standard cages. The cages were placed in a specific pathogen-free facility, in which a 12-h light/dark cycle was maintained. The animals were subjected to free access to food and water. Liver-specific SIRT1-knockout (SIRT1^{-/-}) mice featuring conditional delete of SIRT1 exon four were the result of crossing between mice with floxed alleles of SIRT1 and liver Cre recombinase-expressing mice (Cheng et al., 2003). For the DIO model and the normal diet model used as control, mice were fed *ad libitum* with either a normal chow (10% fat, Lab Diet) or high-fat diet (60% fat, Research Diets) with free access to water. For adenovirus injection, mice were injected *via* their tail vein with adenovirus expressing 1) green fluorescent protein (Ad-GFP), 2) PLZF (Ad-PLZF), and 3) short-hairpin (sh) RNA against luciferase (Ad-shCON) or shRNA against PLZF (Ad-shPLZF) as controls ($0.5\text{--}1.0 \times 10^9$ pfu/mouse in 150 μ l PBS). In the next step, after 5–7 days elapsed from the infection, the liver and plasma of the mice were retrieved for further analysis. The grouping of all the mice was performed in a random manner, and the researchers performing the experiments were blind to the assignment of the groups and the evaluation of the outcome.

Preparation of expression plasmids and recombinant adenoviruses

The full-length mouse PLZF and SIRT1 gene were amplified from liver cDNA of C57BL/6J mice. Afterward, Myc-tagged PLZF and Flag-tagged SIRT1 were cloned into pcDNA3.1 utilizing the following PCR primers: 5'-CCGGGTACCATG GATCTGACAAAGATGGGGAT-3' (Forward) and 5'-CCGG ATATCCAGATCCTCTTCAGAGATGAGTTTCTGCTCCAC ATAACACAGGTAGAGGTACGT-3' (Reverse) for PLZF or 5'-CCGGGTACCATGGCGGACGAGGTGGCGCT-3' (Forward) and 5'-CCGCTCGAGGCTTATCGTCGTCATCCTTGTAAT CTGATTTGTCTGATGGATAGT-3' (Reverse) for SIRT1. PLZF- or SIRT1-expressing recombinant adenoviruses were generated following what was described in ref. (Luo et al., 2007). PCR was used for the amplification of the mouse SREBP-1c gene promoter (-500 to -1 bp) utilizing mouse genomic DNA. Then, SREBP-1c gene promoter was inserted into a pGL3-basic luciferase reporter vector (p-SREBP-1c-500). A series of 5' truncated constructs of the SREBP-1c gene promoter (p-SREBP-1c-224, p-SREBP-1c-119, p-SREBP-1c-71) were prepared by PCR using p-SREBP-1c-500 as a template. The primer sequences used are listed in [Supplementary Table S1](#).

RNA interference

The design and synthesis of shRNAs targeting PLZF gene (shPLZF), SIRT1 (shSIRT1), or luciferase (shCON) were both carried out using the shRNA design program of Genepharma website (Genepharma, Shanghai, China). The shRNAs were constructed into adenovirus plasmids, where the adenoviruses were generated based on procedures given in the reference (Luo et al., 2007). The sequences of the shRNAs were shown as follows: shPLZF: TGGAAATGATGCAGGTAGA, shSIRT1: GCACCG ATCCTCGAACAAATTC and shCON: 5'-CTTACGCTGAGTACTTCGA-3'.

Isolation of mouse primary hepatocytes and their culture

The isolation of mouse primary hepatocytes and their culture was done following reference (Zhang et al., 2013). In brief, type II collagenase (0.5 mg/ml) perfusion *via* the inferior vena cava was administered for the isolation of primary hepatocytes from C57BL/6J and Ko-SIRT1 mice. The viability assessment of hepatocytes was carried out using the trypan blue exclusion method. For the experiments, cells with viability >95% were used. For the culture of mouse hepatocytes, RPMI-1640, which contained FBS (10%), penicillin (with concentration of 100 units/ml), and streptomycin (with concentration of 0.1 mg/ml), was used. In general, for overexpression experiments, we used

100 multiplicity of infection (MOI), and for shRNA knockdown experiments six00 MOI. Afterward, the harvesting of the cells was carried out after elapse of 1–2 days from the infection.

Analytical procedures and chemicals

A commercial kit (Jiancheng, Nanjing, China) was used for the purpose of determining the serum concentrations of TG and cholesterol following the manufacturer's instructions. For determining the intracellular TG and cholesterol content, first cells were lysed with Triton X-100 (0.1%) and then a commercial kit (Jiancheng, Nanjing, China) was employed for assessing the TG and cholesterol content of cell lysates. Hepatic TG and cholesterol were extracted with chloroform-methanol (2:1) according to reference. (Folch et al., 1957). and then their concentrations were measured by a commercial kit (Jiancheng, Nanjing, China). The concentrations of serum TNF α and IL-6 were measured using ELISA (R&D Systems, Minneapolis, United States). EX-52 and Resveratrol were purchased from MedChemExpress.

Real-time qRT-PCR analysis

The isolation of the RNA present in the mouse primary hepatocytes or fresh liver tissues was conducted by means of a TRIzol-based method (Invitrogen). Reverse transcription was performed according to the instructions of the manufacturer of the 5 \times All-In-One RT MasterMix kit (Applied Biological Materials Inc., Richmond, Canada). qRT-PCR was carried out utilizing SYBR Green Master mix with LightCycler[®] 96 Real-Time PCR System (Roche). Three independent biological replicates were carried out, and the genes' relative expression levels were calculated with the 2^{- $\Delta\Delta C_T$} method. The data of the gene expression were normalized to the expression levels of β -actin. The sequences of the primer can be found in [Supplementary Table S2](#).

Immunoprecipitation

For adenoviral transductions, HEK293T cells were transduced with adenovirus expressing Myc-tagged PLZF or Flag-tagged SIRT1. Once 36 h elapsed from transduction, whole cell lysates were retrieved by centrifuging (12,000 rpm; 10 min; 4°C). An amount of 1–1.2 mg of the lysates was utilized for the immunoprecipitation test. The incubation of lysates was carried out with anti-Flag antibody or anti-Myc antibody overnight (4°C). Then, a 2 h treatment with protein A/G Sepharose was performed. After three-time rinsing with PBS, the process of retrieving the immunoprecipitated proteins from

the beads was carried out through a 10 min boiling in sample buffer or by competition with the tag peptide. Afterward, immunoblotting was used for the analysis of immunoprecipitated proteins. Anti-FLAG mouse mAb (8146; CST) and Myc mouse mAb (2276; CST) were used against epitope tags.

Western blotting

The lysis of cells and tissues was carried out in RIPA lysis buffer [Tris-HCl (with concentration of 50 mM, pH 8), NaCl (with concentration of 150 mM), Triton (1%), SDS (with concentration of 0.1%), EDTA (with concentration of 1 mM), and deoxycholic acid (with concentration of 0.5%)] plus a cocktail containing protease and phosphatase inhibitors (Roche), and another one comprising deacetylase inhibitors (Santa Cruz) for 30 min at 4°C. SDS-PAGE was used for the separation of an amount of 30–50 µg of proteins, which was transferred to PVDF membranes (Merck Millipore). Overnight incubation (4°C) with antibodies was applied to the membranes; the antibodies were the following: anti-SREBP-1 (sc-13551, Santa Cruz), anti-SIRT1 (13161-1-AP, Proteintech), PLZF (sc-28319, Santa Cruz), anti-FAS (3180, CST), anti-acetyl Lysine antibody (9441, CST) and β -Actin (bs-0061R, Bioss). For ac-PLZF examination, immunoprecipitation with an anti-PLZF antibody was introduced into cells and tissues extracts, which was followed by immunoblotting with an anti-acetyl-lysine antibody (α -AcK), so that only the acetylated PLZF protein was detected (McConnell et al., 2015; Sadler et al., 2015). Detection of protein signals was carried out by incubation with horseradish peroxidase-conjugated secondary antibodies, where ECL detection reagent (Pierce) was employed in the next step following the manufacturer's instructions.

Histological and immunohistochemistry analyses

For H&E staining, neutral-buffered formalin (10%) was used for fixing the liver tissues; afterward, the tissues were paraffin-embedded, followed by being cut into sections (thickness = 7 µm). Liquid nitrogen was used for freezing the liver tissues for Oil red O staining; the frozen tissues were then cut into sections with a thickness of 10 µm. After staining the sections, their analysis was carried out at magnification of $\times 200$ utilizing a Zeiss Axio Observer microscope.

Analysis of glucose output assay

Primary mouse hepatocytes were seeded into six-well plates. In the next step, the indicated adenovirus was used for infecting

them. Once 36 h elapsed from infection, the cells were washed with PBS (three times); afterward, they were incubated in 1 ml/well of phenol-red-free, glucose-free DMEM that contained dexamethasone (1 µM), pyruvate (2 mM), lactate (20 mM) and forskolin (10 µM) for 3–6 h. An Amplex Red Glucose/Glucose Oxidase Assay Kit (Applygen Technologies, Beijing, China) was used for determining the concentration of glucose in the medium. The lysis of the cells was performed, and for each lysate, the protein concentration was measured (Bio-Rad, Hercules, CA, United States). The normalization of the glucose output rate was carried out using the cellular protein content.

Analysis of luciferase reporter gene assay

The co-transfection of mouse SREBP-1c promoter constructs (PGL3-SREBP-1c-500, PGL3-SREBP-1c-224, PGL3-SREBP-1c-119, and PGL3-SREBP-1c-71) with PLZF-expressing plasmid (pcDNA3.1-PLZF) or empty vectors (pcDNA3.1) was carried out into HepG2 cells utilizing Lipofectamine™ 2000 (Invitrogen), in accordance with the instructions of the manufacturer. As an internal control, a vector expressing Renilla luciferase was utilized. After elapse of 48 h, the harvesting of the cells was performed to evaluate the luciferase activity utilizing the Dual-Luciferase reporter assay system (Promega), following the manufacturer's instruction.

Analysis of chromatin immunoprecipitation assay

ChIP assays were carried out using the procedure of a previous report (Sun et al., 2021). In brief, the crosslinking of the tissues was performed in formaldehyde (1%) at 37°C (15 min), followed by resuspension in 200 ml of lysis buffer [Tris-HCl (with concentration of 50 mM; pH 8.1), SDS (with concentration of 1%), and EDTA (with concentration of 10 mM)]. Lysates were sonicated; afterward, they were diluted using CHIP dilution buffer [SDS (with concentration of 0.01%), Triton X-100 (with concentration of 1.1%), Tris-HCl (with concentration of 16.7 mM; pH 8.1), NaCl (with concentration of 167 mM), and EDTA (with concentration of 1.2 mM)]. The diluted lysates were subjected to immunoprecipitation utilizing anti-PLZF antibody or normal mouse IgG. afterward, the immunoprecipitates were washed followed by elution with 300 µl of elution buffer [NaHCO₃ (with concentration of 0.1 M) and SDS (with concentration of 1%)] and reversed. The amplification of promoter region of SREBP-1c was carried out by PCR utilizing these primers: 5'-GATTGGCCA TGTGCGCTCA-3' as a forward primer and 5'-CCTTCAAAT GTGCAATCCATG -3' as a reverse primer.

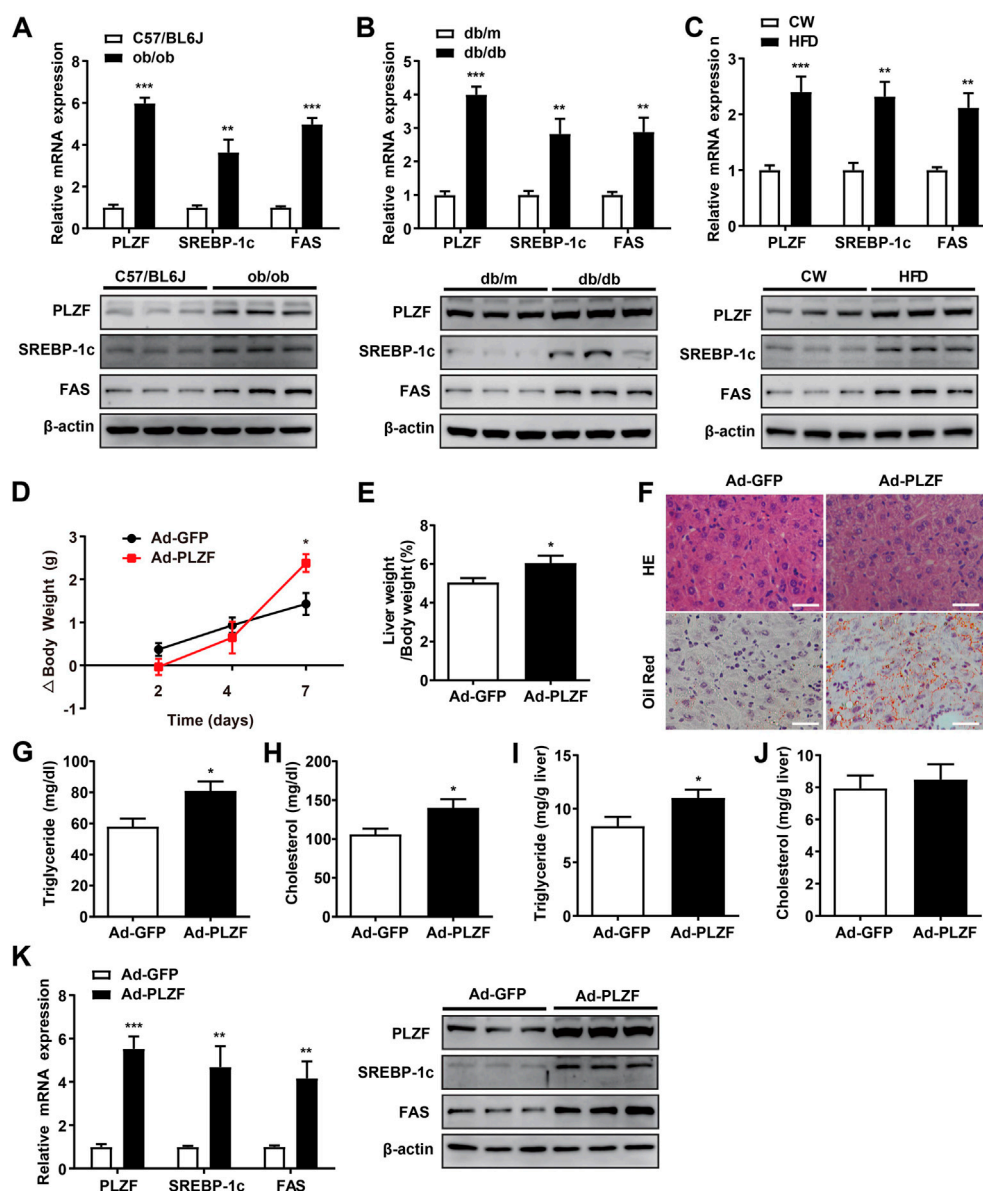


FIGURE 1

Hepatic PLZF gene expression is upregulated in NAFLD mice and adenovirus-mediated PLZF overexpression in C57BL/6J mouse livers leads to improvement in the fatty liver phenotype. PLZF, SREBP-1c, and Fas expression is presented in qPCR analysis (top panel) and western blot analysis (bottom panel). (A) C57BL/6J control mice and ob/ob mice, (B) db/m control mice and db/db mice, and (C) C57BL/6J mice that were fed a normal chow or a high-fat diet for 16 weeks (DIO mice). Ad-GFP or Ad-PLZF adenovirus was injected into C57BL/6J mice (male). Mice were sacrificed for further analysis. Depicted are (D) body weight change, (E) liver weight to body weight ratio, (F) representative section staining of livers with H&E (top panel) and Oil Red O (bottom panel), (G) serum TG, (H) serum cholesterol, (I) hepatic TG, (J) hepatic cholesterol. SREBP-1c and Fas in livers of mice treated with the indicated adenovirus were analyzed with (K) qPCR analysis (left panel) and western blot analysis (right panel). N = 6–8/group. For adenovirus injection, mice were injected via their tail vein with adenovirus. Then, 5–7 days after infection, mice livers and plasma were collected for further analysis. The data shown are the means \pm SEM. Scale bar, 50 μ m * p < 0.05, ** p < 0.01, *** p < 0.001.

Statistical analysis

Data shown were presented as mean \pm standard error of the mean (SEM). The software package IBM SPSS statistics (version 22.0) was employed for performing the statistical

analysis. One-way ANOVA was utilized for the purpose of evaluating differences among groups followed by Bonferroni's post hoc test. For making comparisons between two groups, differences were assessed by Student's t-test. p < 0.05 was set as statistically significant.

Results

Hepatic PLZF expression was increased in hepatic steatosis

Previous reports indicate that hepatic PLZF expression is upregulated depending on the time course of fasting and stimulation of hepatic gluconeogenesis (Chen et al., 2014). However, whether and how PLZF plays role in hepatic lipogenesis are still unclear. This prompted us to examine its role in hepatic lipid metabolism. Three different NAFLD mouse models, namely ob/ob, db/db, and DIO mice, were used to detect hepatic expression of PLZF by qPCR and western blot analysis. The results demonstrate that hepatic PLZF expression is dramatically increased in NAFLD mice in comparison to the control mice, where a significant elevation of lipogenic genes, including SREBP-1c and fatty acid synthase (FAS) was observed (Figures 1A–C). In line with this findings, 75 μ mol/L palmitic acid treatment, which mimics the high-fat stress to establish an *in vitro* model of lipid accumulation, significantly upregulated PLZF expression in primary mouse hepatocytes (Supplementary Figure S1A). To further study the contributions of PLZF to hepatic steatosis, adenovirus expressing Myc-tagged PLZF (Ad-PLZF) was generated and was injected *via* tail vein into wild-type mice with standard chow diet, which resulted in a specifically increased hepatic PLZF overexpression. Although no change was observed in the food intake (Supplementary Figure S1B), hepatic PLZF overexpression induced significant increases in the body weight and the value of the ratio of liver weight/body weight (Figures 1D,E). Furthermore, our histologic analysis (including Oil red O and HE stainings) demonstrated that Ad-PLZF treatment apparently stimulated the hepatosteatosis, including inducing massive deposit of large lipid droplets and ballooning degeneration of liver cells, which marked a process that leads to NAFLD and finally to non-alcoholic steatohepatitis (NASH) (Figure 1F). In line with histological analysis, biochemical analysis showed that adenovirus-mediated overexpression of PLZF dramatically increased the hepatic TG and serum TG and cholesterol levels (Figures 1G–J). We also examined the role of PLZF overexpression on hepatic lipogenesis genes. Similar to the ob/ob, db/db, and DIO mice, hepatic PLZF overexpression robustly induced an increase in SREBP-1c and Fas gene expression in liver (Figure 1K), which could lead to hepatic steatosis.

Silencing of hepatic PLZF protects db/db mice against hepatic steatosis

To further comprehend the pathogenic role of hepatic PLZF in NAFLD progression, we produced an adenovirus that expressed PLZF-specific shRNA (Ad-shPLZF) and

injected Ad-shPLZF into NAFLD models, db/db mice with chow diet *via* tail vein. As expected, hepatic PLZF knockdown slightly, but significantly, slowed body weight gain, where Ad-shPLZF infection decreased the liver weight (Figures 2A,B). Moreover, knockdown of PLZF in the liver showed an obvious reduction in both hepatic and serum TG content, where the serum cholesterol level also decreased (Figures 2C–F). Thus, in db/db mice, hepatic-specific knockdown of PLZF visibly alleviated the phenotype of the fatty liver, as there was reduction in large lipid droplets and ballooning degeneration of liver cells (Figure 2G). Importantly, similar results were also obtained for DIO mice (Supplementary Figure S2), except for body weight gain was not significantly changed. To further evaluate the underlying molecular mechanism in place, we performed *in vitro* assay tests, where we found that consistent with the phenotype, the lipogenic genes' expression, including SREBP-1c and Fas, was dramatically suppressed by the knockdown of PLZF in the liver tissues obtained from db/db and DIO mice (Figure 2H and Supplementary Figure S2H), which contributed to the attenuation of NAFLD phenotype.

Hepatic PLZF enhances SREBP-1c expression *via* binding its promoter

To further delineate the mechanism of PLZF-induced hepatic steatosis, we performed *in vitro* experiments. According to the *in vitro* tests, consistent with previous reports (Chen et al., 2014), primary hepatocytes with Ad-PLZF transfection showed a robust increase in glucose production, where the TG levels contents were also dramatically increased (Figures 3A,B). Subsequent qPCR analysis also indicated that overexpression of PLZF in primary hepatocytes upregulated both glucogenic genes and lipogenic genes, especially SREBP-1c and Liver X receptor α (LXR α) (Figure 3C). SREBP-1c is regulated by multiple molecular pathways and has been found to be a predominant transcription factor playing a part in lipid homeostasis in liver (Eberlé et al., 2004). To determine whether PLZF protein can bind to the promoters of SREBP-1c gene and regulate the expression of this gene, we cloned and fused the promoter fragment of SREBP-1c gene (500 bp) to a luciferase reporter gene (pSREBP-1c-500). Also, a number of luciferase reporter constructs were generated that had shorter fragments of the promoter of SREBP-1c gene (pSREBP-1c-224 and p-SREBP-1c-119, p-SREBP-1c-71). The data of the luciferase reporter gene assay revealed that PLZF overexpression enhanced the pSREBP-1c-500, pSREBP-1c-224 and p-SREBP-1c-119 reporter gene transcription in HepG2 cells. Nonetheless, the stimulatory effects of PLZF were eliminated following further truncation of the promoter region to -71 bp (p-SREBP-1c-71) (Figure 3D), which suggests that the sequence between -71 and -119 bp is the

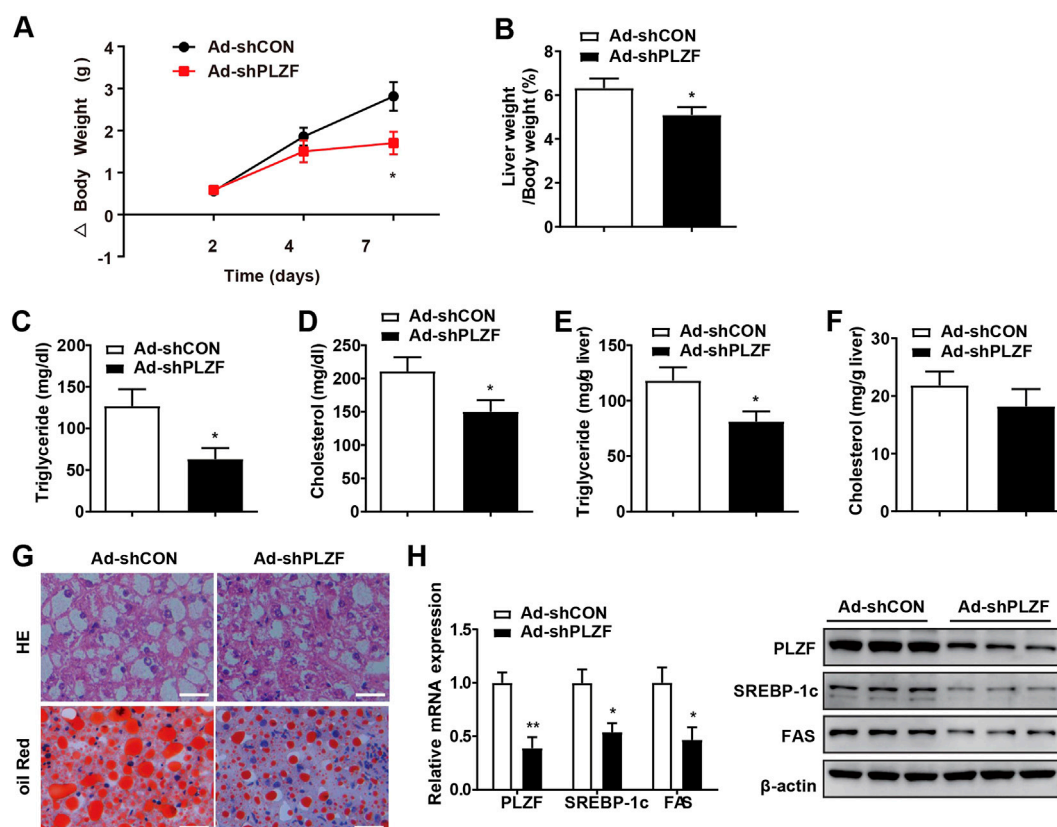


FIGURE 2

Knockdown of hepatic PLZF in db/db mice induced improvement in the fatty liver phenotype. Db/db mice were injected with Ad-shCON or Ad-shPLZF adenovirus and then were for further analysis. Depicted are (A) body weight change, (B) liver weight to body weight ratio, (C) serum TG, (D) serum cholesterol, (E) hepatic TG, (F) hepatic cholesterol, (G) liver sections stained with H and E (top panel) and Oil Red O (bottom panel). SREBP-1c and Fas in livers of mice that were treated with the indicated adenovirus were analyzed by (H) qPCR analysis (left panel) and western blot analysis (right panel). N = 6–8/group. For adenovirus injection, mice were injected via their tail vein with adenovirus. Then, 5–7 days after infection, mice livers and plasma were collected for further analysis. The data shown are the means ± SEM. Scale bar, 50 μm **p* < 0.05, ***p* < 0.01.

mediator for inducing the effects of PLZF on the transcription of SREBP-1c gene. In the next step, using ChIP assays, we examined if endogenous PLZF protein was able to bind directly to the SREBP-1c promoter *in vivo*. Our results indicated that the promoter fragment of SREBP-1c (from +85 bp to –83 bp), which containing the E-box could be amplified while precipitating the DNA complex with anti-PLZF antibody treatment, but not when using normal mouse IgG (negative control) in the liver tissue lysate from C57BL/6J mice (Figure 3E). Finally, mutation of E-box (from CCATGTGC to CaAaTGC) almost abolished the PLZF regulatory effects (Figure 3D). These data suggested that the effects of PLZF on SREBP-1c gene expression are mediated by the E-box element. These findings indicate that PLZF enhances the transcription of SREBP-1c *via* directly binding to the promoter fragment of the gene.

Hepatic PLZF increases lipogenesis dependent on interaction with SIRT1

Previous study has revealed PLZF activates interferon-stimulated genes and facilitates natural killer cell functions. The authors' mechanistic investigation suggests that interferon-induced PLZF phosphorylation and histone deacetylase 1 (HDAC1) recruitment probably mediates the repressor-to-activator conversion (Xu et al., 2009). SIRT1 was identified as an energy sensor and characterized as deacetylates proteins, therefore, we hypothesized that hepatic PLZF-induced dysfunction of lipid metabolism might be mediated by SIRT1 dependent on its deacetylation. As expected, the acetylation level of PLZF was dramatically lowered in the ob/ob, db/db, and DIO mice in comparison to the littermate controls (Figure 4A). Furthermore, our co-immunoprecipitation study on

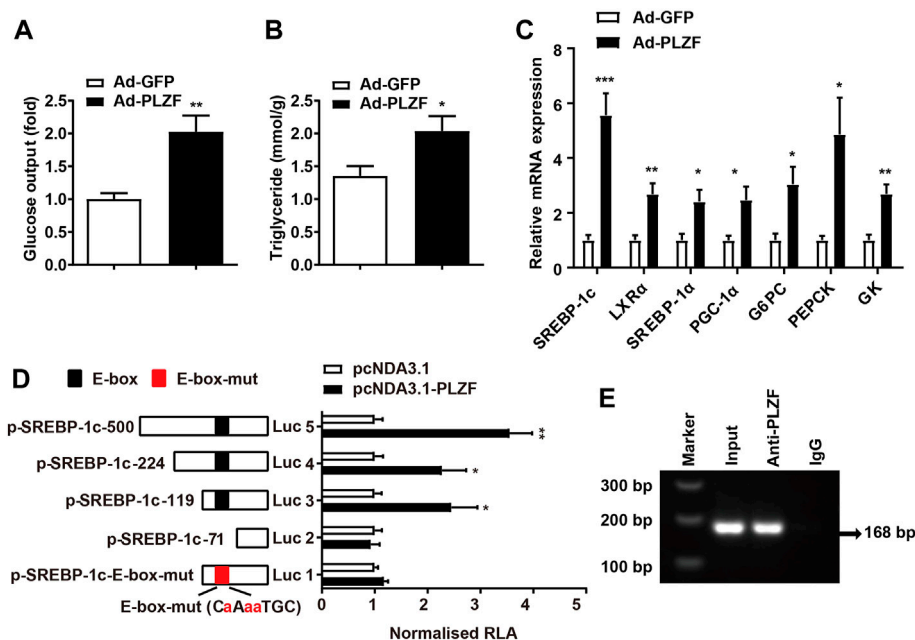


FIGURE 3

PLZF stimulates transcription of the SREBP-1c gene by directly binding to its promoter. (A) Glucose production and (B) TG levels in the primary hepatocytes treated with the indicated adenovirus. (C) qPCR analysis of glucogenic genes and lipogenic genes in the primary hepatocytes treated with the indicated adenovirus. (D) Luciferase reporter gene assay in HepG2 cells transfected with the indicated plasmids. A number of truncated SREBP-1c promoters that were fused to the luciferase reporter gene were co-transfected with pcDNA3.1 or pcDNA3.1-PLZF plasmid into HepG2 cells. (E) For the purpose of assessing endogenous PLZF occupancy of the SREBP-1c promoter, ChIP analysis was performed on liver tissues isolated from C57BL/6J mice. N = 4–6/group. The data shown are the means \pm SEM. * p < 0.05, ** p < 0.01, *** p < 0.001. Luc, luciferase. RLA, relative luciferase activity.

primary hepatocytes, which was incubated with 75 μ mol/L palmitic acid for 24 h to mimic the high-fat stress to establish an *in vitro* model of lipid accumulation, revealed that there is a remarkable interaction between PLZF and SIRT1 (Figure 4B). Consistent with our above-mentioned results, silencing of SIRT1 with EX-527, an inhibitor of SIRT1, significantly blocked the PLZF-induced upregulation of lipogenic genes, including SREBP-1c and Fas, while resveratrol treatment, an activator of SIRT1, impeded the PLZF-induced imbalance of lipogenesis (Figure 4C). This phenomenon was also detected in the primary hepatocytes that were Ad-shSIRT1- or Ad-SIRT1-adenovirus-infected (Figure 4D). Notably, SIRT1 knockdown obviously increased the acetylation level of PLZF, which was reduced when Ad-SIRT1 adenovirus was used to overexpress SIRT1 (Figure 4E). Additionally, the PLZF-induced output of TG was also reduced by SIRT1 knockdown and was increased by SIRT1 overexpression (Figure 4F).

Hepatic SIRT1 knockout impedes PLZF-induced hepatic steatosis

Previous research reports have described that overexpression of hepatic SIRT1 induces protection against the metabolic

impairment induced through a high-fat diet in mice (Pfluger et al., 2008; Purushotham et al., 2009). Nonetheless, in the basal state, the role of SIRT1 on hepatic lipid metabolism remains poorly understood. Based on co-immunoprecipitation results, SIRT1 interacts with PLZF in a cell-autonomous manner, which will change it from a transcriptional repressor into a transcriptional activator depending on its deacetylation. Therefore, we tested the requirements of SIRT1 in PLZF-induced hepatic steatosis *in vivo*. According to our results, although the hepatic SIRT1 interruption did not diminish the increase in the body weight induced by overexpression of PLZF in the liver, the PLZF-induced increase in the ratio of liver weight to body weight in hepatic-SIRT1-deleted mice was significantly decreased (Figures 5A,B). Moreover, the H&E and Oil Red O stainings results indicated that hepatic SIRT1 knockout partly, but significantly, rescued the apparent hepatosteatosis induced by PLZF overexpression, as was reflected in the decrease of lipid droplets and ballooning degeneration of liver cells (Figure 5C). In contrast to the PLZF-overexpression-induced increase in the intracellular hepatic TG, serum TG and serum cholesterol levels contents of WT mice, in hepatic SIRT1 knockdown mice, PLZF-overexpression induced a partly, but significant, abrogation in the increase of intracellular hepatic TG, serum TG and serum cholesterol contents (Figures 5D–G). Consistent

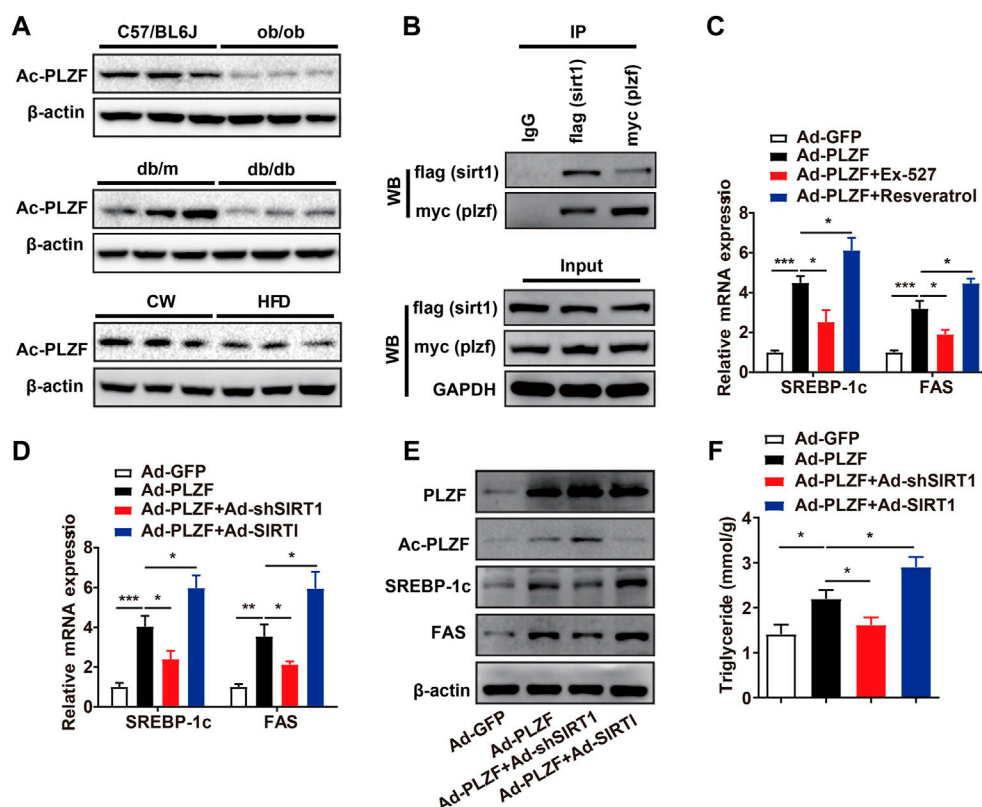


FIGURE 4

Hepatic PLZF increases lipogenesis, which is dependent on interaction with SIRT1. (A) The acetylation level of PLZF in the ob/ob, db/db, and DIO mice, and corresponding littermate controls. (B) Co-IP assay showing that PLZF interacts with SIRT1 in the primary hepatocytes. (C,D) qPCR analysis of lipogenic genes, including SREBP-1C and Fas with indicated treatment in the primary hepatocytes. (E) Western blot analysis of acetylation level of PLZF as well as expression of lipogenic genes in the primary hepatocytes with indicated treatment. (F) TG content in the primary hepatocytes treated with indicated treatment. N = 4–6/group. The data shown are the means \pm SEM. * p < 0.05, ** p < 0.01, *** p < 0.001. EX-527, SIRT1 inhibitor. Resveratrol, SIRT1 activator.

with the attenuation of hepatic steatosis phenotype, our *in vitro* assays further demonstrated a slight, but significant, decrease in deacetylation levels of PLZF in hepatic SIRT1 knockout mice (Figure 5H). Moreover, compared to the littermate controls, the PLZF overexpression induced upregulation of lipogenic genes, including SREBP-1c and Fas, which were obviously abolished by SIRT1 knockout in the liver (Figure 5I).

Hepatic PLZF overexpression impaired glucose tolerance and insulin sensitivity dependent on SIRT1 deacetylases

A previous report has demonstrated a pivotal role for PLZF in the homeostasis of the metabolism of glucose by the positive regulation of gluconeogenesis and negative effects on the insulin signaling pathway (Chen et al., 2014). To further investigate whether SIRT1 was involved in PLZF-induced impairments of systemic glucose/insulin sensitivity, we carried out the glucose-

tolerant test (GTT) and insulin-tolerant test (ITT) in SIRT1^{-/-} mice with hepatic overexpression of PLZF. Consistent with this previous report, in our study, mice on a standard diet with PLZF overexpression in the liver showed a clear impairment of glucose tolerance and insulin sensitivity (Figures 6A,B). Interestingly, when SIRT1 was knocked down in the liver, the dysfunction of systemic glucose tolerance and insulin sensitivity induced by overexpression of hepatic PLZF appeared to be partly rescued (Figures 6A,B). Meanwhile, SIRT1 knockout in the liver also alters PLZF-induced disorder of hepatic glucose production, which was illustrated by the results of the pyruvate tolerance test (PTT) (Figure 6C). To further examine the underlying mechanism in place, we examined the task of SIRT1 loss-of-function in the PLZF-regulated change of gluconeogenic genes. Our results showed that the increase of glucose production from primary hepatocytes with PLZF overexpression was obviously rescued by SIRT1 knockout (Figure 6D). In addition, the upregulation of gluconeogenic genes, including PGC-1 α , PEPCK, and G6PC that are mediated by the overexpression of

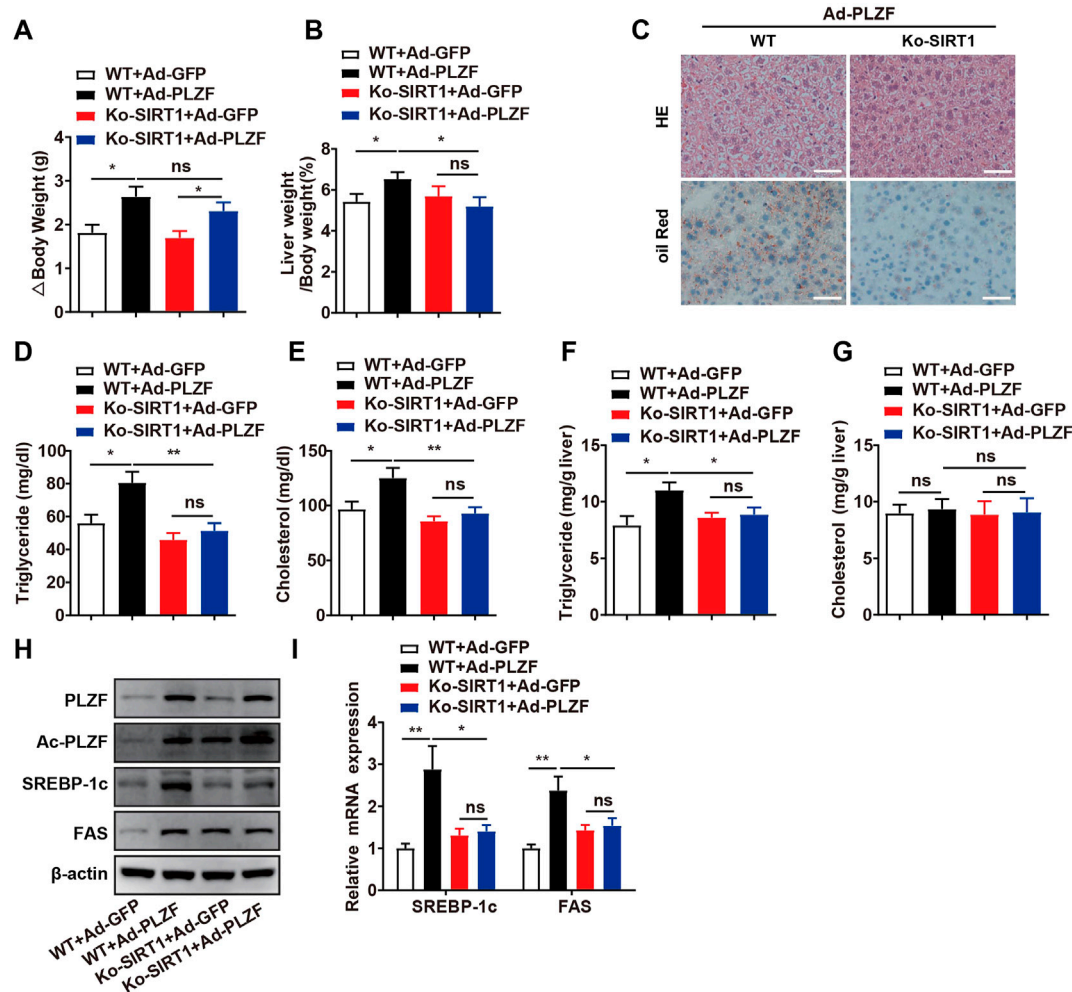


FIGURE 5

Hepatic SIRT1 knockout impedes PLZF-induced hepatic steatosis. Male C57BL/6J mice or Ko-SIRT1 mice were injected with Ad-GFP or Ad-PLZF adenovirus and then were sacrificed for further analysis. Depicted are (A) body weight change, (B) liver weight to body weight ratio, liver sections stained with (C) H and E (top panel) and Oil Red O (bottom panel), (D) serum TG, (E) serum cholesterol, (F) hepatic TG, (G) hepatic cholesterol, (H) acetylation levels of PLZF. (I) SREBP-1c and Fas in livers of mice that were treated with the indicated adenovirus were analyzed by qPCR. $N = 6-8/\text{group}$. For adenovirus injection, mice were injected via their tail vein with adenovirus. Then, 5–7 days after infection, mice livers and plasma were collected for further analysis. The data shown are the means \pm SEM. Scale bar, 50 μm * $p < 0.05$, ** $p < 0.01$.

hepatic PLZF, was reversed by disruption of SIRT1 in the liver (Figure 6E). These data suggested that hepatic PLZF manipulated lipid and glucose metabolism that is dependent on SIRT1 deacetylase.

Hepatic PLZF overexpression induces the expression of inflammatory factors and inhibits mitochondrial biogenesis *via* SIRT1

Inflammatory processes play a crucial role in the pathogenesis of fatty liver diseases, where constant inflammation contributes to the further advancement of

hepatic steatosis (Sutti and Albano, 2020). Taking into account that hepatic PLZF overexpression induces hepatic steatosis and PLZF plays a crucial role in the natural killer cell function, we hypothesized that overexpression of PLZF will increase the contents of intrahepatic pro-inflammatory cytokine TNF α and IL-6. Indeed, hepatic PLZF overexpression significantly increased the serum TNF α and IL-6 levels (Figures 7A,B), and their mRNA expression in the liver was also dramatically promoted (Figures 7C,D). In contrast, the upregulation of TNF α and IL-6 induced by the overexpression of PLZF was blocked by SIRT1 disruption (Figures 7A–D). Many studies have been indicative of an association between hepatic steatosis and the mitochondrial dysfunction (Sunny et al., 2017).

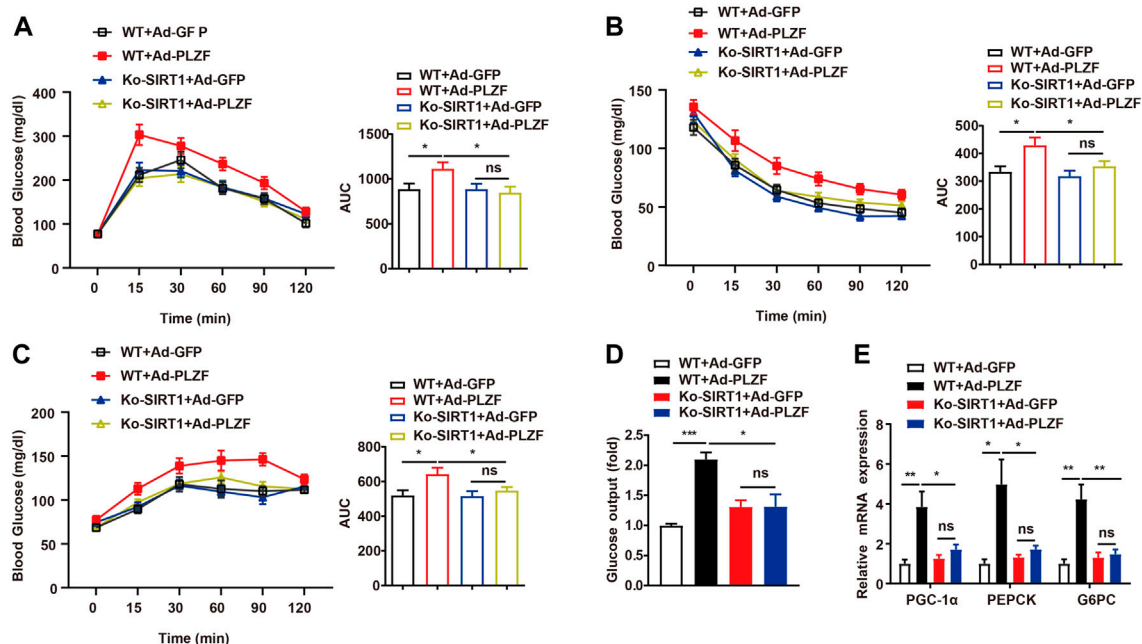


FIGURE 6

Hepatic PLZF overexpression impaired glucose tolerance and insulin sensitivity, which was dependent on SIRT1 deacetylases. Ad-GFP or Ad-PLZF adenovirus was injected into C57BL/6J mice (male) or Ko-SIRT1 mice. Blood glucose levels during (A) GTT, (B) ITT, and (C) PTT in mice that were infected with the indicated adenovirus. (D) Glucose production of the primary hepatocytes isolated from male C57BL/6J mice or Ko-SIRT1 mice infected with the indicated adenovirus. (E) For livers of mice infected with the indicated adenovirus, PGC-1 α , PEPCK, and G6PC were analyzed using qPCR. N = 6–8/group. For adenovirus injection, mice were injected via their tail vein with adenovirus. Then, 5–7 days after infection, mice livers and plasma were collected for further analysis. The data shown are the means \pm SEM. * p < 0.05, ** p < 0.01.

Therefore, we also decided to examine how PLZF overexpression regulates the function of mitochondria and whether SIRT1 mediates this regulation. Interestingly, the expression of mitochondrial transcription factor A (TFAM) and cytochrome c (Cyt C) was decreased in the liver with PLZF overexpression (Figures 7E,F). However, the PLZF-induced mitochondrial dysfunction was eliminated by SIRT1 knockdown (Figures 7E,F).

Discussion

Herein, we showed that PLZF expression was upregulated in mouse models. C57BL/6J mice with PLZF-overexpressed livers displayed fatty liver phenotype, while the knockdown of hepatic PLZF in db/db and DIO mice alleviated the hepatic steatosis. Molecular mechanisms studies indicated that PLZF activates SREBP-1c gene transcription through binding directly to the promoter fragment of this gene, which would induce a repressor-to-activator conversion depending on its interaction with SIRT1 in the role played by PLZF in the transcription process through deacetylation.

PLZF is recognized as a repressor of transcription *via* the mechanism of recruiting nuclear receptor corepressors one and 2

(NCoR1 and NCoR2) and HDACs for achieving repression; it also takes part in regulating a large number of target genes *via* zinc-finger-recognizable promoter elements (Li et al., 1997; Grignani et al., 1998; Lin et al., 1998; Chauchereau et al., 2004; Guidez et al., 2005). However, in our study, we found that PLZF could be a transcriptional activator instead of a transcriptional repressor, depending on SIRT1-mediated deacetylation. This is in accordance with a recent study, which reported on the PLZF-activation of genes that are stimulated by interferon and the PLZF-promotion of the functions of natural killer cells (Xu et al., 2009). This study clearly showed that upon stimulation of PLZF by IFN, PLZF would act as an activator of transcription instead of a repressor of it, as was recognized beforehand. The mechanistic analysis of this study indicated that IFN enhanced phosphorylation-dependent binding of PLZF to HDAC1 to mediate the conversion of repressor-to-activator. The phosphorylation of PLZF was performed within the BTB domain, probably *via* the c-Jun amino-terminal kinase (JNK) cascades. This phosphorylation was required for interferon-stimulated gene induction. Considering there is no commercial anti-phospho PLZF antibody is available at present, we have not detected the phosphorylation level of PLZF. However, in the future, further examination of the level

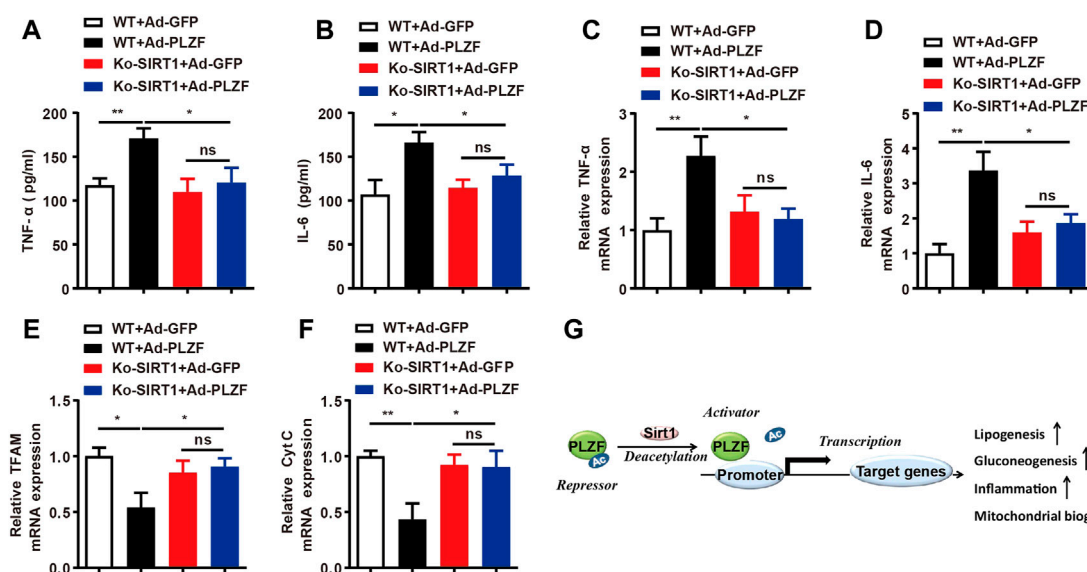


FIGURE 7

Hepatic PLZF overexpression induces the expression of inflammatory factors and inhibits mitochondrial biogenesis through SIRT1. (A,B) Serum TNF α and IL-6 levels were determined with ELISA assay in the mice with indicated treatment. (C,D) Liver TNF α and IL-6 mRNA expression was determined with qPCR assay in the mice with indicated treatment. (E,F) Liver TFAM and Cyt C mRNA expression was determined with qPCR assay in the mice with indicated treatment. (G) Schematic representation of PLZF mediated hepatic lipid homeostasis. N = 6–8/group. For adenovirus injection, mice were injected via their tail vein with adenovirus. Then, 5–7 days after infection, mice livers and plasma were collected for further analysis. The data shown are the means \pm SEM. * p < 0.05, ** p < 0.01.

of phosphorylated PLZF in the primary hepatocytes or tissues derived from mouse model of NAFLD could be detected by immunoprecipitated with a PLZF antibody firstly and then immunoblotted with anti-phospho Ser, anti-phospho Tyr antibodies. In addition, it was found that cyclin-dependent kinase CDK2 induced phosphorylation of another domain of PLZF, which resulted in impairment of the repression of the transcription; this indicated that phosphorylation could be counteracted by repression (Costoya et al., 2008). Interestingly, another study revealed that following IFN stimulation, the phosphorylated STAT1 (STAT = signal transducers and activators of transcription) was acetylated by one HAT, namely CREB binding protein (CBP) (Krämer et al., 2009). The acetylated STAT1 was then sequestered in the cytoplasm, and could no longer stimulate transcription. Therefore, HDACs induce deacetylation of STAT1 and restore its transcriptionally activated state. Thus, the need for HDAC in the transcription that is stimulated by INF may not be to the degree of chromatin, but might be representative of an acetylation-to-deacetylation switch that finely regulates the function of an activator important for interferon-stimulated genes transcription. The reciprocal dynamic action of HATs and HDACs was suggested to account for the need for HDAC activity for the functioning of other genes. Another finding that provides support to a dynamic exchange of acetylation-deacetylation between HDACs and HATs is that some

HDACs and HATs have been found to be in the near vicinity of each other (Yamagoe et al., 2003). The HAT-HDAC dynamics-regulated STAT1 acetylation is interesting because the acetylation of PLZF is also carried out by p300, which is a HAT with close connections to CBP (Guidez et al., 2005). Also, this acetylation has been found to be a requirement for the transcriptional repressor activity of PLZF. Thus, we propose that the state of PLZF transcription might be characterized by a dynamic switching between acetylation and phosphorylation, because IFN stimulation induces the phosphorylation of PLZF, similar to STAT1. Formation of these different transcriptional complexes may be regulated by complicated post-transcriptional modifications of PLZF. Further studies are necessary for elucidating the double character of PLZF as a transcriptional repressor and a transcriptional activator and the dynamic post-translational modifications in place (Ozato, 2009).

Previous studies have demonstrated that among lymphoid cells, PLZF expression is highly restricted to iNKT cells and has not been detected in B cells and NK cells. PLZF was also not detected in eosinophils, neutrophils, or macrophages (Kovalovsky et al., 2008; Fu et al., 2020), which was consistent with the data in BioGPS database (<http://biogps.org/#goto=genereport&id=235320>). In addition, with qPCR and western blotting analysis, we conformed that PLZF was relatively high expressed in liver and adipose tissues (Supplementary Figure S3). PLZF is a transcription factor specific to iNKT cells, which is required for the full

functionality of such cells (Kovalovsky et al., 2008). In models of NAFLD, activation of the immune system played a role in the further progress of damage caused by the fatty liver, where iNKT cells were found to be sensitive to lipid antigens and could show cytotoxicity against hepatocytes (Crosby and Kronenberg, 2018). It is possible to induce NASH-like liver pathology using diets that are deficient in choline, or methionine choline or contain high amounts of fat and cholesterol; this would result in the elevated expression levels of CD1d, accumulation of intrahepatic iNKT cells and consequently, enhanced fibrinogenesis, higher levels of alanine aminotransferase (ALT) and increased NASH disease scores (Syn et al., 2010; Syn et al., 2012; Wolf et al., 2014; Bhattacharjee et al., 2017). In addition, activation of iNKT cells by lipid excess contributes to inflammation of the tissue, resistance toward insulin, and hepatic steatosis in obese mice (Wu et al., 2012). All these data indicated that PLZF may control hepatic metabolism through iNKT cells by producing paracrine mediators.

SNP (783C>G) in the PLZF coding sequence results in nonsynonymous amino acid substitution—serine to threonine at position 208 (T208S)—which affects total body weight, adiposity, and the insulin sensitivity of skeletal muscle (Seda et al., 2005). PLZF is an element of a transcription factor family that is a carrier of the Pox virus and Zinc finger-Bric-a-brac Tramtrack Broad complex (POZ-BTB) domain and Kruppel type C2H2 zinc fingers. PLZF takes part in the regulation of numerous target genes *via* zinc-fingers-recognizable promoter elements. The protein region flanking the substitution containing POZ-BTB domain and C2H2 zinc fingers may be affected by the SNP. Therefore, the target genes regulating hepatic steatosis and related metabolic disorders could not be recognized and transcribed by the zinc fingers. However, further studies utilizing PLZF containing this SNP are necessary to determine whether this minor difference is metabolically “active” or “silent” and reveal the possible underlying mechanisms.

Hyperglycemia is the most effective predictor of hepatic steatosis, where a hyperglycemia-stimulating diet has been found to induce liver steatosis in sheep (Sanders et al., 2018; Kalyesubula et al., 2020). The excess glucose levels not only fuel hepatic *de novo* lipogenesis (DNL) due to being a carbon source for both fatty acids and glycerol synthesis, but also signally prompt upregulation of genes responsible for regulating fatty acid synthesis. The latter could be induced *via* direct and indirect processes: 1) in the direct scenario, the carbohydrate response element binding protein (ChREBP) is essential (Postic et al., 2007), and 2) in the indirect one, insulin-mediated activation of sterol regulatory element binding protein 1c (SREBP-1c) is an important element (Horton et al., 2002). ChREBP is a transcription factor tasked with the regulation of lipogenesis that is stimulated *via* mediation by carbohydrates (glucoses). The activation of ChREBP by glucose is *via* the regulation of the entry of ChREBP into the nucleus and by inducing the activation of transcription factor-DNA binding. Stimulation by glucose is required for binding of ChREBP to the

promoter of liver-type pyruvate kinase (L-PK), which is a crucial enzyme that takes part in the regulation of glycolysis. The L-PK catalyzes phosphoenolpyruvate-to-pyruvate conversion, which steps into Krebs cycle to produce citrate, which is another source of acetyl-CoA utilized for the synthesis of fatty acids (Stoeckman et al., 2004; Ahmed and Byrne, 2007). Srebf1 encodes SREBP-1c, a key transcription factor that is tasked with the regulation of the biosynthesis of lipids by putting under control the expression of various different enzymes essential for endogenous cholesterol, fatty acid, triacylglycerol, and phospholipid synthesis (Eberlé et al., 2004; Fu et al., 2020). Herein, we report that PLZF regulates the biosynthesis of lipids by binding to the SREBP-1c promoter region that regulates the expression of SREBP-1c. Interestingly, a recent report revealed that PLZF contributed to the expression of gluconeogenic genes and hepatic glucose output, resulting in hyperglycemia (Chen et al., 2014). Thus, all these data indicated that PLZF regulates both glucose and lipid production. It is worth noting that our results cannot rule out the possibility that PLZF may induce lipid synthesis, which was partially mediated by hyperglycemia; thus, this issue warrants further investigation in future studies.

In the present study, by means of luciferase reporter gene assay and CHIP analysis, we found that the sequence between +85 and −83 bp that contains the E-box element mediates the effects of PLZF on SREBP-1c gene transcription. In addition, mutation of E-box (from CCATGTGC to CaAaaTGC) almost abolished the PLZF regulatory effects. Thus, such data indicated that the effects of PLZF on SREBP-1c gene expression are through mediation by the E-box element. These findings suggest that PLZF promotes the transcription of SREBP-1c *via* directly binding to its promoter region. However, due to the dual-luciferase reporter assay was conducted in HepG2 cells which are cancer cells and might not really reflect the physiological activity of PLZF on SREBP-1c, therefore, a “normal” hepatocyte cell line, such as AML12 cell, maybe used to confirm this data in future. Furthermore, many studies have revealed the presence of an E-box in the promoter region of both PPAR γ (Lee and Ge, 2014; Deng et al., 2016) and FAS gene (Latasa et al., 2000; Jeon et al., 2012; Li et al., 2015). However, whether PLZF directly regulates PPAR γ and FAS gene expression *via* binding to E-box elements needs to be further studied, as the neighboring structure of the E-box element may also be important for effective gene transactivation, our results cannot rule out this possibility. In a recent study, Fu et al. (2020) demonstrated that PLZF and PPAR γ 2 synergically promotes SREBP-1c transcription to increase lipid biosynthesis in iNKT cells. However, the synergism of PPAR γ 2 and PLZF in regulating the SREBP-1c expression was not investigated in our study. In the future, co-immunoprecipitation of PLZF and PPAR γ in HFD mice derived liver tissues should be performed to determine the interaction between them. In addition, PLZF and PPAR γ 2 should be co-overexpressed to further evaluate the SREBP-1c expression in primary hepatocytes.

In conclusion, we report on the identification of hepatic PLZF as a novel candidate gene for NAFLD *via* binding to the promoter of SREBP-1c and upregulating lipogenic genes. Most importantly, we found that the requirement of hepatic SIRT1 for the dynamic switch from being a transcriptional repressor to being a transcriptional activator of PLZF depends on its deacetylase. This may present a potential therapeutic target for future attempts to treat NAFLD.

Data availability statement

The original contributions presented in the study are included in the article/Supplementary Material, further inquiries can be directed to the corresponding authors.

Ethics statement

The animal study was reviewed and approved by Animal Care and Use Committee of Zhongshan Ophthalmic Center of Sun Yat-sen University.

Author contributions

All authors made significant contributions to this work. ML and CD supervised the whole project. HH and NS conceived the study and carried out most of the experiments, performed the data analysis, and wrote the manuscript. HD, YH, KP, and XLL participated in conducting some of the animal experiments. XXL did some cellular experiments. JW contributed to the revision of the manuscript. The final version of the manuscript was reviewed by all authors and was approved by them.

References

- Ahmed, M. H., and Byrne, C. D. (2007). Modulation of sterol regulatory element binding proteins (SREBPs) as potential treatments for non-alcoholic fatty liver disease (NAFLD). *Drug Discov. Today* 12 (17–18), 740–747. doi:10.1016/j.drudis.2007.07.009
- Bedossa, P. (2017). Pathology of non-alcoholic fatty liver disease. *Liver Int.* 37, 85–89. doi:10.1111/liv.13301
- Bhattacharjee, J., Kirby, M., Softic, S., Miles, L., Salazar-Gonzalez, R. M., Shivakumar, P., et al. (2017). Hepatic natural killer T-cell and CD8+ T-cell signatures in mice with nonalcoholic steatohepatitis. *Hepatology* 65 (4), 299–310. doi:10.1002/hep4.1041
- Browning, J. D., and Horton, J. D. (2004). Molecular mediators of hepatic steatosis and liver injury. *J. Clin. Invest.* 114 (2), 147–152. doi:10.1172/JCI22422
- Chauchereau, A., Mathieu, M., de Saintignon, J., Ferreira, R., Pritchard, L. L., Mishal, Z., et al. (2004). HDAC4 mediates transcriptional repression by the acute promyelocytic leukaemia-associated protein PLZF. *Oncogene* 23 (54), 8777–8784. doi:10.1038/sj.onc.1208128
- Chen, S., Qian, J., Shi, X., Gao, T., Liang, T., and Liu, C. (2014). Control of hepatic gluconeogenesis by the promyelocytic leukemia zinc finger protein. *Mol. Endocrinol.* 28 (12), 1987–1998. doi:10.1210/me.2014-1164
- Cheng, H.-L., Mostoslavsky, R., Saito, S. i., Manis, J. P., Gu, Y., Patel, P., et al. (2003). Developmental defects and p53 hyperacetylation in Sir2 homolog (SIRT1)-deficient mice. *Proc. Natl. Acad. Sci. U. S. A.* 100 (19), 10794–10799. doi:10.1073/pnas.1934713100
- Ching, Y.-H., Wilson, L. A., and Schimenti, J. C. (2010). An allele separating skeletal patterning and spermatogonial renewal functions of PLZF. *BMC Dev. Biol.* 10 (1), 33. doi:10.1186/1471-213X-10-33
- Costoya, J., Hobbs, R., and Pandolfi, P. (2008). Cyclin-dependent kinase antagonizes promyelocytic leukemia zinc-finger through phosphorylation. *Oncogene* 27 (27), 3789–3796. doi:10.1038/onc.2008.7
- Crosby, C. M., and Kronenberg, M. (2018). Tissue-specific functions of invariant natural killer T cells. *Nat. Rev. Immunol.* 18 (9), 559–574. doi:10.1038/s41577-018-0034-2
- Deng, B., Zhang, F., Chen, K., Wen, J., Huang, H., Liu, W., et al. (2016). MyoD promotes porcine PPAR γ gene expression through an E-box and a MyoD-binding site in the PPAR γ promoter region. *Cell. Tissue Res.* 365 (2), 381–391. doi:10.1007/s00441-016-2380-3
- Eberlé, D., Hegarty, B., Bossard, P., Ferré, P., and Foulle, F. (2004). SREBP transcription factors: Master regulators of lipid homeostasis. *Biochimie* 86 (11), 839–848. doi:10.1016/j.biochi.2004.09.018

Funding

Financial support for the present research was provided by Guangdong Basic and Applied Basic Research Foundation (2019A1515010980, 2020A1515011467), Guangzhou Science and Technology Plan Project (202201010994), and the Open Project Program of Guangdong Provincial Key Laboratory of Major Obstetric Diseases.

Conflict of interest

The authors declare that the research was conducted in the absence of any commercial or financial relationships that could be construed as a potential conflict of interest.

The handling editor XC declared a shared parent affiliation with several of the authors HH, KP, XLL, XXL, and CD at the time of review.

Publisher's note

All claims expressed in this article are solely those of the authors and do not necessarily represent those of their affiliated organizations, or those of the publisher, the editors and the reviewers. Any product that may be evaluated in this article, or claim that may be made by its manufacturer, is not guaranteed or endorsed by the publisher.

Supplementary material

The Supplementary Material for this article can be found online at: <https://www.frontiersin.org/articles/10.3389/fphar.2022.1039726/full#supplementary-material>

- Folch, J., Lees, M., and Stanley, G. S. (1957). A simple method for the isolation and purification of total lipides from animal tissues. *J. Biol. Chem.* 226 (1), 497–509. doi:10.1016/s0021-9258(18)64849-5
- Fu, S., He, K., Tian, C., Sun, H., Zhu, C., Bai, S., et al. (2020). Impaired lipid biosynthesis hinders anti-tumor efficacy of intratumoral iNKT cells. *Nat. Commun.* 11 (1), 438–515. doi:10.1038/s41467-020-14332-x
- Grignani, F., De Matteis, S., Nervi, C., Tomassoni, L., Gelmetti, V., Cioce, M., et al. (1998). Fusion proteins of the retinoic acid receptor- α recruit histone deacetylase in promyelocytic leukaemia. *Nature* 391 (6669), 815–818. doi:10.1038/35901
- Guidez, F., Howell, L., Isalan, M., Cebrat, M., Alani, R. M., Ivins, S., et al. (2005). Histone acetyltransferase activity of p300 is required for transcriptional repression by the promyelocytic leukemia zinc finger protein. *Mol. Cell. Biol.* 25 (13), 5552–5566. doi:10.1128/MCB.25.13.5552-5566.2005
- Horton, J. D., Goldstein, J. L., and Brown, M. S. (2002). SREBPs: Activators of the complete program of cholesterol and fatty acid synthesis in the liver. *J. Clin. Invest.* 109 (9), 1125–1131. doi:10.1172/JCI15593
- Jeon, B.-N., Kim, Y.-S., Choi, W.-I., Koh, D.-I., Kim, M.-K., Yoon, J.-H., et al. (2012). Kr-pok increases FASN expression by modulating the DNA binding of SREBP-1c and Sp1 at the proximal promoter. *J. Lipid Res.* 53 (4), 755–766. doi:10.1194/jlr.M022178
- Kalyesubula, M., Mopuri, R., Rosov, A., Alon, T., Edery, N., Moallem, U., et al. (2020). Hyperglycemia-stimulating diet induces liver steatosis in sheep. *Sci. Rep.* 10 (1), 12189–12212. doi:10.1038/s41598-020-68909-z
- Kovalovsky, D., Uche, O. U., Eladad, S., Hobbs, R. M., Yi, W., Alonzo, E., et al. (2008). The BTB-zinc finger transcriptional regulator PLZF controls the development of invariant natural killer T cell effector functions. *Nat. Immunol.* 9 (9), 1055–1064. doi:10.1038/ni.1641
- Krämer, O. H., Knauer, S. K., Greiner, G., Jandt, E., Reichardt, S., Gührs, K.-H., et al. (2009). A phosphorylation-acetylation switch regulates STAT1 signaling. *Genes. Dev.* 23 (2), 223–235. doi:10.1101/gad.479209
- Latasa, M.-J., Moon, Y. S., Kim, K.-H., and Sul, H. S. (2000). Nutritional regulation of the fatty acid synthase promoter *in vivo*: Sterol regulatory element binding protein functions through an upstream region containing a sterol regulatory element. *Proc. Natl. Acad. Sci. U. S. A.* 97 (19), 10619–10624. doi:10.1073/pnas.180306597
- Lee, J.-E., and Ge, K. (2014). Transcriptional and epigenetic regulation of PPAR γ expression during adipogenesis. *Cell. Biosci.* 4 (1), 29–11. doi:10.1186/2045-3701-4-29
- Li, J., Luo, J., Xu, H., Wang, M., Zhu, J., Shi, H., et al. (2015). Fatty acid synthase promoter: Characterization, and transcriptional regulation by sterol regulatory element binding protein-1 in goat mammary epithelial cells. *Gene* 561 (1), 157–164. doi:10.1016/j.gene.2015.02.034
- Li, X., Lopez-Guisa, J. M., Ninan, N., Weiner, E. J., Rauscher, F. J., and Marmorstein, R. (1997). Overexpression, purification, characterization, and crystallization of the BTB/POZ domain from the PLZF oncoprotein. *J. Biol. Chem.* 272 (43), 27324–27329. doi:10.1074/jbc.272.43.27324
- Lin, R. J., Nagy, L., Inoue, S., Shao, W., Miller, W. H., and Evans, R. M. (1998). Role of the histone deacetylase complex in acute promyelocytic leukaemia. *Nature* 391 (6669), 811–814. doi:10.1038/35895
- Liška, F., Landa, V., Zidek, V., Mlejnek, P., Šilhavý, J., Šimáková, M., et al. (2017). Downregulation of plzf gene ameliorates metabolic and cardiac traits in the spontaneously hypertensive rat. *Hypertension* 69 (6), 1084–1091. doi:10.1161/hypertensionaha.116.08798
- Liu, T. M., Lee, E. H., Lim, B., and Shyh-Chang, N. (2016). Concise review: Balancing stem cell self-renewal and differentiation with PLZF. *Stem Cells* 34 (2), 277–287. doi:10.1002/stem.2270
- Luo, J., Deng, Z.-L., Luo, X., Tang, N., Song, W.-X., Chen, J., et al. (2007). A protocol for rapid generation of recombinant adenoviruses using the AdEasy system. *Nat. Protoc.* 2 (5), 1236–1247. doi:10.1038/nprot.2007.135
- McConnell, M. J., Durand, L., Langley, E., Coste-Sarguet, L., Zelent, A., Chomienne, C., et al. (2015). Post transcriptional control of the epigenetic stem cell regulator PLZF by sirtuin and HDAC deacetylases. *Epigenetics Chromatin* 8 (1), 38–14. doi:10.1186/s13072-015-0030-8
- Ozato, K. (2009). PLZF outreach: A finger in interferon's pie. *Immunity* 30 (6), 757–758. doi:10.1016/j.immuni.2009.06.003
- Pfluger, P. T., Herranz, D., Velasco-Miguel, S., Serrano, M., and Tschöp, M. H. (2008). Sirt1 protects against high-fat diet-induced metabolic damage. *Proc. Natl. Acad. Sci. U. S. A.* 105 (28), 9793–9798. doi:10.1073/pnas.0802917105
- Postic, C., Dentin, R., Denechaud, P.-D., and Girard, J. (2007). ChREBP, a transcriptional regulator of glucose and lipid metabolism. *Annu. Rev. Nutr.* 27, 179–192. doi:10.1146/annurev.nutr.27.061406.093618
- Purushotham, A., Schug, T. T., Xu, Q., Surapureddi, S., Guo, X., and Li, X. (2009). Hepatocyte-specific deletion of SIRT1 alters fatty acid metabolism and results in hepatic steatosis and inflammation. *Cell. Metab.* 9 (4), 327–338. doi:10.1016/j.cmet.2009.02.006
- Sadler, A. J., Suliman, B. A., Yu, L., Yuan, X., Wang, D., Irving, A. T., et al. (2015). The acetyltransferase HAT1 moderates the NF- κ B response by regulating the transcription factor PLZF. *Nat. Commun.* 6 (1), 6795–6811. doi:10.1038/ncomms7795
- Sanders, F. W., Acharjee, A., Walker, C., Marney, L., Roberts, L. D., Imamura, F., et al. (2018). Hepatic steatosis risk is partly driven by increased de novo lipogenesis following carbohydrate consumption. *Genome Biol.* 19 (1), 79. doi:10.1186/s13059-018-1439-8
- Seda, O., Liska, F., Sedova, L., Kazdová, L., Krenova, D., and Kren, V. (2005). A 14-gene region of rat chromosome 8 in SHR-derived polydactylous congenic substrain affects muscle-specific insulin resistance, dyslipidaemia and visceral adiposity. *Folia Biol.* 51 (3), 53–61.
- Shen, L., Cui, A., Xue, Y., Cui, Y., Dong, X., Gao, Y., et al. (2014). Hepatic differentiated embryo-chondrocyte-expressed gene 1 (Dec1) inhibits sterol regulatory element-binding protein-1c (Srebp-1c) expression and alleviates fatty liver phenotype. *J. Biol. Chem.* 289 (34), 23332–23342. doi:10.1074/jbc.M113.526343
- Shimomura, I., Shimano, H., Horton, J. D., Goldstein, J. L., and Brown, M. S. (1997). Differential expression of exons 1a and 1c in mRNAs for sterol regulatory element binding protein-1 in human and mouse organs and cultured cells. *J. Clin. Invest.* 99 (5), 838–845. doi:10.1172/JCI119247
- Stoekman, A. K., Ma, L., and Towle, H. C. (2004). Mlx is the functional heteromeric partner of the carbohydrate response element-binding protein in glucose regulation of lipogenic enzyme genes. *J. Biol. Chem.* 279 (15), 15662–15669. doi:10.1074/jbc.M311301200
- Sun, N., Shen, C., Zhang, L., Wu, X., Yu, Y., Yang, X., et al. (2021). Hepatic Krüppel-like factor 16 (KLF16) targets PPAR α to improve steatohepatitis and insulin resistance. *Gut* 70 (11), 2183–2195. doi:10.1136/gutjnl-2020-321774
- Sunny, N. E., Bril, F., and Cusi, K. (2017). Mitochondrial adaptation in nonalcoholic fatty liver disease: Novel mechanisms and treatment strategies. *Trends Endocrinol. Metab.* 28 (4), 250–260. doi:10.1016/j.tem.2016.11.006
- Sutti, S., and Albano, E. (2020). Adaptive immunity: An emerging player in the progression of NAFLD. *Nat. Rev. Gastroenterol. Hepatol.* 17 (2), 81–92. doi:10.1038/s41575-019-0210-2
- Syn, W.-K., Agboola, K. M., Swiderska, M., Michelotti, G. A., Liaskou, E., Pang, H., et al. (2012). NKT-associated hedgehog and osteopontin drive fibrogenesis in non-alcoholic fatty liver disease. *Gut* 61 (9), 1323–1329. doi:10.1136/gutjnl-2011-301857
- Syn, W. K., Htun Oo, Y., Pereira, T. A., Karaca, G. F., Jung, Y., Omenetti, A., et al. (2010). Accumulation of natural killer T cells in progressive nonalcoholic fatty liver disease. *Hepatology* 51 (6), 1998–2007. doi:10.1002/hep.23599
- Wolf, M. J., Adili, A., Piotrowitz, K., Abdullah, Z., Boege, Y., Stemmer, K., et al. (2014). Metabolic activation of intrahepatic CD8 $^{+}$ T cells and NKT cells causes nonalcoholic steatohepatitis and liver cancer via cross-talk with hepatocytes. *Cancer Cell* 26 (4), 549–564. doi:10.1016/j.ccell.2014.09.003
- Wu, L., Parekh, V. V., Gabriel, C. L., Bracy, D. P., Marks-Shulman, P. A., Tamboli, R. A., et al. (2012). Activation of invariant natural killer T cells by lipid excess promotes tissue inflammation, insulin resistance, and hepatic steatosis in obese mice. *Proc. Natl. Acad. Sci. U. S. A.* 109 (19), E1143–E1152. doi:10.1073/pnas.1200498109
- Xu, D., Holko, M., Sadler, A. J., Scott, B., Higashiyama, S., Berkofsky-Fessler, W., et al. (2009). Promyelocytic leukemia zinc finger protein regulates interferon-mediated innate immunity. *Immunity* 30 (6), 802–816. doi:10.1016/j.immuni.2009.04.013
- Yamagoe, S., Kanno, T., Kanno, Y., Sasaki, S., Siegel, R. M., Lenardo, M. J., et al. (2003). Interaction of histone acetylases and deacetylases *in vivo*. *Mol. Cell. Biol.* 23 (3), 1025–1033. doi:10.1128/mcb.23.3.1025-1033.2003
- Zhang, H., Chen, Q., Yang, M., Zhu, B., Cui, Y., Xue, Y., et al. (2013). Mouse KLF11 regulates hepatic lipid metabolism. *J. Hepatol.* 58 (4), 763–770. doi:10.1016/j.jhep.2012.11.024

Frontiers in Pharmacology

Explores the interactions between chemicals and living beings

The most cited journal in its field, which advances access to pharmacological discoveries to prevent and treat human disease.

Discover the latest Research Topics

[See more →](#)

Frontiers

Avenue du Tribunal-Fédéral 34
1005 Lausanne, Switzerland
frontiersin.org

Contact us

+41 (0)21 510 17 00
frontiersin.org/about/contact



Frontiers in Pharmacology

